Valorization of non-recycled plastic waste by catalytic reforming to produce synthesis gas

Aida Younis

Aida Younis. Valorization of non-recycled plastic waste by catalytic reforming to produce synthesis gas. Analytical chemistry. Université du Littoral Côte d'Opale; Université de Balamand (Tripoli, Liban), 2022. English. NNT : 2022DUNK0640 . tel-04047063

HAL Id: tel-04047063
https://theses.hal.science/tel-04047063v1

Submitted on 27 Mar 2023

Thèse de Doctorat

Mention Chimie
Spécialité Chimie théorique, physique, analytique

présentée à *l'Ecole Doctorale en Sciences Technologie et Santé (ED 585)* **de**
l'Université du Littoral Côte d'Opale

par

Aida YOUNIS

pour obtenir le grade de Docteur de l'Université du Littoral Côte d'Opale

Valorisation du plastique non recyclé par reformage catalytique en gaz de synthèse

Soutenue le 09/12/2022, après avis des rapporteurs, devant le jury d'examen :

M.B. Taouk, Professeur INSA Rouen	**Président**
M. J. Randrianalisoa, Professeur Université de Reims	**Rapporteur**
Mme S. Ojala, Professeur Université de Oulu	**Rapportrice**
Mme J. Estephane, Maître de Conférences University of Balamand	**Co-directrice**
M. E Abi Aad, Professeur Université du Littoral Côte d'Opale	**Directeur**
M. S. Aouad, Professeur University of Balamand	**Co-directeur**
M. C Gennequin, Professeur Université du Littoral Côte d'Opale	**Co-directeur**
Mme H. Guy, Docteur, Opale Environnement	**Examinatrice**

Acknowledgements

This experience was more of a journey with its share of ups and downs. This work turned out to be successful despite all the external impediments, such as the global epidemic, national revolution, and economic crisis. Here are my words of gratitude to everyone who helped make this journey plausible.

This PhD would not have been possible without the tangible support provided by the Université du Littoral Côte d'Opale (ULCO) and the Lebanese National Center for Scientific Research (CNRS-L) which granted me the opportunity as well as the financial support required to accomplish this thesis. I would also like to thank the University of Balamand (UOB) research council through the RGA/FAS/19-20/008 research grant.

I am deeply indebted to Prof. Edmond ABI AAD, my thesis director in France, for providing me with this opportunity, for his trust, guidance, and kindness. Thank you for seeing my potential. I would like to express my deepest gratitude to Prof. Samer AOUAD, my thesis director in Lebanon, for his constructive criticism, valuable advice, and guidance. Thank you for being an incredible mentor. I am extremely grateful to Prof. Cédric GENNEQUIN, my thesis supervisor in France, for his encouragement and help all throughout my thesis. Thank you for creating a stress-free environment that was well needed during my PhD. Words cannot express my gratitude to Dr. Jane ESTEPHANE, my thesis supervisor in Lebanon, for her motivation and kindness. Thank you for your motherly nature and care.

I also could not have undertaken this journey without the jury members Prof. Bechara TAOUK, Prof. Satu OJALA, Dr. Jaona RANDRIANALISOA, and Dr. Helene GUY, who generously provided knowledge and expertise to improve this work.

My gratitude goes to Prof. Stéphan SIFFERT, director of UCEIV at ULCO, for his warm welcome in his lab. I extend my gratitude to Prof. Hanna EL NAKKAT, dean of Faculty of Arts and Sciences at the University of Balamad, for his continuous support and encouragement throughout my years at UOB.

I want to express my profound gratitude to my wonderful family at the Chemistry Lab at UOB. Eng. Bilal EL KOURY, I appreciate all your assistance with the setup and your willingness to help me anytime I needed it. Thank you, Ms. Amal AOUN, for the motivational speeches you gave

during the daily breakfast and tea breaks. My office mate Eliane DAHDAH, I appreciate all your assistance and support, as well as your creative stress-relieving techniques. In addition to the research assistants at the UOB's department of Chemical Engineering. Cherine SALIBA, a lifelong friend of mine, for being there and helping me in the lab before I ever began my PhD. Thanks to engineers Lena INATY and Yorgo FARAH for their assistance.

Additionally, I want to express my gratitude to the TCEP team at UCEIV for accepting me into their lab. I sincerely appreciate Lucette TIDAHY's assistance and care throughout the years. I also want to thank Dr. Christophe POUPIN for running the XRD experiments and Prof. Renaud COUSIN for his assistance. I'd like to extend my gratitude to Dr. Fabrice CAZIER and M. Paul GENEVRAY for their assistance with the GC-MS and Pyro/GC-Ms analyses. A sincere thank you to Dr. Carmen CIOTONEA for her assistance and encouragement.

I'm grateful for all the lovely folks who have grown closer to being family along the journey. Muriel and Rebecca, you are two lovely beings, and I will always count myself fortunate to have encountered you. I couldn't have wished for a finer travel companion than Rita. Thank you, Myriam, for your humorous nature, and Mariebelle, for your kind heart and the delicious pot you prepared. My heartfelt gratitude to Sara for her warm welcome on my first day. Madan, I appreciate all your assistance and the fact that you never decline a cup of coffee. Micho, Manon, Caroline, Mireille, Lamia, Marc, Hamed, Bastien, Mahdi, Charad, Lilian, Pedro, Sarah, Abir, Julien, Leila, Nour, Guillaume, Thamy, and Nathalie, each one of you has been a part of so many memories that will always make me smile. I also want to thank my friends in Lebanon, Helena, Souad, Sami, and Maha, who have always stood by my side. I want to thank my cousin Farah in Canada for all the zoom meetings and the assistance in understanding ASPEN.

Lastly, I would love to thank my family. My sisters, Mira and Lara, your belief in me has kept my spirits and motivation high during this process. My brother-in-law Barbar for assisting me with my relocation to France and for all the wonderful cuisine in Paris. Uncle Isaac for being the first to inspire me to be ambitious and pursue my aspirations. Mom and Dad, I owe everything I am and everything I have become to you. I would like to dedicate my work to my late uncle Raif. Thank you for shaping me into the scientist that I am today.

I humbly close my acknowledgements by expressing my thankfulness to You for walking beside me every step of the way.

Abstract

This work aims to study the pyrolysis-catalytic dry reforming of plastic for syngas production over different catalysts. The alumina and alumina promoted by cerium have been chosen as catalytic supports. For syngas production, the influence of nickel loading and the promotion with ruthenium are studied.

For dry reforming of polypropylene, the activity of Ni impregnated pure metal oxides is first investigated, since pure metal oxides are often used as catalytic supports. The 25NiAl$_2$O$_3$ catalyst is found to be the most efficient for syngas production. The promoted Ni-based catalysts with 1 wt.% Ru are studied. Inserting a small percentage of Ru enhanced the catalytic activity by enhancing the surface properties. The effect of the calcination temperature (500 °C and 800 °C) on the catalytic activity is studied. The catalysts calcined at 550 °C exhibit larger surface area and porosity, are easily reduced, and possess higher basicity compared to the same catalyst calcined at 800 °C. The aging of 25NiAl$_2$O$_3$ and 1Ru25NiAl$_2$O$_3$ catalysts is performed, and the 1Ru25NiAl$_2$O$_3$ catalyst calcined at 550 °C, prepared by impregnation of 25 wt% Ni and 1wt.%Ru on stabilized Al$_2$O$_3$ support, shows the best catalytic performance. For Ru-Ni based catalysts, the supports are modified with cerium. The activities of the Ce promoted catalysts are compared to the non-promoted catalyst, and all catalysts produce similar syngas quantities. Although less coke is formed on the Ce promoted catalysts, these catalysts rapidly deactivate and result in clogging of the reactor due to the amorphous carbon formed on the catalyst surface.

The pyrolysis-dry reforming of other types of plastics (polyethylene, polystyrene, and mixture of polyethylene and polypropylene) is performed. The results show that 1Ru25NiAl$_2$O$_3$ catalyst is successful in converting any type of plastic into significant quantities of syngas.

A simulation model on ASPEN Plus platform is developed to evaluate the influence of the reforming temperature and carbon dioxide flow rate on the syngas composition in the product stream. It is concluded from the sensitivity analysis that the optimal process conditions for high H$_2$ and CO yields: 800 °C reforming temperature and 3000 kg/h CO$_2$ flow rate.

Keywords: carbon dioxide; catalyst; cerium; dry reforming; nickel; polypropylene; pyrolysis; ruthenium; syngas.

Résumé

Ce travail de thèse vise à étudier la réaction de reformage à sec des gaz du plastique pour la production de gaz de synthèse en présence de différents catalyseurs supportés. L'alumine (gamma Al_2O_3) et l'alumine promue par le cérium (Ce-Al_2O_3) ont été choisies comme supports catalytiques. Les effets de la teneur en nickel et du ruthénium sur les propriétés catalytiques des matériaux pour la production de gaz de synthèse ont été étudiés.

Pour l'étude de reformage à sec du polypropylène, l'activité des oxydes métalliques purs imprégnés de Ni a d'abord été étudiée. Le catalyseur $25NiAl_2O_3$ s'est avéré être le plus efficace pour la production de gaz de synthèse. Les catalyseurs à base de Ni promus avec 1 % en masse de Ru ont été étudiés. L'ajout d'une faible teneur de Ru a augmenté l'activité catalytique en améliorant les propriétés de surface du matériau. L'effet de la température de calcination (550 °C et 800 °C) sur l'activité catalytique a également été étudié. Les catalyseurs calcinés à 550 °C ont montré une plus grande surface spécifique, une porosité plus importante, une meilleure réductibilité et une basicité plus élevée par rapport au même catalyseur calciné à 800 °C. Le vieillissement des catalyseurs $25NiAl_2O_3$ et $1Ru25NiAl_2O_3$ a été effectué pendant neuf passages. Le catalyseur $1Ru25NiAl_2O_3$ calciné à 550 °C, préparé par imprégnation de 25 % en masse de Ni et 1 % en masse de Ru sur un support stabilisé Al_2O_3, a montré la meilleure performance catalytique.

Pour les catalyseurs à base de Ru-Ni, les supports ont été modifiés avec du cérium. Les activités des catalyseurs promus au cérium ont été comparées à celles du catalyseur non promu, et tous les catalyseurs ont produit des quantités de gaz de synthèse similaires. Bien que moins de coke se soit formé sur les catalyseurs promus par le cérium, ces catalyseurs se sont rapidement désactivés et ont entraîné le blocage du réacteur en raison du carbone amorphe formé à la surface du catalyseur.

La pyrolyse et le reformage à sec d'autres types de plastiques (polyéthylène, polystyrène et mélange de polyéthylène et de polypropylène) ont été réalisés. Les résultats ont montré que le catalyseur $1Ru25NiAl_2O_3$ réussissait à convertir tout type de plastique en quantités significatives de gaz de synthèse. Un modèle de simulation sur la plateforme ASPEN Plus a été développé pour évaluer l'influence de la température de reformage et du débit de dioxyde de carbone sur la composition du gaz de synthèse dans le flux de produit. L'analyse de sensibilité a permis de conclure que les conditions optimales du procédé pour des rendements élevés en H_2 et CO : une température de reformage de 800 °C et un débit de CO_2 de 3000 kg/h.

Mots clés : polypropylène ; gaz de synthèse ; dioxyde de carbone ; pyrolyse ; reformage à sec ; catalyseur ; nickel ; cérium ; ruthénium.

Introduction générale

D'après l'étude "Plastics the Facts" réalisée en 2021 [1], 55 millions de tonnes de déchets plastiques ont été enregistrées pour l'Europe, dont 36 % ont été recyclées. En raison de leur résistance et du fait qu'ils mettent des centaines d'années à se décomposer naturellement, les plastiques constituent une part importante de déchets non valorisés. La mise en décharge est inefficace et nuisible à l'environnement en raison de la contamination du sol et de l'eau. Ainsi, l'utilisation intensive de plastiques et la mise en décharge excessive constituent un danger pour les écosystèmes marins et terrestres, puisque ces matériaux non biodégradables s'accumulent. Par ailleurs, la combustion incontrôlée de ces déchets libère des composés dangereux dans l'atmosphère, contribuant ainsi à la pollution atmosphérique. Le recyclage de ces matières s'avère donc primordiale pour diminuer l'impact néfaste sur l'environnement.

Depuis plusieurs années, les recherches se portent vers le recyclage chimique.

Une méthode prometteuse est la réaction de reformage à sec des gaz de pyrolyse des plastiques. En effet, Les plastiques étant principalement composés d'hydrocarbures, ils peuvent être recyclés chimiquement pour créer du gaz de synthèse (syngas : H_2 et CO), une ressource pour la fabrication de produits chimiques à haute valeur ajoutée. Le plastique pourrait donc devenir une matière première peu coûteuse pour la production de gaz de synthèse. Ce procédé offrirait une nouvelle approche de la gestion des déchets plastiques.

Le reformage à sec est un processus endothermique, qui nécessite donc des températures élevées. La présence d'un catalyseur accélère la réaction et régule la sélectivité pour garantir la formation des produits souhaités. Le catalyseur optimal ne doit pas seulement être actif, mais aussi peu couteux, stable et durable. La sélection du support et de la phase active est donc essentielle. Ce travail de thèse vise donc à synthétiser un catalyseur efficace et actif pour la réaction de reformage à sec des gaz de pyrolyse des plastiques. Cette étude compare plusieurs catalyseurs ayant différentes phases actives supportés par de l'alumine. L'influence des promoteurs sur l'activité catalytique et la stabilité sera également évaluée dans ce travail. En outre, cette étude l présente la production de gaz de synthèse à partir du reformage de déchets plastiques, où le processus de reformage à sec est modélisé à l'aide du logiciel de simulation ASPEN Plus. Différents paramètres seront étudiés afin de déterminer les paramètres optimaux du processus pour la production de gaz de synthèse.

Ce manuscrit est divisé en quatre chapitres :

Le premier chapitre commence par une description des matières plastiques. Les structures et les propriétés des polymères sont décrites, ainsi que les quatre méthodes de recyclage connues. La pyrolyse non catalytique des polymères est étudiée ainsi que la cinétique de la pyrolyse, le mécanisme et les paramètres du processus. Une description détaillée de la réaction de reformage à sec suivra et les catalyseurs fréquemment utilisés dans cette réaction seront présentés. Le phénomène de désactivation du catalyseur sera évoqué. Les paramètres qui affectent la performance catalytique seront également discutés. Enfin, l'explication de la sélection des catalyseurs qui sont examinés dans cette thèse est abordée.

Le deuxième chapitre étudie le matériau plastique utilisé. L'analyse par calorimétrie différentielle à balayage/thermogravimétrie (DSC/TG) est utilisée pour étudier le comportement thermique des plastiques sous une atmosphère inerte. La technique de pyrolyse liée à la chromatographie en phase gazeuse/spectrométrie de masse (Pyro-GC/MS) est utilisée pour étudier les produits gazeux issus de la pyrolyse des plastiques. Ce chapitre donne également un descriptif complet de la synthèse et de la caractérisation physico-chimique du support et des catalyseurs qui ont été testés dans la réaction étudiée. De nombreuses méthodes physico-chimiques ont été utilisées, notamment la diffraction des rayons X (DRX), l'adsorption/désorption de N_2, la réduction en température programmée sous hydrogène (RTP-H_2) et la désorption en température programmée (DTP-CO_2).

Le troisième chapitre sera consacré à l’étude de l'activité des catalyseurs à base de Ni pour la réaction de reformage à sec des gaz de pyrolyse des plastiques de polypropylène. Dans une première section, l'influence de différentes charges de Ni sur l'activité catalytique sera étudiée. Ensuite, l'impact de la promotion des catalyseurs à base de Ni avec du ruthénium sera analysé. Dans la troisième section, l'effet de la température de calcination sur les catalyseurs les plus prometteurs sera étudié et le meilleur sera déterminé par vieillissement. La quatrième section étudiera l'influence de la promotion du support avec du Ce. L'influence du ratio plastique/catalyseur sera examinée, et le catalyseur optimal sera comparé à un catalyseur commercial. Enfin, la production du gaz de synthèse avec de différents types de plastique sera effectuée en présence du catalyseur optimal.

Le quatrième et dernier chapitre est une introduction à la modélisation du processus de pyrolyse-reformage à sec du plastique à l'aide du logiciel de simulation ASPEN Plus. Dans ce chapitre, les effets du type de plastique, de la température de reformage et du débit massique de CO_2 sont étudiés afin de déterminer les paramètres optimaux du procédé pour la production de gaz de synthèse.

Les principaux résultats de cette thèse sont résumés dans une conclusion générale, ainsi que quelques perspectives.

Chapitre 1 : Etat de l'Art

La fabrication et la consommation de produits en plastique ont augmenté à un rythme sans précédent en raison de l'augmentation du niveau de vie et de la croissance démographique [2]. En raison de leurs faibles coûts de production, les plastiques sont l'un des matériaux les plus recherchés pour une utilisation dans un large éventail d'applications, notamment la construction, l'électronique, la biomédecine, l'ingénierie, le transport, les loisirs, l'alimentation aérospatiale et l'emballage des produits [3]. L'un des défis de la transformation des plastiques résulte du volume élevé d'emballages produits chaque jour et des cycles d'utilisation courts de la production de plastique [2].

Les plastiques sont des polymères macromoléculaires à longue chaîne qui ont subi une polymérisation organique. Ils sont durables car les longues chaînes de polymères contiennent des milliers d'unités monomères répétées. Par conséquent, il faut des centaines d'années pour que le plastique se décompose dans l'environnement [3]. Le plastique a donc une très faible biodégradabilité et doit passer par plusieurs processus coûteux (tri, lavage, broyage et extrusion) pour être recyclé efficacement. Cela pose de sérieux problèmes pour l'environnement, la société et l'économie [4].

Ces dernières années, la production mondiale de plastique a augmenté, pour atteindre 367 millions de tonnes de déchets plastiques en 2020 (**fig. 1**), dont 15 % pour l'Europe [1]. Ces chiffres devraient plus que doubler au cours des deux prochaines décennies [5].

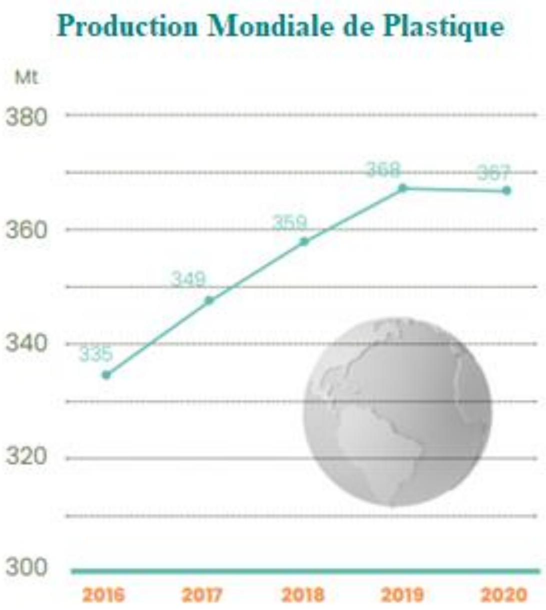

Fig. 1 Évolution de la production mondiale de plastique [1]

La **fig. 2** montre les plastiques les plus produits : le polypropylène (PP) représente 19,7%, suivi du polyéthylène basse densité (PEBD) (17,4%), du polyéthylène haute densité (PEHD) (12,9%), du chlorure de polyvinyle (PVC) (9,6%), du polyéthylène téréphtalate (PET) (8,4%), du polyuréthane (PUR) (7,8%), du polystyrène (PS) (6,1%) et des autres plastiques (18,1%) [1]. Cette demande toujours croissante de plastiques a entraîné une plus grande accumulation de cette matière dans les déchets. Bien que la gestion optimale des déchets plastiques passe par le recyclage et la production d'énergie, la part restante déposée dans les décharges est encore élevée.

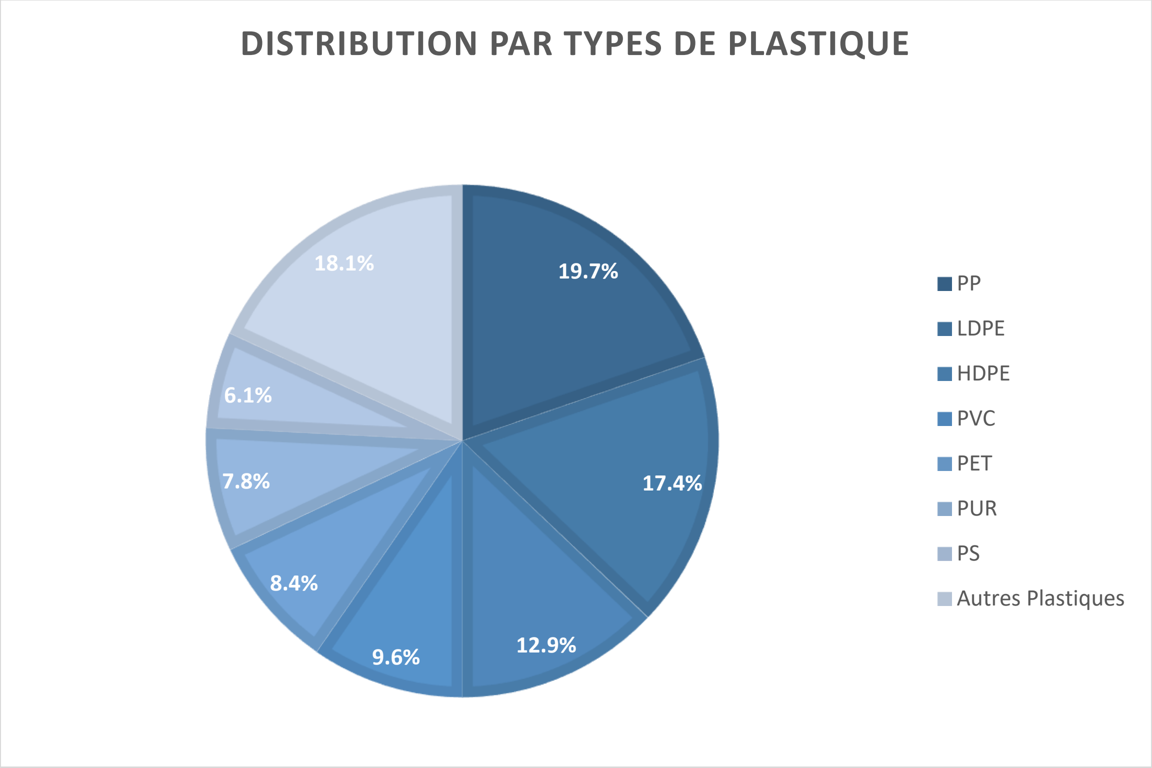

Fig. 2 Répartition de la production de plastiques en fonction des types de résine [1]**.**

Au cours du siècle dernier, la production de matières plastiques a connu une forte augmentation. La fabrication mondiale de plastique devrait tripler d'ici 2050 [3]. En Europe, près de 29,5 millions de tonnes de déchets plastiques post-consommation sont collectés : 42% sont utilisés pour la valorisation énergétique et 34,6% sont recyclés. Les 23,4 % restants sont mis en décharge [1]. La plupart des déchets plastiques sont mis en décharge, une solution moins chère que le recyclage.

Les déchets plastiques contribuent à la contamination des décharges et constituent une contrainte pour l'environnement. Lorsqu'ils sont mis en décharge, les déchets plastiques se décomposent, et du méthane et du dioxyde de carbone sont libérés dans l'atmosphère. Bien que la combustion des plastiques génère de l'énergie, ce processus libère également des gaz dangereux, des particules (notamment des métaux lourds), des oxydes d'azote et de soufre, des dioxines et des furanes, qui ont tous des effets néfastes sur la santé des êtres humains [3]. En outre, en raison de leur petite taille, les microplastiques sont biodisponibles pour une variété d'organismes marins. Les créatures marines avalent accidentellement des débris plastiques ou s'y empêtrent, ce qui entraîne une restriction des mouvements, une diminution de la production reproductive, des troubles de l'alimentation et la mortalité [3]. Ainsi, la mise en décharge et l'incinération ne sont pas des

techniques recommandées pour gérer les déchets plastiques, et des mesures doivent être prises pour traiter ces derniers d'une manière plus durable et plus respectueuse de l'environnement. En raison de l'augmentation des coûts de mise en décharge et de la diminution de l'espace disponible dans les décharges, d'autres alternatives pour l'élimination des déchets plastiques sont examinées. Par conséquent, le traitement des plastiques est devenu un problème important qui doit être résolu rapidement pour faire progresser la technologie du recyclage et de la réutilisation des plastiques [2].

Il était donc essentiel de développer et de mettre en œuvre des stratégies rentables de réduction, de réutilisation ou de recyclage des déchets plastiques. Les quatre catégories de techniques de traitement et de recyclage des déchets plastiques sont le recyclage primaire (réextrusion), secondaire (mécanique), tertiaire (chimique) et quaternaire (valorisation énergétique) [3]. Le recyclage primaire est la forme de recyclage la plus simple, où les déchets plastiques post-industriels sont recyclés en entreprise [6]. Le recyclage secondaire est la méthode de recyclage la plus courante, dans laquelle les déchets plastiques sont recyclés pour générer un produit ayant des caractéristiques différentes du produit intial [6,7]. Le recyclage tertiaire convertit les déchets plastiques en nouveaux produits par des moyens chimiques [8]. Le recyclage quaternaire consiste à brûler les déchets plastiques pour produire de l'énergie [3]. Chaque approche offre un ensemble unique d'avantages qui en font le meilleur choix pour les situations, les utilisations ou les exigences. Même si le recyclage mécanique est la méthode de gestion des déchets la plus courante, le recyclage chimique a gagné en importance au cours des dernières années [9]. La modification structurelle des déchets plastiques par le recyclage chimique les transforme en un produit entièrement nouveau.

En raison de leur contenu énergétique élevé, les déchets plastiques sont utilisés comme matière première pour la production d'énergie dans des procédés thermochimiques tels que la combustion, l'hydrogénation, la pyrolyse et la gazéification [3]. L'un des procédés de valorisation des déchets plastiques est la pyrolyse thermique sous atmosphère inerte qui donne une variété de produits : charbon, hydrocarbures liquides (carburants) et hydrocarbures gazeux [4]. Le type de catalyseur utilisé, les conditions de fonctionnement, la quantité et la nature de la matière première utilisée ont tous un impact sur ces résultats [3]. Le recyclage chimique des déchets plastiques réduit efficacement les déchets et les émissions de CO_2 tout en formant des produits de valeur.

Les émissions totales de CO_2 provenant de la combustion d'énergie et des processus industriels ont augmenté depuis les années 1900, et les préoccupations concernant la poursuite des émissions se sont considérablement accrues au cours des dix dernières années [10]. En raison de la poursuite de la combustion de combustibles fossiles et des changements dans l'utilisation des sols, on prévoit que les niveaux de CO_2 dans l'atmosphère vont encore augmenter. La pandémie de COVID-19 a eu un impact significatif sur la demande énergétique en 2020, réduisant les émissions mondiales de CO_2 de 5,1 %. Cependant, depuis lors, l'économie mondiale s'est redressée à un rythme alarmant. Selon l'étude menée par l'Agence Internationale de l'Energie (AIE), une augmentation de 6 % par rapport à 2020 a fait grimper les émissions de CO_2 à 36,3 gigatonnes (Gt), faisant de 2021 l'année où les émissions de CO_2 liées à l'énergie ont le plus augmenté d'une année à l'autre [11]. C'est pourquoi de nombreuses solutions ont été proposées pour réduire la concentration atmosphérique de dioxyde de carbone, notamment le captage et le stockage du carbone [3] et la conversion en d'autres produits utiles [12]. Le reformage à sec est une voie intéressante pour recycler le CO_2, un GES, comme matière première [13].

En raison de sa grande efficacité et des exigences relativement simples du procédé, la réaction de reformage à sec a fait l'objet de nombreuses recherches [14]. Dans ce procédé, les hydrocarbures se décomposent avec du dioxyde de carbone pour produire du gaz de synthèse [9]. Le gaz de synthèse est un mélange de monoxyde de carbone et d'hydrogène qui peut être utilisé pour fabriquer de nouveaux monomères ou d'autres composés [15]. Le gaz de synthèse contient normalement du H_2 et du CO dans des proportions variables et constitue un intermédiaire commun pour de nombreuses réactions chimiques à grande échelle [16]. Il s'agit d'une réaction industrielle importante qui sert de point de départ à de nombreux procédés de l'industrie chimique, tels que la synthèse de Fischer-Tropsch, les piles à combustible, etc. [13]. Les déchets plastiques représentant une charge d'hydrocarbures, le reformage à sec du plastique (1) est devenu une méthode potentielle pour résoudre le problème des déchets plastiques.

$$C_xH_y + xCO_2 \rightarrow 2xCO + y/2H_2 \tag{1}$$

La réaction de reformage à sec présente un triple intérêt : elle permet de se débarrasser des déchets plastiques, tout en valorisant le gaz à effet de serre CO_2, et en produisant un gaz de synthèse précieux [9]. Cependant, cette réaction endothermique nécessite des températures élevées. Elle est également limitée cinétiquement, ce qui nécessite l'emploi d'un catalyseur pour augmenter son

efficacité [17]. L'emploi d'un catalyseur dans tout procédé de recyclage peut réduire considérablement le besoin de chaleur élevée, ce qui peut contribuer à réduire les coûts opérationnels. La surface spécifique, le volume des pores, la taille des pores et l'acidité sont parmi les caractéristiques clés qui affectent le processus catalytique dans le recyclage du plastique [3].
Le problème clé qui doit être abordé dans la réaction de reformage à sec est le dépôt de coke qui conduit à la désactivation catalytique [14]. Cette désactivation est causée par le dépôt de carbone à la surface des catalyseurs produits par les réactions de décomposition du méthane (2) et de Boudouard (3) [18]. Par conséquent, le développement d'un catalyseur efficace dans ces conditions est nécessaire.

$$CH_4 \leftrightarrow 2H_2 + C \quad (2)$$

$$2CO \leftrightarrow CO_2 + C \quad (3)$$

En raison de ses grandes surfaces spécifiques, de la taille ajustable de ses pores et de sa grande stabilité thermique, l'alumine mésoporeuse a suscité beaucoup d'intérêt en tant que support de catalyseur. Différentes teneurs en métaux Au, Pd, Pt, Re et Ru ont été supportés sur l'alumine dans divers processus catalytiques [14]. La structure ordonnée et la distribution étroite des pores de l’alumine permet une meilleure dispersion des phases actives métalliques déposées, empêchant efficacement l'agglomération à haute température [14].

Les métaux nobles présentent une bonne résistance au coke et de bonnes performances catalytiques, mais leur coût élevé et leur disponibilité limitée les empêchent d'être utilisés dans de vastes opérations industrielles [14]. Les métaux de transition constituent une famille de catalyseurs très efficaces et économiques lorsqu'ils sont utilisés dans la réaction catalytique de reformage à sec. En raison de leur faible coût et de leur bonne activité catalytique, les catalyseurs à base de nickel ont été largement utilisés dans le reformage à sec du méthane et d'autres hydrocarbures. Bien que le nickel soit plus sensible au frittage et à la production de coke que les métaux nobles, il est le matériau catalytique le plus fréquemment utilisé dans les processus de reformage pour des raisons économiques [19]. Par conséquent, d'importants efforts de recherche ont été déployés pour rendre les catalyseurs à base de nickel plus résistants au frittage à haute température, d'autant plus que ces problèmes empêchent l'utilisation généralisée des catalyseurs à base de nickel [20]. Les inconvénients du nickel sont compensés par des modifications avec des promoteurs et des supports appropriés [19]. Par conséquent, plusieurs tentatives ont été faites ces dernières années pour améliorer la dispersion du nickel, réguler les particules de nickel à l'échelle nanométrique et stabiliser cette dimension nanométrique même à des températures de fonctionnement extrêmement élevées [14].

La technique la plus populaire dans la conception des catalyseurs consiste à ajouter un autre métal au catalyseur en tant que promoteur. Ces métaux peuvent améliorer les performances de diverses manières. Il a été démontré que le coke est principalement généré sur les plus grosses particules de Ni. Les promoteurs empêchent la désactivation du catalyseur en bloquant ces sites hautement réactifs [16]. La combinaison de métaux nobles, comme le Ru, avec des catalyseurs en nickel empêche le métal de se fritter et stabilise les performances du catalyseur dans les réactions de reformage [12]. Les avantages du mélange du nickel et du ruthénium comprennent une interaction qui favorise l'auto-activation et la stabilité du catalyseur. La plus grande stabilité résulte du fait que les espèces carbonylées sont essentielles pour les catalyseurs contenant du Ru. De plus, il semble que le développement de clusters bimétalliques Ni-Ru améliore la dispersion du nickel [12]. Par conséquent, dans cette étude, le nickel est promu avec le ruthénium pour former une phase active bimétallique. Il est à noter qu'un faible pourcentage de ruthénium (1 % en masse) est utilisé en raison du coût élevé de ce métal noble.

Chapitre 2 : Synthèse et caractérisation des matériaux de départ

Les plastiques utilisés dans cette étude sont nommés par leur code d'identification de résine, et classés en polypropylène (PP), polyéthylène (PE), polystyrène (PS) et polyéthylène téréphtalate (PET). Chaque type de plastique a été caractérisé par des techniques d'analyse thermique : DSC/TG et Py/GC-MS.

La gamme de température où la pyrolyse commence et se termine a été déterminée à l'aide des profils DSC-TG. Ces résultats nous aident à déterminer les conditions de pyrolyse. La technique Py-GC/MS s'est avérée être une méthode efficace pour déterminer les produits de pyrolyse obtenus lors de la pyrolyse des plastiques qui seront reformés en présence de CO_2 et d'un catalyseur. En se basant sur les résultats obtenus, ce travail de thèse se concentrera sur la pyrolyse du polyéthylène, du polypropylène et du polystyrène. La pyrolyse du polyéthylène téréphtalate est évitée en raison de la formation de l’acide benzoïque, qui pourrait endommager notre montage catalytique.

Synthèse du support d'alumine

L'alumine a été préparée selon la méthode de Vosoughi et al. [21] en mélangeant un bécher A contenant de l'isopropoxyde d'aluminium dissous dans un mélange d'éthanol et d'isopropanol et un bécher B contenant le copolymère F127 dissous dans de l’éthanol et d'isopropanol. La suspension obtenue a été agitée pendant neuf passages, puis soumise à un traitement hydrothermique. Le solide blanc résultant a été lavé avec de l'éthanol, séché, puis calciné sous air à 550 °C pendant 4 heures et à une vitesse de 1 °C/min.

Synthèse des catalyseurs sur support d'alumine

La technique d'imprégnation humide a été utilisée pour synthétiser les catalyseurs. 2 g du support d'alumine ont été imprégnés avec des solutions de précurseurs métalliques ($Ni(NO_3)_2.6H_2O$ (P> 97%)) et/ou ($Ru(NO)(NO_3)_3$) (1,5% Ru). Les catalyseurs ont été stabilisés thermiquement par calcination à 800 °C. Les différents catalyseurs synthétisés avec différentes teneurs en Ni et ceux promus avec 1 % en masse de Ru sont résumés dans la **fig. 3**.

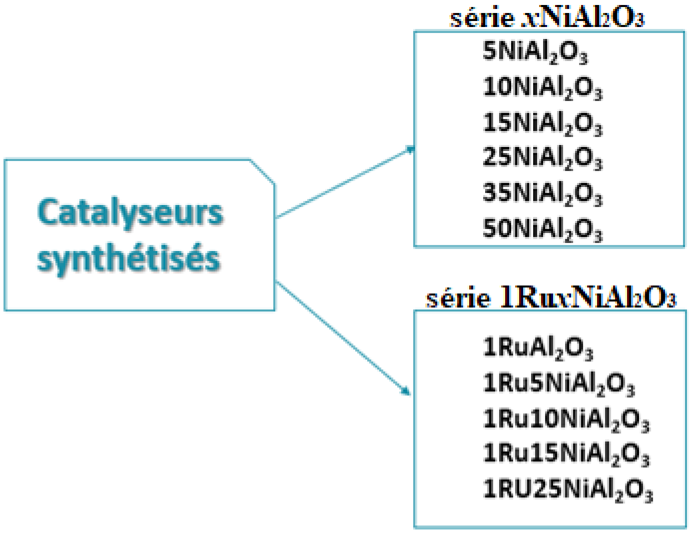

Fig. 3 Résumé des catalyseurs synthétisés à base de Ni et Ru supportés sur de l’alumine

Caractérisation des catalyseurs synthétisés

Les techniques de caractérisation suivantes sont appliquées pour les deux séries de catalyseurs : Analyse de diffraction des rayons X (DRX) pour étudier la structure cristalline des catalyseurs ; analyse d'adsorption/désorption de N_2 pour étudier leur structure poreuse ; la réduction en température programmée sous hydrogène (RTP-H_2) pour étudier les propriétés redox des catalyseurs ; désorption en température programmée de CO_2 (DTP-CO_2) pour étudier les propriétés propriétés basiques des catalyseurs.

D'après l'analyse DRX, la phase aluminate de nickel est observée à une température de calcination élevée pour tous les catalyseurs. Lorsque la charge en Ni augmente au-delà de 25 % en masse, la phase NiO est identifiée. Après réduction, les oxydes de Ni ont été réduits en Ni métallique (Ni^0). L'ajout du catalyseur avec Ru a révélé une bonne dispersion, puisque la phase RuO_2 n'était détectable qu'en présence de faibles pourcentages de nickel. Le support et les catalyseurs ont montré des isothermes d'adsorption de type IV, indiquant leur nature mésoporeuse. Tous les catalyseurs ont montré une diminution de l'aire spécifique de surface après avoir été imprégnés. De plus, après la promotion avec Ru, une augmentation de la surface est remarquée. Les profils RTP-H_2 montrent que la réduction des catalyseurs a été améliorée par la présence de Ru. D'après les profils DTP-CO_2, les catalyseurs promus présentent plus de sites actifs, ce qui améliore l'adsorption du CO_2.

Chapitre 3: Pyrolyse catalytique au reformage à sec du gaz issus des polypropylène: Résultats expérimentaux

La pyrolyse et le reformage à sec du polypropylène sont réalisés dans un réacteur à lit fixe à deux étages, sous pression atmosphérique. La pyrolyse du plastique a lieu dans le premier étage à 500 °C et la réaction de reformage à sec des hydrocarbures produits a lieu dans la deuxième étape à 800 °C, en présence de dioxyde de carbone et d'un catalyseur.

Influence du taux de Ni sur la production de gaz de synthèse

Dans la première section de ce chapitre, l'effet du dioxyde de carbone sur la réaction de reformage a été testé en l'absence de catalyseur. Il a été conclu que l'ajout de CO_2 a conduit à la réaction de reformage à sec des hydrocarbures (polypropylène), augmentant ainsi la production d'hydrogène et de monoxyde de carbone [22].

Dans la deuxième section, l'activité des oxydes métalliques purs imprégnés de Ni a été étudiée dans la réaction de reformage à sec du polypropylène. L'effet du taux de Ni sur la production de gaz de synthèse a été étudié lorsque différents taux de Ni (de 5 à 50 % en masse) ont été imprégnées sur le support alumine stabilisé et calciné à 800 °C. Comme le montre la **fig. 4**, les différents pourcentages de nickel imprégnés sur le support Al_2O_3 mésoporeux ont produit des quantités substantielles de gaz de synthèse, où la production de gaz de synthèse a augmenté de 76 mmol/gPP à 170 mmol/gPP avec l'augmentation de la charge de nickel de 5 à 50 % en poids. De plus, la quantité de H_2 produite est passée de 0,04 mole à 0,09 mole pour les catalyseurs respectifs. Les analyses DRX et RTP-H_2 ont montré qu'avec l'augmentation de la teneur en nickel, plus d'espèces NiO sont formées sur la surface du catalyseur. L'abondance de ces espèces réductibles influence positivent l'activité catalytique. Les résultats de la DTP-CO_2 ont montré que la basicité des catalyseurs augmente avec le taux de Ni, ce qui augmente l'adsorption du CO_2 et donc sa conversion. Les résultats ont montré que le goudron était effectivement craqué en présence d'un catalyseur content de 25 % en masse de Ni et que la quantité de H_2 produite se stabilisait à environ 0,08 mole et ne changeait considérablement pas lorsque la teneur en phase active augmentait. Ainsi, d'un point de vue économique, il est préférable d'utiliser une faible teneur de Ni tout en conservant une conversion plastique appropriée en gaz de synthèse.

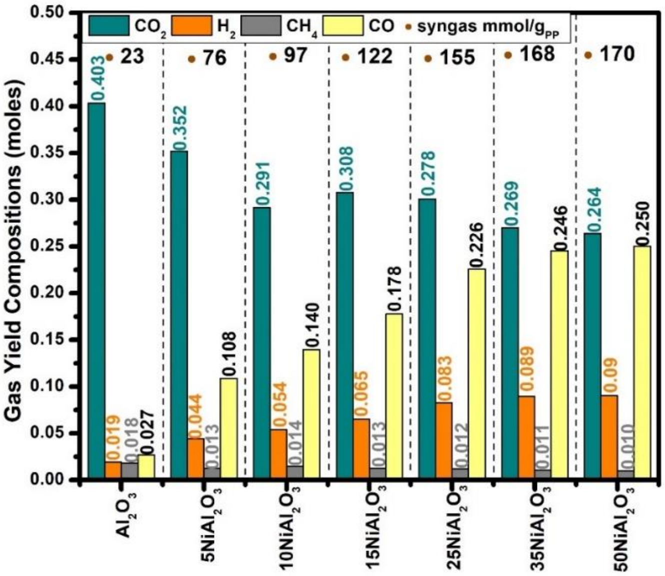

Fig. 4 Composition du gaz produit lors de la pyrolyse et du reformage à sec du polypropylène sur des catalyseurs au *x*NiAl$_2$O$_3$

Influence de la promotion du catalyseur par le ruthénium

Dans ce paragraphe, l'effet de ruthénium comme promoteur métallique va être abordé. Les catalyseurs à base de nickel ont été promus avec du ruthénium pour étudier l'effet du promoteur métallique sur la production de gaz de synthèse. Le ruthénium a été co-imprégné avec le nickel pendant la synthèse du catalyseur. En se basant sur les résultats du paragraphe précédent, les catalyseurs avec un pourcentage de Ni allant jusqu'à 25 % en masse ont été promus avec 1 % en masse de ruthénium. L'activité catalytique des catalyseurs à base de Ni a été considérablement augmentée par la co-imprégnation d’une faible quantité de Ru. Comme le montre la **fig. 5**, le catalyseur $1Ru15NiAl_2O_3$ a produit 0,078 mol de H_2 par rapport au catalyseur $15NiAl_2O_3$, qui a produit seulement 0,065 mol de H_2. Le ruthénium augmente la surface spécifique du catalyseur (table 2.4). Ceci est apparent dans les propriétés texturales après la promotion du catalyseur avec 1 % en masse de Ru. Cette augmentation de l'aire spécifique pourrait être attribuée à une meilleure dispersion de Ni après la promotion du catalyseur avec Ru. Cela a amélioré la capacité du catalyseur à interagir avec les molécules réactives, ce qui a amélioré la performance catalytique [12,23]. En outre, les résultats du H_2-RTP ont montré qu'une fois que les catalyseurs ont été promus avec Ru, la température maximale de réduction du nickel s'est déplacée vers des valeurs plus basses. Cela indique que le ruthénium a eu un impact bénéfique sur la réduction du Ni, peut-être en raison de l'effet de débordement, où un contact étroit entre le nickel et le ruthénium devrait exister pour observer cet effet. Cela signifie que l'introduction de Ru a amélioré la réductibilité des catalyseurs, affectant ainsi positivement la performance catalytique [16]. Les résultats du CO_2-DTP (fig. 2.21) ont montré qu'avec la présence de Ru, plus de sites basiques sont disponibles, ce qui entraîne une meilleure adsorption du CO_2 à la surface des catalyseurs et donc une meilleure conversion du CO_2. La forte adsorption du CO_2 par le catalyseur diminue la formation de carbone au cours du processus, ce qui améliore les performances catalytiques [6]. En outre, la promotion des catalyseurs à base de nickel améliore la conversion du goudron. Les catalyseurs promus craquent efficacement les composés du goudron et diminuent les concentrations de benzène et de toluène dans le goudron par rapport à leurs homologues non promus. Par conséquent, les caractéristiques catalytiques améliorées du catalyseur promu avec Ru ont amélioré la gazéification du carbone et le craquage du goudron, et par conséquent ont augmenté l'activité catalytique pour une production accrue de gaz de synthèse [15]. Le catalyseur à base de nickel promu avec 1 % en masse de Ru s'est avéré plus actif et plus stable que le catalyseur non promu. Les résultats de ce chapitre soulignent l'importance de la teneur de la phase active et de la promotion avec un métal noble, car ils déterminent les propriétés physicochimiques du catalyseur, qui définissent ses performances dans la réaction de reformage à sec. Les résultats des deux premiers chapitres ont été publiés dans le journal "International Journal of Hydrogen Energy" [9].

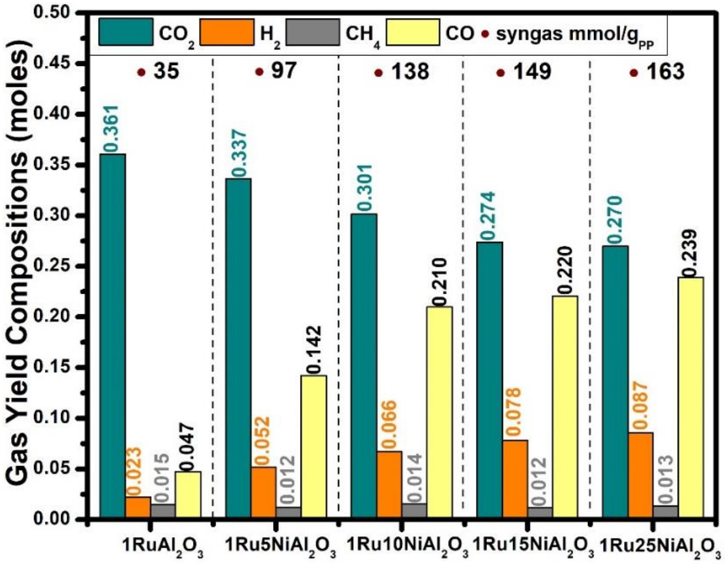

Fig. 5 Composition du gaz produit lors de la pyrolyse et du reformage à sec du polypropylène sur des catalyseurs 1Ru*x*NiAl$_2$O$_3$

Effet de la température de calcination sur la production de gaz de synthèse

La **fig.6** montre que le catalyseur 1Ru25NiAl$_2$O$_3$ calciné à 550 °C a légèrement produit plus de H_2 et de gaz de synthèse (0,089 mol ; 168 mmolsyngas/gPP) par rapport au même catalyseur calciné à 800 °C (0,087 mol H_2 ; 163 mmolsyngas/gPP). Comme les catalyseurs ont été réduits avant test, les oxydes NiO se transforment plus facilement en Ni^0 actif bien dispersé comparées aux espèces $NiAl_2O_4$, ce qui affecte l'activité catalytique. L'activité et la stabilité des catalyseurs dans le reformage à sec des plastiques sont liées aux résultats de leur caractérisation après avoir été calcinés à deux températures différentes (550 °C et 800 °C). Les analyses d'adsorption/désorption de N_2 ont montré une diminution de l'aire de surface à des températures de calcination plus élevées. Une surface plus petite est généralement associée à une cristallinité accrue du catalyseur [24]. L'amélioration de la performance catalytique des catalyseurs calcinés à basse température pourrait être attribuée à la plus grande surface et à la plus petite taille des pores. D'après les profils RTP-H_2, les catalyseurs ont montré une meilleure réductibilité à des températures plus basses de calcination. D'après les résultats de la DTP-CO_2, à mesure que la température de calcination diminue, l'intensité du pic de désorption augmente, indiquant que moins de sites acides étaient présents dans les échantillons calcinés à 550 °C. Par conséquent, les catalyseurs calcinés à des températures plus basses avaient des sites basiques plus forts, ce qui est cohérent avec l'ordre d'activité. L'interaction métal-support, la dispersion des particules métalliques actives et le degré de réduction sont fortement influencés par la température de calcination, qui a un impact sur la stabilité et l'activité des catalyseurs. On peut conclure qu'une température de calcination élevée du catalyseur favorise une plus grande interaction entre la phase active et le support en provoquant le développement d'espèces inactives comme la phase spinelle $NiAl_2O_4$. Ainsi, les catalyseurs calcinés à 550 °C ont montré de meilleures performances catalytiques par rapport à ceux calcinés à 800 °C.

Ces deux catalyseurs ont été soumis à plusieurs tests catalytiques successifs pour étudier leur degré de désactivation. Les résultats ont montré que les catalyseurs à base de nickel ont commencé à se désactiver après neuf passages, tandis que les catalyseurs promus ne se sont pas désactivés. Étant donné que les deux catalyseurs ont été synthétisés en utilisant la même technique d'imprégnation humide et la même teneur en nickel, cela montre clairement que la co-imprégnation avec du ruthénium peut améliorer de manière significative la stabilité des catalyseurs à base de nickel à des températures élevées et allonger la durée de vie du catalyseur pendant le reformage à sec du polypropylène. Aucune désactivation significative du catalyseur $1Ru25NiAl_2O_3$ n'a été observée après les passages successifs. Cela pourrait être dû au fait que la quantité de carbone déposée n'a pas atteint le niveau nécessaire pour provoquer la désactivation du catalyseur dans les cas présents. D'autres essais devraient être effectués pour pouvoir déterminer la durée de vie du catalyseur.

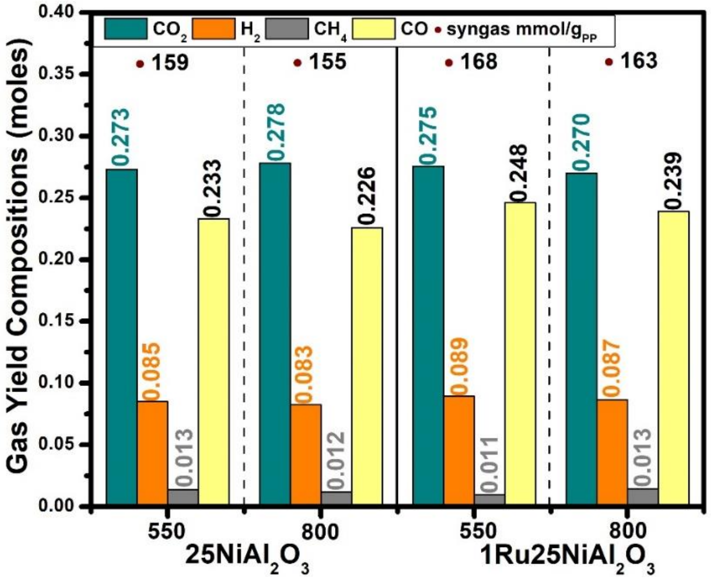

Fig. 6 Product gas composition of the pyrolysis-dry reforming of polypropylene over $25NiAl_2O_3$ and $1Ru25NiAl_2O_3$ catalysts at different calcination temperatures

Influence de la promotion du support avec Ce

La cérine CeO_2 est utilisée comme promoteur pour les catalyseurs supportés à base de l'Al_2O_3. Cela permet de combiner la capacité de CeO_2 à stocker et à libérer l'oxygène avec la grande surface de ces supports mésoporeux. En outre, une méthode largement utilisée pour stabiliser l'alumine consiste à la doper ou à la combiner avec divers oxydes métalliques [25]. Plusieurs études ont porté sur l'utilisation de l'oxyde de cérium comme agent stabilisant de l'alumine, et cette combinaison s'est avérée très prometteuse pour le reformage à sec du méthane [26]. D'après la littérature [27], l'oxyde de cérium joue un rôle crucial dans le transport des espèces d'oxygène actif qui oxydent le carbure sur les surfaces du catalyseur. Par conséquent, l'objectif est d'étudier l'effet du CeO_2 sur la formation de coke sur le catalyseur $1Ru25NiAl_2O_3$ modifié par le Ce dans le reformage à sec du polypropylène.

D'après les propriétés texturales, nous remarquons la surface d'aire spécifique diminue avec l'augmentation de la charge en Ce. Ceci est dû à l'agglomération des particules de Ni et à la formation de Ni-CeO_2, d'autant plus qu'il est plus difficile de réduire le Ni dans le Ni-CeO_2 [27]. De plus, la dispersion du métal actif sur un support à haute surface spécifique améliore l'activité et la stabilité du catalyseur [28]. Par conséquent, la différence de performance catalytique semble être liée à la dispersion de Ni et à la surface. L'activité catalytique diminue lorsque les catalyseurs sont promus avec des charges élevées de Ce en raison de l'agglomération des particules de Ni et de la ségrégation de CeO_2 [27].

Nous pouvons expliquer que la promotion du Ce a fourni des espèces d'oxygène actif, inhibant ainsi la formation de carbure. Le CeO_2 agit comme un transporteur pour les espèces d'oxygène qui oxydent le carbure à la surface du catalyseur et renforce le contact métal-support [27]. La dissociation du dioxyde de carbone est améliorée par l'oxyde de cérium réduit et les espèces d'oxygène absorbées réagissent avec le carbone de surface pour produire H_2, CO et CO_2. Par conséquent, moins de carbone est formé à la surface des catalyseurs promus par le Ce. En outre, le support promu au Ce a révélé sa capacité à inhiber de manière significative la croissance du carbone filamenteux. Cependant, il n'a pas été capable d'arrêter le développement du carbone amorphe. Le vieillissement des catalyseurs promus au Ce a montré que ce type de catalyseurs se désactivent progressivement.

Par conséquent, il est suggéré que le carbone amorphe formé à la surface des catalyseurs promus par le Ce est responsable de la faible activité catalytique due au blocage des réactifs gazeux vers le catalyseur pendant la pyrolyse et le reformage à sec du polypropylène.

Pyrolyse et reformage à sec de différents types de matières plastiques sur un catalyseur au 1Ru25NiAl$_2$O$_3$

Le 1Ru25NiAl$_2$O$_3$, a été utilisé pour étudier la pyrolyse-réformage d'autres types de plastiques (PE et PS), ainsi qu'un mélange de deux plastiques (50% PP + 50% PE). Le comportement du catalyseur vis-à-vis de la production de gaz de synthèse peut varier en fonction du type de plastique utilisé. En termes de production de gaz de synthèse à partir du reformage à sec de différents types de plastique sur le catalyseur 1Ru25NiAl$_2$O$_3$, on peut résumer comme suit : Comme le montre la **fig. 7**, le PP produit une grande quantité de gaz de synthèse, suivi du PS, d'un mélange de PP et de PE, puis du PE. On note une différence dans la production de gaz de synthèse entre les différents types de plastiques. Cela peut être attribué au carbone formé sur la surface du catalyseur après le reformage. On peut donc en conclure que, selon l'échantillon de déchets utilisé, la formation du dépôt de carbone sur les catalyseurs à base de nickel varie [29]. Le rendement du gaz de synthèse varie légèrement entre ces plastiques, ce qui montre que le catalyseur synthétisé dans cette étude peut convertir avec succès différents types de plastiques en quantités significatives de gaz de synthèse.

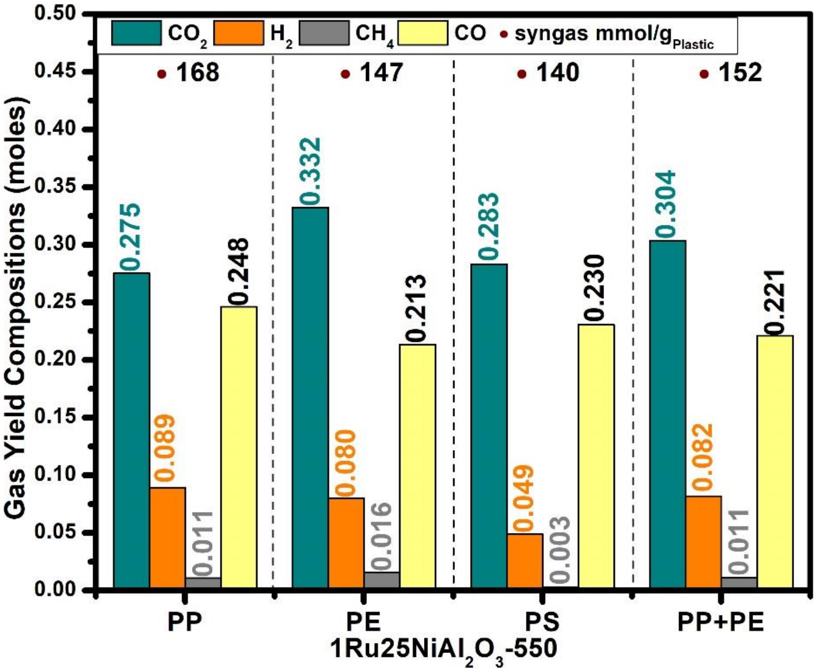

Fig. 7 Composition des gaz produits lors de la pyrolyse et du reformage à sec de différents types de plastiques sur 1Ru25NiAl$_2$O$_3$

Chapitre 4 ASPEN Plus: Simulation de la pyrolyse et du reformage à sec des plastiques

Dans ce chapitre, un modèle de simulation sur la plateforme ASPEN Plus a été développé pour évaluer l'influence du type de plastique, de la température de reformage et du débit de dioxyde de carbone sur la composition du gaz de synthèse dans le flux de produits. Les différents plastiques utilisés (PP, PE et PS) présentant des valeurs similaires dans les analyses proximale et finale, la composition des produits gazeux est presque équivalente après la pyrolyse et le reformage à sec de ces plastiques. En outre, les résultats de la simulation indiquent que l'augmentation de la température de reformage favorise la production de H_2 et de CO, tandis que la production de CH_4 et de CO_2 diminue. Cela implique que lorsque la température augmente, la réaction de reformage à sec prédomine et consomme à la fois du CH_4 et du CO_2. L'analyse de sensibilité a donc permis de déterminer les conditions optimales du procédé pour obtenir des rendements élevés en H_2 et en CO: température de reformage de 800 °C et débit de CO_2 de 3 000 kg/h.

Conclusion

Ce travail vise à trouver une solution à la problématique des déchets plastiques tout en valorisant le gaz à effet de serre : le dioxyde de carbone. Différents matériaux catalytiques sont synthétisés

afin d'évaluer le rôle de la phase active dans la réaction de reformage à sec des plastiques. L'étude décrit la synthèse et la caractérisation de catalyseurs à base de Ni et Ru-Ni supportés sur de l'alumine mésoporeuse et souligne l'impact des supports à base d'oxyde de cérium. Certains paramètres du procédé sont étudiés afin de déterminer les conditions optimales pour la réaction de reformage à sec.

Avant les tests catalytiques, les supports et les catalyseurs ont été étudiés de manière exhaustive pour leur porosité, leurs structures cristallines, leur réductibilité et leur basicité. Tous les catalyseurs calcinés ont montré une isotherme de type IV, indiquant leurs structures mésoporeuses. Après l'imprégnation de la phase active, la structure mésoporeuse du support a été partiellement détruite, menant à un changement des isothermes de sorption de N_2, et la diminution des surfaces spécifiques et des volumes des pores. Une fois que les catalyseurs à base de nickel ont été promus avec du Ru, la dispersion du métal, la réductibilité du NiO à des températures plus basses et les surfaces ont été améliorées.

Dans cette étude, le craquage des hydrocarbures est favorisé en présence d'un catalyseur, ce qui a entraîné une production d'hydrogène plus élevée mais des concentrations plus faibles de méthane et d'autres hydrocarbures. Pour le reformage à sec des plastiques de polypropylène, la charge de nickel imprégnée sur le support d'alumine mésoporeuse a affecté la production de gaz de synthèse. Plus la teneur de nickel augmente, plus l'activité catalytique s'améliore et plus la production de gaz de synthèse est importante. Les résultats de cette étude ont démontré que le Ru réduit la production de carbone tout en améliorant l'activité du catalyseur monométallique dans la pyrolyse et le reformage à sec des plastiques. L'ajout de ruthénium à proximité des sites actifs du nickel stabilise une surface réduite et encourage la gazéification du carbone en empêchant l'accumulation de carbone à l'intérieur de la particule de nickel. Le catalyseur le plus performant dans la réaction étudiée est le $1Ru25NiAl_2O_3$ calciné à 550 °C. Ceci est due aux particules de Ni bien dispersées, du dégrée de réduction élevée, et de la quantité élevée de sites basiques. Les catalyseurs Ru-Ni sont plus performants que les catalyseurs Ni dans la réaction de reformage à sec des plastiques, où le catalyseur $1Ru25NiAl_2O_3$ est resté actif après plusieurs cycles, alors que le catalyseur $25NiAl_2O_3$ s'est désactivé. Cela indique que la stabilité et l'activité catalytique des catalyseurs au nickel ont été grandement améliorées par l'ajout de Ru sur les catalyseurs au nickel. Le support joue également un rôle crucial dans la prévention du développement du coke, ce qui améliore la stabilité du catalyseur. Le dépôt de carbone plus faible lors de la pyrolyse et du reformage à sec du PP était probablement dû à la réaction entre le carbone filamenteux et le dioxyde de carbone, ce qui a augmenté la production de monoxyde de carbone. La production de gaz de synthèse après reformage à sec sur les catalyseurs optimaux était 8,4 fois supérieure à celle du reformage non catalytique du PP. L'augmentation de la production de H_2 et de CO et la diminution du CH_4 dans le rendement gazeux lors du reformage au CO_2 du PP sont dues à la promotion de la réaction de reformage à sec dans le second réacteur. Cela peut être confirmé par l'augmentation de la conversion du CO_2, qui passe de 10 % pour le reformage à sec non catalytique du PP à environ 40 % après le reformage sur des catalyseurs à base de nickel. Un dépôt de carbone plus faible a entraîné une conversion plus élevée du CO_2 et une production plus importante de gaz de synthèse. La promotion du support avec certains pourcentages de Ce n'a pas affecté de manière significative la production de gaz de synthèse et a conduit à la désactivation du catalyseur après des cycles consécutifs. Ceci est dû au carbone amorphe formé après le test qui a couvert les sites actifs et a entravé la performance catalytique. Les résultats optimaux pour le reformage à sec pyrolytique-catalytique du polypropylène ont été découverts à une température de calcination du catalyseur de 550 °C et un rapport plastique:catalyseur de 2:1. Le catalyseur $1Ru25NiAl_2O_3$ synthétisé par imprégnation humide et calciné à 550 °C s'est avéré efficace pour le reformage de différents types de plastiques et la production de quantités importantes de gaz de synthèse.

Un modèle de simulation sur le logiciel ASPEN Plus a été développé pour évaluer l'influence du type de plastique, de la température de reformage et du débit de dioxyde de carbone sur la composition du gaz de synthèse dans le flux de produit. La pyrolyse et le reformage à sec de différents types de plastique ont donné lieu à une composition similaire du produit gazeux. De plus, la température de reformage de 800 °C et le débit de CO_2 de 3000 kg/h étaient les conditions optimales du procédé pour des rendements élevés en H_2 et CO. Ces paramètres ont été déterminés à l'aide d'une étude d'analyse de sensibilité.

Des recherches supplémentaires doivent être menées pour contribuer à la mise à l'échelle des procédés micro-pilote à l'échelle industrielle. Pour commencer, des techniques de caractérisation supplémentaires doivent être réalisées sur les catalyseurs, notamment la cartographie MEB-EDX (pour la dispersion de la phase active), les techniques de microscopie (pour les morphologies du carbone formé), SPX (pour déterminer la capacité d'oxygène de surface) et ICP-OES (pour vérifier

la charge de la phase active, en particulier dans les catalyseurs bimétalliques). En outre, des études des mécanismes industriels pourraient être appliquées, dans lesquelles les intermédiaires réactifs seront identifiés pour comprendre la fonction de chaque composant catalytique dans la réaction. Il sera intéressant d'étudier l'effet de la méthode de synthèse sur la performance catalytique et d'optimiser davantage les paramètres de la réaction pour augmenter la production de gaz de synthèse. De plus, des essais supplémentaires devraient être effectués sur le catalyseur pour étudier son degré de désactivation. Des charges de Ce plus faibles pourraient être utilisées pour étudier de manière exhaustive l'effet du Ce sur la performance catalytique. De plus, l'utilisation du biochar comme support pourrait être une nouvelle approche verte à mettre en œuvre pour cette réaction. En outre, il convient de souligner que la vapeur pourrait être utilisée pour faire progresser le processus en faisant subir au monoxyde de carbone du produit une réaction de déplacement de gaz vers l'eau, ce qui entraînerait la production d'hydrogène [10]. Cela augmenterait le rapport H_2:CO et le rendrait plus proche de 1. Une analyse complète des plastiques et de leurs produits de pyrolyse ajouterait à la valeur de ce travail. En outre, des plastiques propres et purs ont été utilisés dans cette étude. Cependant, afin d'augmenter l'échelle du procédé, il serait intéressant de réaliser le reformage à sec de plastiques impurs mélangés pour étudier l'effet des impuretés sur la performance catalytique. De plus, dans cette étude, un réacteur batch a été utilisé. Par conséquent, une alimentation continue de déchets plastiques sera plus attrayante pour une utilisation industrielle potentielle.

En outre, pour développer un modèle plus réaliste à l'aide du logiciel ASPEN Plus, la cinétique des réactions impliquées dans le processus de reformage à sec doit être déterminée. Par conséquent, dans une perspective, la réaction de pyrolyse-reformage à sec peut être réalisée à différentes températures de fonctionnement et vitesses spatiales horaires du gaz. Les résultats expérimentaux ainsi obtenus peuvent être utilisés pour déterminer les différents paramètres cinétiques par régression du modèle et incorporés dans les modèles de réacteur intégrés comme RPLUG (basé sur le modèle de réacteur à écoulement piston) pour la validation du modèle de simulation.

Références

[1] PlascticsEurope, Plastics-the Facts 2021 An analysis of European plastics production, demand and waste data, 2021.

[2] Y. Zheng, J. Wang, C. Liu, Y. Lu, X. Lin, W. Li, Z. Zheng, Catalytic copyrolysis of metal impregnated biomass and plastic with Ni-based HZSM-5 catalyst: Synergistic effects, kinetics and product distribution, Int J Energy Res. 44 (2020) 5917–5935. https://doi.org/10.1002/ER.5370.

[3] S. Kumar, E. Singh, R. Mishra, A. Kumar, S. Caucci, Utilization of Plastic Wastes for Sustainable Environmental Management: A Review, ChemSusChem. 14 (2021) 3985–4006. https://doi.org/10.1002/CSSC.202101631.

[4] S. Klaimy, C. Ciotonea, J. Dhainaut, S. Royer, M. Casetta, S. Duquesne, G. Tricot, J.F. Lamonier, Flash Catalytic Pyrolysis of Polyethylene over (Alumino)silicate Materials, ChemCatChem. 12 (2020) 1109–1116. https://doi.org/10.1002/CCTC.201901819.

[5] L. Lebreton, A. Andrady, Future scenarios of global plastic waste generation and disposal, Palgrave Commun. 5 (2019). https://doi.org/10.1057/s41599-018-0212-7.

[6] I.A. Ignatyev, W. Thielemans, B. vander Beke, Recycling of polymers: A review, ChemSusChem. 7 (2014) 1579–1593. https://doi.org/10.1002/CSSC.201300898.

[7] S.M. Al-Salem, P. Lettieri, J. Baeyens, Recycling and recovery routes of plastic solid waste (PSW): A review, Waste Management. 29 (2009) 2625–2643. https://doi.org/10.1016/J.WASMAN.2009.06.004.

[8] K. Ragaert, L. Delva, K. van Geem, Mechanical and chemical recycling of solid plastic waste, Waste Management. 69 (2017) 24–58. https://doi.org/10.1016/J.WASMAN.2017.07.044.

[9] A. Younis, J. Estephane, C. Gennequin, L. Tidahy, B. el Khoury, S. Aouad, E. Abi Aad, Influence of promoting Ni-based catalysts with ruthenium in the dry reforming of polypropylene plastics for syngas production, Int J Hydrogen Energy. (2022). https://doi.org/10.1016/J.IJHYDENE.2022.07.156.

[10] W.D. Fletcher, C.B. Smith, Introduction, Reaching Net Zero. (2020) 1–8. https://doi.org/10.1016/B978-0-12-823366-5.00001-4.

[11] I. Energy Agency, Global Energy Review: CO_2 Emissions in 2021 Global emissions rebound sharply to highest ever level, (2021). www.iea.org/t&c/ (accessed March 23, 2022).

[12] N. Elia, J. Estephane, C. Poupin, B. el Khoury, L. Pirault-Roy, S. Aouad, E.A. Aad, A Highly Selective and Stable Ruthenium-Nickel Supported on Ceria Catalyst for Carbon Dioxide Methanation, ChemCatChem. 13 (2021) 1559–1567. https://doi.org/10.1002/cctc.202001687.

[13] A.G. Bhavani, W.Y. Kim, J.W. Lee, J.S. Lee, Influence of Metal Particle Size on Oxidative CO_2 Reforming of Methane over Supported Nickel Catalysts: Effects of Second-Metal Addition, ChemCatChem. 7 (2015) 1445–1452. https://doi.org/10.1002/CCTC.201500003.

[14] X. Fang, C. Peng, H. Peng, W. Liu, X. Xu, X. Wang, C. Li, W. Zhou, Methane Dry Reforming over Coke-Resistant Mesoporous Ni-Al2O3 Catalysts Prepared by Evaporation-Induced Self-Assembly Method, ChemCatChem. 7 (2015) 3753–3762. https://doi.org/10.1002/CCTC.201500538.

[15] S. Svadlenak, S. Rochefort, K.A. Goulas, Syngas production from polyolefins in a semi-batch reactor system, AIChE Journal. 67 (2021) e17479. https://doi.org/10.1002/AIC.17479.

[16] R. Franz, F.D. Tichelaar, E.A. Uslamin, E.A. Pidko, Dry reforming of methane to test passivation stability of Ni/ Al_2O_3 catalysts, Appl Catal A Gen. 612 (2021). https://doi.org/10.1016/j.apcata.2021.117987.

[17] A. Younis, J. Estephane, C. Gennequin, S. Aouad, E. Abi Aad, Valorization of plastics in the presence of Ru-Ni/Al_2O_3 catalysts to produce syngas, in: IEEEXplorer, 2021.

[18] J. Estephane, S. Aouad, S. Hany, B. el Khoury, C. Gennequin, H. el Zakhem, J. el Nakat, A. Aboukaïs, E. Abi Aad, CO_2 reforming of methane over Ni-Co/ZSM5 catalysts. Aging and carbon deposition study, Int J Hydrogen Energy. 40 (2015) 9201–9208. https://doi.org/10.1016/j.ijhydene.2015.05.147.

[19] C.J. Liu, J. Ye, J. Jiang, Y. Pan, Progresses in the Preparation of Coke Resistant Ni-based Catalyst for Steam and CO_2 Reforming of Methane, ChemCatChem. 3 (2011) 529–541. https://doi.org/10.1002/CCTC.201000358.

[20] J. Ashok, M.H. Wai, S. Kawi, Nickel-based Catalysts for High-temperature Water Gas Shift Reaction-Methane Suppression, ChemCatChem. 10 (2018) 3927–3942. https://doi.org/10.1002/CCTC.201800031.

[21] V. Vosoughi, A.K. Dalai, N. Abatzoglou, Y. Hu, Performances of promoted cobalt catalysts supported on mesoporous alumina for Fischer-Tropsch synthesis, Appl Catal A Gen. 547 (2017) 155–163. https://doi.org/10.1016/j.apcata.2017.08.032.

[22] J.M. Saad, M.A. Nahil, P.T. Williams, Influence of process conditions on syngas production from the thermal processing of waste high density polyethylene, J Anal Appl Pyrolysis. 113 (2015) 35–40. https://doi.org/10.1016/J.JAAP.2014.09.027.

[23] S. Andraos, R. Abbas-Ghaleb, D. Chlala, A. Vita, C. Italiano, M. Laganà, L. Pino, M. Nakhl, S. Specchia, Production of hydrogen by methane dry reforming over ruthenium-nickel based catalysts deposited on Al2O3, $MgAl_2O_4$, and YSZ, Int J Hydrogen Energy. 44 (2019) 25706–25716. https://doi.org/10.1016/j.ijhydene.2019.08.081.

[24] B.C. Kwon, N.K. Park, M. Kang, D. Kang, M.W. Seo, D. Lee, S.G. Jeon, H.J. Ryu, CO_2 hydrogenation activity of Ni-Mg-Al_2O_3 catalysts: Reaction behavior on $NiAl_2O_4$ and $MgAl_2O_4$, Korean Journal of Chemical Engineering. 38 (2021) 1188–1196. https://doi.org/10.1007/s11814-021-0778-4.

[25] K.M.S. Khalil, Synthesis and characterization of mesoporous ceria/alumina nanocomposite materials via mixing of the corresponding ceria and alumina gel precursors, J Colloid Interface Sci. 307 (2007) 172–180. https://doi.org/10.1016/J.JCIS.2006.11.039.

[26] S. Damyanova, B. Pawelec, R. Palcheva, Y. Karakirova, M.C. Capel-Sanchez, G. Tyuliev, E. Gaigneaux, J.L.G. Fierro, Structure and surface properties of ceria-modified Ni-based catalysts for hydrogen production, Appl Catal B. 225 (2018) 340–353. https://doi.org/10.1016/J.APCATB.2017.12.002.

[27] K.Y. Koo, H.S. Roh, U.H. Jung, W.L. Yoon, CeO_2 promoted Ni/Al_2O_3 catalyst in combined steam and carbon dioxide reforming of methane for gas to liquid (GTL) process, Catal Letters. 130 (2009) 217–221. https://doi.org/10.1007/S10562-009-9867-4.

[28] M. Safariamin, L.H. Tidahy, E. Abi-Aad, S. Siffert, A. Aboukaïs, Dry reforming of methane in the presence of ruthenium-based catalysts, Comptes Rendus Chimie. 12 (2009) 748–753. https://doi.org/10.1016/j.crci.2008.10.021.

[29] J.M. Saad, P.T. Williams, Pyrolysis-Catalytic-Dry Reforming of Waste Plastics and Mixed Waste Plastics for Syngas Production., Energy and Fuels. (2016). https://doi.org/10.1021/acs.energyfuels.5b02508.

Table of Contents

General Introduction

“Plastics will be the main ingredient of all our grandchildren’s recipes.” – Anthony Hincks

According to the “Plastics the Facts” study done in 2021, 55 million tons of waste plastic were recorded for Europe, of which 36% were recycled. Due to their strength and the fact that they take hundreds of years to naturally decay, plastics make up a significant portion of the deposited materials. Landfilling is inefficient and environmentally harmful due to the soil and water contamination caused by this process. Furthermore, extensive plastic usage and excessive landfilling pose a hazard to the marine and terrestrial ecosystems as these non-biodegradable materials build up in municipal solid waste. The uncontrolled combustion of these wastes, which releases hazardous compounds into the atmosphere, also contributes to air pollution. Although mechanical recycling still accounts for the great majority of plastic waste recycled, interest in chemical recycling is rising. Several chemical recycling methods have been implemented to recycle plastics. One method gaining popularity is the pyrolysis-catalytic dry reforming of plastics. Since plastics are mainly made of hydrocarbons, they can be chemically recycled to create synthesis gas (syngas: H_2 and CO), a resource for manufacturing chemical products. Therefore, plastic is a low-cost feedstock for syngas production. This process would provide a novel approach to managing waste plastics while attaining a solution to the considerable quantities of carbon dioxide in the atmosphere. Because of the worry over climate change, large amounts of carbon dioxide are expected to be produced by future carbon capture methods. Dry reforming is an endothermic process, so high temperatures are required. Also, this reaction requires the presence of a catalyst since it speeds up the process and regulates selectivity to ensure that the desired products are formed. The optimal catalyst should not only be active but also affordable, stable, and durable. When looking for the optimal catalyst, the selection of both the support and the active phase is essential. This research aims to synthesize a suitable catalyst that will make the dry reforming of plastics economically viable. This study compares several alumina-supported catalysts with various active phases. According to the literature, using catalytic promoters changes the catalyst's characteristics and improves its activities. Therefore, the influence of promoters on the catalytic activity and stability will also be studied in this work. Furthermore, this work presents the synthesis gas production from reforming of plastic waste, where the dry reforming process is modeled using ASPEN Plus simulation software. Different parameters will be investigated to determine the optimum process parameters for syngas production.

This manuscript is divided into four chapters

Chapter 1: State of the Art

This chapter begins with an overview of plastics. The polymers' structures and properties will be described, followed by the four known recycling methods. The non-catalytic pyrolysis of polymers is investigated along with the pyrolysis kinetics, mechanism, and process parameters. A detailed description of the dry reforming reaction will follow. Carbon dioxide emissions will be investigated. The thermodynamics and catalysts frequently employed in this reaction will be presented. The unavoidable phenomenon of catalyst deactivation will be highlighted. The catalytic parameters that affect catalytic performance will also be discussed. Finally, the explanation of the selection of the catalysts that are examined in this thesis is addressed.

Chapter 2: Analysis of Plastics and Synthesis/Characterization of the Catalysts

This chapter studies the plastic material used. The differential scanning calorimetry/ thermogravimetry (DSC/TG) analysis is used to study the thermal behavior of plastics under an inert atmosphere. The pyrolysis linked to gas chromatography/mass spectrometry (Pyro-GC/MS) technique is used to study the produced gaseous products from the pyrolysis of plastics.

This chapter also gives a thorough overview of the synthesis and physicochemical characterization of the support and catalysts that were tested in the under-study reaction. Numerous physicochemical methods were used, including X-Ray Diffraction (XRD), N_2 adsorption/desorption, H_2-Temperature Programmed Reduction (H_2-TPR), and CO_2-Temperature Programmed Desorption (CO_2-TPD). The catalysts under investigation were Ni and Ru-Ni supported on mesoporous alumina.

Chapter 3: Catalytic Dry Reforming of Plastics Pyrolysates

In this chapter, a detailed representation of the catalytic setup is presented. The activity of Ni-based catalysts will first be investigated in the dry reforming of polypropylene plastics. In the first section, the influence of different Ni loadings on the catalytic activity and the impact of promoting Ni-based catalysts with ruthenium will be investigated. In the second section, the most performing catalysts will be compared and the best one will be determined through aging. The third section will study the influence of promoting the support with Ce. The influence of plastic to catalyst ratio will be examined, and the best catalyst will be compared with a commercial one. Finally, the reforming of different types of plastic will be performed over the optimum catalyst.

Chapter 4: Simulation of a Process for the Pyrolysis-Dry Reforming of Plastics

In this chapter an ASPEN Plus simulation software was used to model pyrolysis-dry reforming of plastic process. In this chapter, the effects of plastic type, the reforming temperature, and the CO_2 mass flow rate are investigated to determine the optimum process parameters for syngas production. The aim of this chapter is to develop a preliminary model, validate it, and use it in the future to incorporate kinetic characteristics specific to the synthesized catalyst.

The key findings of this thesis are summarized in a general conclusion, along with some perspectives. Furthermore, the characterization techniques and supplementary data for the dry reforming of plastics are covered in two appendices (Appendix A and Appendix B).

Chapter 1

State of the Art

Table of Contents

List of Figures

List of Tables

1. Introduction

Since 1907, plastic materials have been synthesized as a solution for the substitution of scarce and non-sustainable resources such as ivory, tortoiseshell, or animal bones [1]. Since their first synthesis, plastics have replaced many types of materials such as wood, metals, stones, skins, horns, glasses, ceramics, and fibers in the production of consumer products [2,3]. Plastics' production has increased over the years, particularly since they have become one of the foundations of our lifestyles due to their low production cost, low density, durability, and corrosion resistance [4].

Initially, plastics supported the development of modern society by enabling new technologies and achievements in various sectors such as packaging, building and construction, microelectronics, transport, industrial applications, automotive, healthcare, food and water safety, agriculture, and various others [5,6]. Plastics production and consumption have increased significantly worldwide due to their strength, versatility, permanence, and ease of manufacture. Moreover, plastics are inexpensive, making them economically favorable in various application sectors. However, these characteristics that make them successful account for their abundance in the environment [7]. The plastic demand has been increasing due to the increased population, thus producing a global amount of over 300 million tons of plastic annually [8]. According to the "Plastics-the facts" study done in 2021, around 367 million tons of plastic are produced worldwide, out of which 55 million tons are recorded for Europe [9]. These figures are expected to more than double over the next two decades [10]. This ever-increasing demand for plastics has resulted in a greater accumulation of the material in waste. Although the optimum plastic waste management is through recycling and energy production, the remaining portion deposited in landfills is still high.

Since the COVID-19 outbreak, the global demand for plastic products has skyrocketed to unprecedented levels due to the contribution of plastic material in single-use products such as surgical face masks, gloves, personal protective equipment, hand sanitizer bottles, cleaning agents, food packaging, and takeout plastics [11,12]. The large percentage of landfilling is due to plastics' durability; plastics may take up to a billion years to degrade naturally due to the molecular bonds that contain carbon, hydrogen, and sometimes nitrogen, oxygen, chlorine, and other elements [13,14]. This constant disposal of plastic waste in landfills would lead to detrimental environmental problems.

The extensive use of plastics poses significant environmental risks as well as potential health risks to aquatic and terrestrial animals as these non-biodegradable materials accumulate in municipal solid waste [15]. Inadequate waste management has a grave environmental impact, including the accumulation of marine debris [16]. Moreover, for the first time, a recent study has discovered and quantified microplastics in human blood [17]. Furthermore, air pollution is caused by the uncontrollable incineration of such wastes, which releases harmful chemicals such as furans, mercury, and polychlorinated biphenyls [18].

To reduce plastic waste landfilling, mechanical recycling is considered the best plastic waste management alternative. However, the percentage of this type of recycling is still low due to several drawbacks accompanied by this method. Mechanical recycling requires separation and additional washing steps, thus making the process costly and time-consuming [19]. Although this process can reduce plastic waste, alternative methods to produce fuels and petrochemical feedstocks have been investigated [20]. As a result of the rise in energy demand and fossil fuel reduction, researchers have tried to find alternative energy resources. Examples of new energy resources include wind energy, solar energy, geothermal energy, and hydropower technology [13].

Recently, the conversion of waste into energy has emerged as an intriguing method of meeting the world's energy demand. This method is suitable for plastic waste since they are of petrochemical origin and possess high calorific values. An example of these methods is the pyrolysis of plastic waste which has gained attention not only at the plastic waste management level. Pyrolysis of plastics is a potential response to the energy supply problem, especially since the energy crisis is escalating globally and the main sources of energy (fossil fuels, coal, petroleum, and natural gases) are non-renewable energy sources [21].

2. Polymers’ structures and properties

Plastic is a high molecular weight material invented in the mid-nineteenth century by the English inventor Alexander Parkes, who was the first to treat cellulose nitrate with various solvents to produce what he called "Parkesine" (known today as celluloid, the first thermoplastic made) [3]. Plastics are also known as polymers; a molecule formed by the repetition of a single unit called a monomer. Plastics are a wide family of different materials. Each plastic is designed with specific characteristics that make it ideal for its intended application, providing individuals with resource-efficient solutions [1]. Plastic materials can be derived from a variety of sources. They could be of fossil (gas, crude oil, etc.), renewable (vegetable oils, starch, sugar cane, etc.), or mineral-based (salt) origin. Plastic materials, regardless of where they come from, are valuable resources that can either be used as new materials or as an alternative source of energy [1].

Polymers are classified into two distinctive classes: thermoplastics and thermosets. These classes are differentiated based on how they react in the presence of heat [21]. Thermoplastics are a class of plastics that can be melted when heated and hardened when cooled. They are referred to as reversible plastics because they can be repeatedly reheated, reshaped, and frozen [1]. Thermosets, on the other hand, are always in a permanent solid state and can only be shaped once during their synthesis [22]. Once they are heated, thermosets cannot be re-melted or reformed. Moreover, thermoplastics have low melting points, while thermosets can withstand high temperatures.

Around 85% of the polymers produced in the world are thermoplastics, mainly polyethylene (30.3%), polypropylene (19.7%), polyvinyl chloride (9.6%), polyethylene terephthalate (8.4%), polystyrene (6.1%), and 10.7% accounting for other types of thermoplastics. Thermosets make up the remaining 15% such as polyurethane, silicone, unsaturated polyesters, vinyl esters, melamine resins, epoxy resins, urea, phenol, etc. [9].

Polyolefins such as polyethylene (PE) and polypropylene (PP) are the most abundant plastics produced worldwide, accounting for roughly half the global demand for plastics. Polyethylene and polypropylene polymers are solely comprised of carbon and hydrogen. Due to the lack of oxygen and moisture in plastic-derived fuels, they are inclined to have high calorific values, in addition to fewer acidity and corrosivity problems [7].

As a result of their dominance in plastic waste, polyethylene and polypropylene have been used as the primary raw materials in this research, alongside a more complex material, polystyrene.

2.1.Polyethylene (PE)

Polyethylene (PE), belonging to the family of polyolefins, is the simplest and most widespread polymer in the world and accounts for around 30.3% of plastic production in 2020 [9]. Polyethylene is made by the radical polymerization of ethylene monomers. As shown in **fig. 1.1**, Ziegler-Natta process and metallocene catalysts are used for the polymerization of polyethylene [23].

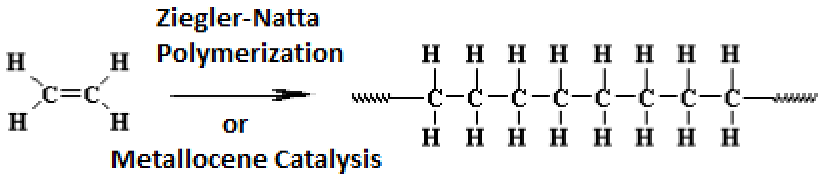

Fig. 1.1 Polymerization of ethylene monomer to form polyethylene polymer

This versatile material has a very simple structure that results from the polymerization of ethylene molecules ($CH_2 = CH_2$) and whose main chain is formed by carbon atoms, with two hydrogen atoms attached to each carbon atom [24].

Polyethylene is one of the most used and lowest-cost plastic polymers. Polyethylene is an ideal material for a variety of industrial applications due to its excellent combination of properties. They are used in a variety of applications, including packaging bottles and films, medical and healthcare, pipes, hoses and fittings, household products, consumer goods, wiring and cables, agriculture, and many others [25].

Polyethylene has a density of between 0.910 and 0.967 g/cm^3 at room temperature, resulting in a range of hardness and flexibility [26]. Their molecular weight can vary from 30,000 g.mol^{-1} to 60,000 g.mol^{-1} with a crystallinity range of 30-90%. When the temperature increases to around 135 °C, polyethylene starts to melt, and the melt density drops to 0.8 g/cm^3 [27,28]. Even though polyethylene is recyclable, its vast majority ends up in landfills. Polyethylene is extremely stable and non-biodegradable unless exposed to UV radiation from the sun, which takes centuries to degrade [29]. This polymer is resistant to most chemical products and solvents, apart from some substances that dissolve polyethylene at high temperatures. Polyethylene can only be chemically destroyed by strong oxidizing agents such as sulfuric acid or nitric acid.

Depending on the melting point, the PE is divided into several categories: low, medium, and high density, each having a specific industrial application. Polyethylene can be linear or branched and can be classified according to:

Density and Branching

The most common types of polyethylene are:

The branched versions:

- Low-density polyethylene (LDPE)

- Linear low-density polyethylene (LLDPE)

The linear version:

- High-density polyethylene (HDPE)
- Ultra-high molecular weight polyethylene (UHMWPE)

In addition, PE is found in other types such as:

- Very-low density polyethylene (VLDPE)
- Medium-density polyethylene (MDPE)

Molecular Weight

The PE can have extremely long chains with high molecular weight, and the most common types are:

- High-molecular-weight polyethylene (HMWPE)
- Ultra-low molecular weight polyethylene (ULMWPE)

Crosslinking

The polyethylene crosslinking rate reflects the presence of covalent bonds between the chains created after polymerization. The common types are:

- Crosslinked polyethylene (XLPE)
- High-density cross-linked polyethylene (HDXLPE)

The structures of the different categories of polyethylene are shown in **fig. 1.2**.

Low Density Polyethylene (LDPE)

Linear Low-Density Polyethylene (LLDPE)

Medium Density Polyethylene (MDPE)

High Density Polyethylene (HDPE)

Ultra-High Molecular Weight Polyethylene (UHMWPE)

Crosslinked Polyethylene

Fig 1.2 Structures of different categories of polyethylene

The main families of polyethylene are low-density polyethylene and high-density polyethylene:

2.1.1. High-density Polyethylene (HDPE)

HDPE is a linear structural compound with no or very little branching and a density ranging from 0.941 to 0.967 g/cm^3 [26]. HDPE is formed using a low-pressure process (10-80 bar) and temperature (70-300 °C). HDPE is mainly produced by slurry polymerization or gas phase polymerization and has the structure displayed in **fig. 1.3**:

$$-CH_2-CH_2-CH_2-CH_2-CH_2-CH_2-CH_2-$$

Fig. 1.3 Structure of high-density polyethylene

The longer the main chain, the more atoms there are, and thus the higher the molecular weight. The physical and chemical properties of the final product are determined by the molecular weight, degree of branching, and distribution of molecules.

Linear polyethylene is much stronger than branched polyethylene. Due to its high degree of crystallinity (70-90%), HDPE is opaque, rigid, and has high tensile strength [26,28]. Therefore, it is commonly used in the production of milk bottles, detergent bottles, organic solvent bottles, pipes (water pipes, chemical-resistant pipes, gas distribution pipes, etc.), kids' toys, fuel tanks for vehicles, etc. [28,30]. HDPE is the third most common type of plastic found in municipal solid waste and contributes to around 12.9% of the total plastic waste [9].

2.1.2. Low-density Polyethylene (LDPE)

Some of the carbons in polyethylene have long chains or branches of polyethylene attached to them instead of hydrogen atoms. LDPE has a higher degree of short and long side-chain branching compared to HDPE, and its structure is displayed in **fig. 1.4**.

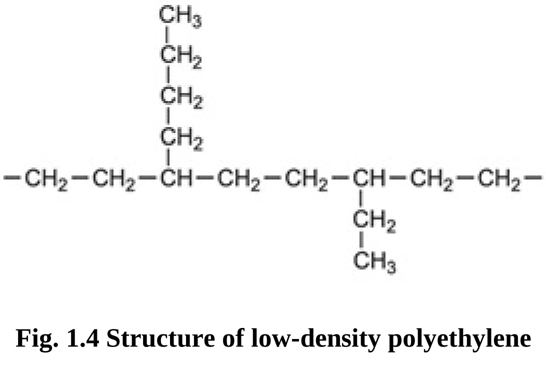

Fig. 1.4 Structure of low-density polyethylene

When compared to high-density polyethylene, branched or low-density polyethylene is less expensive, easier to manufacture, and has greater flexibility [31]. Until 1950, the only polyethylene produced was low-density polyethylene density (LDPE) via free radical polymerization at very high pressures (1000-3000 bar) and moderate temperatures (147-297 °C). Due to the transfer of intermolecular and intramolecular chains during polymerization, this high-pressure polymerization produced polyethylene with many connections [21]. LDPE has more branching and a density ranging from 0.910 to 0.925 g/cm^3, resulting in a lower intermolecular force. This reduces tensile strength, melting point, crystallinity, and hardness [32]. LDPE is made up of 4,000 to 40,000 carbon atoms with numerous short branches. Because the lateral branch makes the structure less crystalline, LDPE is easier to mold, semi-rigid, and has higher ductility than HDPE [21]. Furthermore, due to its lower crystallinity (30-50%), this type of plastic is translucent rather than opaque. [32]. LDPE has high water resistance and is used in plastic bags, packaging, garbage bags, and other products. Because these items are commonplace in our lives, they have become the second most common plastic in municipal solid waste, accounting for approximately 17.4% of total global plastic waste [9].

2.2. Polypropylene (PP)

Polypropylene, like polyethylene, is a polyolefin with a methyl group attached to one of the main chain's two carbons, with the formula $(-CH_2-CH(CH_3)-)_n$. As illustrated in **fig. 1.5**, polypropylene is synthesized by radical polymerization of propylene $[(CH_2=CH-CH_3)]$ monomers using Ziegler-Natta polymerization in the presence of metallocene catalysts [32].

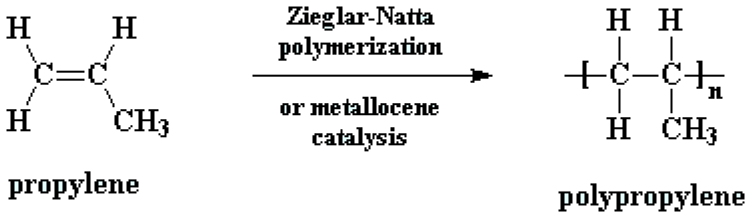

Fig. 1.5 Polymerization of propylene monomer to form polypropylene polymer

Upon polymerization, polypropylene can form three basic chain structures based on the position of the methyl group: isotactic, atactic, and syndiotactic [33].

The basic chain structures are shown in **fig. 1.6**. The most used polypropylene is isotactic (1), where all the methyl groups are on the same side of the chains. Other than isotactic, atactic (2) polypropylene is also used, where the methyl groups are randomly placed on both sides of the chain. The third structure of polypropylene is the syndiotactic (3) polypropylene, where the methyl groups are alternatingly placed on both sides of the chain.

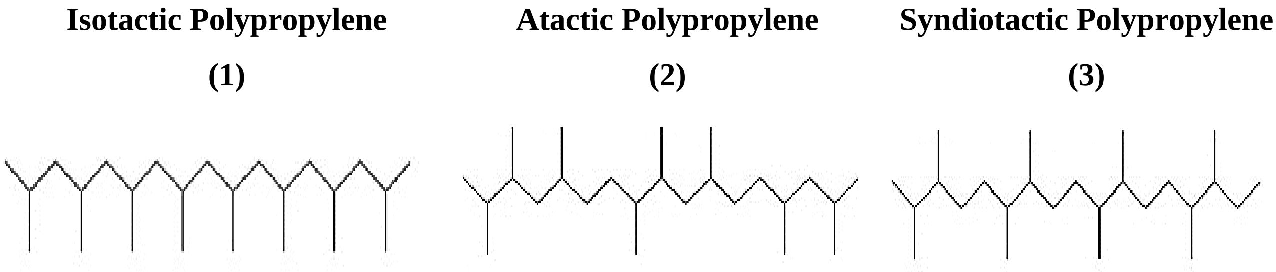

Isotactic Polypropylene (1) **Atactic Polypropylene (2)** **Syndiotactic Polypropylene (3)**

Fig. 1.6 Basic chain structures of polypropylene

Polypropylene is a saturated polymer with a linear hydrocarbon chain that has high tensile strength and can withstand temperatures above 100 °C [32]. It has a lower density than HDPE but a higher rigidity, making it a preferred material in the plastics industry. Polypropylene is one of the most affordable plastics available today, accounting for approximately 19.7% of plastic waste and accounting for the greatest proportion of material plastics found in municipal solid waste [9].

The various applications of polypropylene in our daily lives include consumer goods (food packaging, sweet and snack wrappers, etc.), the furniture market (hinged caps, microwave containers, etc.), industrial applications (pipes, etc.), the automotive industry (automotive parts), and other applications [6].

2.3.Polystyrene (PS)

Polystyrene is a long hydrocarbon chain with a phenyl group attached to one of the main chain's two carbons. As displayed in **fig. 1.7**, polystyrene is produced through free radical vinyl polymerization of the monomer styrene (C_8H_8) [34].

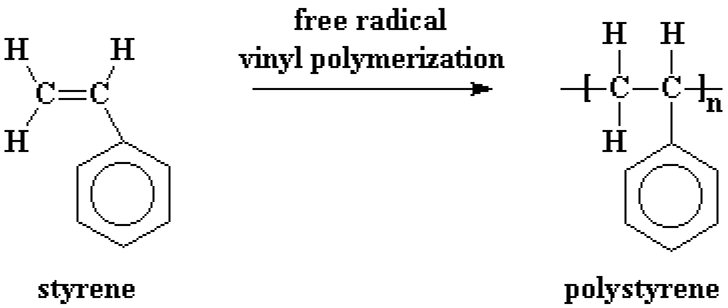

Fig. 1.7 Polymerization of styrene monomer to form polystyrene

Polystyrene is a low-cost, clear, hard, and brittle plastic with a melting point of around 240 °C. It is a transparent thermoplastic that is available as standard solid plastics as well as rigid foam materials. The solid plastic form of polystyrene is commonly used in medical device applications (test tubes, Petri dishes, etc.) and is commonly used in our daily lives in food packaging (dairy, fishery), electrical and electronic equipment, building insulation, eyeglass frames, CD cases, etc. [6]. Polystyrene plastic's wide range of applications resulted in it accounting for 6.1% of plastic production in 2020 [9].

2.4. Polyethylene Terephthalate (PET)

Polyethylene terephthalate (PET) is also one of our most used plastics. It is a thermoplastic polymer belonging to the polyester family. As shown in **fig. 1.8**, PET is synthesized from ethylene glycol and terephthalic acid [35]. PET has excellent thermal, mechanical, and chemical resistance. It is characterized by good strength, hardness, stiffness, and ductility [36]. PET is the most recyclable kind of plastic, having the number “1” as a recycling symbol. It has the molecular formula $(C_{10}H_8O_4)_n$ and a density of 1.397g/cm^3. PET is flexible, colorless, and semi-crystalline in its natural state [21].

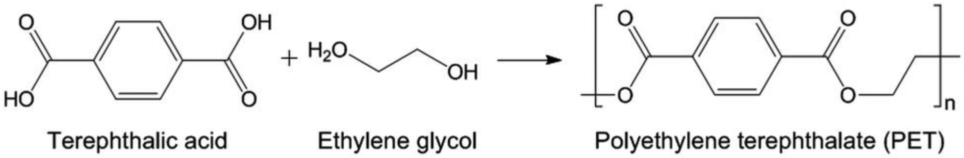

Fig. 1.8 Reaction between terephthalic acid and ethylene glycol to produce polyethylene terephthalate

Due to being excellent water and moisture barrier material, PET is widely used in food packaging, mineral water bottles, soft drink bottles, fruit juice bottles, transparent films, microwavable containers, magnetic tapes, printing sheets, cosmetic jars, and many others [37]. In 2020, PET accounts for 8.4% of plastic used worldwide [9].

2.5. Polyvinyl Chloride (PVC)

Polyvinyl chloride (PVC) is a widely used thermoplastic manufactured from 57% chlorine and 43% carbon [38]. As shown in **fig. 1.9**, PVC is produced from the polymerization of vinyl chloride monomer (VCM).

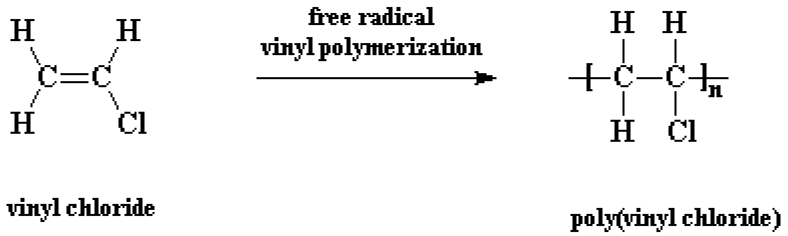

Fig. 1.9 Polymerization of vinyl chloride monomer to form polyvinyl chloride

PVC is used in pipes, medical appliances, wire cables, etc. It is characterized by its high-strength properties. Furthermore, the high chlorine content of PVC makes it fire resistant and thus ideal for electrical insulation [34]. It is the world's third most used plastic after PE and PP and accounts for 9.6% of worldwide used plastic [9].

3. Recycling methods

The number of plastics accumulating in the waste stream has increased in response to the increased demand for plastics. Increased landfilling without adequate feedstock or energy recovery has resulted in major health and environmental concerns such as increased greenhouse gas emissions, underground water contamination, increased risk of fire and explosion, human health hazards, and sanitary issues [29]. As a result, the valorization of plastic wastes has received considerable attention in the research field, with a focus on recovering energy and valuable products from these wastes.

Two major solid waste plastics are produced during the life cycle of polymers. The first type of solid waste plastic, known as post-industrial waste plastic, is formed during the polymer's manufacturing process. When a product reaches the end of its useful life, it is discarded, resulting in the second type of solid waste plastic, post-consumer waste plastic [39]. The source of waste can make a big difference in these two broad categories of solid waste plastics. Furthermore, some properties will influence how much of this waste can be recycled. The properties include whether the waste is mono-plastic (one component) or a mixed plastic (multiple components), whether it is contaminated with organic or inorganic wastes, and whether the composing polymers and their respective ratios in these wastes are known [39].

The “Plastics the Facts” study in 2021 has shown that 29.5 million tons of plastic post-consumer waste were collected in Europe in 2020. 42% is used to recover energy, and 34.6% is recycled. However, the remaining 23.4% is still disposed of in landfills [9]. As illustrated in **fig. 1.10**, recycling and energy recovery rates have increased over the past 14 years, thus reducing the amount of plastic waste disposed of in landfills.

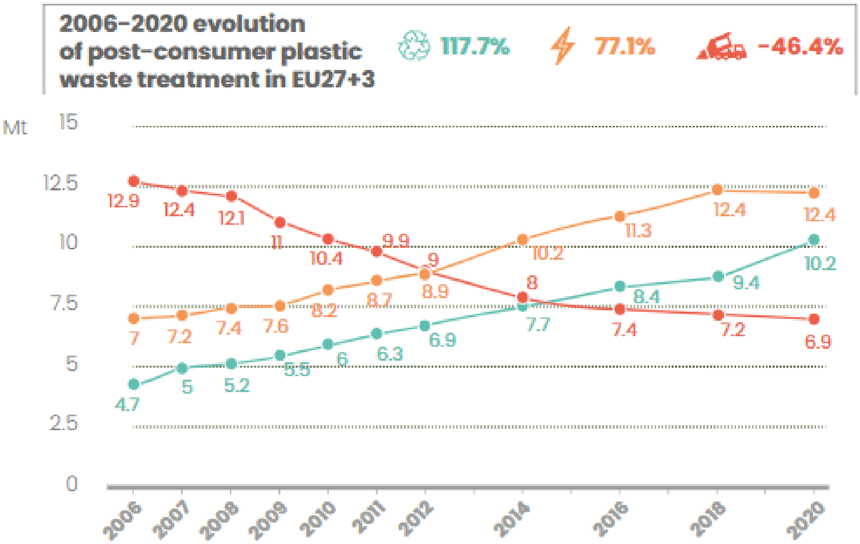

Fig. 1.10 Evolution of landfilling, recovery, and recycling of SPW in the EU [9]

Therefore, the recycling of plastics has received a lot of attention in recent decades and has grown at a rapid pace. Plastic recycling can be divided into four categories as shown in **fig. 1.11**: primary, secondary, tertiary, and quaternary recycling [40].

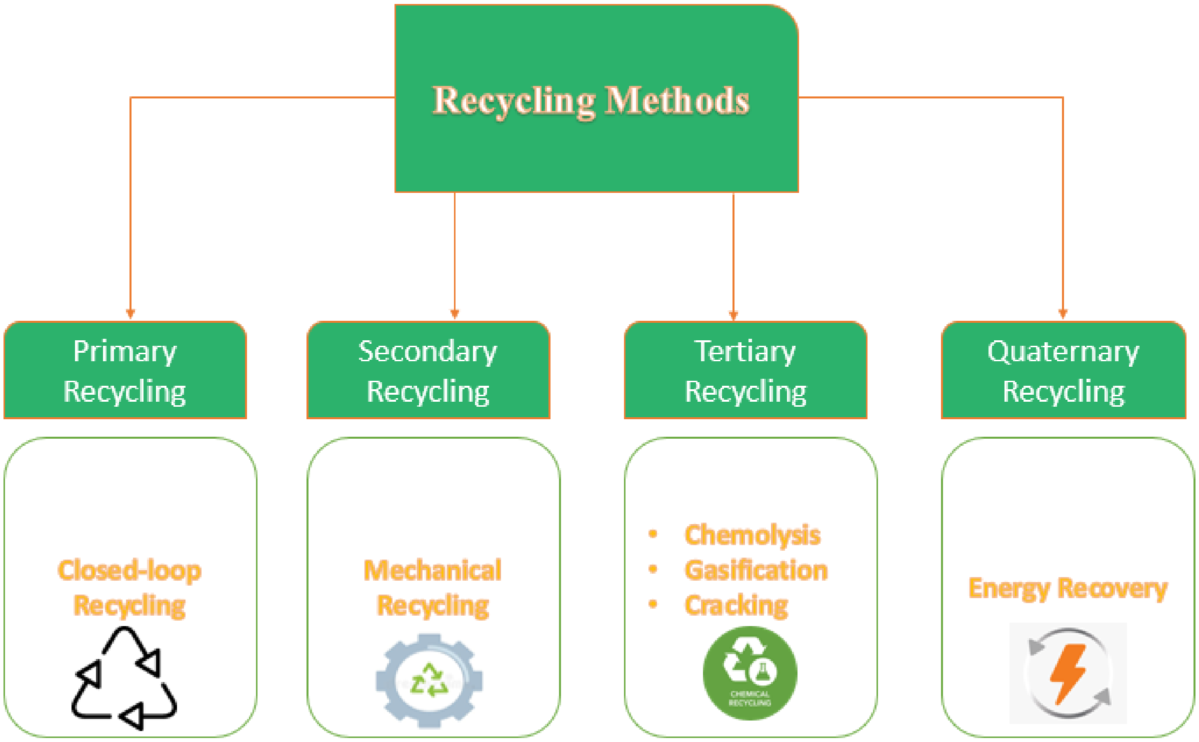

Fig. 1.11 Schematic representation of the different recycling methods

3.1. Primary recycling

Primary recycling, also known as closed-loop recycling or re-extrusion, entails the recycling of clean, uncontaminated plastics of only one type into a product with similar properties to the original [40]. Plastics from post-industrial waste are recycled first [41]. Recycled waste is typically blended with virgin material to ensure the quality of the product, or it can be utilized as second-grade material [42]. Because of its simplicity and low cost, this is the most popular recycling method. This method, however, cannot deal with accumulated plastic waste in urban areas, and it is sensitive to the age and type of plastic. Moreover, subjecting the plastic wastes to additional heating cycles will cause molecular damage, lowering the accuracy of the resulting final product. Furthermore, quantitative data on post-industrial waste plastics is obscured, as it is not publicly available and is kept within the company [39].

3.2. Secondary recycling

Secondary recycling, also known as mechanical or physical recycling, is the most common method for recycling plastics [43]. In 2020, around 10.2 million tons of plastic waste, which accounts for around 35% of this waste, were recycled in Europe by mechanical means [9].

Secondary recycling involves recycling plastic waste to create a product with different characteristics and less stringent performance requirements than the original [41]. This process entails separating the plastic from its contaminants before dividing it into generic types or melting it as a mixture without division [40]. Secondary recycling produces products that could replace other materials such as wood, metals, and concrete. It is mainly used in our daily lives in products such as benches, fences, windows, doors, desks, etc. [44]. Mechanical recycling is only possible with single-polymer plastics. This category primarily includes polyethylene (PE), polypropylene (PP), and polystyrene (PS) [43]. However, because this treatment process involves several steps such as size reduction, separation, cleaning, and drying, it is expensive to achieve the desired quality [39]. Furthermore, before being processed, the plastics should be free of contaminants, necessitating additional washing and drying steps. Hence, the more contaminated the waste plastics are, the more difficult it is to mechanically recycle them [42].

3.3. Tertiary recycling

Due to the drawbacks associated with mechanical recycling, such as processing difficulties, difficulty in maintaining high product quality, and fluctuating market prices, interest has increased in a less commonly used type of recycling: tertiary or chemical recycling [39].

Chemical recycling is a type of recycling in which plastic materials are broken down into smaller molecules using heat or chemical processes. The chemical intermediates produced, mainly liquids or gases, are used as feedstocks to produce new plastics and petrochemicals [42,43]. Chemical recycling has a high potential for mixed, contaminated plastic wastes when their separation is not feasible, neither on economic nor technical levels [39].

In this process, the polyolefins in plastic waste are converted back into their oil or hydrocarbon components, while polyesters and polyamides are converted back into monomers. The latter could be used as a raw material to produce new polymers [45]. All types of plastics could be used in this process apart from polyethylene terephthalate (PET) and polyvinyl chloride (PVC). These latter plastics, respectively release benzoic acid and hydrochloric acid, which are hazardous substances and would lead to corrosion and clogging, thus destroying the setup [46].

Chemical recycling could be divided into chemolysis (hydrolysis, alcoholysis, glycolysis), gasification, and cracking.

3.3.1. Chemolysis

Chemolysis, also known as solvolysis, is the process of depolymerizing plastics and converting them back to monomers using chemical agents as catalysts. Hydrolysis, alcoholysis, and glycolysis are examples of chemolysis processes. Hydrolysis recovers raw materials through the reaction of the water molecule at the starting materials' linkage point. Alcholysis is the chemical breakdown of a polymer using alcohol or diols as a solvent. In glycolysis, polymers are degraded in the presence of glycol. Methanolysis, which is an example of transesterification, occurs when the degradation occurs in the presence of methanol [42]. However, some polymers, such as polyolefins, which make up a large portion of municipal solid waste, cannot be easily depolymerized to their original monomer. As a result, other methods are employed to mitigate these waste polymers [47].

3.3.2. Gasification

Despite the high calorific values of plastic wastes, their direct combustion would cause significant environmental problems due to the release of toxic substances such as dioxins, SO_x, NO_x, and light hydrocarbons [42]. However, gasification (or partial oxidation) can convert any non-pre-treated feed comprising organic materials into a gaseous mixture containing carbon dioxide, synthesis gas (syngas: a mixture of hydrogen and carbon monoxide), methane, and some light hydrocarbons [48].

The gasification process is carried out at high temperatures with the aid of a gasifying agent, typically air or oxygen, and/or steam. Because the separation of air to obtain oxygen is complex and costly, the air is used instead of oxygen to simplify the gasification process and reduce operating costs [43]. Even though the air is the cheapest option, it has several drawbacks, including a higher gas flow rate that produces a greater amount of NO_x, which should be closely monitored [39].

The primary product of the gasification process is syngas. However, the latter contains impurities such as ammonia, NO_x, alkali metals, hydrogen sulfide, and tars [39]. As a result, special attention should be paid to the presence of these contaminants, which could be detrimental to various processes. Therefore, the purification of the produced syngas is an additional important step in the process, raising the production costs [49].

3.3.3. Cracking

Thermal cracking, also known as pyrolysis, is the thermochemical degradation of long-chained polymer molecules at high temperatures in the absence of oxygen or the presence of an inert gas [50]. This process will be thoroughly discussed in section 4 (Non-catalytic Pyrolysis).

3.4. Quaternary recycling

Quaternary recycling, also known as energy recovery, involves burning plastic waste under controlled conditions to produce energy [43]. It recovers energy from plastic waste and applies to all types of plastic [44]. Plastics have a high energy content (1 kg of plastic releases 11,000 kcal of energy) in comparison with 1 L of heating oil (10,200 kcal) or 1 kg of coal (4800 kcal). However, this recycling method is rational when the other types of recycling cannot be used due to specific restraints [40,51]. As a result, this type of recycling is avoided due to the need for advanced pollution control measures, as plastic incineration generates toxic pollutants such as furans and dioxins, which are hazardous to the environment and human health [52].

4. Non-catalytic pyrolysis

As mentioned in section 3.3.3, non-catalytic pyrolysis, also known as thermal cracking, is the thermal degradation of long-chain polymers into smaller molecules under elevated temperatures and in the absence of oxygen [53]. This process is usually operated at temperatures between 400 °C and 800 °C to produce hydrocarbon oil, gas possessing a high calorific value, and char [42]. The proportion of these fractions differs based on the manipulation of process conditions (temperature, residence time, reactor design, fluidizing agent, and catalyst type) and the type of polymer used [54].

Pyrolysis has both environmental and financial benefits. Environmentally, pyrolysis offers an alternative to landfilling plastic waste and reduces greenhouse gases (GHG). Financially, pyrolysis generates a fuel with a high calorific value that could be readily marketed and used in internal combustion engines to supply heat and electricity [43].

According to a study done by Wongkhorsub and Chindaprasert [55], the liquid oil produced has a similar high heating value (HHV = 46.19912 MJ/kg) as diesel fuel (HHV = 45.81474 MJ/Kg). This liquid can be used without prior treatment in furnaces, boilers, turbines, and diesel engines [56,57].

Over time, various types of plastic pyrolysis, slow, fast, and flash pyrolysis, have been initiated, with process parameters being upgraded to optimize product yield [58,59].

Slow Pyrolysis

A slow heating rate and a long heating residence time characterize this type of pyrolysis. Slow pyrolysis involves heating the material to temperatures ranging from 350 °C to 500 °C at a rate of 1-10 °C/min for a vapor residence time of 5 to 30 minutes [58,59]. Slow pyrolysis not only promotes the formation of solid char but also produces low yields of liquid and gaseous products. A slow heating rate combined with a long residence time would result in secondary reactions that would increase char formation [58,60].

Fast Pyrolysis

In this type of pyrolysis, the reactor is rapidly heated at a rate of 10-200 °C/s to a temperature of 850 °C to 1250 °C, over a short residence time of 1 to 10 s [60]. The pyrolysis vapors are swept out of the reactor and condensed immediately. Fast pyrolysis is advantageous to producing liquid fuels because the oil product yield exceeds that of coal and gas [58,61]. Fast pyrolysis typically yields 60–75% liquid products, 15–25% char, and 10–20% non-condensable gaseous products [56].

Flash Pyrolysis

Flash pyrolysis can be viewed as a refined and improved version of fast pyrolysis. The heating rate in this pyrolysis is very high, around 1000 °C/s, to achieve a temperature range of 900 °C to 1200 °C in 0.1-1 s [60]. The high heating rate, combined with the high temperature and short vapor residence time, results in an increased liquid yield and reduced char formation [58].

From the literature, it is evident that the focus is on the pyrolysis of polyolefins (polyethylene and polypropylene), since the latter account for the major bulk of plastic waste and are the best candidates for producing liquid fuel. However, there are several disadvantages to the non-catalytic pyrolysis of polyolefins. To begin with, thermal degradation necessitates high temperatures. Moreover, the products of this process are distinguished by their high molecular weight (carbon chains ranging from C_5 to C_{28}), thus requiring additional processing to achieve the desired quality [62].

Different plastic types have different compositions, according to the proximate analysis of each type found in the literature. Proximate analysis is a technique for determining the chemical properties of plastics based on four factors: moisture content, fixed carbon content, volatile matter, and ash content [13]. The main elements that influence the yield of the liquid product are volatile matter and ash content. The increase in volatile matter content favors the production of liquid oil, while the increase in ash content favors the production of gas and char [63]. According to the literature [13], proximate analysis of plastics reveals that they have high volatile matter and low ash content, indicating that plastics have the potential to produce a higher yield of liquid oil from the pyrolysis process.

The following section includes the pyrolysis of various plastic types, performed by several researchers, under different process parameter conditions.

4.1. Polyethylene pyrolysis

PE is made up of a long chain of carbon atoms, each of which has two hydrogen atoms attached to it. This is referred to as high-density polyethylene (HDPE). When one of these hydrogen atoms is replaced by another PE chain, the carbon backbone branches, resulting in low-density polyethylene (LDPE). HDPE is crystalline, whereas LDPE is amorphous [64].

4.1.1. High-density Polyethylene pyrolysis

Based on the process parameters, HDPE has a tremendous potential for application in the pyrolysis process since it can give high liquid yields. Several studies on the pyrolysis of HDPE plastic under various experimental conditions have been carried out, and the product yield obtained has been investigated. Kumar et al., [42] investigated the pyrolysis of HDPE in a semi-batch reactor at temperatures ranging from 400 °C to 550 °C. They concluded that the highest liquid yield of 79.08 wt.% and the gaseous product of 24.75 wt.% were obtained at 550 °C. Ahmad et al., [52] investigated the pyrolysis of HDPE in a micro steel reactor at temperatures ranging from 300 °C to 400 °C and a heating rate of 5-100 °C /min under nitrogen flow. They concluded that the highest conversion occurred at 350 °C, with a liquid yield of 80.88 wt.%. Moreover, the solid residue decreased from 33.05 wt.% to 0.54 wt.% as the temperature increased from 300 °C to 400 °C. Al Salem et al., [65] investigated the pyrolysis of HDPE in a fixed bed reactor at temperatures ranging from 500 °C to 800 °C and under a flow of nitrogen. The maximum oil product yield of 70 wt.% was obtained at 550 °C, and the gaseous products increased with increasing temperatures due to the high activity of the C-C chain scission reaction.

4.1.2. Low-density Polyethylene pyrolysis

In comparison to HDPE, LDPE is a branched-chain polymer with weak intermolecular forces, resulting in lower strength and hardness. Because of the branching, LDPE is less crystalline, making it more ductile and easier to mold. The pyrolysis of LDPE to produce oil has piqued the interest of researchers in the fields of energy recovery and waste reduction. Kassargy et al., [66] investigated the pyrolysis of LDPE in a batch reactor at 450 °C, with and without a catalyst. They concluded that in the absence of a catalyst, 80 wt.% of wax was obtained, while the presence of the catalyst allowed the conversion of the polymer into 71 wt.% of liquid fuel with a mixture of C_5-C_{39} compounds. Zhao et al., [67] studied the pyrolysis of LDPE in a fluidized bed reactor at temperatures ranging from 500 °C to 600 °C and residence times ranging from 12.4 s to 20.4 s. They realized that as the temperature increased, the gas yield increased from 8.2 wt.% to 56.8 wt.% while the liquid yield decreased from 81.2 wt.% to 28.5 wt.% when the temperature increased from 500 °C to 600 °C. Chen et al., [68] investigated the pyrolysis of LDPE in a fixed bed quartz tube reactor at temperatures ranging from 300 °C to 600 °C and residence times ranging from 17.7 s to 53 s. They discovered that a high volatilization temperature promotes the cracking of volatiles, resulting in a decrease in carbon chain length and, as a result, in oil yield. Furthermore, for temperatures above 400 °C, the formation of light oil increases as the residence time increases. On the other hand, longer chains form with increased residence time at a temperature of 300 °C.

4.2. Polypropylene pyrolysis

Polypropylene's demand, because of its numerous applications, is increasing, as are polypropylene plastic wastes. As a result, pyrolysis of PP is one way to recover energy from this plastic. Several researchers studied the pyrolysis of polypropylene under several conditions. Sakata et al., [69] studied the pyrolysis of polypropylene at 380 °C in a batch reactor. They obtained a liquid yield of 80.1 wt.%, a gas yield of 6.6 wt.%, and a solid yield of 13.3 wt.%. On the other hand, Demirbas et al., [70] used a batch reactor to investigate the pyrolysis of PP at 740 °C. They obtained a liquid yield of 48.8 wt.%, a gas yield of 49.6 wt.%, and a solid yield of 1.6 wt.%. By comparing these two studies, it is noted that as temperature increases, the liquid yield decreases while the gas yield increases. Jung et al., [71] investigated the pyrolysis of PP in a fluidized bed reactor at temperatures ranging from 660 °C to 750 °C. The feed rate and fluidizing medium were investigated as well. They concluded that increasing the reaction temperature increased gas production (65.9 wt.%) but decreased oil production (from 43.1 wt.% to 29.6 wt.%). Furthermore, a higher feed rate and the use of nitrogen as the fluidizing medium were recommended for improved oil production. Fakhrhoseini et al., [72] studied the pyrolysis of PP at 500 °C using a pyrolysis quartz reactor. The liquid yield obtained was 82.12 wt.%, showing that the results were in accordance with Demirbas et al., where the increase in temperature reduced liquid yield while increasing the gaseous products. Ahmad et al., [52] investigated the pyrolysis of PP using a micro-steel reactor at temperatures ranging from 250 °C to 400 °C. The highest liquid yield was 69.82 wt.% at 300 °C while increasing the temperature led to a decrease in the liquid yield and an increase in the solid yield, proving that coke forms at high temperatures. Honus et al., [73] studied the pyrolysis of PP using a vertical dual-chamber reactor at three different temperatures: 500 °C, 700 °C, and 900 °C, and under helium flow. They concluded that at 900 °C, the highest conversion of PP to gaseous products occurred, with a gas product yield of 66.88 wt.%. It is concluded that at elevated temperatures more gaseous products are produced from the pyrolysis of PP due to the conversion of the heavier components via secondary cracking reactions.

4.3. Polystyrene pyrolysis

Some researchers studied the pyrolysis of polystyrene. Miandad et al., [74] compared the pyrolysis of different types of plastics at 450 °C with a retention time of 75 min using a pyrolysis reactor. In comparison to other types of plastics, PS produced the most liquid oil (80.8 wt.%) and the least gases (13 wt.%). Amjad et al., [75] studied the pyrolysis of PS using a semi-batch pyrolysis reactor at temperatures ranging from 290 °C to 480 °C under a flow of nitrogen. They observed the highest liquid oil yield of 88 wt.% at 350 °C.

4.4. Polyethylene Terephthalate pyrolysis

PET’s widespread use has resulted in an increase in waste accumulation in landfills. Furthermore, the transportation costs of waste collection have increased due to the bulkiness of the containers and their frequent collection. As a result, sorting and size reduction are required to increase the efficiency of PET recycling, which makes the process uneconomical and time-consuming [13]. As a result, alternative methods for the recovery of PET have been investigated, with several researchers studying the product yield from the pyrolysis of this plastic waste. FakhrHoseini et al., [72] investigated the pyrolysis of PET in a fixed bed reactor at 500 °C with a heating rate of 10 °C /min, under a flow of nitrogen. They discovered a liquid yield of 38.9 wt.% and a gas yield of 52.1 wt.%. This is because PET has a low volatile matter content when compared to other plastic types.

Cepeliogullar et al., [76] applied the same conditions as FakhrHoseini for the PET pyrolysis. They noted that the liquid yield produced (21.3 wt.%) was less than the gas produced (76.9 wt.%), with no traces of solid residue. Compared to the previous study, they concluded that the liquid product yield is in the range of 23-40 wt.% and the gas product yield is in the range of 52-77 wt.%. Furthermore, they tested the oil produced by GC-MS and discovered that benzoic acid made up a large portion of the oil composition (49.93%). The oil's acidity was unfavorable due to its corrosiveness, which could cause serious industrial damage. Diaz-Silvarrey et al., [77] investigated the pyrolysis of PET at temperatures ranging from 450 °C to 600 °C using a quartz reactor with a quartz combustion boat. They discovered that when PET is heated above 395 °C, it decomposes into vinyl ester and benzoic acid via random scission. The rate of PET decomposition and product distribution is affected by temperature, the volatiles' residence time, and the amount and type of catalyst used. If the gaseous product is preferred, PET may be the best plastic to use. However, special attention is required due to the production of benzoic acid, which increases the cost of the process and, if not managed properly, can have serious consequences.

4.5. Polyvinyl Chloride pyrolysis

Despite its wide range of applications, pyrolysis of PVC has received little attention due to the presence of chlorine, which causes the release of hazardous chemicals when heated at high temperatures. Miranda et al., 1999 [78] investigated the pyrolysis of PVC in a batch reactor at temperatures ranging from 225 °C to 520 °C, a heating rate of 10 °C /min, and a total pressure of 2 kPa. The percentage of liquid oil produced increased from 0.45 wt.% to 12.79 wt.% as the temperature increased from 225 °C to 520 °C. However, the main product obtained with the highest yield of 58.2 wt.% was hydrochloric acid (HCl). When heated, HCl becomes corrosive and toxic, causing irreversible damage to the experimental equipment. Honus et al., 2018 [73] investigated the pyrolysis of PVC using a vertical dual-chamber reactor at three different temperatures: 500 °C, 700 °C, and 900 °C under helium flow, in comparison to PP, PE, and PS. The HCl produced was collected using a trap containing 0.1 M NaOH. They concluded that PVC produced 6.27 times more gas than other samples. However, pyrolysis of PVC is not preferred because it produces a small amount of liquid oil and the accumulation of PVC in plastic waste is lower than that of any other plastic type. Furthermore, HCl is released during PVC pyrolysis, and chlorinated compounds are present in the pyrolysis oil, both of which are extremely harmful to the environment. As a result, for PVC pyrolysis to be effective, a dichlorination step is required, which could be accomplished through stepwise pyrolysis, catalytic pyrolysis, or pyrolysis with adsorbents added to the plastic [79]. Therefore, the pyrolysis of PVC necessitates supplementary steps and thus additional costs, which is a significant disadvantage on a large scale.

It is concluded that the pyrolysis temperature influences the product compositions. In the pyrolysis of polyolefins (polyethylene and polypropylene), the increase in temperature (>500 °C) resulted in an increase in the production of gaseous products while the liquid products decreased. On the other hand, the pyrolysis of polystyrene plastic resulted in a high yield of liquid products mainly at 350 °C. Even though the pyrolysis of polyethylene terephthalate and polyvinyl chloride results in high yields of gaseous products, the pyrolysis of these two polymers is avoided due the production of benzoic acid (from PET) and hydrochloric acid (from PVC) which are destructive to the setup. The pyrolysis temperature of the plastic used in this study will be determined in Chapter 2 using a specific characterization technique.

5. Pyrolysis kinetics and mechanism

5.1. Kinetic degradation based on thermal gravimetric analysis (TGA)

Thermal degradation of polymers has sparked considerable interest as an alternative chemical raw material or source of energy, as well as a potential solution to environmental problems [80]. Knowing the thermal degradation kinetics of plastics could help to improve their thermal behavior. Thermogravimetric analysis (TGA) is a powerful tool for investigating the kinetics of thermal degradation [81]. This method offers information on the activation energy and kinetic model. As a result, understanding the kinetics of the pyrolysis degradation reaction is critical in determining the parameters that govern the reaction occurring in the pyrolysis reactor. TGA is the most used technique for this type of work.

In general, the rate of conversion in polymer degradation is proportional to the amount of reacted material. The kinetic models are based on an analysis of the mass loss curve obtained during the sample's TGA. The mass loss is determined as a function of temperature [21].

The kinetic study can be used to calculate the activation energy (E) and the pre-exponential factor (A). According to the literature [82], apart from PVC, plastics degrade in a first-order reaction. Several studies have reported the activation energy (Ea) of the pyrolysis of PE and PP. The activation energy values obtained for HDPE varies between 238-247 kJ/mol, 215-221 kJ/mol for LDPE, and 179-188 kJ/mol for PP [81,83].

5.2. Mechanism of thermal degradation

Thermal cracking of plastics occurs through a radical mechanism in which initiating radicals form in the presence of heat. Due to the presence of inconsistent weak links in the polymer, the macromolecules of the polymer tend to be unstable when heated. This is the reason why lower molecular weight chain models are more stable than the polymer itself [42].

The thermal decomposition of polymers initially proceeds by two distinct cracking reactions: random scission and chain-end scission.

5.2.1. Random scission:

Random scission involves the formation of a free radical at some point on the polymer backbone, which causes the macromolecule to fragment into molecules of different chain lengths. Polyolefins such as polyethylene and polypropylene generally degrade by random scission [84]. When a free radical is formed along the chain of polyethylene or polypropylene, chain scission takes place, producing a molecule with an unsaturated end and another with a free radical. This free radical can take hydrogen from a neighboring carbon, producing a saturated end and a new radical, or combine with another free radical to form an alkane. The scission produces molecules small enough to be volatile with a lower molecular weight. Since the scission is random, molecules with different chain lengths are produced.

5.2.2. Chain end scission:

The polymer can separate into end groups when heated above its decomposition temperature. This type of degradation pathway is also known as a depolymerization reaction because it involves the sequential release of monomer units from the end of the chain. Because molecules move more violently at higher temperatures, the shorter end chains will split off from the main chain. This explains why increasing the reaction temperature increases the yield of products with shorter hydrocarbon chains.

Plastics degrade by breaking the bonds between the individual atoms that make up the polymer chain [84]. C-C bonds have a bond dissociation energy of 347 kJ/mol, while C-H bonds have a bond dissociation energy of 413 kJ/mol [42]. As a result, the cracking of the C-C bond requires less energy than the cracking of the C-H bond. Therefore, the C-C bond dissociation, which is the weaker of the two, is the more likely initiation step [84]. Hence, the polymers could be cracked at the C-C bond at low temperatures and both the C-C and C-H bonds at high temperatures, with random scission serving as the first step in thermal degradation.

Thermal degradation involves the following elemental reactions: initiation, propagation, and termination [85]. Polyethylene and polypropylene are decomposed by random chain scission, where the same reaction steps are attributed to the pyrolysis of these two polymers.

Initiation

During the first step, large polymer molecules are broken down into free radicals and smaller molecules. Initiation reactions take place through random scission of the polymer chain into primary radicals.

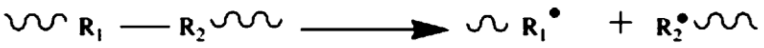

Propagation

During the propagation step, the free radicals and species formed during initiation are further broken down into smaller radicals and molecules. Propagation is the scission of free radicals produced by initiation reactions, which during the pyrolysis process serve as intermediate reactions. The main propagation reaction is β-scission, which also comprises random scission reactions, mid-chain scission reactions, and end-of-chain scission reactions. The propagation reactions primarily produce alkene molecules and smaller free radicals by cracking the large free radicals produced by the reaction initiation.

Hydrogen chain transfer is the transfer of protons to other sites, resulting in a decrease in the molecular weight of the polymer. These reactions include inter/intramolecular transfer reactions.

The intermolecular transfer reaction involves the extraction of a hydrogen atom from a neighboring molecule, resulting in the formation of a stable saturated alkane and a radical secondary in the middle of the neighboring molecule. From the corresponding radicals, saturated hydrocarbon molecules are formed.

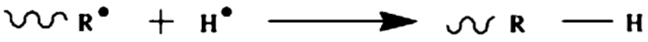

Intramolecular transfer reactions, on the other hand, move the proton of free hydrogen from one end of a free radical to the other. This reaction promotes the formation of isomers during the pyrolysis process.

Termination

During the termination reaction, the unstable produced radicals eventually combine to form stable molecules. The termination reaction occurs because of free radical disproportionation or due to the combination of two free radicals. This reaction has a direct impact on the length of the product chain.

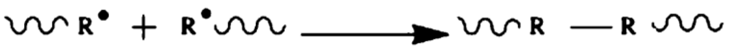

According to the above reactions in the pyrolysis of plastics, β-scission reactions produce alkenes and dienes (double bonds), whereas intermolecular transfer reactions produce alkanes [86].

6. Pyrolysis process parameters

In the pyrolysis of plastic wastes, process parameters have a significant impact on the yield and composition of the pyrolysis products. The process parameters may have an impact on the final product, whether it is liquid oil, a gaseous product, or solid char. The main process parameters include temperature, pressure, residence time, type of reactor, catalysts, fluidizing agents, and flow rate [13]. The requested product could be attained by controlling the already mentioned parameters.

6.1. Temperature

Temperature is one of the most important parameters governing the pyrolysis process because it regulates the cracking reaction of the polymer chain. The increased vibration of the molecules causes the Van der Waals forces that attract the molecules together to evaporate and collapse, causing the breakage of the carbon chain [29]. Moreover, as concluded in section 4, temperature has a significant role in influencing the pyrolysis product and side reactions. At low temperatures, long-chain hydrocarbons are produced, while as the temperature elevates, short-chain hydrocarbons are produced due to the cracking of the C-C bonds [87].

Temperature has a significant impact on the reaction rate, which influences the composition of the final product, whether liquid, gas, or solid. As a result, the operating temperature is primarily determined by the desired product. If a liquid product is preferred, temperatures in the range of 300 °C to 500 °C are suggested. However, if gas or char products are preferred, higher temperatures above 500 °C are recommended [13]. This condition is applied to all types of plastics.

6.2. Pressure and residence time

According to the literature [88], pressure influences the carbon number distribution in liquid products, with high pressure causing lower molecular weight chains to be formed. Moreover, pressure influences the rate of double bond formation, with increased pressure affecting the scission rate of the C-C links and thus decreasing the rate of double bond formation. Furthermore, pressure affects the residence time at low temperatures. However, as the temperature rises, the effect of pressure on residence time diminishes [13,29].

The average length of time a particle spends in a reactor, which may affect the product distribution, is referred to as residence time [89]. The residence time in fast or continuous pyrolysis represents the time the plastic encounters the heated reactor. In slow or batch pyrolysis, the residence time refers to the time from the start of the heating of the plastic to the end of the reaction [13]. A longer residence time increases polymer conversion due to secondary cracking reactions, resulting in more thermally stable products such as light molecular weight hydrocarbons and non-condensable gaseous products [29].

Pressure and residence time are temperature-dependent factors that influence product distribution at low temperatures. As the pressure rises, the yield of gaseous products rises as well, as does the molecular weight of the resulting liquid product [29]. However, most studies carry out their pyrolysis processes at atmospheric pressure because the effect of pressure at high temperatures is less noticeable. Considering pressure as a factor in the processes will also necessitate additional operational costs from an economic standpoint. As a result, pressure and residence time should only be considered when working at temperatures below 450 °C [13].

6.3. Reactor type

There are various types of reactors used in the pyrolysis process. The type of reactors used has a significant impact on the mixing of plastics and catalysts, heat transfer, residence time, and reaction efficiency to achieve the desired products [13].

Most of the lab-scale pyrolysis processes were performed using batch reactors (batch and semi-batch) or continuous flow reactors (fluidized bed, fixed bed, and conical spouted bed reactors), in addition to microwave-assisted technology.

6.3.1. Batch and semi-batch reactors

A batch reactor (**fig. 1.12**) is a closed system, where reactants and products cannot flow in or out while the reaction is taking place. In the batch reactor, high conversion of reactants can be achieved by extending the residence time. A semi-batch reactor, on the other hand, allows the addition of reactants and removal of products at the same time, even when the reaction starts. However, while using a batch or semi-batch reactor, the products vary from one batch to another. Moreover, there are high labor costs per batch, and it is difficult to implement on a large industrial scale [13].

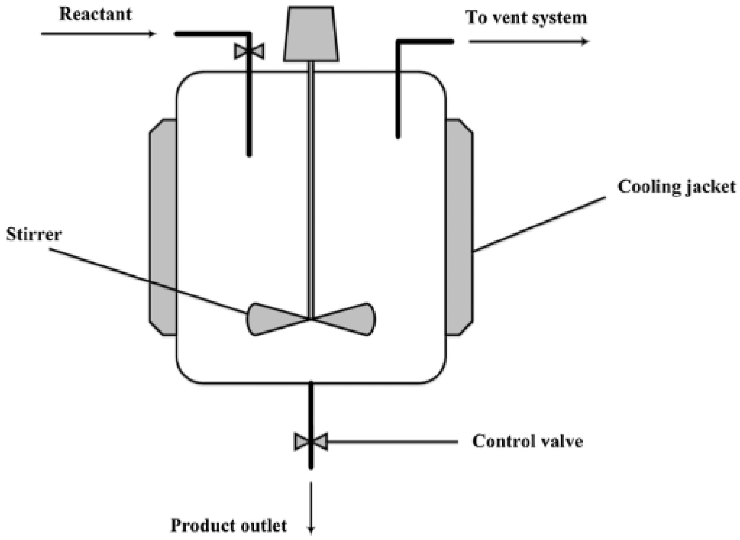

Fig. 1.12 Schematic representation of batch reactor [13]

Batch and semi-batch reactors are preferred for laboratory-scale use by researchers due to their simple design and the ability to control the process parameters when initiating the reaction [90]. Normally, pyrolysis of plastics in batch reactors takes place at temperatures ranging from 300 °C to 800 °C. Furthermore, some researchers used batch reactors in catalytic pyrolysis to increase the hydrocarbon yield by mixing the plastics with catalysts. However, this method of catalytic pyrolysis is prone to coke formation, which can deactivate the catalyst and result in a high residue at the end of the process [13].

As a result, batch reactors are ideal for laboratory-scale thermal pyrolysis due to their ability to achieve high liquid yields and the ease with which the parameters can be controlled. However, due to the high operating costs and coke generation, which lowers catalyst efficiency, these types of reactors are not advised for catalytic pyrolysis or large-scale applications.

6.3.2. Continuous flow reactor

Fixed and Fluidized Bed Reactors

The pelletized catalyst is packed in a static bed in a fixed bed reactor (**fig. 1.13**). This reactor is simple to construct. However, the irregular shape and size of the plastic feedstock may pose a challenge during the reactant feeding process [29]. In the pyrolysis process, the fixed bed reactor was used in a variety of studies. Some researchers used this type of reactor for secondary pyrolysis because the products of primary pyrolysis (mostly liquid and gas) could be easily fed into it [91].

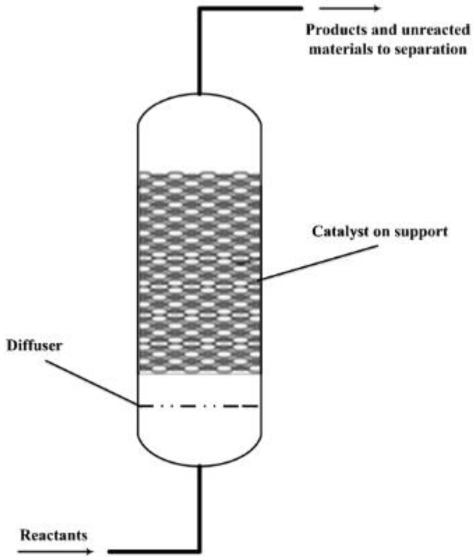

Fig. 1.13 Schematic representation of a fixed bed reactor [13]

Although the two-step process eliminates some of the problems associated with batch reactors, such as the difficulty of catalyst recovery and rapid deactivation, this design is rarely used on a large scale because it is not cost-effective, and the outcomes are comparable to those of a one-step process [13].

The catalyst in a fluidized bed reactor (**fig. 1.14**) is placed on a distributor plate, through which the fluidizing gas passes, carrying the particles in a fluid state [92]. As a result, because the catalyst is well mixed with the fluidizing agent, there is a larger surface area for the reaction to occur and thus better access to the catalyst [29]. Fluidized bed reactors are ideal for fast pyrolysis due to their high heating rate [89].

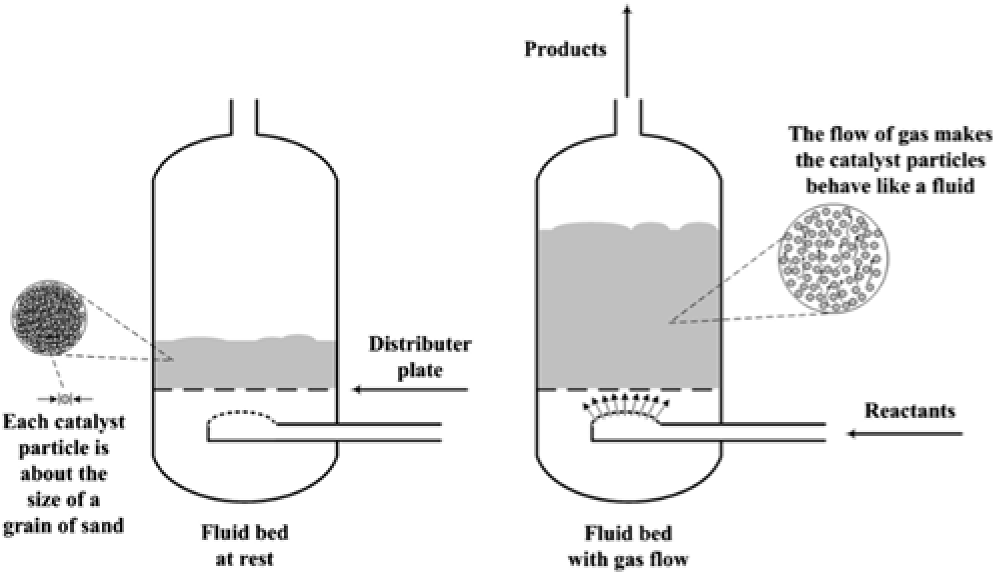

Fig. 1.14 Schematic representation of the fluidized bed reactor [13]

As a result, the fluidized bed reactor is ideal for catalytic pyrolysis, especially since the catalyst can be reused multiple times. Because of its low operating costs, this reactor is also suitable for large-scale processes [13].

Conical Spouted Bed Reactor (CSBR)

When using a conical spouted bed reactor (**fig. 1.15**), different sizes and densities of particles could be used [91]. When treating sticky solids, this type of reactor has good heat transfer between phases and avoids the de-fluidization problem [29]. The CSBR, on the other hand, has a complicated design in which numerous pumps are introduced into the system, posing numerous challenges in terms of catalyst feeding, transport, and product collection. Because of these obstacles, the use of CSBR is both costly and unfavorable [13].

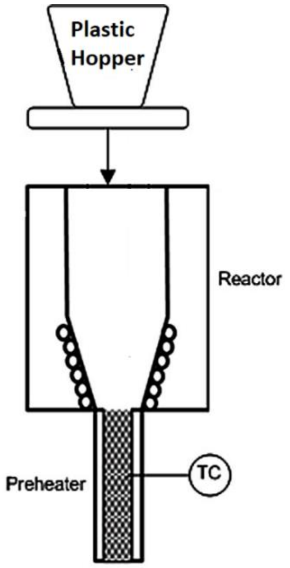

Fig. 1.15 Schematic representation of the conical spouted bed reactor [13]

6.3.3. Microwave-assisted technology

Several alternative reactor designs for the pyrolysis of plastic wastes have been developed over the years to improve heat transfer to the polymer and facilitate the handling of plastics. Microwave-assisted technology is gaining popularity as a new method for the pyrolysis of plastic waste. In this process, a high microwave absorbent (such as carbon) is combined with the polymer and absorbs microwave energy to reach the required pyrolysis temperature [13]. Microwave-assisted technology allows for rapid and selective heating, making the process easier to control and thus increasing production speed while decreasing costs [93]. However, this process is difficult to implement on an industrial scale due to a lack of data to quantify the dielectric properties of the treated wastes, which is used to calculate heating efficiency [13].

6.4. Fluidizing agent and flow rate

The fluidizing agent, also known as the carrier gas, is a gas that transports the produced vapors without participating in the pyrolysis process. Several fluidizing agents, including hydrogen, helium, nitrogen, argon, ethylene, and propylene, could be used in pyrolysis. Each fluidizing agent has a unique reactivity based on its molecular weight [13]. The fluidizing agent’s molecular weight aids in the determination of the product composition. The lighter gas can generate more condensable liquid oil products. This illustrates the significance of the carrier gas in increasing product yield during the pyrolysis process [94].

Most researchers use nitrogen as a fluidizing agent in the pyrolysis of plastics because it is safer and easier to handle than other highly reactive and flammable gases such as hydrogen and ethylene. Helium, on the other hand, has high liquid yields but is less common and more expensive than nitrogen [13]. Argon is both safe and easy to handle, and it is not as expensive as other fluidizing agents.

Aside from the fluidizing gas agent, the flow rate can affect product distribution. When the flow rate is low, the contact time of the primary products is long, resulting in the formation of more coke and secondary products [92]. Increasing the flow rate is thus preferable.

7. Dry reforming

Dry reforming (DR) is the catalytic conversion of hydrocarbon feedstock using CO_2 to synthesis gas, a mixture of hydrogen and carbon monoxide. Because DR processes are highly endothermic, a high operating temperature (700 °C to 1000 °C) is required to achieve the desired conversion levels. Ni-based catalysts supported on metal oxides, zeolites, perovskites, and carbides are commonly used for DR processes because they are competitive with noble metals in catalytic activity and cost-effectiveness [95]. However, catalytic deactivation resulting from either coke deposition, or the sintering of nickel catalysts is one of the challenges that accompany the dry reforming process [96]. In order to address this issue, numerous research have been carried out, including testing for various combinations of active metals, promoters, and supports, where the interactions between these components are among the most crucial aspects determining the activity of the nickel catalysts [97]. The proper ratio of specific components, as well as the basicity of the support, results in high dispersion, particle size preservation, and delayed coke formation [95].

Methane is the most well-known feedstock for dry reforming research, where the dry reforming reaction allows for the conversion of two of the most copious greenhouse gases, CO_2 and CH_4, instantaneously [98]. However, there has recently been increased interest in the dry reforming process with alternative feedstocks such as biogas, toluene, ethanol, and glycerol [99].

In recent years, there has been a surge of interest in the use of plastic waste as a hydrocarbon source for DR. Plastic waste contains a high concentration of CH–CH molecular chains, making it a potential hydrocarbon feedstock for dry reforming [2,100]. Furthermore, dry reforming of plastic waste is a promising solution to the waste treatment problem. In this context, dry reforming combines environmentally friendly methods for managing both waste plastics and carbon dioxide.

As a result, dry reforming of plastics is the focus of extensive research in the areas of carbon dioxide capture and disposal/storage processes [95].

7.1. CO_2 emissions and utilization

Carbon dioxide is the most common greenhouse gas, accounting for approximately 76% of total greenhouse gas emissions. 90 % of carbon dioxide is produced by the combustion of fossil fuels, specifically coal, oil, and natural gas. Electricity is generated by coal and natural gas power plants. Most of the energy for transportation comes from oil-based products such as gasoline, aviation fuel, and diesel fuel. Also, industrial processes require the use of fossil fuels to generate the necessary power and heat [101]. In 1958, Charles Keeling, an atmospheric scientist, initiated measuring CO_2 levels in the atmosphere. Since then, the concentration of CO_2 in the atmosphere has been steadily increasing [101]. As shown in **fig. 1.16**, the total CO_2 emissions from energy combustion and industrial processes have increased since the 1900s. The COVID-19 pandemic had a significant impact on energy demand in 2020, lowering global CO_2 emissions by 5.1%. However, since then, the global economy has recovered at an alarmingly rapid pace. According to the study conducted by the International Energy Agency (IEA) [102], a 6% increase from 2020 drove the CO_2 emissions to 36.3 gigatonnes (Gt), making 2021 the year with the greatest year-on-year increase in energy-related CO_2 emissions.

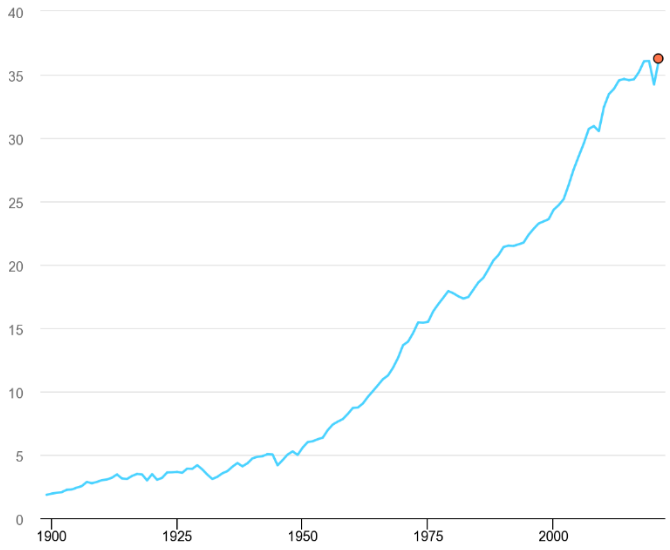

Fig. 1.16 Total CO_2 emissions from energy combustion and industrial processes and their annual change from 1900 till 2021 [102]

In recent years, the rise of human activities, as well as the diminution of the world's natural reserves, has prompted extensive research for alternative energy sources. Moreover, due to the severe environmental consequences of climate change, considerable effort has recently been expended to reduce carbon dioxide emissions in the atmosphere [96].

One strategy for reducing these significant emissions is carbon capture and storage (CCS), which produces a large amount of CO_2 [103]. CCS processes are gaining traction in the scientific community as a means of reducing CO_2 emissions and lowering their concentration in the atmosphere while preserving the primary energy source. It entails capturing CO_2 at the source, compressing it to a supercritical fluid, and then sequestering it [104]. The recent progress in carbon capture and sequestration as a key component in the global effort to reduce emissions is providing significant quantities of CO_2 as a renewable feedstock for conversions to commodity chemicals, fuels, and polymeric materials at a reasonable cost. Several conversion processes have been implemented, such as artificial photoreduction, electrochemical reduction, hydrogenation, synthesis of organic carbonates, photocatalytic reduction of carbon dioxide with water, biological fixation, and reforming [105]. Carbon dioxide is a low-cost, recyclable, and non-toxic carbon source, so using it in reforming hydrocarbons would benefit both the economy and the environment [106]. Dry reforming is one such process in which carbon dioxide is used instead of steam or air to catalyze the reforming of high molecular weight hydrocarbons to produce synthesis gas [16,106].

Synthesis gas (syngas) is a combination of hydrogen and carbon monoxide that can be utilized to synthesize many chemical intermediates having higher values than methane [99]. Synthesis gas is produced through the thermochemical conversion of various wastes and is regarded as an energy vector for a sustainable energy future [107]. It has the potential to be used as a raw material in a variety of reactions, and its potential end-use is influenced by the H_2:CO ratio [108]. When the H_2:CO ratio is close to 1, syngas can be used to produce ethanol, methanol, ammonia, acetic acid, aldehydes, and synthetic fuels via Fischer-Tropsch synthesis [109]. As a result, syngas could be considered a viable alternative to fossil fuels. The chemical industry typically uses feedstocks that are the most cost-effective to obtain or produce. **Fig. 1.17** shows that syngas is most used in the chemical industry [110].

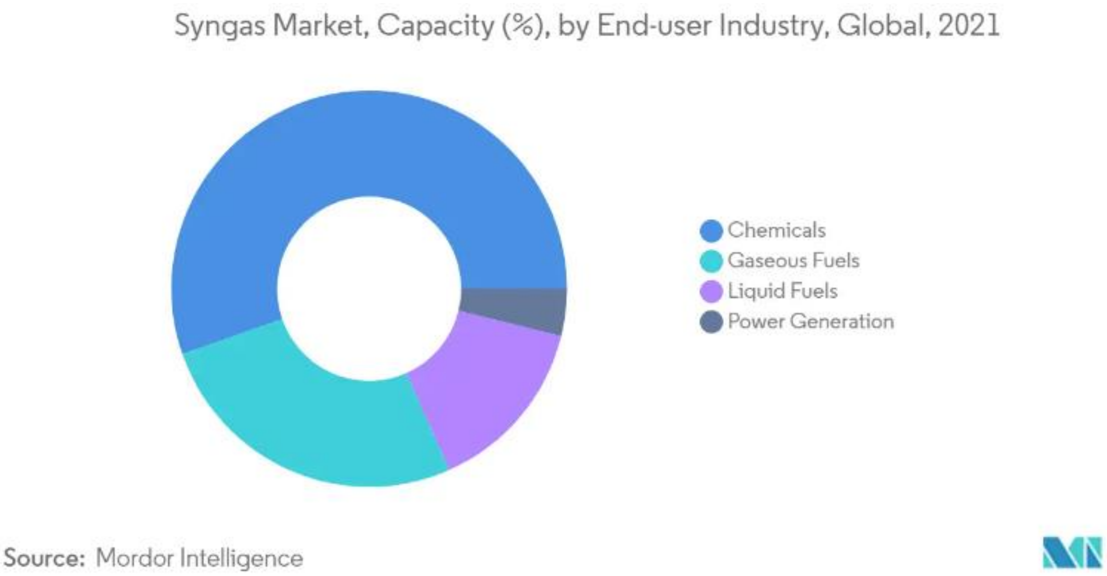

Fig. 1.17 Global applications of synthesis gas, 2021 [110]

7.2. Pyrolysis catalytic dry reforming of plastics

The pyrolysis catalytic dry reforming (PCDR) process combines the pyrolysis of hydrocarbon sources, such as plastic waste, with in-line dry reforming of the produced pyrolyzed gases, in the presence of a catalyst, to generate liquid chemicals and valuable synthesis gas.

For PCDR processes, three main reactor systems have already been proposed and tested in the laboratory. The most common are two-stage reactor systems [8,111–114] (**fig. 1.18** a and b): **Fig. 1.18** (a) is made up of a single tubular reactor divided into two stages, while **fig. 1.18** (b) is made up of two stages each containing a separate tubular reactor. In both systems, each stage is heated by a separate heating unit. The pyrolysis process takes place in the first stage, while the catalytic dry reforming process takes place in the second stage. An inert atmosphere is created by feeding an inert gas, such as nitrogen or argon, into the first stage reactor, while a stream of carbon dioxide is fed into the second stage reactor. On the other hand, **fig. 18** (c) depicts a less common reactor system for PCDR, where only one reactor and one heating unit are used [113,115]. The hydrocarbon source is pyrolyzed in the presence of carbon dioxide, resulting in partial gasification. The mixture of pyrolysis gases, inert gases, and carbon dioxide is then transferred directly into the catalyst bed, where the dry reforming reaction occurs. Fixed bed reactors are the most used type of reactor in laboratory-scale PCDR processes and large-scale chemical synthesis. It consists of a tube filled with a plastic feedstock and a gaseous stream that flows through the bed and converts the plastic into pyrolytic products [95].

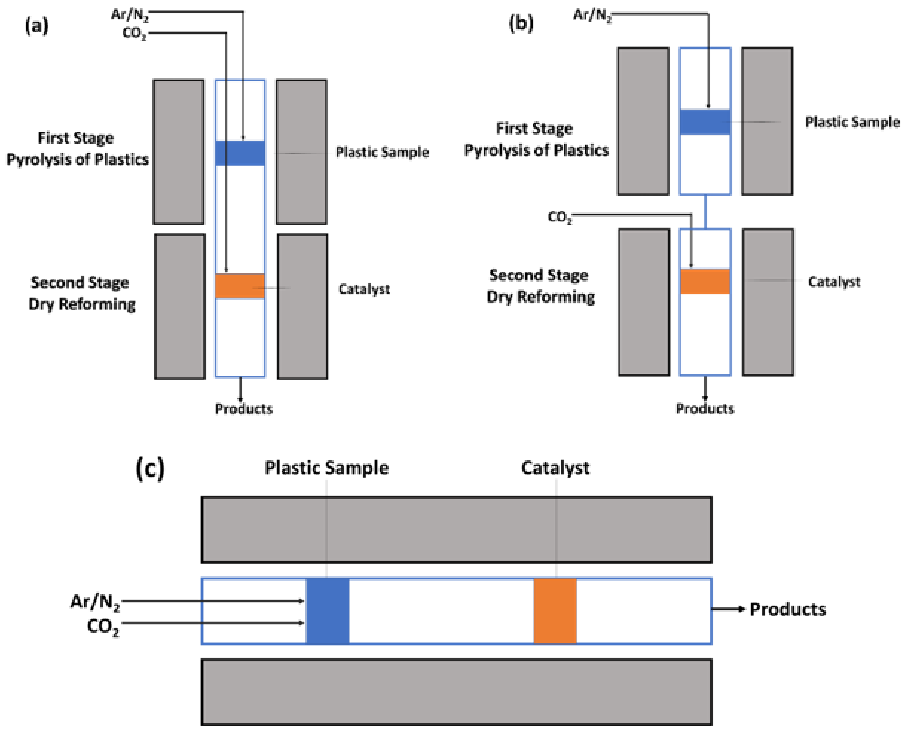

Fig. 1.18 Laboratory-scale pyrolysis-catalytic dry reforming setups: (a) Two-stage reactor; (b) Two-stage reactor system consisting of two separate reactors;(c) One-stage reactor [95]

PCDR processes are typically carried out under atmospheric pressure with temperatures varying depending on the stage: the pyrolysis step is performed at temperatures ranging from 400 °C to 500 °C, and the DR step is favored at higher temperatures ranging from 630 °C to 830 °C [95]. The two-stage pyrolysis catalytic dry reforming process is more manageable than one-stage processes because the contaminants produced by the pyrolysis unit do not reach the second stage and thus do not affect the catalyst. Because the gaseous products generated by the PCDR process are tar-free, they avoid the major issue associated with gasification processes. Therefore, PCDR is a promising method for valorizing waste plastics.

Table 1.1 summarizes some of the catalysts used in the two-stage catalytic dry reforming of plastics.

Table 1.1 Syngas yields obtained from the pyrolysis-catalytic dry reforming of plastics reported in the literature under different process parameters

Catalyst	Plastic Used	Operating Conditions	Catalyst: Plastic	Syngas Yield	Reference
Ni-Co-Al	LDPE	T_{pyr}=500°C	0.5	154.7mmol/g_{LDPE}	[116]
	HDPE	T_{DR}= 800°C		149.4 mmol/g_{HDPE}	
	PP			136 mmol/g_{PP}	
	PS			126.3 mmol/g_{PS}	
	PET			63 mmol/g_{PET}	
Ni-Co/Al$_2$O$_3$	SPW	T_{pyr}=500°C T_{DR}= 600°C	0.5	116.2mmol/g_{MPW}	[111]
		T_{pyr}=500°C T_{DR}= 700°C		144.0mmol/g_{MPW}	
		T_{pyr}=500°C T_{DR}= 800°C		148.6mmol/g_{MPW}	
		T_{pyr}=500°C T_{DR}= 900°C		125.8mmol/g_{MPW}	
Ni-Co/Al$_2$O$_3$	SPW	T_{pyr}=500°C	0.25	141.3mmol/g_{MPW}	[111]
		T_{DR}= 800°C	0.5	148.6mmol/g_{MPW}	
			1	143.9mmol/g_{MPW}	
			1.5	139.9mmol/g_{MPW}	
Ni-Co/Al$_2$O$_3$	SPW	T_{pyr}=500°C T_{DR}= 800°C CO_2:Steam 4:0	0.5	96mmol/g_{MPW}	[112]
		T_{pyr}=500°C T_{DR}= 800°C CO_2:Steam 4:0.5		107mmol/g_{MPW}	
		T_{pyr}=500°C T_{DR}= 800°C CO_2:Steam 4:1		136mmol/g_{MPW}	
		T_{pyr}=500°C T_{DR}=800°C CO_2:Steam 4:1.5		159mmol/g_{MPW}	
		T_{pyr}=500°C T_{DR}= 800°C CO_2:Steam 4:2		156mmol/g_{MPW}	
Ni-Mg/Al$_2$O$_3$	SPW	T_{pyr}=500°C	0.5	108mmol/g_{MPW}	[112]

		T_{DR}= 800°C CO_2:Steam 4:0			
		T_{pyr}=500°C T_{DR}= 800°C CO_2:Steam 4:0.5		113mmol/g_{MPW}	
		T_{pyr}=500°C T_{DR}= 800°C CO_2:Steam 4:1		147mmol/g_{MPW}	
		T_{pyr}=500°C T_{DR}= 800°C CO_2:Steam 4:1.5		144mmol/g_{MPW}	
		T_{pyr}=500°C T_{DR}= 800°C CO_2:Steam 4:2		132mmol/g_{MPW}	
Ni/Al_2O_3	SPW from Agricuture	T_{pyr}=500°C T_{DR}= 800°C	0.5	153.67mmol/g_{MPW}	[117]
$Ni-Co/Al_2O_3$				121.26mmol/g_{MPW}	
Ni/Al_2O_3	SPW from building and consrtruction	T_{pyr}=500°C T_{DR}= 800°C	0.5	143.85mmol/g_{MPW}	[117]
$Ni-Co/Al_2O_3$				141.47mmol/g_{MPW}	
Ni/Al_2O_3	SPW from household packaging	T_{pyr}=500°C T_{DR}= 800°C	0.5	146.32mmol/g_{MPW}	[117]
$Ni-Co/Al_2O_3$				156.45mmol/g_{MPW}	
Ni/Al_2O_3	SPW from electrical and electronic equipment	T_{pyr}=500°C T_{DR}= 800°C	0.5	85.49mmol/g_{MPW}	[117]
$Ni-Co/Al_2O_3$				87.26mmol/g_{MPW}	
$Ni-Mg/Al_2O_3$	HDPE	T_{pyr}=500°C T_{DR}= 800°C	0.5	132mmol/g_{HDPE}	[113]
Ni-Al	HDPE	T_{pyr}=500°C T_{DR}= 800°C	0.5	138.81mmol/g_{HDPE}	[114]

Ni-Cu-Al	130.56mmol/g_{HDPE}
Ni-Co-Al	149.92mmol/g_{HDPE}
Ni-Mg-Al	146.96mmol/g_{HDPE}

It is concluded from **table 1.1** that nickel-based catalysts containing various metal promoters (Ca, Ce, Co, Cu, Fe, La, Mg, Mn, and Ru) as well as supports (activated carbon, alumina, molecular sieves, and zeolites), have been primarily used in PCDR processes. According to the literature [95], the most common PCDR catalysts are Ni-Co/Al_2O_3 and Ni–Mg/Al_2O_3 in a two-stage setup due to their high catalytic activity and stability in the dry reforming of hydrocarbons.

7.3. Dry reforming reaction: thermodynamics study

According to the literature [118], the thermodynamic calculations for plastic pyrolysis show only two phases: solid carbon and a gas phase, in which two species, hydrogen, and methane, dominate and are thermodynamically stable at 1100 °C. During plastic pyrolysis, the polymer is converted into hydrocarbons (mainly methane) **(1.1)**, which act as a sink for carbon dioxide, thus producing syngas **(1.2)**.

$$\text{Polymers} \rightarrow C_xH_y \tag{1.1}$$

$$C_xH_y + CO_2 \rightarrow 2x\text{CO} + \frac{y}{2}H_2 \tag{1.2}$$

Since there are different available types of plastics with different chemical compositions and since, after the pyrolysis of plastics, methane is one of the major hydrocarbons produced, we will study the thermodynamics of the dry reforming of methane.

In 1928, Fisher and Tropsch realized that the dry reforming of methane is thermodynamically favored at elevated temperatures ranging between 630 °C and 1000 °C [97,106]. Since CO_2 and CH_4 are very stable compounds with low potential energy, high temperatures are mandatory for a desirable methane conversion, making methane dry reforming an endothermic process [99].

The primary chemical reaction that occurs during methane dry reforming is the reaction between methane and carbon dioxide, which produces syngas **(1.3)**. This reaction is favored at low pressure yet requires high temperatures. Furthermore, due to the elevated temperature, other side reactions may occur such as the Boudouard reaction (BR) **(1.4)**, methane decomposition (MD) **(1.5)**, and the reverse water gas shift reaction (RWGS) **(1.6)**. The BR and MD reactions influence the formation of carbon and its deposition on the catalyst's surface, leading to its deactivation. The RWGS reaction influences the H_2:CO ratio, pushing it below 1 since more CO is generated from this reaction [119]. This is beneficial for a variety of industrial applications, including the synthesis of oxygenated chemicals such as dimethyl ether and acetic acid [120].

$$CH_4 + CO_2 \rightarrow 2H_2 + 2CO \qquad \Delta H_{298} = 247.0\ kJ.mol^{-1} \qquad \textbf{(1.3)}$$

$$2CO \rightarrow C + CO_2 \qquad \Delta H_{298} = -172.4\ kJ.mol^{-1} \qquad \textbf{(1.4)}$$

$$CH_4 \rightarrow C + 2H_2 \qquad \Delta H_{298} = 74.6\ kJ.mol^{-1} \qquad \textbf{(1.5)}$$

$$CO_2 + H_2 \rightarrow CO + H_2O \qquad \Delta H_{298} = 41.1\ kJ.mol^{-1} \qquad \textbf{(1.6)}$$

As shown in **fig. 1.19**, the equilibrium constant of the DRM reaction increases sharply with temperature due to its strong endothermic character, whereas the equilibrium constants of reactions with moderate endothermic character, such as MD and RWGS, increase moderately with temperature. On the other hand, exothermic reactions, such as BR, are less thermodynamically favored at high temperatures [99]. In conclusion, the DRM reaction is favored at temperatures exceeding 700 °C.

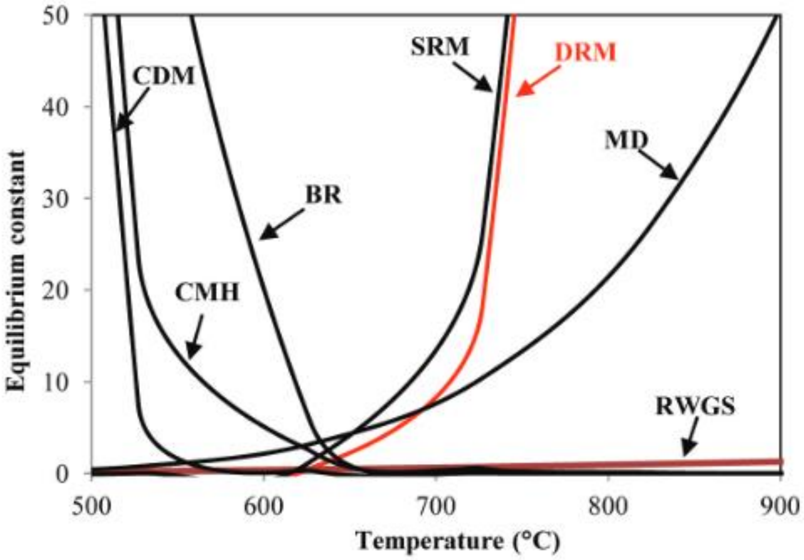

Fig. 1.19 Evolution of equilibrium constant versus temperature [99]

In practice, the residence time in the reactor is shorter than the time required to achieve theoretical equilibrium. As a result, the use of a catalyst is required to reduce activation energy while favoring the DRM reaction pathway over other side reactions [99]. Therefore, the presence of a catalyst makes the DRM process more economically viable.

7.4.Challenges accompanying dry reforming:

Even though the dry reforming process has aroused the interest of the industry and academia due to its ability to convert greenhouse gas carbon dioxide into syngas, this process is fraught with difficulties. There are several reasons why this process has not yet been fully commercialized. The main challenges are the high energy requirements due to the endothermic nature of the reaction, low syngas quality, and high sensitivity to coke formation, leading to catalytic deactivation [121]. Moreover, to minimize coke formation, high temperatures are also required. Furthermore, there is a shortage of a constant clean source of carbon dioxide [99]. On the other hand, finding a cost-effective catalyst with high performance and low susceptibility to deactivation is also strenuous. All these obstacles raise the cost of the process, impeding its commercialization.

7.5. Catalytic deactivation

For a catalyst to be considered ideal, it should exhibit high activity, selectivity, and stability over an extended period. Catalyst deactivation is a phenomenon that occurs during a reaction and causes a loss of catalytic activity and product selectivity. At some point, all catalysts degrade and must be substituted. However, depending on the catalyst, this deactivation can take anywhere from seconds to years [122]. To address catalytic deactivation, industries must frequently perform catalyst replacements, regeneration, and plant shutdowns, all of which result in increased energy consumption, lost production time, and require additional costs [122].

Nickel-based catalysts have received a lot of attention due to their low cost, wide availability, and high activity in the reforming process. However, their main disadvantage is that they are prone to catalytic deactivation due to coking sensitivity [96]. Moreover, under reforming conditions, which necessitate high temperatures, these catalysts tend to form clusters of nickel on which unreactive carbon can effortlessly form, eventually causing catalytic deactivation due to pore blockage and active site confinement [122]. As a result, it is critical to understand the mechanisms underlying catalyst deactivation to implement more precautionary measures to extend the time before a catalyst starts deactivating.

There are two types of catalyst deactivation mechanisms: physical and chemical.

Sintering (fig 1.20) is an irreversible physical property that is commonly used to describe the crystalline growth that leads to an increase in particle size and, as a result, loss of catalytic activity. Dry reforming reactions, as previously mentioned, are endothermic and thus thermodynamically favored at high temperatures. Therefore, the active phase or support sintering is likely to happen. To avoid this, it is recommended that appropriate promoters be used, the metal support interaction is increased, and a suitable catalyst preparation method is chosen [99].

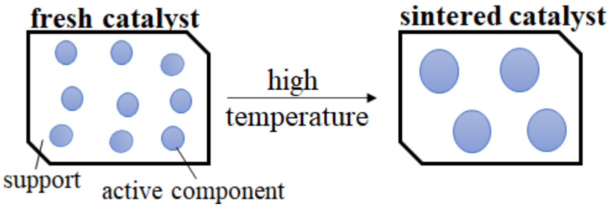

Fig. 1.20 Catalyst sintering

Fouling (fig. 1.21) is the physical deposition of species from the reacting medium onto the active surface of the catalyst, resulting in the blockage of sites and pores and, as a result, the loss of catalytic activity [122]. Coke and carbon deposition are the most common types of fouling resulting from the Boudouard reaction. It is a partly reversible process where these carbonaceous species can be eliminated through gasification or burning in the presence of air, oxygen, carbon dioxide, hydrogen, or water [120].

Fig 1.21 Catalyst fouling [122]

Poisoning (fig. 1.22) is the loss of catalytic activity resulting from the chemisorption of impurities (chlorine, ammonia, sulfur, tar, etc.) found in the feed stream onto the catalyst's active sites. The most common catalyst poison during reforming is sulfur. Once the catalyst has been poisoned, the chemical substance is irreversibly chemisorbed on the catalyst's active sites, necessitating chemical retreatment to attempt to regenerate the catalyst [120].

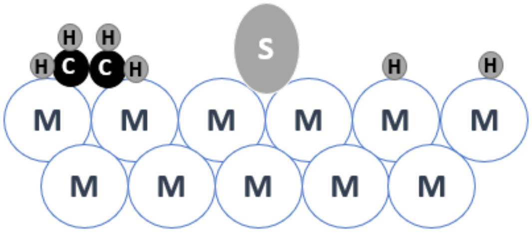

Fig. 1.22 Catalyst poisoning

Carbon is primarily formed during the dry reforming reaction from side reactions, each of which is favored at a specific temperature. Methane decomposition and the Boudouard reaction, as shown earlier in **fig.1.19**, are thermodynamically possible at temperatures ranging from 500 °C to 900 °C [99]. These reactions generate solid carbon, which can deposit on the catalyst. As a result, carbon deposition can cause physical blockage of the active sites. This has a significant impact on the stability and activity of the catalyst.

The distinction between the terms "carbon" and "coke" must be made. Even though the definitions of the two terms can occasionally be used interchangeably, this is not the case in general. Carbon is the product of CO disproportionation while coke is the substance that results from the condensation or decomposition of hydrocarbons [122]. Heavy hydrocarbons that have been polymerized typically make up coke. Nevertheless, depending on the circumstances of the reaction, the composition of coke could range from high molecular weight hydrocarbons to primary carbons like graphite [122].

Mechanisms of carbon deposition on metal catalysts from carbon monoxide are illustrated in **fig 1.23**.

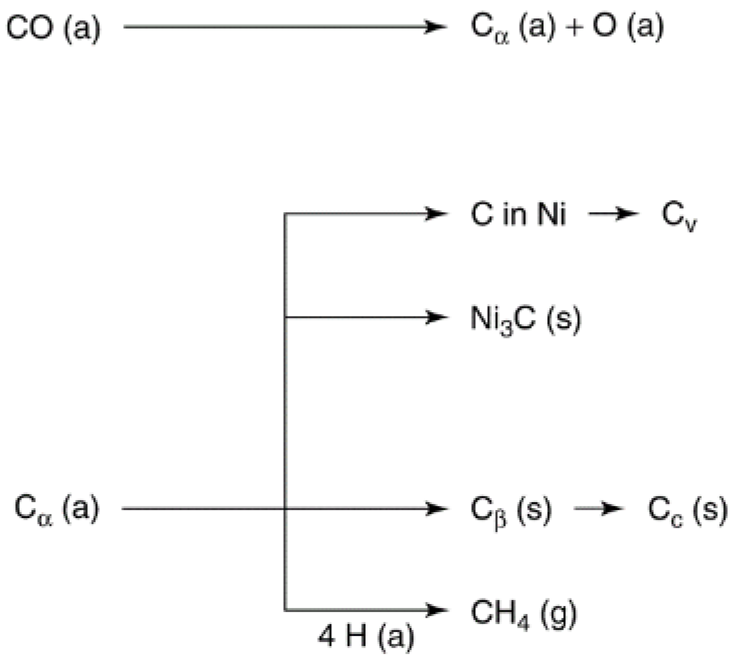

Fig. 1.23 Formation, transformation, and gasification of carbon on Nickel ((a) adsorbed state; (g) gaseous state; (s) solid state) [123]

Different kind of carbon and coke, which vary in morphology and reactivity, are formed in these reactions. CO dissociates on metals to form adsorbed atomic carbon (Cα). $C_α$ are the reaction's intermediates, primarily responsible for the syngas formation [124]. This type of carbon is highly unstable and easily re-oxidized. It can produce CO by reacting with water, oxygen, or carbon dioxide, and it is made up of carbon that has been adsorbed and bound to metallic centers [99]. If this type of carbon accumulates on the surface, it can be converted into polymeric carbon film (Cβ). These types of carbon (Cα and Cβ) are amorphous in structure, highly reactive, and form at low temperatures. Over an extended period and at high temperatures, these types of carbon can be converted into a less reactive graphitic carbon (Cc). The most stable carbonaceous compounds are those found in the form of graphite carbon. They are the primary causes of catalyst deactivation since they can only be oxidized at high temperatures [125]. Cα can also form vermicular carbon (Cv) or metal carbide (Cγ).

Filamentous carbon, also known as whisker carbon, is the most harmful to nickel-based catalysts. This carbon nucleates, forming a strong whisker with a nickel crystal that eventually pushes it out of the catalyst. Whisker carbon may also cause the catalyst pellets to fracture [99,126]. These types of carbon are not involved in the dry reforming reaction and can only be removed at high temperatures and in the presence of a strong oxidant [123].

The properties of each carbon type, formation temperature, and gasification temperature are listed in **table 1.2**.

Table 1.2 Carbon species formed by CO decomposition on Ni [123]

Designation	Structure	Formation Temperature (°C)	Gasification Temperature (°C)
Cα	Adsorbed, atomic	200-400	200
Cβ	Polymeric, amorphous, filamentous	250-500	400
Cv	Vermicular, whisker-like filaments	300-1000	400-600
Cγ	Nickel carbide	150-250	275
Cc	Graphitic, crystalline	500-550	550-850

Mechanisms of coke formation deposition on metal catalysts from hydrocarbons are illustrated in **fig 1.24.**

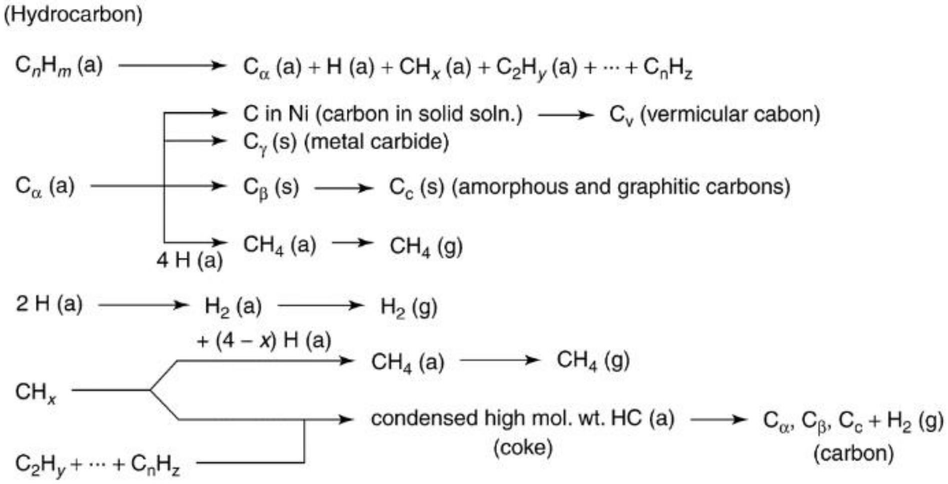

Fig 1.24 Formation, transformation, and gasification of coke on metal surface ((a) adsorbed state; (g) gaseous state; (s) solid state) [123]

As shown from **fig. 1.24**, the process is more complicated than CO dissociation due to the formation of segmented hydrocarbon species. Some of these species may condense to generate greater molecular weight coke.

The regeneration of the deactivated catalyst by the formation of a carbon deposit is an expensive process. This makes it difficult to use this reaction for industrial purposes. Since carbon formation is influenced by the catalyst's composition and structure, numerous studies have been conducted to develop an active and selective catalyst for the dry reforming reaction that is stable and resistant to sintering and carbon deposition [127]. On the other hand, it is possible to avoid sintering and the formation of carbon deposits by using catalysts that are resistant to this type of deactivation. Indeed, certain parameters have been identified in the literature [128] as favoring the catalyst's resistance to deactivation by sintering or carbon deposition. A review of several articles on various materials used in dry reforming revealed that certain parameters have a significant impact on the performance of the catalysts.

7.6. Catalytic parameters

Certain catalytic parameters must be considered when selecting a suitable catalyst for the dry reforming reaction. Such parameters include calcination temperature, metal-support interaction, reduction temperature, basicity, and active phase dispersion.

7.6.1. Calcination temperature

The calcination temperature has a significant impact on the nature of active sites, where high–temperature calcination improves metal-support interaction (MSI), yet also promotes particle size growth, complicating the reduction of the catalyst [99]. Moreover, thermal stability is an important parameter; the activation of the catalysts is done through thermal treatment, and this activation method can influence their stability and reactivity [128] The products obtained after this treatment are the active compounds in the dry reforming reaction.

7.6.2. Metal-support interaction

Metal-support interactions influence the carbon deposition during the dry reforming reaction. Carbon deposition on the catalytic surface, and consequently the catalytic deactivation, are prevented by strong MSI. This is because a strong interaction between the support and the metal provides better dispersion of the active phase by keeping the active species small and precluding agglomeration [128]. This increases particle sizes and thus improves resistance to carbon deposition [99,120].

7.6.3. Reduction temperature

The catalyst is first activated by reducing its metal oxides before the dry reforming reaction. Reduced oxides are thought to be the catalyst's active phases. To obtain the greatest number of available active sites, a catalyst with high reducibility must be synthesized. High activity and low deactivation are favored by support with suitable reducibility.

7.6.4. Basicity

Basic catalysts have been shown to improve CO_2 adsorption in the dry reforming reaction by supplying more surface oxygen species on the catalytic surface. The more active oxygen species there are, the more they will react with the surface carbon. This allows the gasification of intermediate carbonaceous species and thus increases the resistance of the catalyst to deactivation by carbon deposition. Moreover, adding basic oxides to the support improves the catalyst's ability to chemisorb oxidants, such as carbon dioxide and water, thereby enabling coking inhibition.

7.6.5. Active phase dispersion

The active phase dispersion on the catalytic surface may increase the activity of the catalyst and improve its resistance to sintering and particle agglomeration. This increases the specific surface area of the solid and creates a bigger surface contact between the catalyst and the gas mixture. As a result, the dispersion of the active phases influences the activity of the catalyst as well as its resistance to sintering and carbon formation.

These parameters can be enhanced by experimenting with the nature and physicochemical properties of the catalyst.

7.7. Catalyst choice

For a catalyst to be ideal, it should have high catalytic performance, excellent selectivity, and high stability. However, from an industrial standpoint, catalytic performance is important, yet the cost of the catalyst must not be overlooked. Therefore, it is important to choose a suitable catalyst that meets both catalytic and economic points of view.

The activity of dry reforming catalysts is determined by a variety of factors such as the support, the active metal phase, and the interaction of both [126]. Therefore, to create an ideal catalyst, its two main components must be highlighted: the support and the active phase.

Two supports were used in this study: alumina and alumina promoted with ceria. Alumina (Al_2O_3) is distinguished by its ease of accessibility and ability to be synthesized using a variety of catalyst formulations. It is chemically and physically stable, as well as mechanically strong, and it can disperse the active metal phase [129]. Furthermore, it is the most affordable and widely used support in the dry reforming reaction [120]. Ceria (CeO_2) is being studied because of its ability to release and absorb oxygen. These oxides, when used as a support, improve catalytic performance by enhancing the metal support interaction [99]. Moreover, ceria is gaining attention due to its excellent redox properties, where the Ce^{4+} can be quickly reduced to Ce^{3+}. Furthermore, because an oxygen vacancy on the CeO_2 surface is a Lewis base, it facilitates CO_2 adsorption and aids in its activation [103]. On the other hand, alumina can be doped with metal oxides like CeO_2. Because of its coverage, the presence of Ce reduces the density of acidic sites. Ce coats the Al_2O_3 acidic centers and neutralizes or suppresses the Lewis acid sites, increasing oxygen vacancy and preventing coke formation on the support [129,130]. Therefore, in this study, the promotion of alumina support with cerium oxide will also be investigated.

While various active metals have been considered for the dry reforming reaction, noble metals (Ru, Pt, Rd, and Pd) and transition metals (Ni, Co) are mostly studied. While noble metals exhibit good activity and stability in elevated temperature applications, they are deemed uneconomical for large-scale applications. On the other hand, transition metals like Ni and Co have proven to be the most intrinsically active metals. Therefore, Ni is the active phase of choice due to its reasonable cost, high catalytic activity, and high hydrogen selectivity [130]. To achieve the high activity, high loading is required. Therefore, a Ni metal loading of up to 50 wt.% is employed in this study. Nonetheless, Ni-based catalysts withstand sintering at high temperatures, promoting methane decomposition and Boudouard reactions [96]. This results in carbon depositing on the catalyst's surface, making it more susceptible to deactivation [131]. Sometimes a metal promoter is added to address these deficiencies and enhance the catalytic activity [99,132]. Therefore, the incorporation of noble metals into a catalyst inhibits sintering and stabilizes catalytic performance, preventing the catalyst from deactivating [103,133]. Ruthenium appears to have high catalytic properties and is commonly used as an active site in a variety of chemical reactions. Moreover, Ru is less expensive compared to other noble metals. Therefore, in this study, nickel is promoted with ruthenium to form a bimetallic active phase. It is to be noted that a small percentage of ruthenium (1 wt.%) is utilized due to the high cost of this noble metal.

8. Conclusion

In previous decades, the production and consumption of plastic has increased, thus increasing the abundance of plastic waste. Although mechanical recycling of plastics is the most common waste management method, other methods, such as chemical recycling, which produces petrochemical feedstocks and fuels, have prospered in recent years. Chemical recycling of plastic wastes through pyrolysis to produce useful hydrocarbons has been identified as a promising technology. Pyrolysis produces liquid oils, solid chars, and gaseous products. Process parameters, such as temperature, pressure, and residence time, influence the fraction of pyrolysis products.

In recent years, the pyrolysis-catalytic dry reforming of plastic waste to syngas has received increased attention and is being advanced in terms of environmental concerns such as CO_2 emissions and waste management. Dry reforming is the process where the resulting pyrolyzed hydrocarbons are cracked with carbon dioxide to generate synthesis gas. It is well understood that syngas can subsequently be used as a feedstock for chemical processes, such as the Fischer–Tropsch synthesis, to produce a variety of chemical products and fuels. The influence and optimization of many process parameters, such as operating conditions, catalyst, and feedstock, on the efficiency of the PCDR process is a challenge for future research. The type of feedstock is critical because different product distribution and composition can be obtained depending on its composition and the chemical structure of constituents, and it may also affect carbon deposition on the catalyst. To date, nickel-based catalysts have primarily been used in PCDR processes. However, there is a need to overcome the problem of catalyst deactivation while maintaining high catalytic activity. To commercialize syngas production via the PCDR process, it is necessary to develop low-cost, robust catalysts with high performance and long-term stability. It is critical to conduct extensive research on the synergistic interactions of catalyst components, such as active sites, basicity, and metal–support interactions. Strong interactions between metal and support, metal and promoter, and other catalyst components are crucial for improved catalytic activity and deactivation resistance at elevated reaction temperatures. Moreover, understanding these interactions will allow for the development of catalysts with the required selectivity, stability, and conversion rates. As a result, these factors were considered when selecting Ru-Ni supported on alumina as the catalyst of choice in the pyrolysis-catalytic dry reforming of plastic.

9. References

[1] PlasticsEurope, Plastics-the Facts 2019 An analysis of European plastics production, demand and waste data, 2019.

[2] S.L. Wong, N. Ngadi, T.A.T. Abdullah, I.M. Inuwa, Current state and future prospects of plastic waste as source of fuel: A review, Renewable and Sustainable Energy Reviews. 50 (2015) 1167–1180. https://doi.org/10.1016/j.rser.2015.04.063.

[3] M. Gilbert, Plastics Materials: Introduction and Historical Development, in: Brydson's Plastics Materials: Eighth Edition, Elsevier Inc., 2016: pp. 2–18. https://doi.org/10.1016/B978-0-323-35824-8.00001-3.

[4] G. Lopez, M. Artetxe, M. Amutio, J. Alvarez, J. Bilbao, M. Olazar, Recent advances in the gasification of waste plastics. A critical overview, Renewable and Sustainable Energy Reviews. 82 (2018) 576–596. https://doi.org/10.1016/j.rser.2017.09.032.

[5] J.J. Klemeš, Y. van Fan, P. Jiang, Plastics: friends or foes? The circularity and plastic waste footprint, Energy Sources, Part A: Recovery, Utilization and Environmental Effects. 43 (2021) 1549–1565. https://doi.org/10.1080/15567036.2020.1801906.

[6] PlascticsEurope, Plastics-the Facts 2020 An analysis of European plastics production, demand and waste data, 2020.

[7] B.K. Sharma, B.R. Moser, K.E. Vermillion, K.M. Doll, N. Rajagopalan, Production, characterization and fuel properties of alternative diesel fuel from pyrolysis of waste plastic grocery bags, Fuel Processing Technology. 122 (2014) 79–90. https://doi.org/10.1016/j.fuproc.2014.01.019.

[8] J.M. Saad, P.T. Williams, Catalytic dry reforming of waste plastics from different waste treatment plants for production of synthesis gases, Waste Management. 58 (2016) 214–220. https://doi.org/10.1016/j.wasman.2016.09.011.

[9] PlascticsEurope, Plastics-the Facts 2021 An analysis of European plastics production, demand and waste data, 2021.

[10] L. Lebreton, A. Andrady, Future scenarios of global plastic waste generation and disposal, Palgrave Commun. 5 (2019). https://doi.org/10.1057/s41599-018-0212-7.

[11] K.R. Vanapalli, H.B. Sharma, V.P. Ranjan, B. Samal, J. Bhattacharya, B.K. Dubey, S. Goel, Challenges and strategies for effective plastic waste management during and post COVID-19 pandemic, Science of the Total Environment. 750 (2021). https://doi.org/10.1016/j.scitotenv.2020.141514.

[12] S. Dharmaraj, V. Ashokkumar, K.W. Chew, S.R. Chia, P.L. Show, C. Ngamcharussrivichai, Novel strategy in biohydrogen energy production from COVID - 19 plastic waste: A critical review, Int J Hydrogen Energy. (2021). https://doi.org/10.1016/j.ijhydene.2021.08.236.

[13] S.D. Anuar Sharuddin, F. Abnisa, W.M.A. Wan Daud, M.K. Aroua, A review on pyrolysis of plastic wastes, Energy Convers Manag. 115 (2016) 308–326. https://doi.org/10.1016/j.enconman.2016.02.037.

[14] D. Yao, H. Li, Y. Dai, C.H. Wang, Impact of temperature on the activity of Fe-Ni catalysts for pyrolysis and decomposition processing of plastic waste, Chemical Engineering Journal. 408 (2021). https://doi.org/10.1016/j.cej.2020.127268.

[15] B. Kunwar, H.N. Cheng, S.R. Chandrashekaran, B.K. Sharma, Plastics to fuel: a review, Renewable and Sustainable Energy Reviews. 54 (2016) 421–428. https://doi.org/10.1016/j.rser.2015.10.015.

[16] A. Younis, J. Estephane, C. Gennequin, S. Aouad, E. Abi Aad, Valorization of plastics in the presence of Ru-Ni/Al_2O_3 catalysts to produce syngas, in: IEEEXplorer, 2021.

[17] H.A. Leslie, M. J. M. van Velzen, S.H. Brandsma, D. Vethaak, J.J. Garcia-Vallejo, M.H. Lamoree, Discovery and quantification of plastic particle pollution in human blood, Environ Int. (2022) 107199. https://doi.org/10.1016/J.ENVINT.2022.107199.

[18] I. Barbarias, G. Lopez, M. Artetxe, A. Arregi, J. Bilbao, M. Olazar, Valorisation of different waste plastics by pyrolysis and in-line catalytic steam reforming for hydrogen production, Energy Convers Manag. 156 (2018) 575–584. https://doi.org/10.1016/j.enconman.2017.11.048.

[19] R. Kukreja, Advantages and disadvantages of recycling., Conserve Energy Future . (2009) 1–50.

[20] A. Laurent, J. Clavreul, A. Bernstad, I. Bakas, M. Niero, E. Gentil, T.H. Christensen, M.Z. Hauschild, Review of LCA studies of solid waste management systems - Part II: Methodological guidance for a better practice, Waste Management. 34 (2014) 589–606. https://doi.org/10.1016/j.wasman.2013.12.004.

[21] C. Kassargy, Contribution à l'étude de la valorisation énergétique des résidus de plastique par craquage catalytique, 2018. https://tel.archives-ouvertes.fr/tel-01883636.

[22] G.M. Swallowe, Mechanical Properties and Testing of Polymers: An A-Z Reference, 1999.

[23] A.S. Pouzada, Selection of thermoplastics, Design and Manufacturing of Plastics Products. (2021) 87–140. https://doi.org/10.1016/B978-0-12-819775-2.00004-8.

[24] R.A. Ash, Vehicle armor, Lightweight Ballistic Composites: Military and Law-Enforcement Applications: Second Edition. (2016) 285–309. https://doi.org/10.1016/B978-0-08-100406-7.00009-X.

[25] H.N. Dhakal, S.O. Ismail, Introduction to composite materials, Sustainable Composites for Lightweight Applications. (2021) 1–16. https://doi.org/10.1016/B978-0-12-818316-8.00001-3.

[26] W.K. Kupolati, E.R. Sadiku, I.D. Ibrahim, A.O. Adeboje, C. Kambole, O.O.S. Ojo, A.A. Eze, P. Paige-Green, J.M. Ndambuki, The use of polyolefins in geotextiles and engineering applications, Polyolefin Fibres: Structure, Properties and Industrial Applications: Second Edition. (2017) 497–516. https://doi.org/10.1016/B978-0-08-101132-4.00016-3.

[27] L.A. Pruitt, Structural Biomedical Polymers (Nondegradable), Comprehensive Biomaterials. 1 (2011) 373–379. https://doi.org/10.1016/B978-0-08-055294-1.00036-2.

[28] A. Emblem, Plastics properties for packaging materials, Packaging Technology. (2012) 287–309. https://doi.org/10.1533/9780857095701.2.287.

[29] S.M. Al-Salem, A. Antelava, A. Constantinou, G. Manos, A. Dutta, A review on thermal and catalytic pyrolysis of plastic solid waste (PSW), J Environ Manage. 197 (2017) 177–198. https://doi.org/10.1016/J.JENVMAN.2017.03.084.

[30] J. Bayer, L.A. Granda, J.A. Méndez, M.A. Pèlach, F. Vilaseca, P. Mutjé, Cellulose polymer composites (WPC), Advanced High Strength Natural Fibre Composites in Construction. (2017) 115–139. https://doi.org/10.1016/B978-0-08-100411-1.00005-4.

[31] V.R. Sastri, Commodity Thermoplastics: Polyvinyl Chloride, Polyolefins, and Polystyrene, Plastics in Medical Devices. (2014) 73–120. https://doi.org/10.1016/B978-1-4557-3201-2.00006-9.

[32] J.P. Greene, Commodity Plastics, Automotive Plastics and Composites. (2021) 83–105. https://doi.org/10.1016/B978-0-12-818008-2.00004-0.

[33] A. Rohani Shirvan, A. Nouri, C. Wen, Structural polymer biomaterials, Structural Biomaterials. (2021) 395–439. https://doi.org/10.1016/B978-0-12-818831-6.00010-0.

[34] A. Vijayakumar, J. Sebastian, Pyrolysis process to produce fuel from different types of plastic - A review, IOP Conf Ser Mater Sci Eng. 396 (2018). https://doi.org/10.1088/1757-899X/396/1/012062.

[35] M. Lanaro, L. Booth, S.K. Powell, M.A. Woodruff, Electrofluidodynamic technologies for biomaterials and medical devices: melt electrospinning, Electrofluidodynamic Technologies (EFDTs) for Biomaterials and Medical Devices: Principles and Advances. (2018) 37–69. https://doi.org/10.1016/B978-0-08-101745-6.00003-7.

[36] L.W. McKeen, Polyester Plastics, Permeability Properties of Plastics and Elastomers. (2017) 95–114. https://doi.org/10.1016/B978-0-323-50859-9.00006-3.

[37] S.M. Fakhrhoseini, M. Dastanian, Predicting pyrolysis products of PE, PP, and PET using NRTL activity coefficient model, J Chem. (2013). https://doi.org/10.1155/2013/487676.

[38] British Plastic Federation, Polyvinyl Chloride PVC, (2022). https://www.bpf.co.uk/plastipedia/polymers/PVC.aspx (accessed February 25, 2022).

[39] K. Ragaert, L. Delva, K. van Geem, Mechanical and chemical recycling of solid plastic waste, Waste Management. 69 (2017) 24–58. https://doi.org/10.1016/J.WASMAN.2017.07.044.

[40] N. Singh, D. Hui, R. Singh, I.P.S. Ahuja, L. Feo, F. Fraternali, Recycling of plastic solid waste: A state of art review and future applications, Compos B Eng. 115 (2017) 409–422. https://doi.org/10.1016/J.COMPOSITESB.2016.09.013.

[41] I.A. Ignatyev, W. Thielemans, B. vander Beke, Recycling of polymers: A review, ChemSusChem. 7 (2014) 1579–1593. https://doi.org/10.1002/CSSC.201300898.

[42] S. Kumar, A.K. Panda, R.K. Singh, A review on tertiary recycling of high-density polyethylene to fuel, Resour Conserv Recycl. 55 (2011) 893–910. https://doi.org/10.1016/j.resconrec.2011.05.005.

[43] S.M. Al-Salem, P. Lettieri, J. Baeyens, Recycling and recovery routes of plastic solid waste (PSW): A review, Waste Management. 29 (2009) 2625–2643. https://doi.org/10.1016/J.WASMAN.2009.06.004.

[44] O. Parthiba, K. Kirsten, H. Subramanian, S. Muthu, Environmental Footprints and Eco-design of Products and Processes Recycling of Solid Waste for Biofuels and Bio-chemicals, 2016. http://www.springer.com/series/13340.

[45] K. Hamad, M. Kaseem, F. Deri, Recycling of waste from polymer materials: An overview of the recent works, (2013). https://doi.org/10.1016/j.polymdegradstab.2013.09.025.

[46] G. Grause, A. Buekens, Y. Sakata, A. Okuwaki, T. Yoshioka, Feedstock recycling of waste polymeric material, Journal of Material Cycles and Waste Management . 13 (2011) 265–282. https://doi.org/10.1007/s10163-011-0031-z.

[47] A. Akah, J. Hernandez-Martinez, C. Rallan, A.A. Garforth, Enhanced feedstock recycling of post-consumer plastic waste, Chem Eng Trans. 43 (2015) 2395–2400. https://doi.org/10.3303/CET1543400.

[48] S. Heidenreich, P.U. Foscolo, New concepts in biomass gasification, Prog Energy Combust Sci. 46 (2015) 72–95. https://doi.org/10.1016/J.PECS.2014.06.002.

[49] P. Haro, F. Trippe, R. Stahl, E. Henrich, Bio-syngas to gasoline and olefins via DME - A comprehensive techno-economic assessment, Appl Energy. 108 (2013) 54–65. https://doi.org/10.1016/J.APENERGY.2013.03.015.

[50] D. Chen, L. Yin, H. Wang, P. He, Reprint of: Pyrolysis technologies for municipal solid waste: A review, Waste Management. 37 (2015) 116–136. https://doi.org/10.1016/J.WASMAN.2015.01.022.

[51] E.M. Abdel-Bary, Handbook of Plastic Films, Rapra Technology Ltd. , Shawbury, United Kingdom, 2003.

[52] I. Ahmad, M. Ismail Khan, H. Khan, M. Ishaq, R. Tariq, K. Gul, W. Ahmad, Pyrolysis study of polypropylene and polyethylene into premium oil products, Int J Green Energy. 12 (2015) 663–671. https://doi.org/10.1080/15435075.2014.880146.

[53] I. Kremer, T. Tomić, Z. Katančić, M. Erceg, S. Papuga, J.P. Vuković, D.R. Schneider, Catalytic pyrolysis of mechanically non-recyclable waste plastics mixture: Kinetics and pyrolysis in laboratory-scale reactor, J Environ Manage. 296 (2021) 113145. https://doi.org/10.1016/J.JENVMAN.2021.113145.

[54] K.B. Park, Y.S. Jeong, B. Guzelciftci, J.S. Kim, Two-stage pyrolysis of polystyrene: Pyrolysis oil as a source of fuels or benzene, toluene, ethylbenzene, and xylenes, Appl Energy. 259 (2020) 114240. https://doi.org/10.1016/J.APENERGY.2019.114240.

[55] C. Wongkhorsub, N. Chindaprasert, A Comparison of the Use of Pyrolysis Oils in Diesel Engine, Energy Power Eng. 05 (2013) 350–355. https://doi.org/10.4236/EPE.2013.54B068.

[56] A. v. Bridgwater, Review of fast pyrolysis of biomass and product upgrading, Biomass Bioenergy. 38 (2012) 68–94. https://doi.org/10.1016/J.BIOMBIOE.2011.01.048.

[57] H. Panchasara, N. Ashwath, Effects of Pyrolysis Bio-Oils on Fuel Atomisation-A Review, Energies (Basel). 14 (2021). https://doi.org/10.3390/en14040794.

[58] S. Papari, H. Bamdad, F. Berruti, Pyrolytic conversion of plastic waste to value-added products and fuels: A review, Materials. 14 (2021). https://doi.org/10.3390/ma14102586.

[59] D. Czajczyńska, L. Anguilano, H. Ghazal, R. Krzyżyńska, A.J. Reynolds, N. Spencer, H. Jouhara, Potential of pyrolysis processes in the waste management sector, Thermal Science and Engineering Progress. 3 (2017) 171–197. https://doi.org/10.1016/J.TSEP.2017.06.003.

[60] M. Tripathi, J.N. Sahu, P. Ganesan, Effect of process parameters on production of biochar from biomass waste through pyrolysis: A review, Renewable and Sustainable Energy Reviews. 55 (2016) 467–481. https://doi.org/10.1016/J.RSER.2015.10.122.

[61] Y. Xue, S. Zhou, R.C. Brown, A. Kelkar, X. Bai, Fast pyrolysis of biomass and waste plastic in a fluidized bed reactor, Fuel. 156 (2015) 40–46. https://doi.org/10.1016/J.FUEL.2015.04.033.

[62] E. Butler, G. Devlin, K. Mcdonnell, Waste Polyolefins to Liquid Fuels via Pyrolysis: Review of Commercial State-of-the-Art and Recent Laboratory Research, Waste Biomass Valorization. 2 (2011) 227–255. https://doi.org/10.1007/s12649-011-9067-5.

[63] F. Abnisa, W.M.A. Wan Daud, A review on co-pyrolysis of biomass: An optional technique to obtain a high-grade pyrolysis oil, Energy Convers Manag. 87 (2014) 71–85. https://doi.org/10.1016/J.ENCONMAN.2014.07.007.

[64] S.C. Moldoveanu, Pyrolysis GC / MS, present and future (recent past and present needs), Journal of Microcolumn Separations. 13 (2001) 102–125. https://doi.org/10.1002/MCS.1028.

[65] S.M. Al-Salem, Thermal pyrolysis of high density polyethylene (HDPE) in a novel fixed bed reactor system for the production of high value gasoline range hydrocarbons (HC), Process Safety and Environmental Protection. 127 (2019) 171–179. https://doi.org/10.1016/J.PSEP.2019.05.008.

[66] C. Kassargy, S. Awad, G. Burnens, K. Kahine, M. Tazerout, Experimental study of catalytic pyrolysis of polyethylene and polypropylene over USY zeolite and separation to gasoline and diesel-like fuels, J Anal Appl Pyrolysis. 127 (2017) 31–37. https://doi.org/10.1016/J.JAAP.2017.09.005.

[67] D. Zhao, X. Wang, J.B. Miller, G.W. Huber, The Chemistry and Kinetics of Polyethylene Pyrolysis: A Process to Produce Fuels and Chemicals, ChemSusChem. 13 (2020) 1764–1774. https://doi.org/10.1002/CSSC.201903434.

[68] Z. Chen, X. Zhang, L. Che, H. Peng, S. Zhu, F. Yang, X. Zhang, Effect of volatile reactions on oil production and composition in thermal and catalytic pyrolysis of polyethylene, Fuel. 271 (2020) 117308. https://doi.org/10.1016/J.FUEL.2020.117308.

[69] Y. Sakata, M.A. Uddin, A. Muto, Degradation of polyethylene and polypropylene into fuel oil by using solid acid and non-acid catalysts, J Anal Appl Pyrolysis. 51 (1999) 135–155. https://doi.org/10.1016/S0165-2370(99)00013-3.

[70] A. Demirbas, Pyrolysis of municipal plastic wastes for recovery of gasoline-range hydrocarbons, J Anal Appl Pyrolysis. 72 (2004) 97–102. https://doi.org/10.1016/J.JAAP.2004.03.001.

[71] S.H. Jung, M.H. Cho, B.S. Kang, J.S. Kim, Pyrolysis of a fraction of waste polypropylene and polyethylene for the recovery of BTX aromatics using a fluidized bed reactor, Fuel Processing Technology. 91 (2010) 277–284. https://doi.org/10.1016/j.fuproc.2009.10.009.

[72] S.M. Fakhrhoseini, M. Dastanian, Predicting pyrolysis products of PE, PP, and PET using NRTL activity coefficient model, J Chem. (2013). https://doi.org/10.1155/2013/487676.

[73] S. Honus, S. Kumagai, G. Fedorko, V. Molnár, T. Yoshioka, Pyrolysis gases produced from individual and mixed PE, PP, PS, PVC, and PET—Part I: Production and physical properties, Fuel. 221 (2018) 346–360. https://doi.org/10.1016/J.FUEL.2018.02.074.

[74] R. Miandad, M.A. Barakat, A.S. Aburiazaiza, M. Rehan, I.M.I. Ismail, A.S. Nizami, Effect of plastic waste types on pyrolysis liquid oil, Int Biodeterior Biodegradation. 119 (2017) 239–252. https://doi.org/10.1016/J.IBIOD.2016.09.017.

[75] U. e. S. Amjad, M. Ishaq, H. ur Rehman, N. Ahmad, L. Sherin, M. Hussain, M. Mustafa, Diesel and gasoline like fuel production with minimum styrene content from catalytic pyrolysis of polystyrene, Environ Prog Sustain Energy. 40 (2021). https://doi.org/10.1002/EP.13493.

[76] Ö. Çepelioɫullar, A.E. Pütün, A pyrolysis study for the thermal and kinetic characteristics of an agricultural waste with two different plastic wastes, Waste Management and Research. 32 (2014) 971–979. https://doi.org/10.1177/0734242X14542684.

[77] L.S. Diaz-Silvarrey, A. McMahon, A.N. Phan, Benzoic acid recovery via waste poly(ethylene terephthalate) (PET) catalytic pyrolysis using sulphated zirconia catalyst, J Anal Appl Pyrolysis. 134 (2018) 621–631. https://doi.org/10.1016/J.JAAP.2018.08.014.

[78] R. Miranda, J. Yang, C. Roy, C. Vasile, Vacuum pyrolysis of PVC I. Kinetic study, Polym Degrad Stab. 64 (1999) 127–144. https://doi.org/10.1016/S0141-3910(98)00186-4.

[79] A. López, I. de Marco, B.M. Caballero, M.F. Laresgoiti, A. Adrados, A. Aranzabal, Catalytic pyrolysis of plastic wastes with two different types of catalysts: ZSM-5 zeolite and Red Mud, Appl Catal B. 104 (2011) 211–219. https://doi.org/10.1016/J.APCATB.2011.03.030.

[80] I. Martín-Gullón, M. Esperanza, R. Font, Kinetic model for the pyrolysis and combustion of poly-(ethylene terephthalate) (PET), J Anal Appl Pyrolysis. 58–59 (2001) 635–650. https://doi.org/10.1016/S0165-2370(00)00141-8.

[81] A. Aboulkas, K. el harfi, A. el Bouadili, Thermal degradation behaviors of polyethylene and polypropylene. Part I: Pyrolysis kinetics and mechanisms, Energy Convers Manag. 51 (2010) 1363–1369. https://doi.org/10.1016/J.ENCONMAN.2009.12.017.

[82] M. Čolnik, D. Pečar, Ž. Knez, A. Goršek, M. Škerget, Kinetics study of hydrothermal degradation of pet waste into useful products, Processes. 10 (2022). https://doi.org/10.3390/pr10010024.

[83] I. Dubdub, M. Al-Yaari, Thermal behavior of mixed plastics at different heating rates: I. pyrolysis kinetics, Polymers (Basel). 13 (2021). https://doi.org/10.3390/polym13193413.

[84] P. Das, P. Tiwari, Thermal degradation kinetics of plastics and model selection, Thermochim Acta. 654 (2017) 191–202. https://doi.org/10.1016/J.TCA.2017.06.001.

[85] A. Marcilla, M.I. Beltrán, R. Navarro, Thermal and catalytic pyrolysis of polyethylene over HZSM5 and HUSY zeolites in a batch reactor under dynamic conditions, Appl Catal B. 86 (2009) 78–86. https://doi.org/10.1016/J.APCATB.2008.07.026.

[86] H. Bockhorn, A. Hornung, U. Hornung, D. Schawaller, Kinetic study on the thermal degradation of polypropylene and polyethylene, J Anal Appl Pyrolysis. 48 (1999) 93–109. https://doi.org/10.1016/S0165-2370(98)00131-4.

[87] A. López, I. de Marco, B.M. Caballero, M.F. Laresgoiti, A. Adrados, Influence of time and temperature on pyrolysis of plastic wastes in a semi-batch reactor, Chemical Engineering Journal. 173 (2011) 62–71. https://doi.org/10.1016/J.CEJ.2011.07.037.

[88] K. Murata, K. Sato, Y. Sakata, Effect of pressure on thermal degradation of polyethylene, J Anal Appl Pyrolysis. 71 (2004) 569–589. https://doi.org/10.1016/J.JAAP.2003.08.010.

[89] F.J. Mastral, E. Esperanza, P. Garciía, M. Juste, Pyrolysis of high-density polyethylene in a fluidised bed reactor. Influence of the temperature and residence time, J Anal Appl Pyrolysis. 63 (2002) 1–15. https://doi.org/10.1016/S0165-2370(01)00137-1.

[90] M.R. Jan, J. Shah, H. Gulab, Catalytic degradation of Waste high-density polyethylene into fuel products using BaCO3 as a catalyst, Fuel Processing Technology. 91 (2010) 1428–1437. https://doi.org/10.1016/J.FUPROC.2010.05.017.

[91] H.S. Fogler, ELEMENTS OF CHEMICAL REACTION ENGINEERING, 2016.

[92] Y.H. Lin, M.H. Yang, Catalytic pyrolysis of polyolefin waste into valuable hydrocarbons over reused catalyst from refinery FCC units, Appl Catal A Gen. 328 (2007) 132–139. https://doi.org/10.1016/J.APCATA.2007.05.039.

[93] Z. Hussain, K.M. Khan, S. Perveen, K. Hussain, W. Voelter, The conversion of waste polystyrene into useful hydrocarbons by microwave-metal interaction pyrolysis, Fuel Processing Technology. 94 (2012) 145–150. https://doi.org/10.1016/J.FUPROC.2011.10.009.

[94] M.S. Abbas-Abadi, M.N. Haghighi, H. Yeganeh, A.G. McDonald, Evaluation of pyrolysis process parameters on polypropylene degradation products, J Anal Appl Pyrolysis. 109 (2014) 272–277. https://doi.org/10.1016/J.JAAP.2014.05.023.

[95] V. la Parola, E. Pawelczyk, I. Wysocka, J. G¿ , Pyrolysis Combined with the Dry Reforming of Waste Plastics as a Potential Method for Resource Recovery—A Review of Process Parameters and Catalysts, Catalysts 2022, Vol. 12, Page 362. 12 (2022) 362. https://doi.org/10.3390/CATAL12040362.

[96] J. Estephane, S. Aouad, S. Hany, B. el Khoury, C. Gennequin, H. el Zakhem, J. el Nakat, A. Aboukaïs, E. Abi Aad, CO_2 reforming of methane over Ni-Co/ZSM5 catalysts. Aging and carbon deposition study, Int J Hydrogen Energy. 40 (2015) 9201–9208. https://doi.org/10.1016/j.ijhydene.2015.05.147.

[97] N.A.K. Aramouni, J.G. Touma, B.A. Tarboush, J. Zeaiter, M.N. Ahmad, Catalyst design for dry reforming of methane: Analysis review, Renewable and Sustainable Energy Reviews. 82 (2018) 2570–2585. https://doi.org/10.1016/J.RSER.2017.09.076.

[98] R. Mahfouz, J. Estephane, C. Gennequin, L. Tidahy, S. Aouad, E. Abi-Aad, CO_2 reforming of methane over Ni and/or Ru catalysts supported on mesoporous KIT-6: Effect of promotion with Ce, J Environ Chem Eng. 9 (2021). https://doi.org/10.1016/j.jece.2020.104662.

[99] S. Aouad, M. Labaki, S. Ojala, P. Seelam, E. Turpeinen, C. Gennequin, J. Estephane, E.A. Aad, A Review on the Dry Reforming Processes for Hydrogen Production: Catalytic Materials and Technologies, in: 2018: pp. 60–128. https://doi.org/10.2174/9781681087580118020007.

[100] T. Namioka, A. Saito, Y. Inoue, Y. Park, T.J. Min, S.A. Roh, K. Yoshikawa, Hydrogen-rich gas production from waste plastics by pyrolysis and low-temperature steam reforming over a ruthenium catalyst, Appl Energy. 88 (2011) 2019–2026. https://doi.org/10.1016/j.apenergy.2010.12.053.

[101] W.D. Fletcher, C.B. Smith, Introduction, Reaching Net Zero. (2020) 1–8. https://doi.org/10.1016/B978-0-12-823366-5.00001-4.

[102] I. Energy Agency, Global Energy Review: CO_2 Emissions in 2021 Global emissions rebound sharply to highest ever level, (2021). www.iea.org/t&c/ (accessed March 23, 2022).

[103] N. Elia, J. Estephane, C. Poupin, B. el Khoury, L. Pirault-Roy, S. Aouad, E.A. Aad, A Highly Selective and Stable Ruthenium-Nickel Supported on Ceria Catalyst for Carbon Dioxide Methanation, ChemCatChem. 13 (2021) 1559–1567. https://doi.org/10.1002/cctc.202001687.

[104] J.C.M. Pires, F.G. Martins, M.C.M. Alvim-Ferraz, M. Simões, Recent developments on carbon capture and storage: An overview, Chemical Engineering Research and Design. 89 (2011) 1446–1460. https://doi.org/10.1016/J.CHERD.2011.01.028.

[105] R. Muthuraj, T. Mekonnen, Recent progress in carbon dioxide (CO2) as feedstock for sustainable materials development: Co-polymers and polymer blends, Polymer (Guildf). 145 (2018) 348–373. https://doi.org/10.1016/J.POLYMER.2018.04.078.

[106] J.M. Saad, DRY REFORMING OF WASTE PLASTICS FOR SYNTHESIS GAS PRODUCTION, 2016.

[107] S. Achinas, J. Mulder, G.J.W. Euverink, A biotechnological overview of syngas fermentation, Handbook of Biofuels. (2022) 511–527. https://doi.org/10.1016/B978-0-12-822810-4.00027-0.

[108] E. Dahdah, S. Aouad, C. Gennequin, J. Estephane, B. Nsouli, A. Aboukaïs, E. Abi-Aad, Glycerol steam reforming over Ru-Mg-Al hydrotalcite-derived mixed oxides: Role of the preparation method in catalytic activity, Int J Hydrogen Energy. 43 (2018) 19864–19872. https://doi.org/10.1016/j.ijhydene.2018.09.042.

[109] M.R. Cesario, G.S. Souza, F.J.A. Loureiro, A.J.M. Araújo, J.P.F. Grilo, S. Aouad, H.L. Tidahy, D.A. Macedo, D.P. Fagg, C. Gennequin, E. Abi-Aad, Synthesis of Co–Ni and Cu–Ni based-catalysts for dry reforming of methane as potential components for SOFC anodes, Ceram Int. 47 (2021). https://doi.org/10.1016/j.ceramint.2021.08.220.

[110] Syngas Market | 2022 - 27 | Industry Share, Size, Growth - Mordor Intelligence, (2022). https://www.mordorintelligence.com/industry-reports/syngas-market (accessed March 24, 2022).

[111] J.M. Saad, P.T. Williams, Pyrolysis-catalytic dry (CO_2) reforming of waste plastics for syngas production: Influence of process parameters, Fuel. 193 (2017) 7–14. https://doi.org/10.1016/j.fuel.2016.12.014.

[112] J.M. Saad, P.T. Williams, Manipulating the H_2/CO ratio from dry reforming of simulated mixed waste plastics by the addition of steam, Fuel Processing Technology. 156 (2017) 331–338. https://doi.org/10.1016/j.fuproc.2016.09.016.

[113] J.M. Saad, M.A. Nahil, P.T. Williams, Influence of process conditions on syngas production from the thermal processing of waste high density polyethylene, J Anal Appl Pyrolysis. 113 (2015) 35–40. https://doi.org/10.1016/J.JAAP.2014.09.027.

[114] J.M. Saad, M.A. Nahil, C. Wu, P.T. Williams, Influence of nickel-based catalysts on syngas production from carbon dioxide reforming of waste high density polyethylene, Fuel Processing Technology. 138 (2015) 156–163. https://doi.org/10.1016/j.fuproc.2015.05.020.

[115] M. Al-asadi, N. Miskolczi, Z. Eller, Pyrolysis-gasification of wastes plastics for syngas production using metal modified zeolite catalysts under different ratio of nitrogen/oxygen, J Clean Prod. 271 (2020). https://doi.org/10.1016/J.JCLEPRO.2020.122186.

[116] J.M. Saad, P.T. Williams, Pyrolysis-Catalytic-Dry Reforming of Waste Plastics and Mixed Waste Plastics for Syngas Production., Energy and Fuels. (2016). https://doi.org/10.1021/acs.energyfuels.5b02508.

[117] J.M. Saad, P.T. Williams, Catalytic dry reforming of waste plastics from different waste treatment plants for production of synthesis gases, Waste Management. 58 (2016) 214–220. https://doi.org/10.1016/J.WASMAN.2016.09.011.

[118] S. Devasahayam, Catalytic actions of $MgCO_3$/MgO system for efficient carbon reforming processes, Sustainable Materials and Technologies. 22 (2019). https://doi.org/10.1016/J.SUSMAT.2019.E00122.

[119] Y. Kathiraser, U. Oemar, E.T. Saw, Z. Li, S. Kawi, Kinetic and mechanistic aspects for CO_2 reforming of methane over Ni based catalysts, Chemical Engineering Journal. 278 (2015) 62–78. https://doi.org/10.1016/J.CEJ.2014.11.143.

[120] R. Mahfouz, Synthèses et Caractérisations de Catalyseurs à Base de Nickel et/ou de Ruthénium pour la Valorisation du CO_2 via la Méthanation ou le Reformage à Sec du Méthane, 2021.

[121] S. Afzal, D. Senguptab, M.M. El-Halwagi, N. Elbashir, Minimizing CO_2 emissions for syngas production units using Dry Reforming of Methane, Computer Aided Chemical Engineering. 40 (2017) 2617–2622. https://doi.org/10.1016/B978-0-444-63965-3.50438-4.

[122] E. Dahdah, The role of Mg-Al hydrotalcite derived mixed oxides as catalytic support materials: Applications in the transesterification of vegetable oils for biodiesel production and in the steam reforming of glycerol for hydrogen production, 2018.

[123] M.D. Argyle, C.H. Bartholomew, Heterogeneous catalyst deactivation and regeneration: A review, Catalysts. 5 (2015) 145–269. https://doi.org/10.3390/catal5010145.

[124] X. Hu, X. Jia, C. jun Liu, The structural effect of Ni/ZrO_2 on the formation and the reactivity of the carbon formed from methane decomposition, Chemical Engineering Science: X. 11 (2021). https://doi.org/10.1016/J.CESX.2021.100104.

[125] Y. Zhang, W. Wang, Z. Wang, X. Zhou, Z. Wang, C.J. Liu, Steam reforming of methane over Ni/SiO_2 catalyst with enhanced coke resistance at low steam to methane ratio, Catal Today. 256 (2015) 130–136. https://doi.org/10.1016/J.CATTOD.2015.01.016.

[126] K. Wittich, M. Krämer, N. Bottke, S.A. Schunk, Catalytic Dry Reforming of Methane: Insights from Model Systems, ChemCatChem. 12 (2020) 2130–2147. https://doi.org/10.1002/CCTC.201902142.

[127] B. Abdullah, N.A. Abd Ghani, D.V.N. Vo, Recent advances in dry reforming of methane over Ni-based catalysts, J Clean Prod. 162 (2017) 170–185. https://doi.org/10.1016/J.JCLEPRO.2017.05.176.

[128] M. Usman, W.M.A. Wan Daud, H.F. Abbas, Dry reforming of methane: Influence of process parameters - A review, Renewable and Sustainable Energy Reviews. 45 (2015) 710–744. https://doi.org/10.1016/J.RSER.2015.02.026.

[129] M. Abou Rjeily, C. Gennequin, H. Pron, E. Abi-Aad, J.H. Randrianalisoa, Pyrolysis-catalytic upgrading of bio-oil and pyrolysis-catalytic steam reforming of biogas: a review, Environ Chem Lett. 19 (2021) 2825–2872. https://doi.org/10.1007/s10311-021-01190-2.

[130] J. Abou Rached, M.R. Cesario, J. Estephane, H.L. Tidahy, C. Gennequin, S. Aouad, A. Aboukaïs, E. Abi-Aad, Effects of cerium and lanthanum on Ni-based catalysts for CO2 reforming of toluene, J Environ Chem Eng. 6 (2018). https://doi.org/10.1016/j.jece.2018.06.054.

[131] M. A. Álvarez, L.F. Bobadilla, V. Garcilaso, M.A. Centeno, J.A. Odriozola, CO_2 reforming of methane over Ni-Ru supported catalysts: On the nature of active sites by operando DRIFTS study, Journal of CO2 Utilization. 24 (2018) 509–515. https://doi.org/10.1016/j.jcou.2018.01.027.

[132] S.-L. Wu, M.-Y. Wey, Synthesis of Ni@Al_2O_3 nanocomposite with superior activity and stability for hydrogen production from plastic-derived syngas by CO_2-sorption-enhanced reforming, Int J Hydrogen Energy. 46 (2021) 39728–39735. https://doi.org/10.1016/j.ijhydene.2021.09.246.

[133] C. Gennequin, S. Hany, L. Tidahy, S. Aouad, J. Estephane,). Influence of the presence of ruthenium on the activity and stability of Co–Mg–Al-based catalysts in CO_2 reforming of methane for syngas production, Environ Sci Pollut Res Int. 23 (2016) 22744–22760.

Chapter 2

Analysis of Plastics and Synthesis/Characterization of the Catalysts

Table of Contents

List of Figures

List of Tables

1. Plastic samples

1.1. Origin

Due to the wide variety of types of plastics, this part considers the major polymers found in industrial and household plastic waste: polyethylene (PE), polypropylene (PP), polystyrene (PS), and polyethylene terephthalate (PET). The plastic samples were identified by their resin identification codes (PE = 2, PP = 5, PS = 6, and PET = 1) and cleaned after all external materials (stickers, labels, etc.) were removed. The clean and dry samples (**fig. 2.1**) were cut into small pieces (around 3 mm) to fit into the pyrolysis reactor and enhance gas distribution during test.

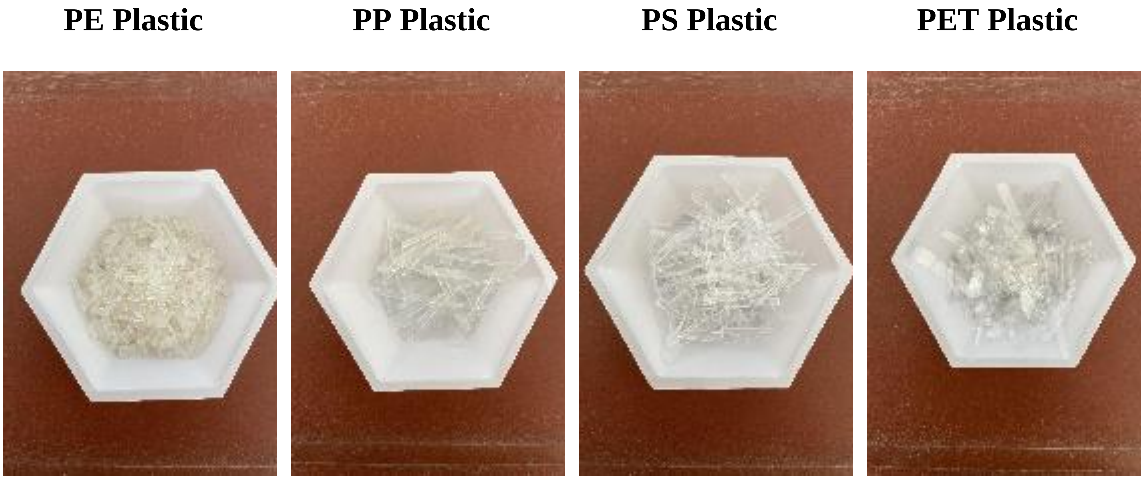

PE Plastic **PP Plastic** **PS Plastic** **PET Plastic**

Fig. 2.1 Clean and cut plastic samples

1.2. Characterization

1.2.1. Thermal analysis of plastics

During the pyrolysis of plastics, temperature is a critical parameter because it regulates the cracking of the polymer chain. Temperature can cause changes in the chemical and physical properties of a solid, which can be accompanied with an exothermic process (heat release) or an endothermic process (heat absorption), as well as weight gain or weight loss [1].

The DSC/TG technique enables the identification of the progressive mass changes (as a percentage of the initial sample mass), and the determination of the temperatures that characterize the stages of mass gain or mass loss [2].

To inspect the thermal analysis of the plastic samples, the two techniques (DSC/TG) were used concurrently. The principle is to measure the difference in heat flux between an aluminum crucible containing the plastic sample and an empty reference crucible. The thermal effects of the plastic were studied by heating the crucibles from ambient temperature to 900 °C with a 10 °C/min heating rate and a 30 ml/min flow of argon. The DSC curve offers information on the occurring degradation steps throughout the process, which is designated by the number of peaks. On the other hand, the TG curve reveals the change in the weight of a substance as a function of temperature and time [3]. The polymer chain is broken down into smaller hydrocarbon molecules during the thermal cracking process. It is an endothermic process that necessitates a certain amount of energy. As a result, we can see this energy directly in the heat flow signal (first endothermic peak). However, when the degradation of the polymer chain begins, the TG signal, which shows the steps associated with weight loss, does not show any weight loss. This is because, after the breakdown of polymer bonds (designated by an endothermic signal in the DSC profile), the initially produced products are very heavy to evaporate. However, with the progression of the reaction, lighter products are produced. These, at the reaction temperature, will eventually become volatile and evaporate from the crucible, resulting in the observed mass loss. The necessary heat for the hydrocarbons' evaporation will contribute to the DSC signal [4]. This trend is observed for polyethylene, polypropylene, and polyethylene terephthalate plastics. On the other hand, polystyrene plastics show a different trend, as will be detailed in the following section.

Polyethylene:

Fig. 2.2 shows the DSC-TG profile obtained for polyethylene plastic. The DSC signal reveals two endothermic peaks. The first, at 124 °C, corresponds to the fusion of the PE sample. Therefore, no corresponding change in weight is noticed. The second peak appears at elevated temperatures, corresponding to the breakdown of the polymer, which is complemented by a major weight loss (84%) attributed to the lighter products' evaporation. From the DSC-TG profile, it is evident that the thermal degradation began at 350 °C and ended at 550 °C. The maximum degradation rate of PE occurred at 484 °C. This temperature will be used when performing the plastic pyrolysis-reforming experiments.

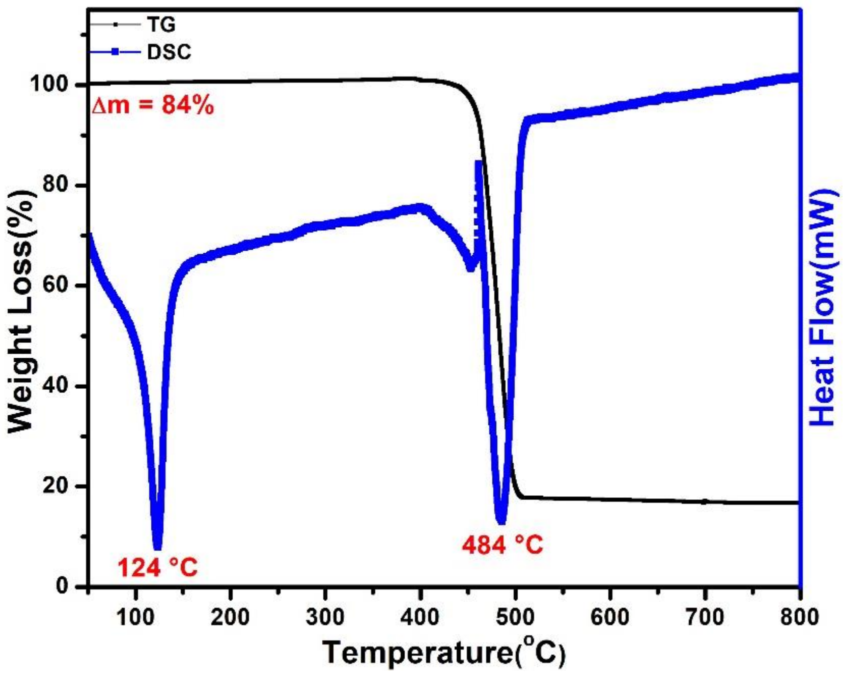

Fig. 2.2 DSC-TG curves of polyethylene plastic

Polypropylene:

As shown in **fig. 2.3**, the main decomposition of polypropylene occurred between 400 °C and 500 °C. The first peak in the DSC curve represents the fusion of the PP sample at 175 °C. The maximum degradation temperature for PP is around 463 °C where the main weight loss (83%) took place. Compared to PE, every second carbon in the PP molecule has a methyl group. This means that half of the carbons in the polypropylene chain are tertiary carbons, making tertiary carbocation formation easier during degradation [5]. Therefore, due to their active decomposition, PP thermally degrades at a faster rate compared to PE, and thus the weight loss found in the TGA graph above starts at a lower temperature compared to PE.

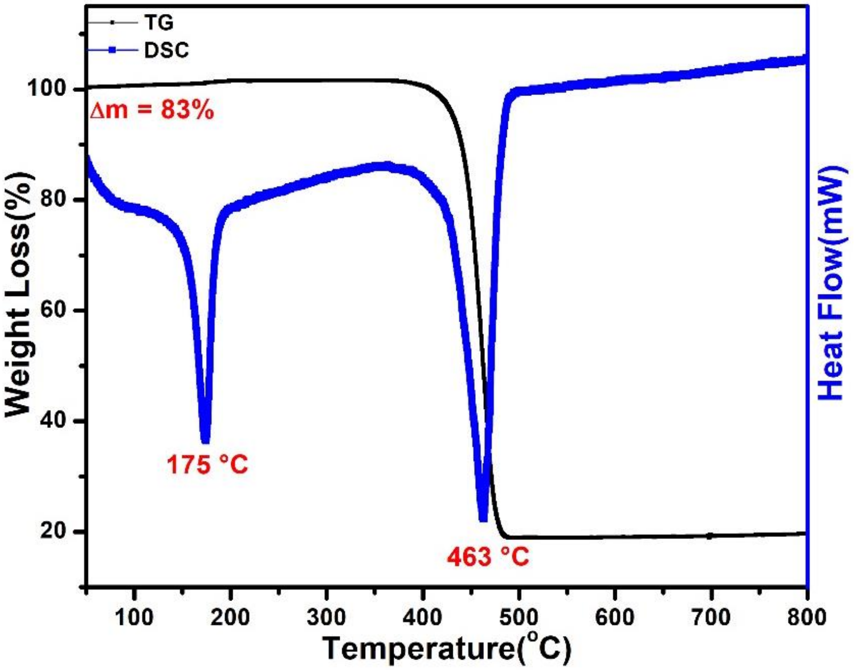

Fig. 2.3 DSC-TG curves of polypropylene plastic

Polyethylene terephthalate:

The PET thermal decomposition in **fig. 2.4** shows that PET fusion occurs at temperatures ranging from 209 °C to 298 °C. The main degradation began at 400 °C, with most of the sample's weight loss (68%) occurring at 428 °C due to structural backbone decomposition. At temperatures above 490 °C, no significant changes occurred. We can deduce that the PET thermal degradation occurred between 380 °C and 500 °C. The results are in accordance with Çepelioğullar and Pütün [6], who noticed that the PET thermal degradation starts above 360 °C, with the most noticeable peak appearing at 428 °C.

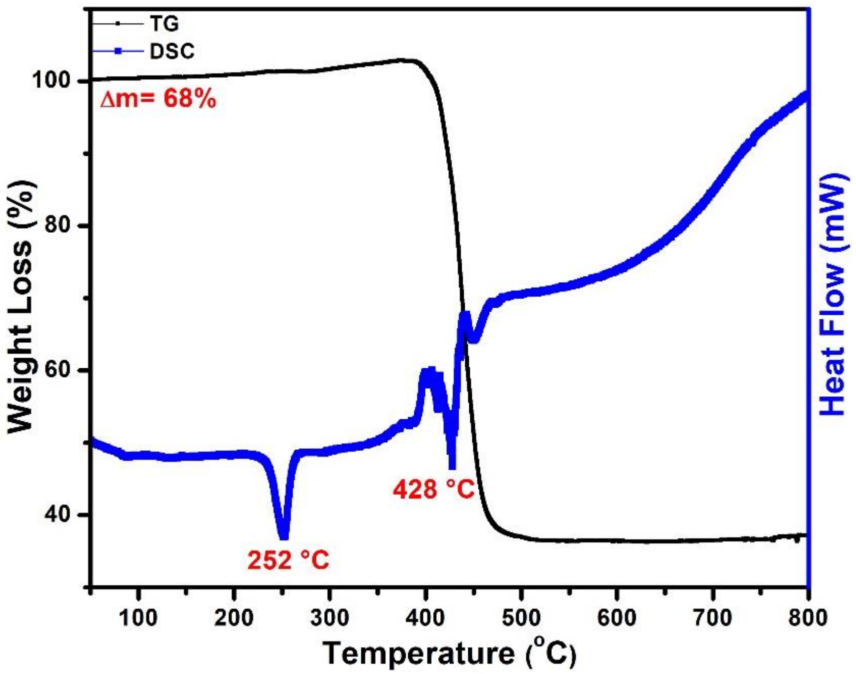

Fig. 2.4 DSC-TG curves of polyethylene terephthalate plastic

Polystyrene:

Fig. 2.5 shows that PS degrades in a single step [7]. In comparison with the pyrolysis of other plastics, PS degrades at the lowest temperature. The DSC-TG profile shows that the PS maximum weight loss of 80% occurred at 423 °C, with only one peak observed on the DSC curve. This is because the PS completely degrades into a dark viscous oil at 350 °C, with the highest amount achieved at 423 °C [8]. We can conclude that PS thermally degrades between 350 °C and 475 °C.

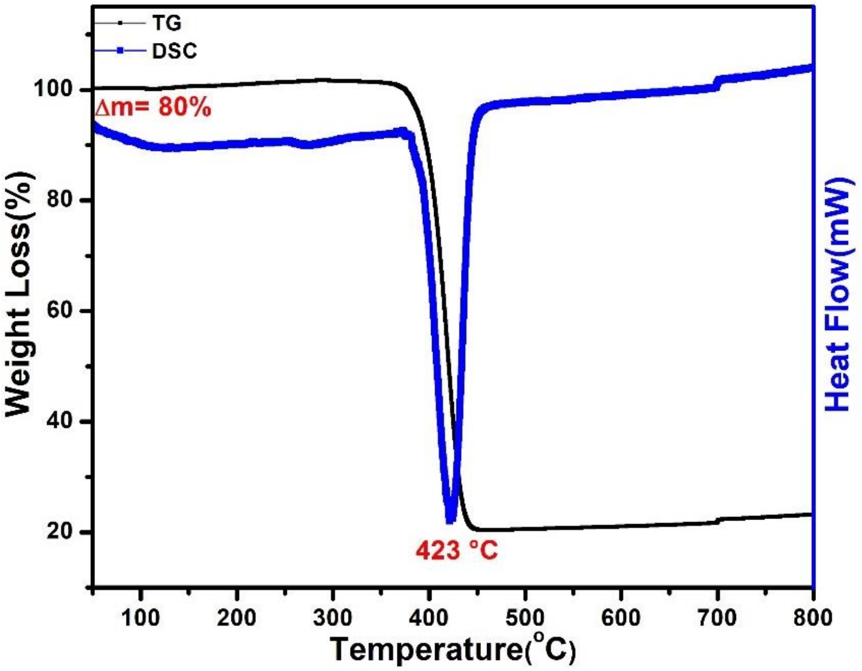

Fig. 2.5 DSC-TG curve of polystyrene plastic

1.2.2. Pyrolysis-Gas Chromatography/Mass Spectrometry

A pyrolyzer linked to gas chromatography and mass spectrometry (Py-GC/MS) is used to analyze the primary reactions of the fast pyrolysis of the subsequent plastics: polyethylene (PE), polypropylene (PP), polyethylene terephthalate (PET), and polystyrene (PS). The equipment setup directly transfers the produced gaseous compounds from the pyrolyzing unit to the gas chromatography for separation. The separated gaseous products are then routed into a detector to be identified and quantified. The identification of unknown substances is frequently performed using an MS detector. However, the MS detector cannot be used for quantification since it produces a total ion chromatogram (TIC), which represents the total number of fragment ions from a molecule. The TIC signal will be strong if a molecule easily breaks, and the inverse is also true [9]. As a result, mass spectrometry is only appropriate for qualitative analysis.

The following section shows the formed products from the pyrolysis of the original sample polymer (PE, PP, PET, and PS) under monitored conditions: a specific temperature of 550 °C and in the presence of helium as an inert gas.

Polyethylene:

During pyrolysis, the carbon backbone of PE is cut into a wider assortment of smaller hydrocarbons with terminal free radicals via a random scission mechanism. These free radicals could be stabilized by either removing hydrogen from a neighboring molecule, resulting in a saturated end group, or by β-scission, resulting in the backbone degradation and the formation of a terminal free radical and an unsaturated end [10]. **Fig. 2.6** shows the proposed mechanism of the PE pyrolysis process, which yields hydrocarbons that are either saturated (*n*-alkanes), unsaturated with a double bond (α-alkene), or unsaturated with double bonds at both ends (α, ω-alkadienes) [9,11,12]. The fast pyrolysis of PE in laboratory studies reveals that aliphatic hydrocarbons (up to C_{31}) are the initial gas products. Alkenes have the highest yield of aliphatic hydrocarbons, followed by alkanes, while alkadienes exhibit the lowest yield [9].

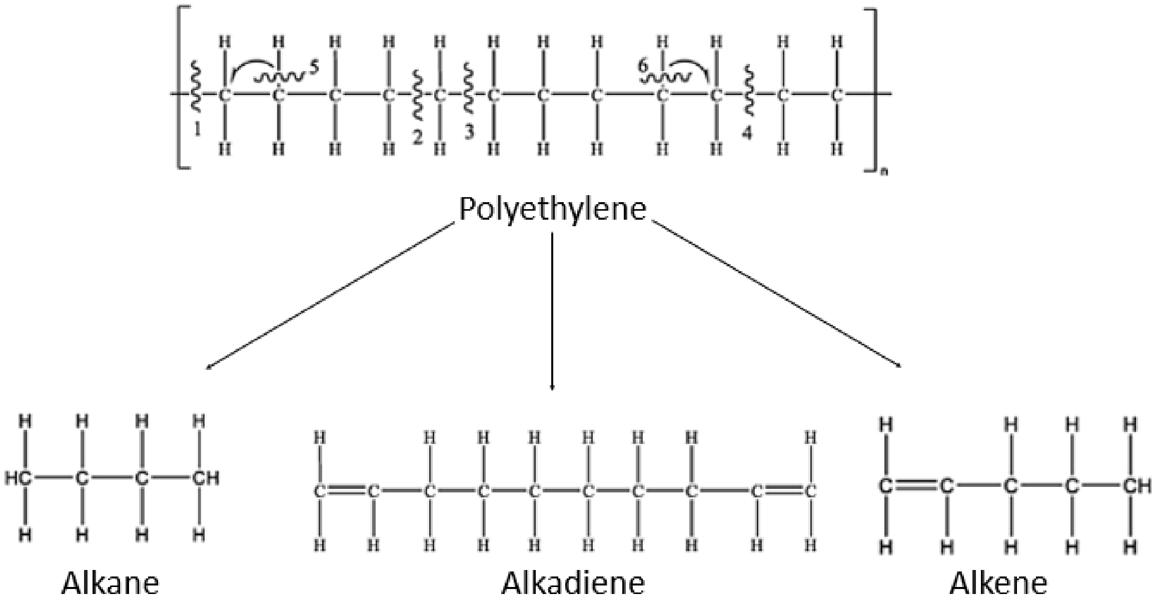

Fig. 2.6 Suggested mechanism of PE pyrolysis [9]

Fig. 2.7 displays the Py-GC/MS chromatogram (pyrogram) obtained following the pyrolysis of polyethylene at 550 °C. The pyrogram of **fig. 2.8** is a zoom-in of **fig. 2.7** and is made up of serial triplets that respectively correspond to C_{17}-C_{32}, α, ω-alkadienes, α-alkene, and *n*-alkanes.

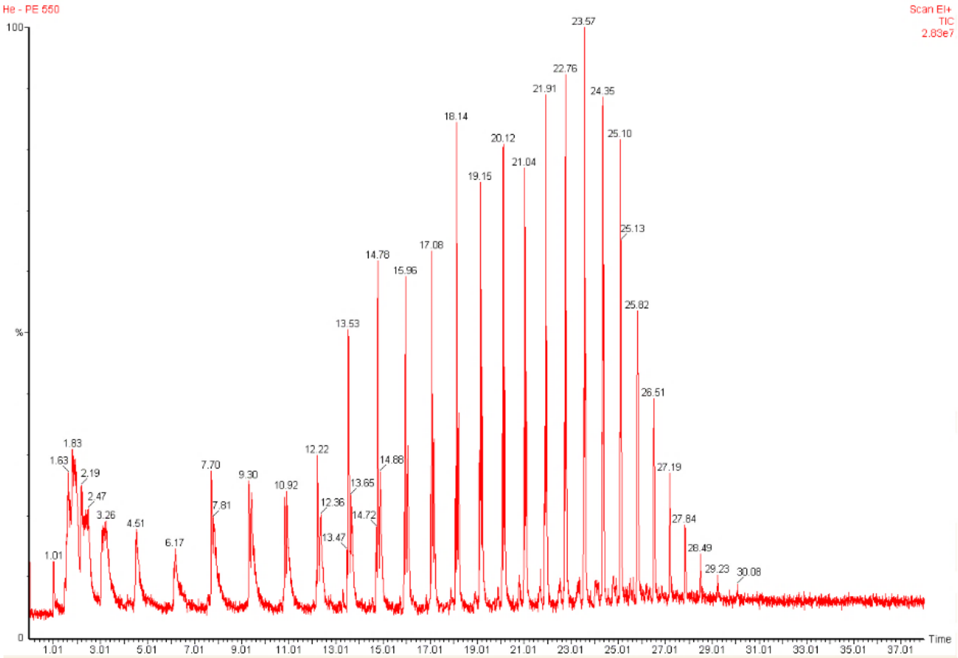

Fig. 2.7 Py-GC/MS (pyrogram) of PE at 550 °C.

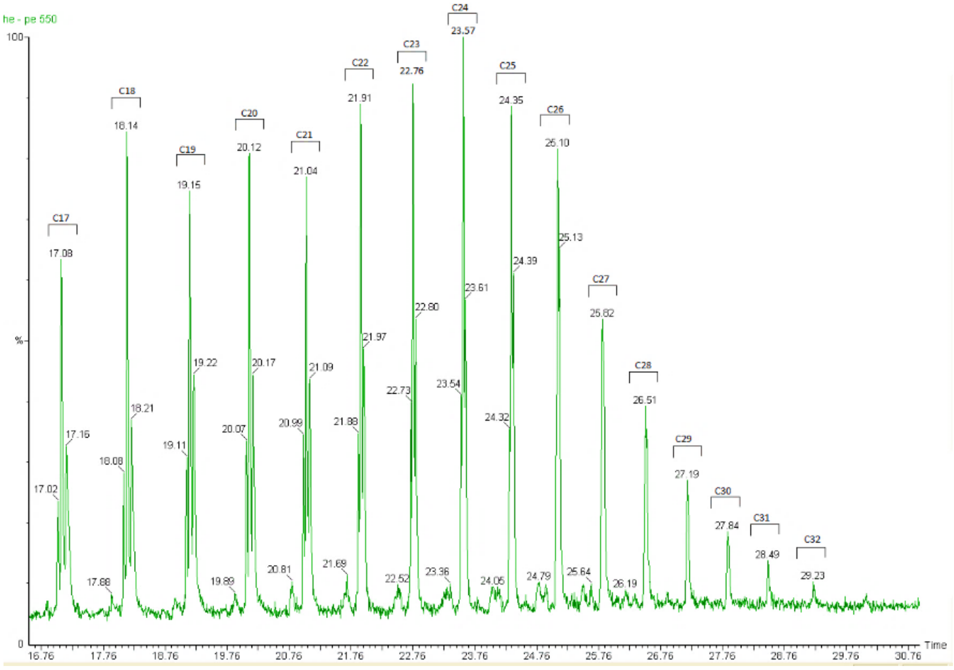

Fig. 2.8 Py-GC/MS (pyrogram) of PE at 550 ºC. Range 16.76-30.76 min.

Compound identification was accomplished by comparing retention times and mass spectra of a standard hydrocarbon sample, analyzing the mass spectra, and comparing the results with the National Institute of Standards and Technology (NIST) webbook data. **Fig. 2.9** depicts a comparison of the identified C_{17}-C_{23} hydrocarbon triplets with the mass spectra of a known hydrocarbon standard.

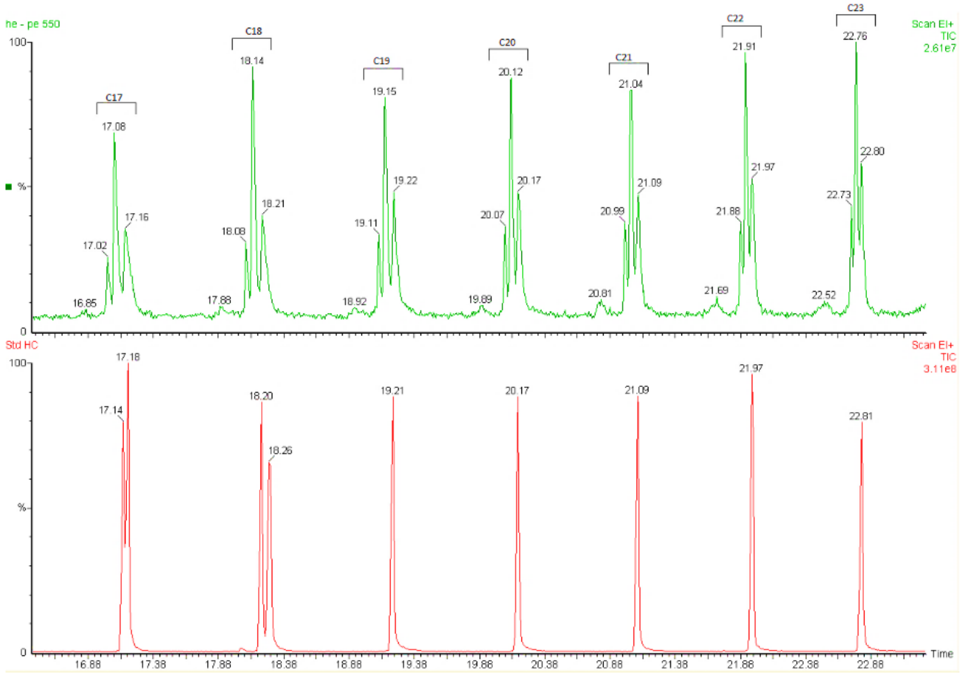

Fig. 2.9 Py-GC/MS (pyrogram) of PE at 550ºC in comparison with a standard hydrocarbon. Range 16.76-30.76 min. Peak identification- triplet C17: 17.02 min-heptadecadiene, 17.08 min- heptadecene, 17.16 min-heptadecane; triplet C18: 18.08 min- octadecadiene, 18.14 min- 3-octadecene, 18.21 min- 2-methylheptadecene; triplet C19: 19.11 min- nonadecadiene, 19.15 min- 1-nonadecene, 19.22 min-nonadecane; triplet C20: 20.07 min- 1,19-eicosadiene, 20.12 min- 3-eicosene, 20.17 min- eicosane; triplet C21: 20.99 min- heneicosadiene, 21.04 min- heneicosene, 21.09 min- heneicosane; triplet C22: 21.88 min-docosadiene, 21.91 min- docosene, 21.97 min- docosane; triplet C23: 22.73 min- tricosadiene, 22.76 min-tricosene, 22.80 min- tricosane.

Polypropylene:

Polypropylene is synthesized through the radical polymerization of propylene [$(CH_2 = CH\text{-}CH_3)$] monomers. The polypropylene polymer's random chain scission generates primary and secondary radicals. Intramolecular radical transfer reactions sequentially form tertiary radicals. These tertiary radicals undergo β-cleavage, which may lead to unsaturated (alkenes) and saturated (alkanes) branch fragments. As shown in **fig. 2.10**, the three most important gas products are pentane, propene, and 2,4-dimethyl-1-heptene. Hydrocarbons up to C_{12} (alkanes, alkenes, and alkyl-alkenes) accounted for 80% of total gas products, with alkenes yielding the highest and alkanes the lowest [9].

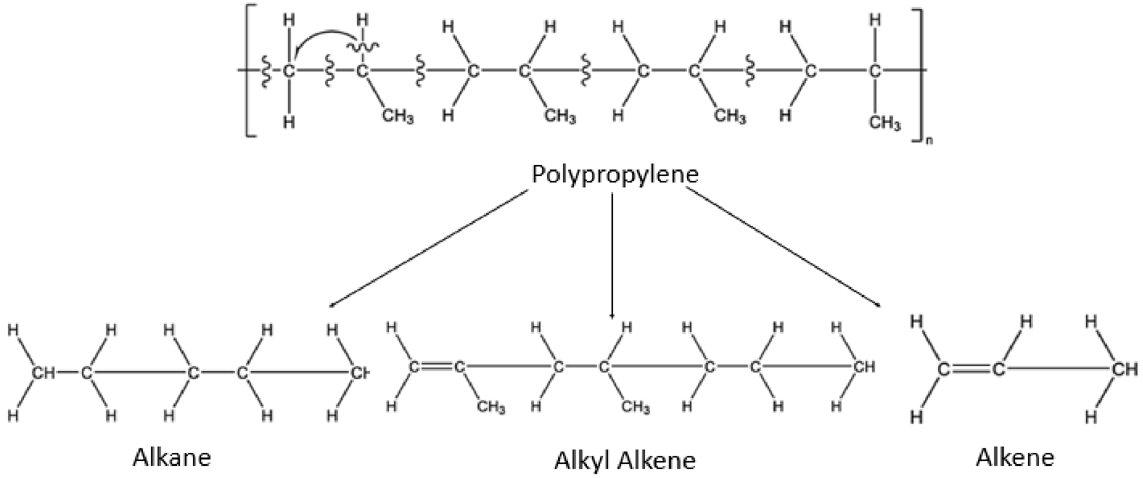

Fig. 2.10 Suggested mechanism of PP pyrolysis [9]

Fig. 2.11 shows the pyrogram of the degradation of polypropylene at 550 °C. As the compound degrades, a pattern of the peaks is noticed, with the main peaks representing the propylene monomer and the branched alkenes such as the propylene dimer (2-methyl-1-pentene), trimer (2,4-dimethyl-1-heptene), tetramer (2,4,6-trimethyl-1-nonene), pentamer (4,6,8-tetramethyl-1-undecene), etc. [13]. Through random chain scission, PP produces the monomer (propene) and oligomers [5].

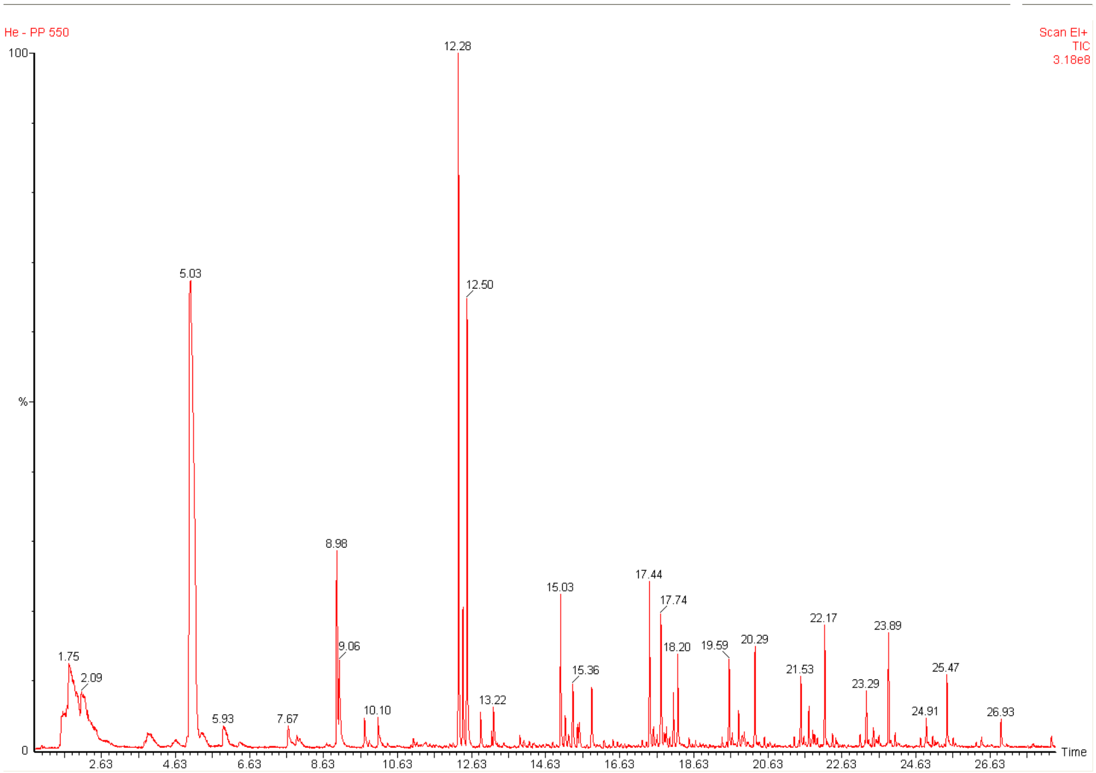

Fig. 2.11 Py-GC/MS (pyrogram) of PP at 550 °C. Peak identification: 5.03 min-propylene; 8.06 min-2-methyl-1-pentene (propylene dimer); 12.28 min-2,4-dimethyl-1-heptene (propylene trimer); 15.03 min-2,4,6-trimethyl-1-nonene (propylene tetramer).

Polyethylene Terephthalate:

Fig. 2.12 shows the pyrogram of the pyrolysis of PET at 550 °C. Peaks representing the phthalate monomer (tr = 15.72 min) and dimer (tr = 25.46 min) are observed. Also, large peaks representing benzoic acid (tr = 11.40 min) and 3-formyl benzoic acid (tr = 16.71 min) are detected. This plastic is hazardous due to the formation of benzoic acid. The pyrolysis of PET would lead to corrosion and clogging, eventually destroying of the setup [14].

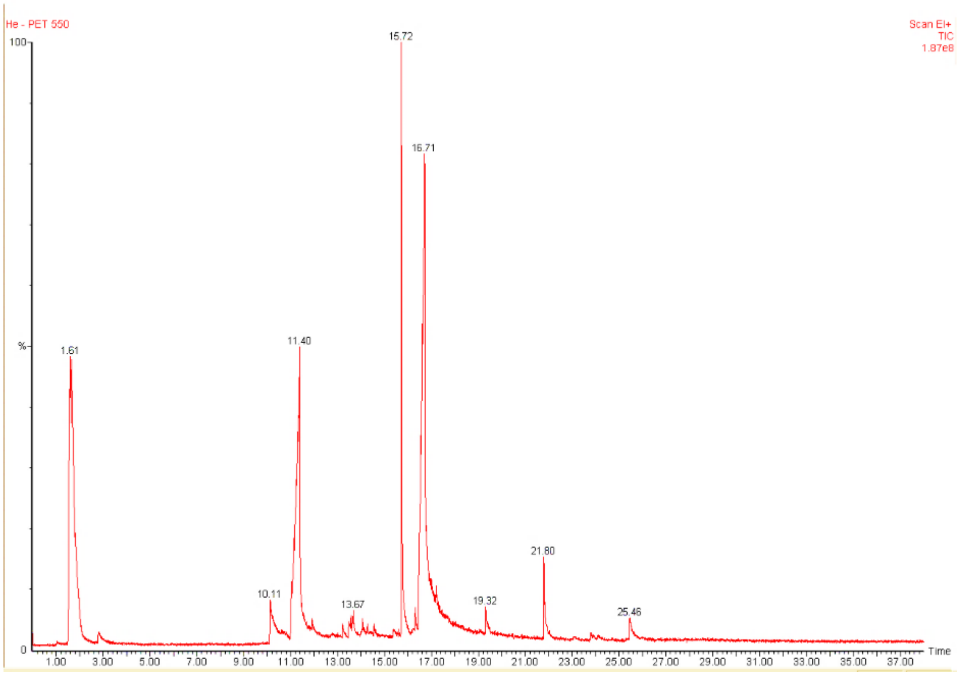

Fig. 2.12 Py-GC/MS (pyrogram) of PET at 550 °C. Peak identification: 1.61 min- carbon dioxide; 2.85 min- benzene; 10.11 min- toluene; 11.4 min- benzoic aicd; 15.72 min- phthalate monomer; 16.71 min-3-formyl benzoic acid; 19.32 min- benzophenone; 21.80 min- benzoyl bromide; 25.46 min- phthalate dimer.

Polystyrene:

According to the literature [15–17], the primary reaction of polystyrene fast pyrolysis produces styrene, as well as less significant yields of aromatic compounds such as benzene, toluene, methyl styrene, styrene dimer, and styrene trimer [9]. **Fig. 2.13** shows the proposed mechanism of PS pyrolysis producing the styrene monomer, dimer, and trimer. The pyrogram in **fig. 2.14** is like what is found in the literature. As shown, the major product from the polystyrene thermal decomposition at 550 °C is the monomer styrene (tr = 6.05 min), while the amounts of styrene dimer (tr = 17.54 min) and styrene trimer (tr = 24.16 min) were lower.

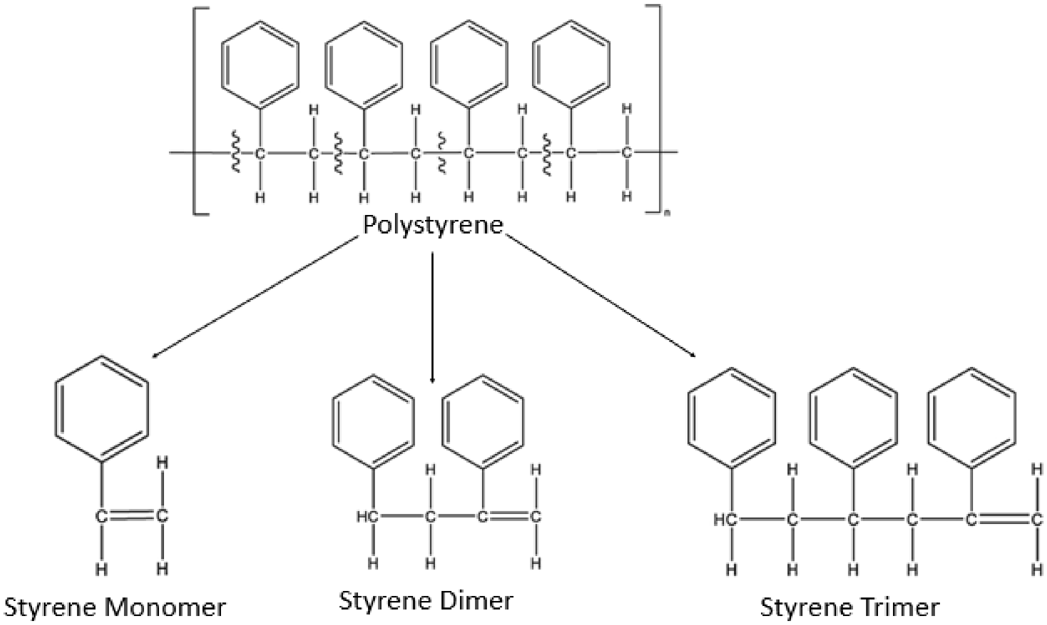

Fig. 2.13 Suggested mechanism of PS pyrolysis [9]

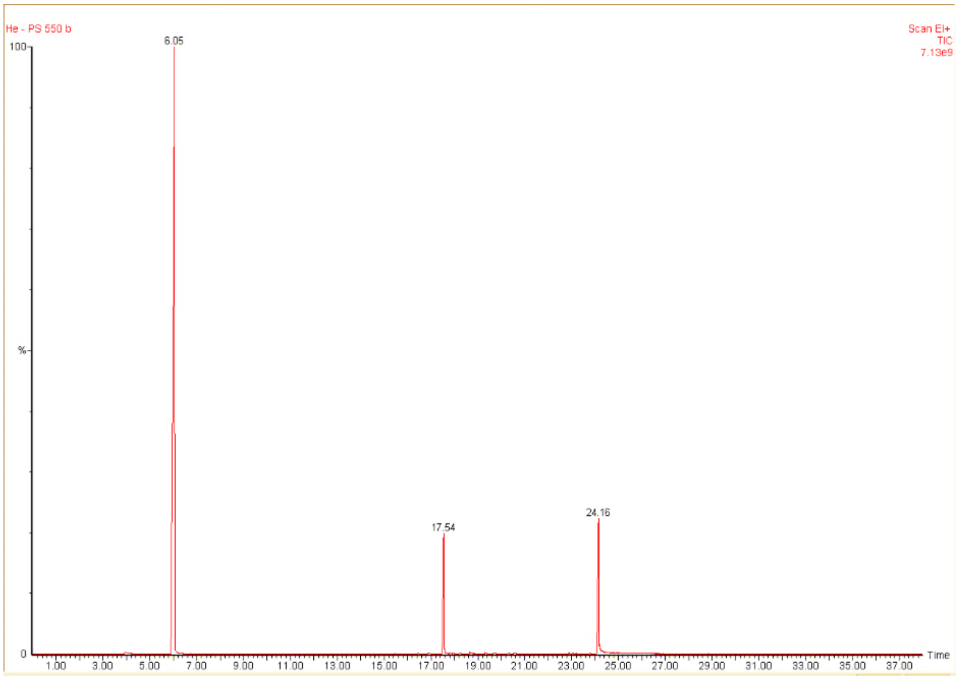

Fig. 2.14 Py-GC/MS (pyrogram) of PS at 550 °C. Peak identification: 6.05 min- styrene monomer; 17.54 min- styrene dimer; 24.16 min- styrene trimer.

1.3. Conclusion:

The thermal degradation of four diverse types of plastics was studied. The temperature range where pyrolysis begins and ends, was determined using the DSC-TG profiles. These outcomes will help in determining the pyrolysis conditions during the pyrolysis-reforming experiments. The Py-GC/MS technique proved to be an efficient method for determining the pyrolysis products obtained from the pyrolysis of plastics. It will be interesting to reform the gases that resulted from the pyrolysis of plastics via the catalytic dry reforming process. Based on the findings, the work will concentrate on the pyrolysis of polyethylene, polypropylene, and polystyrene. The pyrolysis of polyethylene terephthalate is avoided due to the formation of benzoic acid, which could damage the setup. Details concerning the synthesized catalysts will be presented in the next section.

2. Al_2O_3 supported catalysts

2.1. Catalyst preparation

2.1.1. Synthesis of Al_2O_3 support

The preparation of mesoporous Al_2O_3 was adapted from the literature [18]. In a first beaker, aluminum isopropoxide was dissolved in an ethanol/isopropanol mixture and stirred for 1 hour at 50 °C. In a second beaker, a non-ionic F127 copolymer was dissolved in a mixture of ethanol and isopropanol and stirred for half an hour at 50 °C. A limited amount of water was then added dropwise over the latter solution to hydrolyze the polymer. The content of the first beaker was then gradually added to the second beaker, and the resulting white suspension was stirred for 4 hours at 50 °C, then aged at ambient temperature for 24 hours. The mixture was hydrothermally treated for 24 hours at 80 °C, then again at 150 °C. The resulting white material was washed with anhydrous ethanol. To discard the organic template, the powder was filtered, dried, and calcined under airflow at 550 °C at a heating rate of 1 °C/min for 4 hours.

2.1.2. Synthesis of xNiAl$_2$O$_3$ catalysts

The catalysts were synthesized by wet impregnation: 2 g of the Al_2O_3 support was impregnated with 100 ml solution of the nickel metal precursor (Ni $(NO_3)_2.6H_2O$ (P> 97 %)). The mixture was stirred at room temperature for 2 hours before the water was evaporated under vacuum. The resulting slurry was dried at 80 °C overnight and later calcined under air for 4 hours at 800 °C with a heating rate of 1 °C/min. The catalysts were named xNiAl$_2$O$_3$ where x is the mass percentage of Ni in the solid ranging from 5 to 50 wt.%.

2.1.3. Promotion of xNiAl$_2$O$_3$ catalysts with ruthenium

The bimetallic (Ru-Ni) catalysts were synthesized by simultaneously impregnating Ru and Ni on the alumina support using Ru (NO)(NO$_3$)$_3$ (1.5 wt.% Ru) and Ni (NO$_3$)$_2$.6H$_2$O (P> 97 %) as metal precursors. The catalysts were named 1RuxNiAl$_2$O$_3$, where x ranges from 5 to 25 wt.%, and were calcined at 800 °C.

2.2. Catalyst characterization

2.2.1. X-ray Diffraction (XRD)

Fig. 2.15 (a) shows XRD patterns of the synthesized Al$_2$O$_3$ support calcined at 550 °C and the different xNiAl$_2$O$_3$ catalysts calcined at 800 °C. The XRD patterns of the corresponding reduced catalysts (xNiAl$_2$O$_3$-red) at 800 °C are shown in **fig. 2.15** (b).

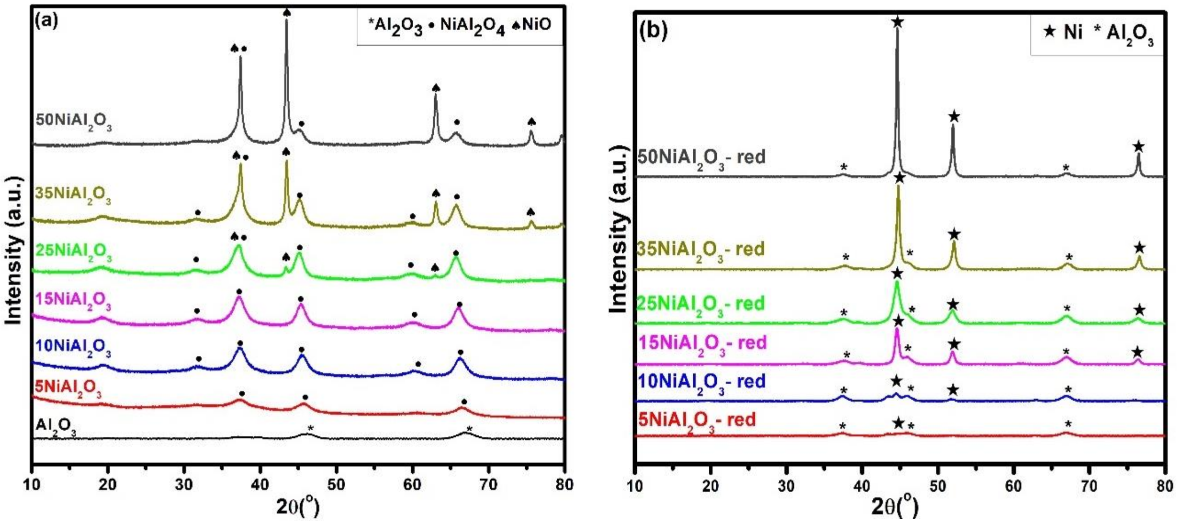

Fig. 2.15 XRD patterns of xNiAl$_2$O$_3$ catalysts (a) calcined at 800 °C and (b) reduced at 800 °C

For the XRD pattern of the Al$_2$O$_3$ support calcined at 550 °C, the γ-Al$_2$O$_3$ cubic structures are identified at 2θ = 37°, 39°, 46°, and 66° (JCPDS 50-0741). In the literature [18], the γ-Al$_2$O$_3$ has been described as a defect spinel structure characterized by oxygen atoms in cubically closed sites together with tetrahedral and octahedral aluminum cations in the lattices. The observed broad peaks indicate that the platelets responsible for pore formation are well disordered, demonstrating the amorphous structure of the alumina support [19].

The catalysts displayed XRD peaks for nickel aluminate (NiAl$_2$O$_4$) and nickel oxide (NiO). The peaks at 2θ = 19°, 32°, 37°, 43.2°, and 62.8° are assigned to the NiAl$_2$O$_4$ phase (JCPDS 10-0339), while the diffraction lines at 2θ = 37.2°, 43.1°, 63°, and 75.4° are assigned to the NiO phase

(JCPDS 44-1159). The NiO phase was observed for catalysts having a nickel loading greater or equal to 25 wt.%. Nickel aluminate is formed at high calcination temperatures when NiO bonds to the alumina support. These results indicate that the catalysts prepared are primarily composed of nickel, aluminum, and oxygen bonded together as nickel aluminate. Due to the strong interaction between the nickel and the support, the metal appears to be evenly dispersed throughout the catalysts. Since these catalysts were not reduced prior to their characterization, the XRD patterns show that all the metals impregnated on the support are in their oxide form [20]. Additionally, the patterns were similar, but a slight difference could be noticed in the diffraction peaks, which became sharper as the amount of nickel loading increases. As depicted in **fig. 2.16**, it is worth noting that the color of the catalysts of 5, 10, and 15 wt.% nickel loadings was blue due to the formation of $NiAl_2O_4$ phases. However, the color became dark green for 25, 35, and 50 wt.% nickel loadings, confirming the presence of NiO phases [21].

$5NiAl_2O_3$-800 **$10NiAl_2O_3$-800** **$15NiAl_2O_3$-800**

$25NiAl_2O_3$-800 **$35NiAl_2O_3$-800** **$50NiAl_2O_3$-800**

Fig. 2.16 Samples of calcined *x*$NiAl_2O_3$ catalysts

After reduction at 800 °C, nickel oxide species were reduced into metallic Ni. This is shown on the XRD pattern, where the diffraction lines of metallic Ni at $2\theta = 44.5°$, 52°, and 76° (JCPDS 04-0850) and γ-Al_2O_3 (JCPDS 50-0741) were observed.

Fig. 2.17 (a) shows the diffraction patterns of the promoted xNiAl$_2$O$_3$ with ruthenium after calcination. For 1RuAl$_2$O$_3$ and 1Ru5NiAl$_2$O$_3$ catalysts, the RuO$_2$ phase is noticeable at $2\theta = 28.1°$, 35.1°, 40°, and 54.1° (JCPDS 40–1290). This is probably due to the presence of ruthenium crystallites formed after the agglomeration of ruthenium oxide nanocrystals [19]. The absence of RuO$_2$ diffraction peaks in the 1Ru10NiAl$_2$O$_3$, 1Ru15NiAl$_2$O$_3$, and 1Ru25NiAl$_2$O$_3$ XRD patterns is probably due to the low content of these crystals or to their high dispersion in these solids [22]. After reduction, the catalysts were reduced to metallic nickel observed at $2\theta = 44.5°$, 52°, and 76° (JCPDS 04-0850) and γ-Al_2O_3 (JCPDS 50-0741), while metallic ruthenium at $2\theta = 38°$, 43°, 58°, and 69° (JCPDS 06-0663) was only observed for the 1Ru5NiAl$_2$O$_3$ catalyst, as shown in **fig. 2.17** (b).

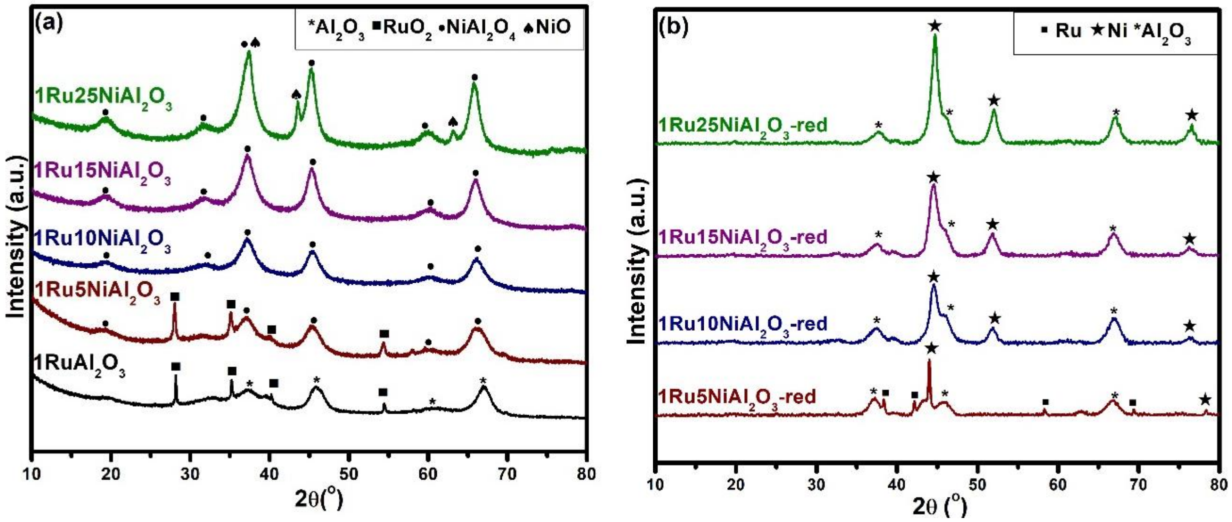

Fig. 2.17 XRD patterns of 1RuxNiAl$_2$O$_3$ catalysts (a) calcined at 800 °C and (b) reduced at 800 °C

The Ni crystallite sizes in the xNiAl$_2$O$_3$ and 1RuxNiAl$_2$O$_3$ catalysts were calculated using the Debye-Scherrer equation (Appendix A). From **table 2.1**, the Ni crystallite size in the reduced catalysts increases with the increase in nickel loading. These results show that when the nickel loading increases, the Ni species are more likely to sinter producing larger Ni crystals [23]. However, the promotion with Ru led to a decrease in Ni crystallite sizes compared to the nonpromoted counterparts. From the literature [24,25], Ru-NiAl_2O_3 catalysts are characterized by their smaller active metal crystallite sizes and a high degree of active metal dispersion.

Table 2.1 Ni crystallite sizes in *x*NiAl_2O_3 and 1Ru*x*NiAl_2O_3 catalysts reduced at 800 °C

Catalysts	Crystallite Size (nm)	Catalysts	Crystallite Size (nm)
	Ni		Ni
5NiAl_2O_3	9.3	**1Ru5NiAl_2O_3**	-
10NiAl_2O_3	9.57	**1Ru10NiAl_2O_3**	7.99
15NiAl_2O_3	12.26	**1Ru15NiAl_2O_3**	8.06
25NiAl_2O_3	14.38	**1Ru25NiAl_2O_3**	9.20
35NiAl_2O_3	18.97		
50NiAl_2O_3	28.95		

2.2.2. N_2 adsorption/desorption analysis

The nitrogen adsorption/desorption isotherms and the pore size distributions of the calcined Al_2O_3 supported catalysts are shown in **fig. 2.18** (a and b) and **fig. 2.19** (a and b), respectively. The textural properties associated with each are listed in **table 2.2**.

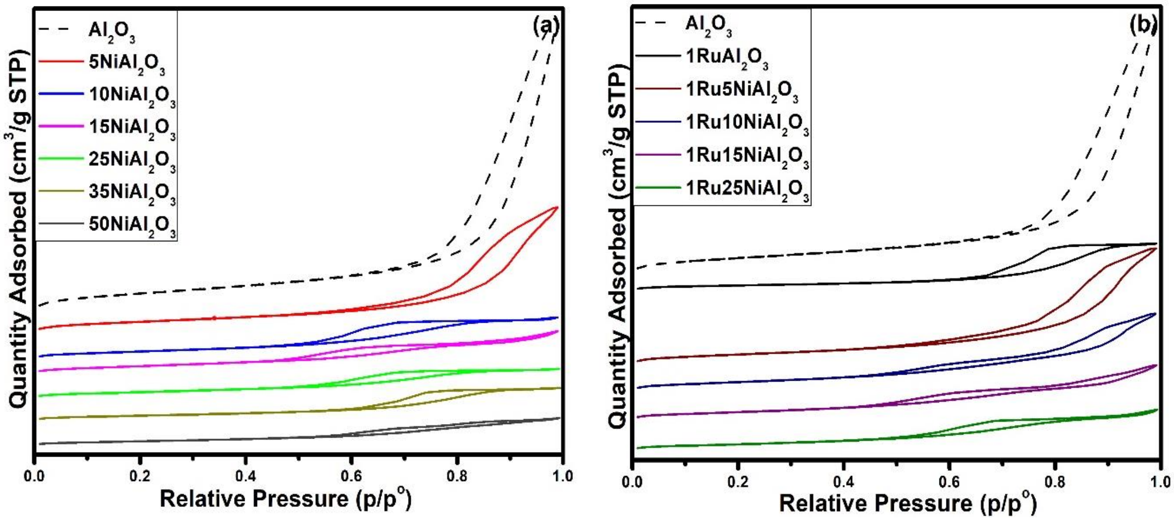

Fig. 2.18 N_2 adsorption/desorption isotherms of calcined (a) *x*NiAl_2O_3 and (b) 1Ru*x*NiAl_2O_3 catalysts

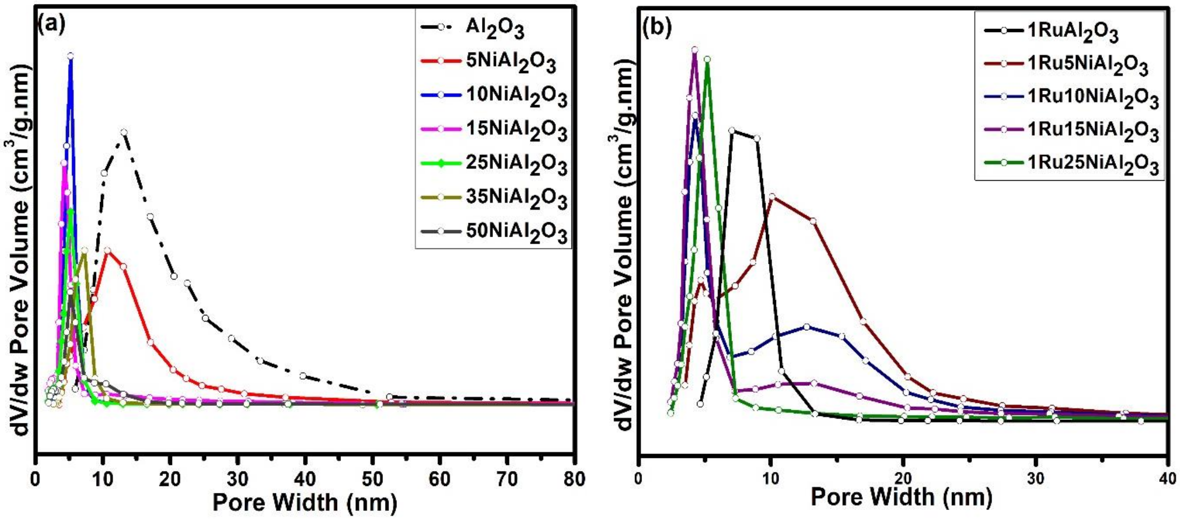

Fig. 2.19 Pore size distribution of calcined (a) *x*NiAl$_2$O$_3$ and (b) 1Ru*x*NiAl$_2$O$_3$ catalysts

According to the IUPAC classification of adsorption isotherms, porous Al$_2$O$_3$ support, *x*NiAl$_2$O$_3$, and 1Ru*x*NiAl$_2$O$_3$ catalysts exhibit a type IV isotherm with an H3 hysteresis loop, which is characteristic of a mesoporous structure with wormhole like pore distribution of the pores [26]. The shape of the isotherms slightly changes upon metal impregnation, suggesting that the synthesized mesoporous alumina material is resilient to textural alterations. It is noticed that the support exhibited larger pores at relative pressure p/p^o of 1. These pores become less evident as the Ni loading increases and disappear for Ni loadings ≥ 25 wt.%. This indicate that there are no macropores in the catalysts with high Ni loading. The adsorption volume in the hysteresis region decreased as the nickel content increased. These results indicate that smaller pores developed with increasing Ni content.

The broad range of pore distribution is a result of the disordered structure of mesoporous alumina [18], which agrees with the XRD results. The peak of pore size distribution shifted to smaller pore diameters, and its intensity decreased with increasing nickel content. The synthesized *x*NiAl$_2$O$_3$ catalysts showed a monomodal pore size distribution ranging between ~2 nm and ~35 nm for 5 wt.% nickel loading, with most of the pores at around 11 nm. The peaks got narrower (between ~2 nm and ~7 nm), with most of the pores at around 5 nm as the active phase loading increases up to 50 wt.%. A bi-modal pore size distribution is exhibited for the promoted 1Ru*x*NiAl$_2$O$_3$ catalysts. However, as the nickel loading increased to 25 wt.%, only one peak was noticed for the promoted catalyst. It is noticed that the promotion of the *x*NiAl$_2$O$_3$ catalysts with Ru reduced the pore diameter, demonstrating a uniform distribution of Ni across the surface and pores of the support

[27]. Moreover, the peaks become narrower as the active phase loading increases. This narrow pore size distribution positioned around 5 nm could be associated with capillary condensation in a mesoporous structure [25]. These results are in line with the crystallite size of the Ni particles which decreased after the promotion with Ru.

Table 2.2 shows the textural properties of the Al_2O_3-supported catalysts calcined at 800 °C. Alumina exhibits a large surface area [28] which is known to significantly improve catalytic activity [29]. The mesoporous support synthesized has a large surface area (388 m^2/g). The impregnation of the nickel active phase led to a decrease in the surface area due to the active phase filling the pores [30]. Moreover, during impregnation, the pore volume of mesoporous alumina drops from 1.281 cm^3/g to 0.162 cm^3/g when increasing the nickel metal loading up to 50 wt.%. This proves that the nickel active phase partially filled the pore structures of the supports. It is noticed for the support that most of the pores were had diameters in the 13 nm range. After impregnation with Ni, the pores were partially occupied with particles resulting in decrease in pore size.

However, the Ru containing catalysts exhibit slightly larger surface areas compared to their ruthenium free counterparts. According to a previous work by Elia et al., [22] the dispersion of the active phase in catalysts containing Ni and Ru was almost 2.5 times greater than in the Ni containing catalysts. This was explained by a synergistic effect between Ru and Ni that improves particles uniformity and structure, resulting in an ameliorated dispersion of metals [22]. Moreover, in the same study [22], the bimetallic catalyst showed smaller metal particle sizes, thus confirming that the presence of Ru enhanced the dispersion of nickel species. A study performed by Hossain et al. [25] showed that promoting $NiAl_2O_3$ catalysts with Ru resulted in smaller metal crystallite sizes and better metal dispersion. Incorporating Ru improved the metal-support interaction and prevented metal particle agglomeration on the catalyst surface.

Table 2.2 Textural properties of xNiAl$_2$O$_3$ and 1RuxNiAl$_2$O$_3$ catalysts

Catalyst	S_{BET}[a] (m^2/g)	Vp[b] (cm^3/g)	d_0[c] (nm)	Catalyst	S_{BET}[a] (m^2/g)	Vp[b] (cm^3/g)	d_0[c] (nm)
Al_2O_3	388	1.281	13.166	**1RuAl_2O_3**	142	0.343	7.989
5NiAl_2O_3	235	0.648	10.737	**1Ru5NiAl_2O_3**	249	0.720	10.348
10NiAl_2O_3	165	0.258	5.254	**1Ru10NiAl_2O_3**	217	0.483	4.276
15NiAl_2O_3	167	0.239	4.313	**1Ru15NiAl_2O_3**	186	0.336	4.275
25NiAl_2O_3	124	0.184	5.124	**1Ru25NiAl_2O_3**	149	0.260	5.125
35NiAl_2O_3	105	0.202	7.317				
50NiAl_2O_3	94	0.162	5.193				

[a] Specific surface area; [b] Pore volume; [c] Pore diameter

2.2.3. H_2-Temperature programmed reduction analyses (H_2-TPR)

H_2-TPR experiments were conducted to investigate the reducibility of NiO species and to have insights regarding their interaction with the support. **Fig. 2.20** (a and b) show the deconvoluted H_2-TPR profiles of the calcined xNiAl$_2$O$_3$ and 1RuxNiAl$_2$O$_3$ catalysts.

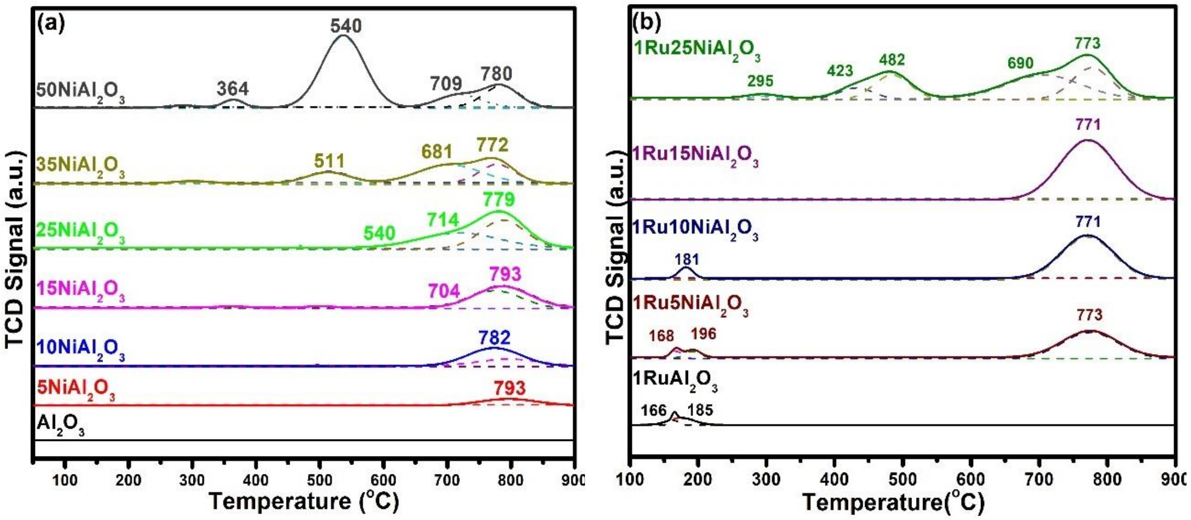

Fig. 2.20 H_2-TPR profiles of calcined (a) xNiAl$_2$O$_3$ and (b) 1RuxNiAl$_2$O$_3$ catalysts

In **fig. 2.20** (a), the H_2-TPR profile of the Al_2O_3 support showed no reduction peak, implying that Al_2O_3 is not reducible in the considered temperature range. It is observed that all xNiAl$_2$O$_3$ catalysts show a reduction peak around 800 ºC corresponding to the reduction of nickel aluminate species. The high reduction temperature is due to the strong interaction between Ni and Al_2O_3 following calcination at high temperatures. Moreover, it is noticed that the reduction temperature shifted to a lower temperature after increasing the Ni loading. The $5NiAl_2O_3$ catalyst showed the strongest interaction between the Ni species and the support. However, for high Ni loading, some of the NiO species will agglomerate rather than interact with the support, weakening its interaction with the support [23]. Therefore, a second reduction peak was obtained, with increasing Ni loading. The latter corresponds to the reduction of the NiO species weakly interacting with the support [31]. The intensity of these peaks increases as the nickel loading increases from 15 wt.% to 50 wt.% indicating that the fraction of agglomerated NiO is more important for higher Ni loadings.

Fig. 2.20 (b) reports the H_2-TPR analysis for the different $1Ru\mathit{x}NiAl_2O_3$ catalysts. The H_2-TPR profiles of $1Ru\mathit{x}NiAl_2O_3$ showed a first reduction event at relatively low temperatures, corresponding to the reduction of RuO_2 species. The $1RuAl_2O_3$, $1Ru5NiAl_2O_3$, and $1Ru10NiAl_2O_3$ catalysts exhibit low reduction peaks attributed to the reduction of well dispersed RuO_2 species [27]. When the Ni loading exceeds 10 wt.% by weight, this peak disappears. These results are in line with the XRD results (**Fig. 2.17** a), where RuO_2 species were only detected in these three catalysts. Furthermore, when compared to the $\mathit{x}NiAl_2O_3$ catalysts, the presence of ruthenium favored nickel reduction at lower temperatures. For example, once the $5NiAl_2O_3$ catalyst was promoted with 1 wt.% Ru, the reduction temperature shifted from 793 °C to 773 °C. The decrease in reduction temperature is due to Ru ability to prevent the migration of Ni ions into the support structure while also reducing the nickel-alumina interaction [27]. According to the literature [32], two primary steps take place: first, adjacent Ru and Ni atoms are reduced, resulting in a bimetallic phase; second, the remaining Ni oxides are reduced, resulting in a separate nickel phase. The lower Ni reduction temperature is due to the easier availability of hydrogen in the presence of ruthenium. This is known as the hydrogen spillover effect: on the Ru metallic surface, hydrogen atoms dissociate to form hydrogen species, which diffuse to the nickel species via the support surface, thereby enhancing their reduction [33].

Table 2.3 shows the experimental and theoretical H_2 consumptions of $\mathit{x}NiAl_2O_3$ and $1Ru\mathit{x}NiAl_2O_3$ catalysts. It is noticed that the total H_2 consumption of promoted catalysts is greater than that of the non-promoted nickel-based catalysts. For example, the reduction of $1Ru25NiAl_2O_3$ consumes 3624 $\mu H_2/g$ which is larger than the 2317 $\mu H_2/g$ obtained for $25NiAl_2O_3$. This shows that the nickel-based catalysts promoted with Ru hold more available Ni active sites than the non-promoted catalysts. Moreover, the difference in value between experimental and theoretical H_2 consumption in the nickel-based catalysts show that Ni is difficult to reduce and the equilibrium between nickel oxide and hydrogen varies depending on how much Ni interacts with the support. Therefore, Ni-support interactions can be characterized by the reducibility of nickel. According to the literature [34,35], nickel supported on alumina is not fully reduced to the metallic nickel due to the strong oxide support interaction. With an increase in reduction temperature and time, the amount of reduction to nickel metal increases, but it cannot be totally attained. This reduction depends on metal loading and calcination temperature and has been ascribed to the formation of $NiAl_2O_4$ spinel.

Table 2.3 Experimental and theoretical H_2 consumptions of *x*$NiAl_2O_3$ and 1Ru*x*$NiAl_2O_3$ catalysts

Catalyst	**H_2 Consumption [μH_2/g catalyst]**				
	Experimental Consumption				**Theoretical Consumption**
	I	**II**	**III**	**Total**	**Total**
5$NiAl_2O_3$	-	-	635	**635**	**897**
10$NiAl_2O_3$	-	-	1502	**1502**	**1843**
15$NiAl_2O_3$	-	-	1846	**1846**	**2879**
25$NiAl_2O_3$	-	85	2963	**3048**	**5315**
35$NiAl_2O_3$	60	541	2963	**3564**	**8394**
50$NiAl_2O_3$	394	6227	2915	**9536**	**15017**

Catalyst	**H_2 Consumption [μH_2/g catalyst]**						
	Experimental Consumption				**Theoretical Consumption**		
	I	**II**	**III**	**Total**	**NiO/Ni**	**RuO_2/Ru**	**Total**
1$RuAl_2O_3$	163	35		**198**	-	200	**200**
1Ru5$NiAl_2O_3$	130		935	**1065**	897	200	**1097**
1Ru10$NiAl_2O_3$	128		1847	**1975**	1843	200	**2043**
1Ru15$NiAl_2O_3$			2430	**2430**	2879	200	**3079**
1Ru25$NiAl_2O_3$		236	3338	**3624**	5315	200	**5515**

2.2.4. CO_2-Temperature Programmed Desorption Analysis (CO_2-TPD)

CO_2-TPD experiments were performed to gain further insight into the basicity of the catalysts by determining the strength of their basic sites. **Fig. 2.21** shows the CO_2-TPD profiles of calcined xNiAl$_2$O$_3$ and 1RuxNiAl$_2$O$_3$ catalysts.

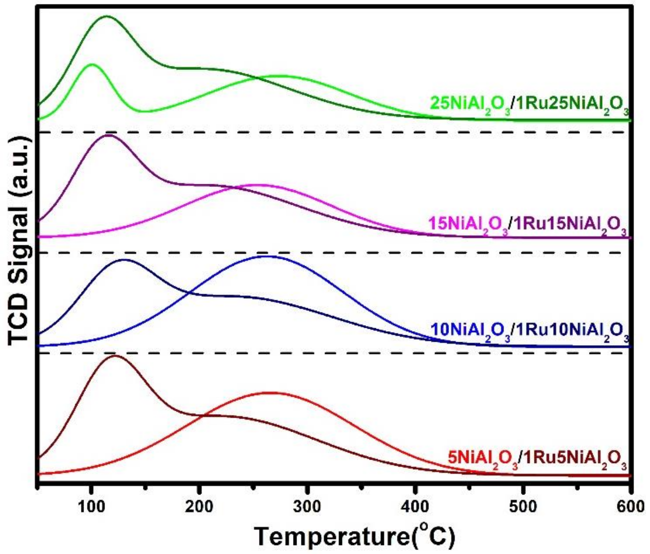

Fig. 2.21 CO_2-TPD profiles of calcined xNiAl$_2$O$_3$ and 1RuxNiAl$_2$O$_3$ catalysts

The curves define the distribution of basic catalyst sites as a function of desorption temperature; hence, a greater desorption temperature indicates a stronger interaction between carbon dioxide and the catalyst, and thus a stronger basic site [36]. According to the desorption temperature, two regions are distinguished: weak basic sites (between 50 °C and 150 °C) and moderate basic sites (between 150 °C and 450 °C).

CO_2-TPD profiles of xNiAl$_2$O$_3$ catalysts show one desorption peak of around 270 °C indicating the presence of medium basic sites. A weak basic site was noticed at around 100 °C for a Ni loading of 25 wt.%. This illustrates the impact of nickel incorporation into the support and may be responsible for the additional CO_2 adsorption sites at higher Ni loadings [37]. Once the catalysts were promoted with Ru, two peaks with different temperature regions are noticed, indicating weak and moderate active sites for CO_2 adsorption on the catalyst surface. The results show CO_2-desorbed peaks at low temperature indicating that in the presence of Ru more weak basic sites are present. Basic catalysts could enhance the CO_2 adsorption, which supplies surface oxygen for the gasification of coke during the dry reforming reaction, thus improving coke resistance. However, it is not plausible to measure catalytic activity and coke resistance solely on basic strength since catalytic performance also depends on several important parameters. These include metal support interaction, dispersion, active metal particle size, and degree of reduction [38].

2.3. Conclusion

From the XRD analysis, the nickel aluminate phase is observed for all catalysts. As the Ni loading increases above 25 wt.%, a NiO phase is formed. After reduction, some nickel phases were reduced to metallic Ni. The promotion of the catalyst with Ru led to a better dispersion of metal oxides species, with the RuO_2 phase only detectable in catalysts having low nickel loadings. The support and the catalysts displayed type IV adsorption isotherms, indicating their mesoporous nature. All the nickel-based catalysts had lower specific surface areas compared to the alumina support. However, enhanced surface areas were obtained after the promotion of the catalysts with ruthenium. From the H_2-TPR profiles, it is noticed that the reduction of the catalysts was enhanced due to the presence of Ru. From the CO_2-TPD profiles, the promoted catalysts exhibited more active sites which would enhance the CO_2 adsorption on the catalyst. Therefore, the promoted catalysts showed better active phase dispersion, higher surface areas, improved reducibility, and enhanced basic properties all of which may have a favorable impact on the catalytic activity.

3. References

[1] E. Dahdah, The role of Mg-Al hydrotalcite derived mixed oxides as catalytic support materials : Applications in the transesterification of vegetable oils for biodiesel production and in the steam reforming of glycerol for hydrogen production, 2018.

[2] C. Kassargy, Contribution à l’étude de la valorisation énergétique des résidus de plastique par craquage catalytique, 2018. https://tel.archives-ouvertes.fr/tel-01883636.

[3] S. Kumar, A.K. Panda, R.K. Singh, A review on tertiary recycling of high-density polyethylene to fuel, Resour Conserv Recycl. 55 (2011) 893–910. https://doi.org/10.1016/j.resconrec.2011.05.005.

[4] A. Coelho, L. Costa, M. das Mercês Marques, I. Fonseca, M.A. Lemos, F. Lemos, Using simultaneous DSC/TG to analyze the kinetics of polyethylene degradation-catalytic cracking using HY and HZSM-5 zeolites, Reaction Kinetics, Mecahnism and Catalysis. 99 (2010) 5–15. https://doi.org/10.1007/s11144-009-0114-1.

[5] S.H. Jung, M.H. Cho, B.S. Kang, J.S. Kim, Pyrolysis of a fraction of waste polypropylene and polyethylene for the recovery of BTX aromatics using a fluidized bed reactor, Fuel Processing Technology. 91 (2010) 277–284. https://doi.org/10.1016/j.fuproc.2009.10.009.

[6] Ö. Çepelioǿullar, A.E. Pütün, A pyrolysis study for the thermal and kinetic characteristics of an agricultural waste with two different plastic wastes, Waste Management and Research. 32 (2014) 971–979. https://doi.org/10.1177/0734242X14542684.

[7] S.A. Mansour, Study of thermal stabilization for polystyrene/carbon nanocomposites via TG/DSC techniques, Thermal Analysis and Calorimetry. 112 (2013) 579–583. https://doi.org/10.1007/s10973-012-2595-9.

[8] J.A. Onwudili, N. Insura, P.T. Williams, Composition of products from the pyrolysis of polyethylene and polystyrene in a closed batch reactor: Effects of temperature and residence time, J Anal Appl Pyrolysis. 86 (2009) 293–303. https://doi.org/10.1016/J.JAAP.2009.07.008.

[9] Supriyanto, P. Ylitervo, T. Richards, Gaseous products from primary reactions of fast plastic pyrolysis, J Anal Appl Pyrolysis. 158 (2021). https://doi.org/10.1016/J.JAAP.2021.105248.

[10] S.C. Moldoveanu, Pyrolysis of Hydrocarbons, Pyrolysis of Organic Molecules. (2019) 35–161. https://doi.org/10.1016/B978-0-444-64000-0.00002-0.

[11] T.P. Wampler, Applied pyrolysis handbook, Chromatographia 2007 66:9. 66 (2007) 827–827. https://doi.org/10.1365/S10337-007-0431-3.

[12] P. Kusch, Application of Pyrolysis-Gas Chromatography/Mass Spectrometry (Py-GC/MS), Comprehensive Analytical Chemistry. 75 (2017) 169–207. https://doi.org/10.1016/BS.COAC.2016.10.003.

[13] S. Tsuge, H. Ohtani, C. Watanabe, Pyrolysis - GC/MS Data Book of Synthetic Polymers, Pyrolysis - GC/MS Data Book of Synthetic Polymers. (2011). https://doi.org/10.1016/C2010-0-68897-3.

[14] G. Grause, A. Buekens, Y. Sakata, A. Okuwaki, T. Yoshioka, Feedstock recycling of waste polymeric material, Journal of Material Cycles and Waste Management . 13 (2011) 265–282. https://doi.org/10.1007/s10163-011-0031-z.

[15] J. Zhou, Y. Qiao, W. Wang, E. Leng, J. Huang, Y. Yu, M. Xu, Formation of styrene monomer, dimer and trimer in the primary volatiles produced from polystyrene pyrolysis in a wire-mesh reactor, Fuel. 182 (2016) 333–339. https://doi.org/10.1016/J.FUEL.2016.05.123.

[16] E.B. Hassan, I. Elsayed, A. Eseyin, Production high yields of aromatic hydrocarbons through catalytic fast pyrolysis of torrefied wood and polystyrene, Fuel. 174 (2016) 317–324. https://doi.org/10.1016/J.FUEL.2016.02.031.

[17] Z. Ahmad, F. Al-Sagheer, N.A. Al-Awadi, Pyro-GC/MS and thermal degradation studies in polystyrene-poly(vinyl chloride) blends, J Anal Appl Pyrolysis. 87 (2010) 99–107. https://doi.org/10.1016/J.JAAP.2009.10.010.

[18] V. Vosoughi, A.K. Dalai, N. Abatzoglou, Y. Hu, Performances of promoted cobalt catalysts supported on mesoporous alumina for Fischer-Tropsch synthesis, Appl Catal A Gen. 547 (2017) 155–163. https://doi.org/10.1016/j.apcata.2017.08.032.

[19] R. Mahfouz, J. Estephane, C. Gennequin, L. Tidahy, S. Aouad, E. Abi-Aad, CO2reforming of methane over Ni and/or Ru catalysts supported on mesoporous KIT-6: Effect of promotion with Ce, J Environ Chem Eng. 9 (2021). https://doi.org/10.1016/j.jece.2020.104662.

[20] J.M. Saad, M.A. Nahil, C. Wu, P.T. Williams, Influence of nickel-based catalysts on syngas production from carbon dioxide reforming of waste high density polyethylene, Fuel Processing Technology. 138 (2015) 156–163. https://doi.org/10.1016/j.fuproc.2015.05.020.

[21] B.C. Kwon, N.K. Park, M. Kang, D. Kang, M.W. Seo, D. Lee, S.G. Jeon, H.J. Ryu, CO_2 hydrogenation activity of Ni-Mg-Al_2O_3 catalysts: Reaction behavior on $NiAl2O_4$ and $MgAl_2O_4$, Korean Journal of Chemical Engineering. 38 (2021) 1188–1196. https://doi.org/10.1007/s11814-021-0778-4.

[22] N. Elia, J. Estephane, C. Poupin, B. el Khoury, L. Pirault-Roy, S. Aouad, E.A. Aad, A Highly Selective and Stable Ruthenium-Nickel Supported on Ceria Catalyst for Carbon Dioxide Methanation, ChemCatChem. 13 (2021) 1559–1567. https://doi.org/10.1002/cctc.202001687.

[23] Y.S. Seo, Y.S. Jung, W.L. Yoon, I.G. Jang, T.W. Lee, The effect of Ni content on a highly active Ni-Al_2O_3 catalyst prepared by the homogeneous precipitation method, Int J Hydrogen Energy. 36 (2011) 94–102. https://doi.org/10.1016/J.IJHYDENE.2010.09.082.

[24] R.Y. Chein, C.C. Wang, Experimental Study on CO_2 Methanation over Ni/Al_2O_3, Ru/Al_2O_3, and Ru-Ni/Al_2O_3 Catalysts, Catalysts 2020, Vol. 10, Page 1112. 10 (2020) 1112. https://doi.org/10.3390/CATAL10101112.

[25] M.Z. Hossain, M.B.I. Chowdhury, A.K. Jhawar, P.A. Charpentier, Supercritical water gasification of glucose using bimetallic aerogel Ru-Ni-Al_2O_3 catalyst for H_2 production, Biomass Bioenergy. 107 (2017) 39–51. https://doi.org/10.1016/J.BIOMBIOE.2017.09.010.

[26] G. Leofanti, M. Padovan, G. Tozzola, B. Venturelli, Surface area and pore texture of catalysts, Catal Today. 41 (1998). https://doi.org/10.1016/S0920-5861(98)00050-9.

[27] N.A. Roslan, S. Zainal Abidin, O.U. Osazuwa, S.Y. Chin, Y.H. Taufiq-Yap, Enhanced syngas production from glycerol dry reforming over Ru promoted -Ni catalyst supported on extracted Al_2O_3, Fuel. 314 (2022). https://doi.org/10.1016/J.FUEL.2021.123050.

[28] E. Saab, S. Aouad, E. Abi-Aad, M.N. Bokova, E.A. Zhilinskaya, A. Aboukaïs, Carbon black oxidation mechanism in loose and tight contacts with Al_2O_3 and CeO_2 catalysts, Kinetics and Catalysis. 48 (2007) 841–846. https://doi.org/10.1134/S0023158407060134.

[29] W. Wang, K. Zhang, Y. Yang, H. Liu, Z. Qiao, H. Luo, Synthesis of mesoporous Al_2O_3 with large surface area and large pore diameter by improved precipitation method, Microporous and Mesoporous Materials. 193 (2014) 47–53. https://doi.org/10.1016/j.micromeso.2014.03.008.

[30] E. Dahdah, S. Aouad, C. Gennequin, J. Estephane, B. Nsouli, A. Aboukaïs, E. Abi-Aad, Glycerol steam reforming over Ru-Mg-Al hydrotalcite-derived mixed oxides: Role of the preparation method in catalytic activity, Int J Hydrogen Energy. 43 (2018) 19864–19872. https://doi.org/10.1016/j.ijhydene.2018.09.042.

[31] S. Andraos, R. Abbas-Ghaleb, D. Chlala, A. Vita, C. Italiano, M. Laganà, L. Pino, M. Nakhl, S. Specchia, Production of hydrogen by methane dry reforming over ruthenium-nickel based catalysts deposited on Al_2O_3, $MgAl_2O_4$, and YSZ, Int J Hydrogen Energy. 44 (2019) 25706–25716. https://doi.org/10.1016/j.ijhydene.2019.08.081.

[32] Z. Ian, S. Das, M. Ing, H. Wai, P. Hongmanorom, S. Kawi, AReview on Bimetallic Nickel-Based Catalysts for CO_2 Reforming of Methane, ChemPhysChem. 18 (2017) 3117–3134.

[33] F.R. Lucci, M.D. Marcinkowski, T.J. Lawton, E.C.H. Sykes, H_2 Activation and Spillover on Catalytically Relevant Pt-Cu Single Atom Alloys, Journal of Physical Chemistry C. 119 (2015) 24351–24357. https://doi.org/10.1021/ACS.JPCC.5B05562/ASSET/IMAGES/MEDIUM/JP-2015-05562K_0004.GIF.

[34] C. Li, Y.W. Chen, Temperature-programmed-reduction studies of nickel oxide/alumina catalysts: effects of the preparation method, Thermochim Acta. 256 (1995) 457–465. https://doi.org/10.1016/0040-6031(94)02177-P.

[35] W.H. Ind Eng, I. Chen, D.-W. Shine, Principles of Polymer Chemistry, Z.; Biesenberger, J. A. Ind. Eng. Chem. Fundam. 27 (1988) 859–863. https://pubs.acs.org/sharingguidelines (accessed September 21, 2022).

[36] D. Méndez-mateos, V. Laura Barrio, J.M. Requies, J.F. Cambra, Effect of the Addition of Alkaline Earth and Lanthanide Metals for the Modification of the Alumina Support in Ni and Ru Catalysts in CO_2 Methanation, Catalysts 2021, Vol. 11, Page 353. 11 (2021) 353. https://doi.org/10.3390/CATAL11030353.

[37] A. Alihosseinzadeh, B. Nematollahi, M. Rezaei, E.N. Lay, CO methanation over Ni catalysts supported on high surface area mesoporous nanocrystalline γ-Al_2O_3 for CO removal in H2-rich stream, Int J Hydrogen Energy. 40 (2015) 1809–1819. https://doi.org/10.1016/J.IJHYDENE.2014.11.138.

[38] A.H. Fakeeha, M.A. Naeem, W.U. Khan, A.E. Abasaeed, A.S. Al-Fatesh, Reforming of methane by CO_2 over bimetallic Ni-Mn/γ- Al_2O_3 catalyst, Chinese Journal of Chemical Physics. 27 (2014) 214–220. https://doi.org/10.1063/1674-0068/27/02/214-220.

Chapter 3

Catalytic Dry Reforming of Plastics Pyrolysates

Table of Contents

List of Figures

List of Tables

In this chapter, the activity of Ni-based catalysts was first studied in the dry reforming of polypropylene plastics. The Al_2O_3 support was synthesized as described in Chapter 2 and impregnated with different metal active phase loadings. In the first section, the effect of different Ni loadings on syngas production will be studied, and the effect of promoting the Ni-based catalysts with ruthenium will be evaluated. In the second section, the most performing catalysts will be tested in consecutive reactions to study its aging behavior. The effect of promoting support with Ce will be tested in the third section. The influence of plastic to catalyst ratio will then be studied, and the best catalyst will be compared with a commercial one. Finally, the reforming of other types of plastics (polyethylene, polystyrene, and a mixture of polypropylene and polyethylene) will be performed over the most performing catalyst.

According to the thermogravimetric analysis outlined in Chapter 2, the main PP degradation peak was identified between 400 °C and 500 °C. As a result, for this series of experiments, a pyrolysis temperature of 500 °C was chosen. It is to be noted that the analysis of the used polypropylene plastics showed the following composition: 83% volatile fraction, less than 1% moisture, and less than 1% ash. Furthermore, the carbon balance was checked during all the performed tests and presented in Appendix B, where more than 98% of the carbon input was tracked down in the obtained gaseous, liquid, and solid products.

1. Catalytic test description

The pyrolysis catalytic dry reforming experiments were conducted at atmospheric pressure. From the thermal gravimetric analysis of the plastic samples (Chapter 2, section 1.2.1) it was possible to determine the pyrolysis temperature of polypropylene at 500 °C. From the thermodynamic study of the dry reforming reaction (Chapter 1, section 7.3), a temperature of 800 °C was chosen as the reforming temperature. The experimental set-up is displayed in the **fig. 3.1.**

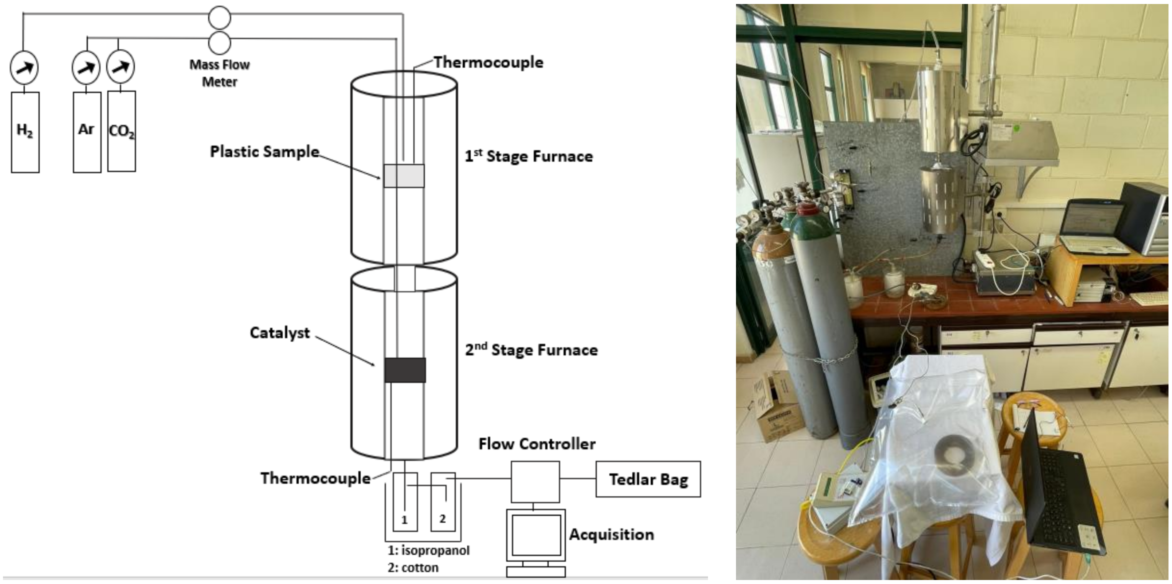

Fig. 3.1 Schematic diagram of the two-stage fixed bed reactors and photograph of the existing setup in the lab

The experimental setup involved two-stage fixed bed reactors, where the pyrolysis of polypropylene plastics and the catalytic dry reforming of produced hydrocarbons occurred. Each stage was heated by a separate electric furnace. The first comprised the pyrolysis reactor which was a 43 cm in length and 3 cm inner diameter quartz reactor. The second comprised the catalytic bed reactor which was 45 cm in length and 4 cm inner diameter quartz reactor with a quartz wool catalytic bed. The pyrolysis furnace was placed on top of the second stage reforming furnace. Each stage had a specific heating system and was controlled by a thermocouple to monitor its temperature. In the first stage, the pyrolysis of the feedstock took place under a flow of Ar that served as a carrier gas. The generated gases were sent into the second stage where the reforming reaction occurred in the presence of CO_2 and a catalyst.

Based on the H_2-TPR results, a reduction temperature of 800 °C is needed to reduce the catalyst. Therefore, 1 g of sieved catalyst (350-800 µm) underwent in-situ reduction at this temperature under 10% H_2 in Ar flow (30 ml/min), preceding the pyrolysis-reforming experiment. The procedure consisted of holding the reforming reactor at 800 ºC, which contained the reduced catalyst. 2 g of pelletized PP plastics were situated in the pyrolysis reactor and heated to the specified pyrolysis temperature. The carrier gas Ar (50 ml/min) was sent throughout the entire experiment, and the reforming gas CO_2 (105 ml/min) was introduced during the reforming reaction. According to the DSC-TG analysis of PP plastic, the pyrolysis starts at 330 °C and ends at 490 °C. During the 32 min required to cover the pyrolysis temperature range at 5 °C/min rate, 6.25 g of CO_2 must be sent into the system to perform the dry reforming reaction of polypropylene. This permitted the calculation of the flow of CO_2 needed for the reforming reaction to be 105 ml/min. This also permitted the calculation of number of moles of CO_2 injected in the setup to be 0.469 mol. Therefore, the conversion of CO_2 (%) was calculated according to the following formula:

$$X_{CO_2} = \frac{[molsCO_2]_{in} - [molsCO_2]_{out}}{[molsCO_2]_{in}} \times 100$$

Where $molsCO_{2in}$ represents the number of moles of carbon dioxide injected into the setup and $molsCO_{2out}$ represents the number of moles of carbon dioxide measured by the GC analysis after the experiment had finished.

The gases produced following the pyrolysis-reforming process were swept into ice-cooled gas bubblers, one comprising isopropanol solution and the other comprising cotton, which served as a tar trap. The uncondensed gases were delivered to a flow controller which totalized the volume of gas collected in a Tedlar^{TM} gas sample bag (25 L) for offline analysis. The total reaction time was 40 min with an additional 60 min wait to ensure that all gases were collected in the gas sample bag. Since the Tedlar bag can only hold 25 L, and after determining the time needed for the experiment to finish, a 50 ml/min Argon flow was used which was sufficient to carry the gases towards the Tedlar bag.

As for the CO_2, CH_4, H_2, and CO quantities, it was calculated using the total volume of gas collected (using the gas totalizer) and the percentages of these gases in the mixture according to microGC results. Several injections were performed to minimize errors and number of moles were obtained from calculated volumes using the ideal gas law.

The syngas production ($mmol_{syngas}/g_{PP}$) was calculated using the formula below:

$$syngas = \frac{n_{H_2} + n_{CO}}{m_{PP}}$$

Where n_{H_2} and n_{CO} correspond to the number of moles (mmol) of hydrogen and carbon monoxide, respectively, and m_{PP} corresponds to the mass of PP placed in the first reactor in grams.

According to theoretical calculations based on equation (**3.1**), 2 g of polypropylene plastic should produce 0.14 mol of H_2, 0.28 mol of CO, and 210 $mmol_{syngas}/g_{PP}$ of syngas.

$$-(CH_2)- + CO_2 \rightarrow H_2 + 2CO \quad (3.1)$$

Using this experimental setup, the pyrolysis-dry reforming reaction was carried out under fixed conditions while changing the used catalyst.

2. Influence of active phase on the syngas production

The pyrolysis-catalytic dry reforming of polypropylene plastic was carried out over xNiAl$_2$O$_3$ and 1RuxNiAl$_2$O$_3$ catalysts at 800 °C. According to “Plastics the Facts” study, polypropylene is the most produced type of plastic [1]. Due to its significant contribution to the plastics waste category in municipal solid waste, it was chosen as the starting material in this study.

2.1. The uncatalyzed reaction

The pyrolysis of PP was first conducted without a catalyst and without CO_2 (pyrolysis-blank test) to be used as a reference to which catalytic activity can be compared. Another test was performed in the absence of a catalyst but with the addition of CO_2 (reforming-blank test). **Fig. 3.2** demonstrates the gas compositions (moles) produced following the pyrolysis-catalytic dry reforming of PP.

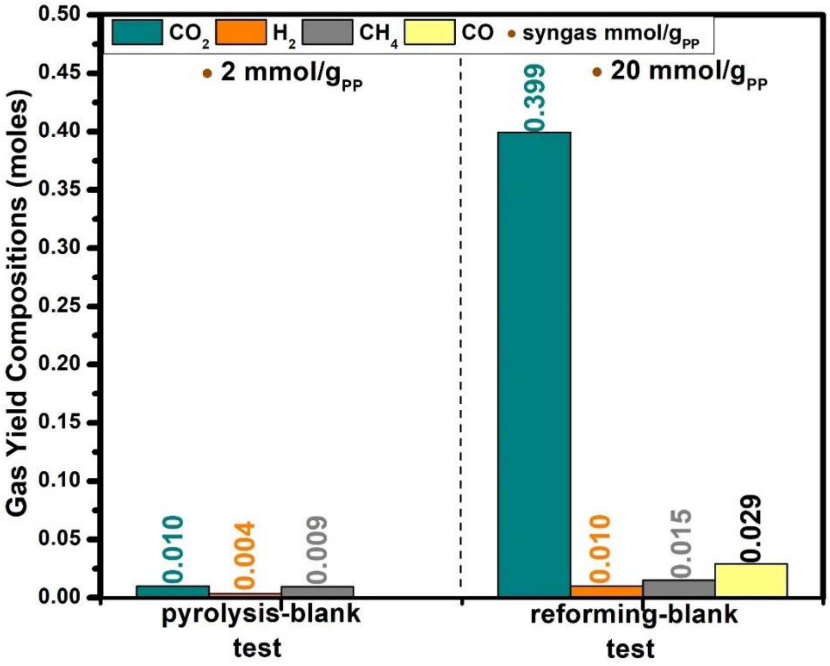

Fig. 3.2 Product gas composition from the uncatalyzed pyrolysis and dry reforming of polypropylene plastic

When CO_2 was added during the reforming-blank test, more hydrogen gas was produced (0.010 mol) than during the pyrolysis-blank test (0.004 mol). Moreover, syngas production increased by ten times once carbon dioxide was inserted. The addition of CO_2 led to the dry reforming reaction (**1.2**) thus increasing the hydrogen and carbon monoxide production [2].

Low hydrogen yields are produced during the pyrolysis of polypropylene plastics. However, high yields of hydrogen can be produced via two-stage processing of polypropylene, which involves thermal decomposition of the plastic in the first stage followed by reforming in the second stage [3]. The pyrolysis process releases volatile compounds, which are then reacted with carbon dioxide during the reforming stage to create synthesis gas. The reaction in the second reactor at 800 °C accelerated the carbon dioxide interaction with hydrocarbons, increasing hydrogen production. No carbon monoxide was detected in the pyrolysis-blank test due to the absence of CO_2. However, once CO_2 was added, the dry reforming reaction took place and 0.029 mol of CO was produced. The hydrocarbons generated from the pyrolysis of PP reacted with the carbon dioxide to produce more H_2 and CO. According to the thermodynamic study of the dry reforming reaction presented in Chapter 1, this reaction is favored at temperatures exceeding 700 °C. Therefore, comparing the results of pyrolysis-blank test and the reforming-blank test, the dry reforming reaction between the hydrocarbons with carbon dioxide occurred in the second stage [3].

Since the introduction of carbon dioxide has influenced the thermal cracking of heavy hydrocarbons in the reforming reactor, all following experiments were conducted with carbon dioxide and argon flows.

2.2. xNiAl$_2$O$_3$ catalysts

This section shows the influence of nickel-based catalysts with different Ni loadings on the production of syngas in the dry reforming of PP. As mentioned in Chapter 1, nickel-based materials are the catalysts of choice due to their low cost and excellent stability and catalytic activity [4].

Fig. 3.3 shows the effect of Ni loading on the gas composition (moles) and syngas production in the pyrolysis-dry reforming of polypropylene.

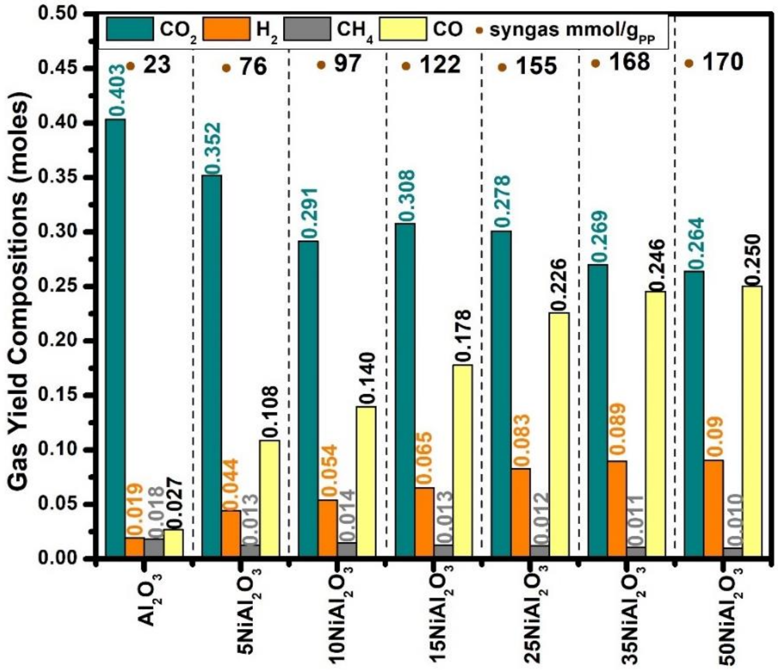

Fig. 3.3 Product gas composition of the pyrolysis-dry reforming of polypropylene over *x*NiAl$_2$O$_3$ catalysts

As shown in **fig. 3.3**, the hydrogen yield reached 0.019 mol during the reforming over mesoporous alumina support. However, in the presence of the *x*NiAl$_2$O$_3$ catalyst, hydrogen and carbon monoxide production increased. The amount of H_2 produced ranged between 0.044 mol in the presence of 5NiAl$_2$O$_3$ catalyst and 0.09 mol in the presence of 50NiAl$_2$O$_3$. The produced quantities of CO increased from 0.029 mol during the reforming-blank test to 0.108 mol over the 5NiAl$_2$O$_3$ catalyst and 0.250 mol over the 50NiAl$_2$O$_3$ catalyst. Furthermore, the produced quantities of CH_4 decreased from 0.013 mol over the 5NiAl$_2$O$_3$ catalyst to 0.010 mol over the 50NiAl$_2$O$_3$ catalyst. The CO_2 quantities also decreased with increasing Ni loading. From the 0.469 mol of CO_2 injected into the setup, 0.403 mol remained after reforming over alumina support. The values of remaining CO_2 decreased to 0.352 mol over 5NiAl$_2$O$_3$ catalysts and further decreased to 0.264 mol over 50NiAl$_2$O$_3$ catalyst. The increase in nickel loading from 5 wt.% to 50 wt.% increased the syngas production from 76 mmol$_{syngas}$/g$_{PP}$ to 170 mmol$_{syngas}$/g$_{PP}$. This increase in H_2 and CO production and the decrease in CH_4 and CO_2 production in the gas yield is because of the promotion of dry reforming reaction in the second reactor, where the addition of the nickel active phase improved catalytic performance. However, it seems that further increasing the Ni loading above 25 wt.% did not drastically increase the amount of H_2 produced, where it stabilized at roughly 0.08 mol.

The amount of carbon dioxide that was consumed throughout the experiment was measured using the CO_2 conversion formula. **Fig. 3.4** shows the relation between the production of syngas, the conversion of carbon dioxide, and the deposition of carbon after the dry reforming reaction over xNiAl$_2$O$_3$ catalysts. (Refer to Appendix B for carbon deposition determination)

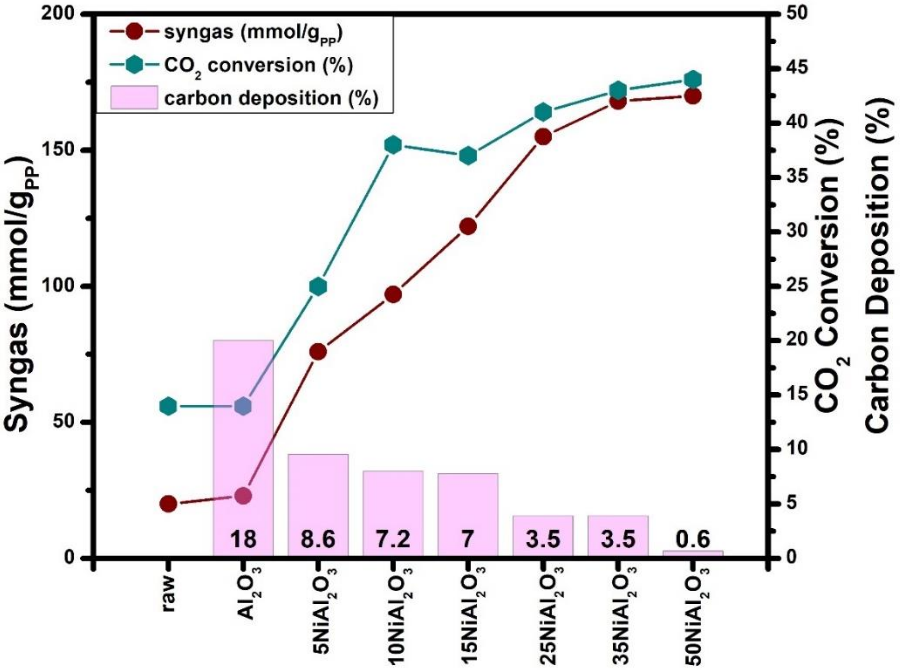

Fig. 3.4 Syngas production, carbon dioxide conversion, and carbon deposition obtained from the pyrolysis-dry reforming of PP over xNiAl$_2$O$_3$ catalysts

The results show that with an increase in Ni loading, the production of syngas increases along with the conversion of carbon dioxide. On the other hand, carbon deposition decreases. The CO_2 conversion increased from 14% in the absence of a catalyst to 25% over 5NiAl$_2$O$_3$ and further increased to 44% as the Ni loading reached 50 wt.%. Meanwhile, the carbon deposition decreased significantly as the Ni loading increased to 50 wt.%. According to the thermodynamic study of the dry reforming reaction in Chapter 1, at 800 °C, the carbon deposited mainly due to the methane decomposition reaction. However, at this temperature, most carbonaceous coke was removed by the reverse-Boudouard reaction (equation **3.2**), thus decreasing the carbon deposition while increasing the CO_2 conversion [5]. This could be correlated to the basicity of the catalyst, which provided better interaction between the CO_2 molecules and the catalyst. The basicity increased with the increase in Nickel loading (refer to Chapter 2, section 2.2.4).

$$C + CO_2 \rightarrow 2CO \qquad \Delta H_{298} = 172.4\ kJ.mol^{-1} \qquad \textbf{(3.2)}$$

Since, with a Ni loading of 25 wt.% the amount of H_2 produced stabilized and did not change considerably as the active phase content increased, the optimum course of action from an economic perspective is to employ low Ni loading while ensuring maximum plastic conversion into synthesis gas.

Researchers have recently become interested in employing Ru as a promoter to lower carbon production and increase catalytic stability [6]. However, using Ru alone is not economical. Moreover, although ruthenium's catalytic activity as a monometallic catalyst is lower than nickel in the dry reforming reaction, co-impregnating Ni and Ru on the support boosted the reducibility of nickel oxides species and prevented deactivation [7]. Therefore, a better approach to increase catalytic activity and prevent carbon formation would be using Ru noble metal as a catalytic promoter [8]. Even though Ru has shown great physicochemical properties and catalytic activity in dry reforming of methane processes, the influence of Ru as a promoter over Ni-based catalysts in pyrolysis-dry reforming of plastics has not been investigated. Therefore, in the following section, the catalysts with a nickel percentage of up to 25 wt.% will be promoted with 1 wt.% of ruthenium.

2.3. 1Ru*x*NiAl$_2$O$_3$ catalysts

According to the literature [7–10], promoting the catalyst with a transition metal might improve the performance of the reaction by increasing its stability. Since ruthenium was known for its stability and lower cost compared to other noble metals [6], this metal was chosen as a promoter, and its effect on the production of syngas was compared to that of Ni-based catalysts. As a result, the nickel and ruthenium precursors were co-impregnated on an alumina support, calcined, and then reduced at 800 °C prior to the dry reforming of polypropylene plastic.

Fig. 3.5 shows the gas compositions (moles) obtained following the reforming of PP over different 1Ru*x*NiAl$_2$O$_3$ catalysts.

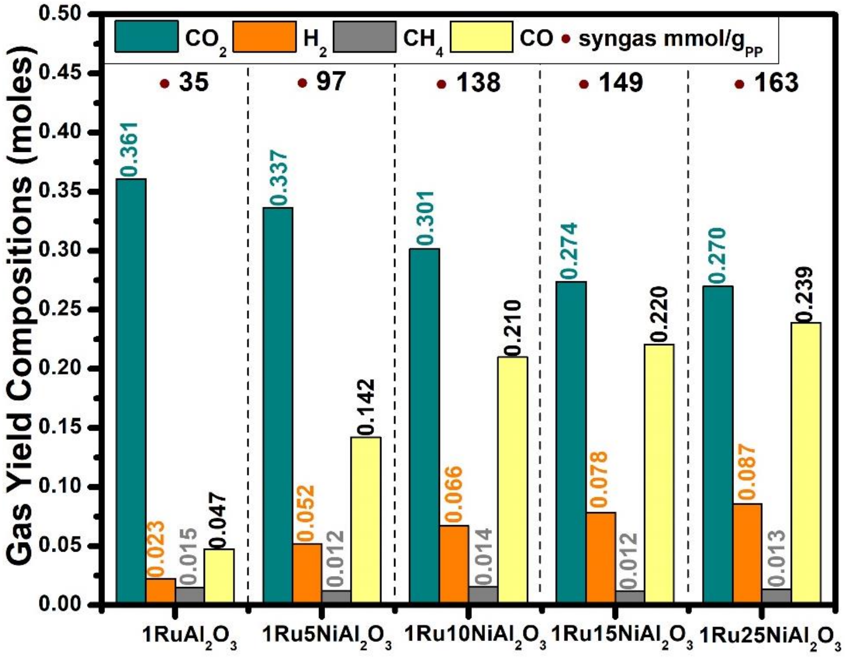

Fig. 3.5 Product gas composition of the pyrolysis-dry reforming of polypropylene over 1Ru*x*NiAl$_2$O$_3$ catalysts

The amount of produced H_2 was only 0.023 mol over 1RuAl$_2$O$_3$ catalyst. However, the presence of both Ru and Ni in the catalysts gave superior results compared to the corresponding *x*NiAl$_2$O$_3$ catalysts. **Table 3.1** shows the produced H_2 quantities for Ru free and corresponding Ru promoted catalysts. The presence of Ru was beneficial as its effect on H_2 production was more than additive.

Table 3.1 Effect of promoting *x*NiAl$_2$O$_3$ catalysts with Ru on the number of moles of H_2 produced

Catalyst	H_2 production (without Ru)	H_2 production (with Ru)	H_2 (with Ru) - H_2 (without Ru)	Expected H_2 if effect is additive	Percentage increase compared to addition
Al$_2$O$_3$	0.019	0.023	0.004	-	-
5Ni Al$_2$O$_3$	0.044	0.052	0.008	0.048	8.3%
10Ni Al$_2$O$_3$	0.054	0.066	0.012	0.058	13.8%
15Ni Al$_2$O$_3$	0.065	0.078	0.013	0.069	13.0%
25Ni Al$_2$O$_3$	0.083	0.087	0.004	0.087	0.0%

When the nickel-based catalysts were promoted with 1 wt.% Ru, the quantity of produced gases from the pyrolysis-dry reforming of polypropylene showed an obvious increase; promoting the $5NiAl_2O_3$ catalyst with ruthenium considerably improved the catalytic activity, increasing the H_2 production to 0.052 mol. The significant impact of co-impregnating the Ni-catalyst with Ru on the catalytic activity was noticed for all Ni-loadings. The $1Ru10NiAl_2O_3$ catalyst produced 0.066 mol compared to 0.054 mol in the presence of the $10NiAl_2O_3$ catalyst. The $1Ru15NiAl_2O_3$ catalyst produced 0.078 mol of H_2 compared to the $15NiAl_2O_3$ catalyst, which produced 0.065 mol of H_2. The beneficial effect of co-impregnating Ru is clearly seen for the $1Ru10NiAl_2O_3$ and the $1Ru15NiAl_2O_3$ catalysts. The amount of H_2 produced is at least 13% greater than what is expected from simple additive effect of active phases. However, it is noticed that for $25NiAl_2O_3$ catalysts, the promotion with Ru did not significantly affect the number of moles of H_2 produced. Only a slight addition impact was noted once the Ni loading increased to 25 wt.%, where the $25NiAl_2O_3$ catalyst produced 0.083 mol of H_2 while the $1Ru25NiAl_2O_3$ catalyst produced 0.087 mol. The promotion of the Ni-based catalyst with Ru also influenced the CO production. The CO production over the $5NiAl_2O_3$ catalyst increased from 0.108 mol to 0.142 mol once Ru was present. The $10NiAl_2O_3$ catalyst produced 0.140 mol of CO, this value increased to 0.210 mol over the $1Ru10NiAl_2O_3$ catalyst. The $15NiAl_2O_3$ catalyst produced 0.178 mol of CO and the values increased to 0.220 mol once the catalyst was promoted with Ru. The $25NiAl_2O_3$ catalyst also produced greater CO amounts after promotion with 1 wt.% Ru, where the values increased from 0.226 mol to 0.239 mol. Moreover, the syngas production increased as the nickel-based catalysts were promoted with Ru. For instance, an increase in syngas production from 122 mmol/g_{PP} to 149 mmol/g_{PP} was noticed as 1 wt.% Ru was introduced to the 15 wt.% nickel catalyst. The Ru-$NiAl_2O_3$ catalysts were more active than $NiAl_2O_3$ catalysts, producing higher amounts of syngas. This suggests that the co-impregnation of nickel and ruthenium improved catalytic performance by boosting the reforming of pyrolysis gases and increasing the production of H_2 and CO.

The CO_2 conversion was calculated, and the results are presented along with the syngas production and carbon deposition in **fig. 3.6**.

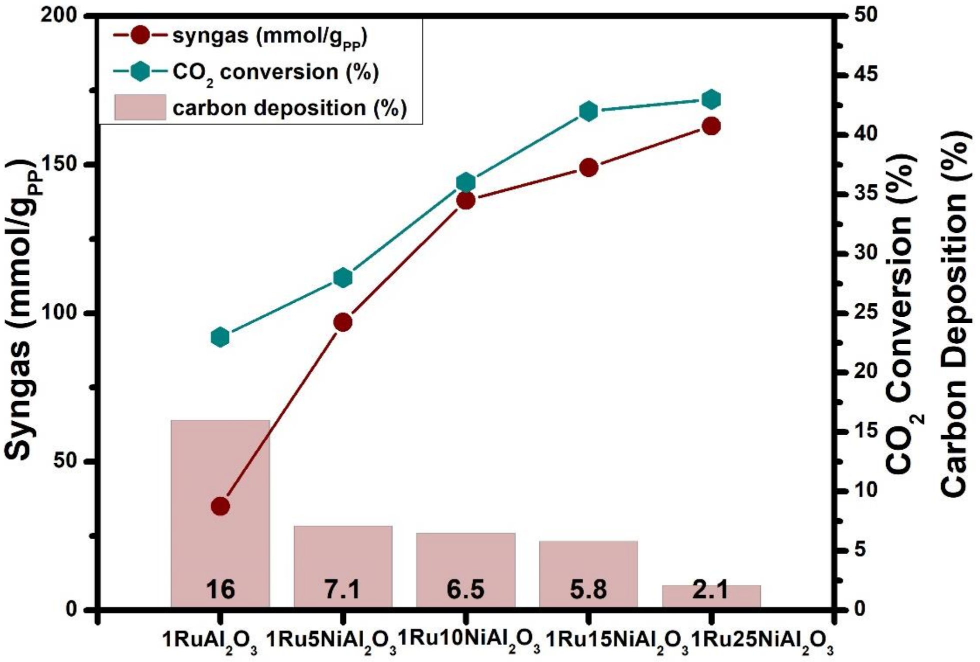

Fig. 3.6 Syngas production, carbon dioxide conversion, and carbon deposition obtained from the pyrolysis-dry reforming of PP over 1Ru*x*NiAl$_2$O$_3$ catalysts

As the CO$_2$ conversion increases, more syngas is produced while the carbon deposition decreases. This trend is observed as the Ni loading in the 1Ru*x*NiAl$_2$O$_3$ catalysts increases. For instance, the CO$_2$ conversion in the 1RuAl$_2$O$_3$ catalyst was 23%. This value increased to 43% as the nickel loading reached 25 wt.%. This resulted in an increase in syngas production from 35 mmol$_{syngas}$/g$_{PP}$ to 163 mmol$_{syngas}$/g$_{PP}$. After comparing these results with the ones presented for *x*NiAl$_2$O$_3$ catalysts, the promotion with 1 wt.% Ru increased the production of syngas along with the conversion of carbon dioxide, while decreasing the carbon deposition. The carbon deposition decreased from 3.5% over 25NiAl$_2$O$_3$ catalyst to 2.1% over 1Ru25NiAl$_2$O$_3$ catalyst. This could be correlated to the basicity of the catalyst, where the CO$_2$-TPD results showed that the 1Ru25NiAl$_2$O$_3$ catalyst possessed more basic sites than the non-promoted catalyst

2.4. Characterization after test

2.4.1. Characterization of the spent catalysts

The used catalysts in the dry reforming reaction were characterized using DSC-TG and XRD analyses.

DSC-TG

Fig. 3.7 shows the DSC curves of spent $x\mathrm{NiAl_2O_3}$ and $1\mathrm{Ru}x\mathrm{NiAl_2O_3}$ catalysts after the reforming of PP plastics.

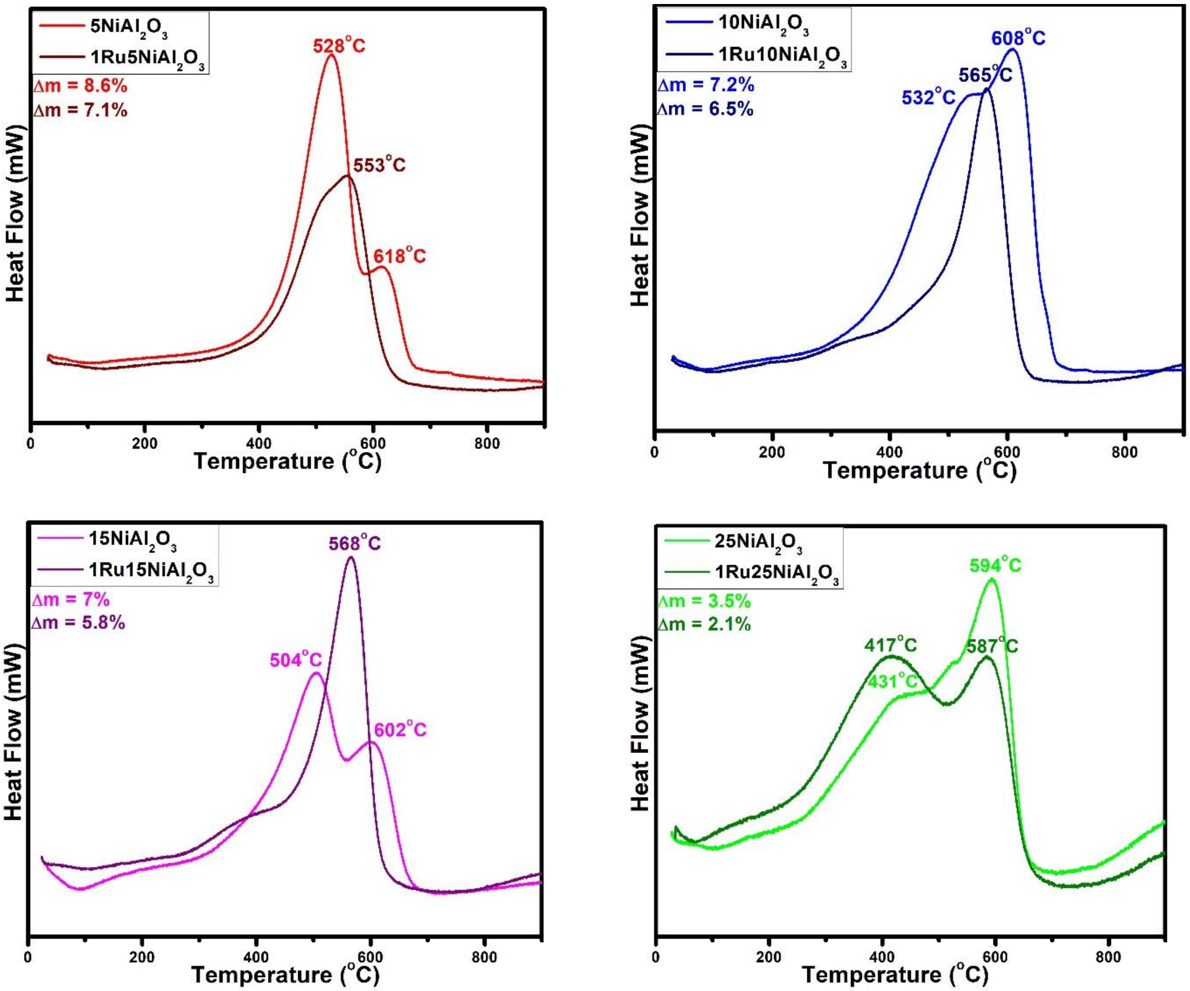

Fig. 3.7 DSC curves of spent $x\mathrm{NiAl_2O_3}$ and $1\mathrm{Ru}x\mathrm{NiAl_2O_3}$ catalysts

The DSC curve of the spent $x\mathrm{NiAl_2O_3}$ catalysts shows two exothermic peaks (details of the nature of carbon deposition are already mentioned in Chapter 1). Two oxidation peaks are also observed for 5, 10, and 15 wt.% of Ni: the first peak around 500 °C corresponds to deposited filamentous carbon species [11]. The second peak around 600 °C corresponds to either graphitic carbon or a more stable form of filamentous carbon that results from the methane decomposition reaction [12]. It should be emphasized that the carbon generated from the methane cracking accumulates on the catalyst's surface without grave deactivation, in contrast to the filamentous carbon that is known to be a deactivating carbon [11]. Both peaks attributed to the oxidation of carbon formed on the catalytic surface are accompanied by weight loss. As the Ni loading is further increased (25 wt.%), a different trend is observed: the first exothermic peak accompanied by a weight gain is attributed to the re-oxidation of the Ni particles present on the catalyst surface [11]. The second exothermic peak accompanied by weight loss is ascribed to the oxidation of carbon species. The lower temperatures of the second peak as the nickel loading increases indicate that the coke formed was easier to oxidize. It is noticed that the carbon deposited decreased as the Ni loading increased on the surface. As already mentioned, this could be due to the reaction between carbon and carbon dioxide (equation **3.2**). After the promotion of the nickel-based catalysts with 1 wt.% Ru, an exothermic peak is observed, corresponding to the oxidation of carbon. For high nickel loading (25 wt.%), a first exothermic peak corresponds to the oxidation of nickel species and a second peak corresponds to the oxidation of carbon. It is noticed that for all catalysts, the intensity of the peaks decreases after the promotion with ruthenium. Moreover, the total weight loss corresponding to the percentage of carbon deposited on the catalyst surface is lower in the Ru promoted nickel-based catalysts. This implies that less carbon is deposited on the catalyst surface once ruthenium is present.

XRD

Fig. 3.8 (a) and (b) show the XRD patterns of the xNiAl$_2$O$_3$ and 1RuxNiAl$_2$O$_3$ catalysts after their use in the reforming reaction of PP plastics.

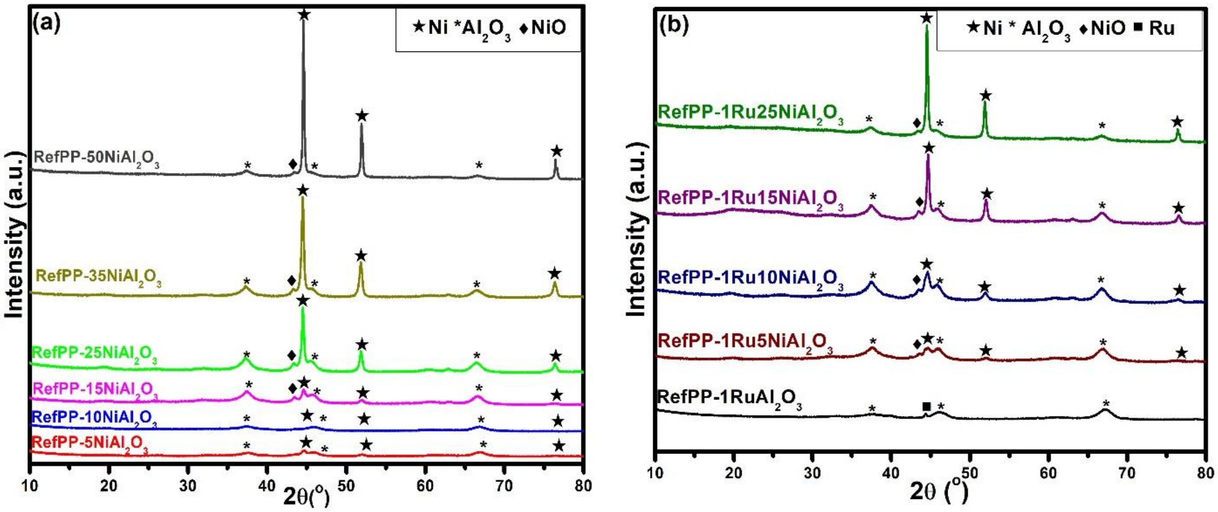

Fig. 3.8 XRD patterns of spent (a) xNiAl$_2$O$_3$ and (b) 1RuxNiAl$_2$O$_3$ catalysts

The XRD analysis of the reduced catalysts in Chapter 2 showed that metal oxides were reduced to their metallic form. Since the metal oxide diffraction peaks in the diffractogram of the spent *x*$NiAl_2O_3$ and 1Ru*x*$NiAl_2O_3$ catalysts (**fig. 3.8** a and b) have very low intensities, it is likely that most Ni species were still in their reduced state during the dry reforming reaction. This is because the evolved products (H_2 and CO) are reducing agents [11]. The XRD patterns of the spent catalysts show that some Ni was partially oxidized (NiO peak at $2\theta = 43.2°$), indicating that Ni was also involved in a redox cycle throughout the reaction. Additionally, the deposited carbon might have formed a coating that prevents the catalysts from being oxidized again [11]. However, no detectable carbon diffraction lines were noticed for the spent catalysts, probably because the carbon formed on the catalyst surface was non-crystalline. This negates the previous hypothesis concerning the formation of graphitic carbon. Hence, the carbon formed at a temperature above 550 °C is a more stable form of filamentous carbon [12]. Furthermore, it can be seen from **table 3.2** that the results for Ni crystallite sizes after testing for *x*$NiAl_2O_3$ and 1Ru*x*$NiAl_2O_3$ catalysts are larger than those after reduction (Chapter 2, table 2.1) because of a potential active phase agglomeration that took place during the dry reforming reaction.

Table 3.2 Ni crystallite sizes in the spent *x*$NiAl_2O_3$ and 1Ru*x*$NiAl_2O_3$ catalysts

Catalysts	Ni Crystallite Size (nm)	Catalysts	Ni Crystallite Size (nm)
5$NiAl_2O_3$	12.85	**1Ru5$NiAl_2O_3$**	-
10$NiAl_2O_3$	13.25	**1Ru10$NiAl_2O_3$**	11.15
15$NiAl_2O_3$	17.23	**1Ru15$NiAl_2O_3$**	15.27
25$NiAl_2O_3$	25.93	**1Ru25$NiAl_2O_3$**	25.31
35$NiAl_2O_3$	26.08		
50$NiAl_2O_3$	40.50		

2.4.2. Characterization of the isopropanol solution

The tar forming chemical compounds that were trapped in the isopropanol solution after each catalytic dry reforming test were studied by GC-MS, and the primary identifiable chemicals with associated retention times have been identified as shown in **fig. 3.9** with the split turned off (up to 4 min, the MS was turned off so that the solvent would be evacuated).

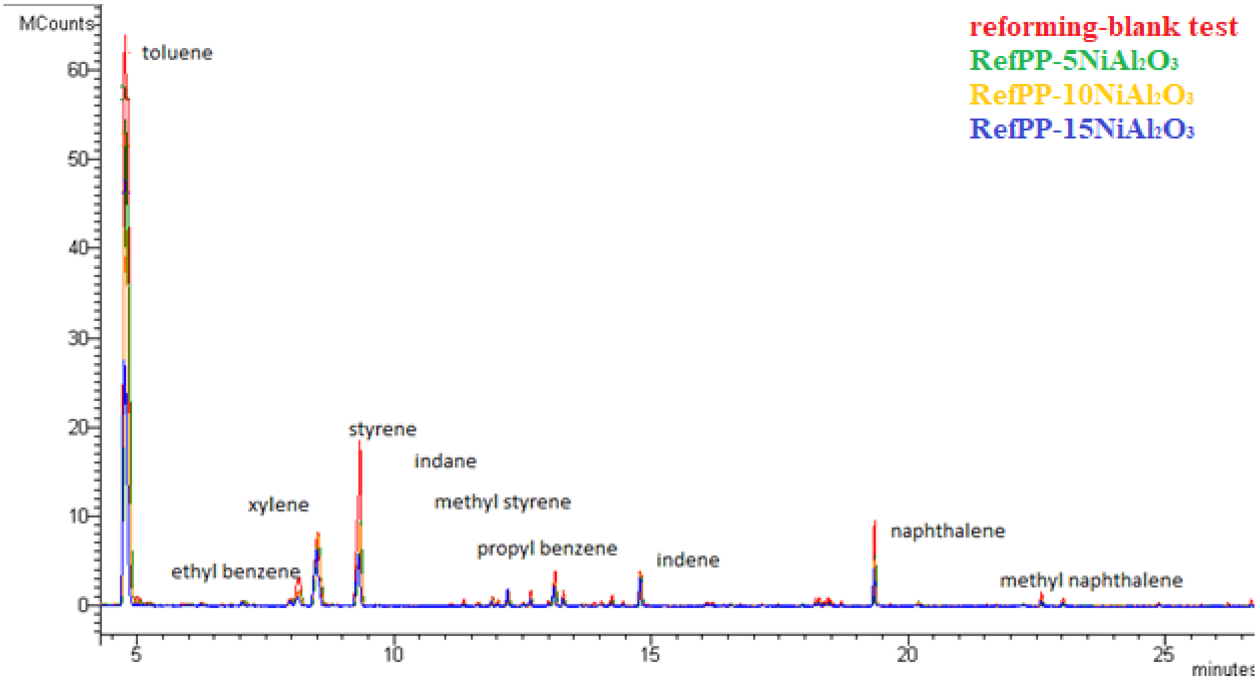

Fig. 3.9 Gas chromatography-mass spectrometry (GC-MS) spectra of tar in the isopropanol solution after PP pyrolysis and PP reforming over xNiAl$_2$O$_3$ catalysts

When polypropylene was catalytically dry reformed over a 15NiAl$_2$O$_3$ catalyst, the relative abundance of tar was reduced compared to when the plastic was pyrolyzed without a catalyst. As shown in **fig. 3.9**, the intensity of the peaks decreased as the metal loading on the catalyst increased, the red curve represents the pyrolysis of PP in the absence of a catalyst and the blue curve represents the reforming of PP over 15 wt.% Ni loading. This shows that the alumina-supported nickel catalysts were effective in cracking aromatic hydrocarbons. Since no tar peaks are detected after reforming over 25 wt.% nickel loading and higher (results are shown later in this section), these three catalysts (5, 10, and 15 wt.%) were chosen for comparison purposes.

As observed, the main components were monocyclic and polycyclic aromatic hydrocarbons. However, the benzene peak was not observed since it emerged during the first 4 minutes of the analysis. With a split ratio of 5, the peak representing benzene is observed at a retention time of 2.4 min as shown in **fig. 3.10**.

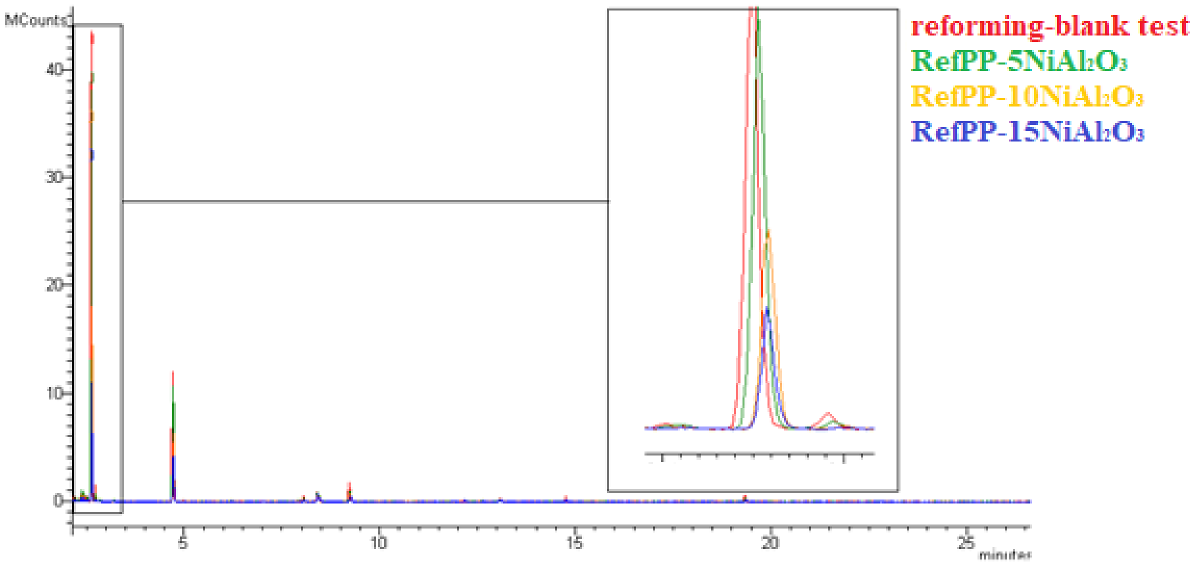

Fig. 3.10 Zoomed in GC-MS of benzene peak at tr = 2.4 min with split of 5

The effect of different Ni loadings on tar conversion efficiency was studied (Appendix B).

Fig. 3.11 shows the tar yield and conversion efficiency over different catalysts at a reforming temperature of 800 °C. The tar conversion efficiency over the 5 wt.% Ni loading is 21% higher compared to the blank-reforming test. This is because the mesoporous structure of the alumina support provides better adsorption of light tar compounds to the active site of the catalyst and plays an important role in enhancing the dispersion of the Ni active phase [13]. Additionally, the effectiveness of tar conversion with various catalysts improved as more nickel metal was impregnated onto the support, indicating that nickel was very active in the cleavage of the C-C and C-H bonds, leading to the destruction of aromatic hydrocarbons [14]. For a nickel loading of 15 wt.%, the tar conversion efficiency reached 67%. Since no peaks representing tar have been detected for 25, 35, and 50 wt.% Ni, it is suggested that at high Ni loadings, almost all tar was cracked during the reforming reaction.

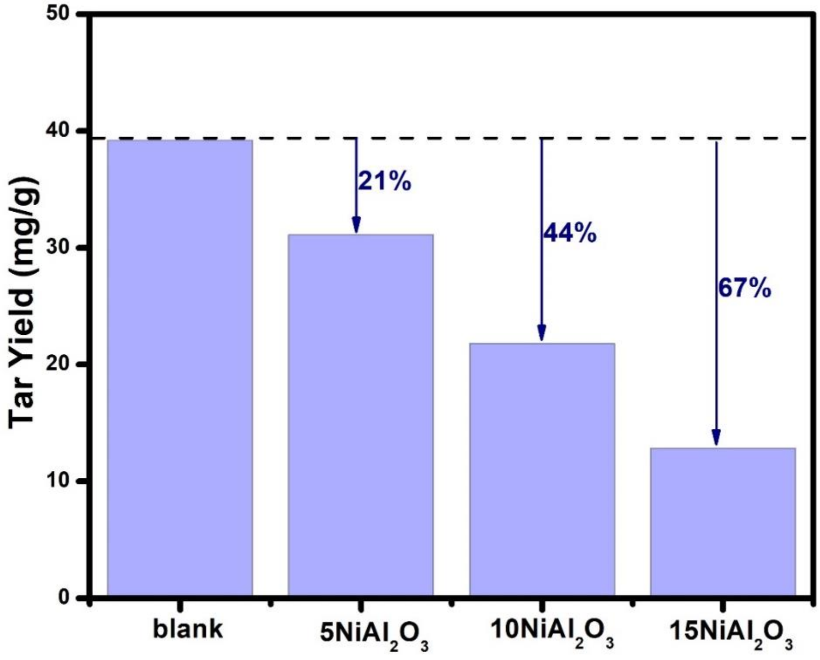

Fig. 3.11 Tar yield and conversion efficiency in the absence of catalyst and with *x*$NiAl_2O_3$ catalysts

Monocyclic aromatic hydrocarbons, heterocyclic compounds, and polycyclic aromatic hydrocarbons are the three primary components found in tar. The primary components with a high relative content (benzene and toluene) were analyzed for clarity, and the findings are displayed below.

Fig. 3.12 shows the benzene (tr = 2.4 min) and toluene (tr = 4.2 min) peaks after the reforming of PP over $xNiAl_2O_3$ (a) and $1RuxNiAl_2O_3$ (b) catalysts.

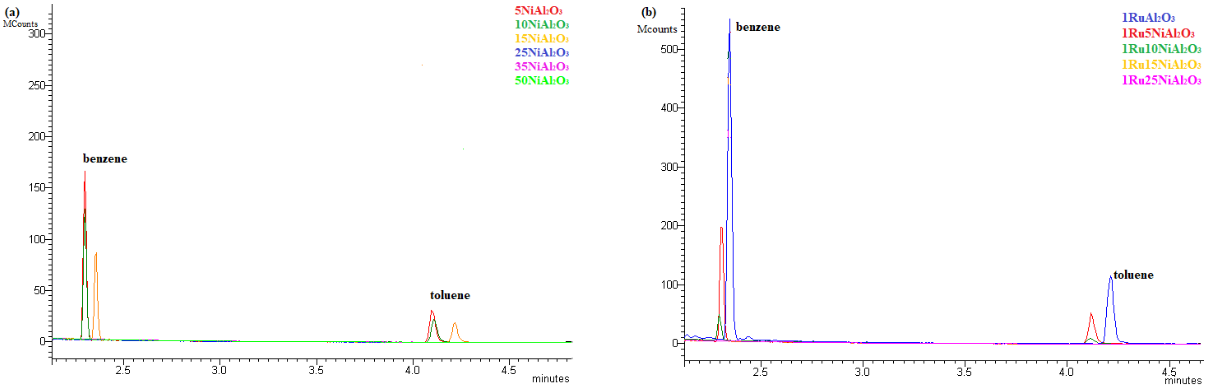

Fig. 3.12 GC-MS spectra of benzene and toluene from tar obtained from PP reforming over (a) *x*$NiAl_2O_3$ and (b) 1Ru*x*$NiAl_2O_3$ catalysts

It is noticed that after reforming over xNiAl$_2$O$_3$ (**fig. 3.12** a) the intensity of the peaks decreased as the nickel loading increased and became negligible at nickel loadings of 25 wt. % and higher. In the tar samples obtained following the reforming of PP over 1RuxNiAl$_2$O$_3$ catalysts (**fig. 3.12** b), the intensity of the peaks decreased as the nickel loading increased and became negligible at nickel loadings of 15 wt.% and higher. For instance, comparing the orange curves representing 15NiAl$_2$O$_3$ catalyst and its promoted counterpart in both figures, it is noticed that the peak representing the tar trapped after the reforming over this catalyst disappears after the co-impregnation with Ru.

Fig. 3.13 shows the concentrations of benzene and toluene in the trapped tar after the dry reforming reaction over xNiAl$_2$O$_3$ (a) and 1RuxNiAl$_2$O$_3$ (b) catalysts.

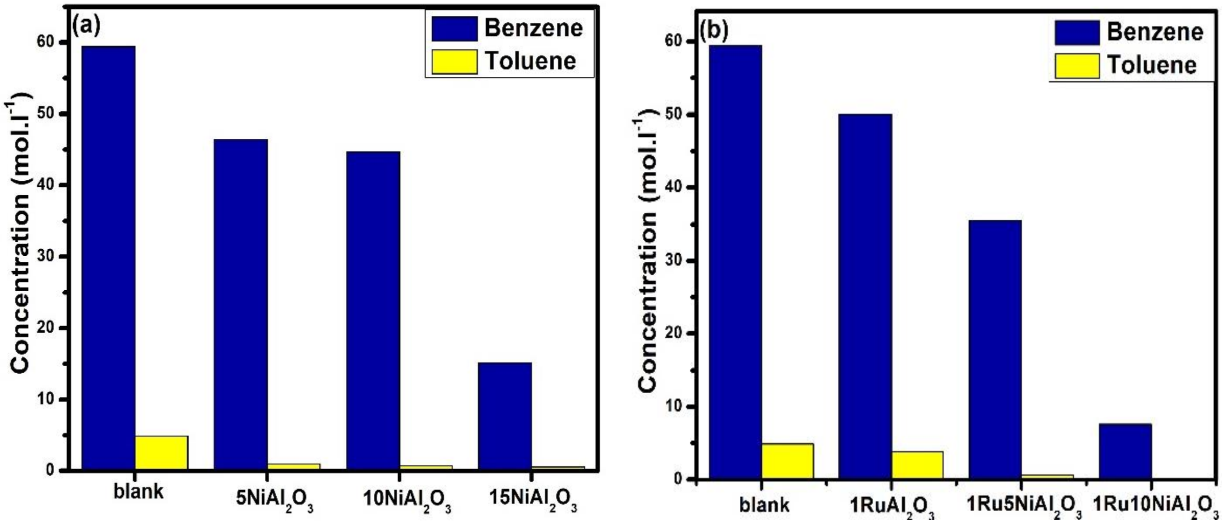

Fig. 3.13 Concentration of benzene and toluene from tar obtained from PP reforming over (a) xNiAl$_2$O$_3$ and (b) 1RuxNiAl$_2$O$_3$ catalysts

It is noticed from **fig. 3.13** (a and b) that the concentrations of these two compounds decreases with the increasing metal loading. Since no peaks were detected for 25 wt.% Ni loading and higher and for 1Ru15NiAl$_2$O$_3$ and 1Ru25NiAl$_2$O$_3$ catalysts (**fig. 3.12** a and b), it is assumed that the concentrations of benzene and toluene in these catalysts are negligible. The concentration of benzene was 46 mol.L^{-1}in tar obtained over the 5NiAl$_2$O$_3$ catalyst, and it decreased to 35 mol.L^{-1} in tar obtained with the Ru promoted counterpart. The concentration of benzene in tar obtained over the 15NiAl$_2$O$_3$ catalyst was 15 mol.l^{-1}, this value became negligible after the promotion with Ru. It is evident that the promotion of 15NiAl$_2$O$_3$ with 1 wt.% Ru effectively cracked the tar and resulted in better syngas production compared to the non-promoted 15NiAl$_2$O$_3$ catalyst.

2.5.Discussion

The increase of nickel loading from 5 wt.% to 50 wt.% led to a considerable improvement in the H_2 and syngas production since the lower nickel content might have favored the production of less reducible nickel species with strong interaction with the support. However, an increase in Ni content produced excess nickel, which formed nickel oxide particles on the nickel—alumina interface [15]. The weaker support interaction increased the reducibility and enhanced the dispersion of the active phase which led to better catalytic activity and syngas generation [16]. These findings correlate with the XRD results, that showed a decrease in the intensity of $NiAl_2O_4$ diffraction lines as the Ni loading increased above 25 wt.%. Moreover, they are in line with the H_2-TPR findings, which showed that decreased Ni content did not result in a reduction peak at a relatively low temperature due to the strong interaction between the nickel species and the support [15]. The catalytic activity of the Ni-based catalysts was significantly increased upon its co-impregnation with a small quantity of Ru which enhanced the catalyst’s surface area. The surface area of $25NiAl_2O_3$ increased, from 124 m^2/g to 149 m^2/g, after promoting the catalyst with 1 wt.% Ru. This increase in the surface area could be attributed to a better Ni dispersion after the catalyst promotion with Ru. This improved the catalyst's ability to interact with reactant molecules, which enhanced the catalytic performance [6,8]. Furthermore, the H_2-TPR results revealed that once the catalysts were promoted with Ru, the maximum reduction temperature of nickel shifted towards lower values thus indicating the beneficial impact of Ru on the reduction of Ni. This can be attributed to the spillover effect, where a close contact between nickel and ruthenium is required to observe this effect. Consequently, the introduction of Ru enhanced the catalysts’ reducibility and enhanced the catalytic performance [17]. The total H_2 consumption of $1Ru25NiAl_2O_3$ (3624 $\mu H_2/g$) was greater than that of the $25NiAl_2O_3$ catalyst (2317 $\mu H_2/g$) thus indicating that the promoted catalyst had a greater availability of active sites compared to the non-promoted catalyst, which led to a higher catalytic activity. (The experimental H_2 consumptions of these catalysts were determined in Chapter 2.)

The beneficial effect of the presence of Ru was clear up to a Ni loading of 15 wt.% and no noticeable enhancement in H_2 yield was observed with higher Ni loading ($1Ru25NiAl_2O_3$ catalyst). These results indicated that Ru probably favored the formation of well dispersed Ni particles. At higher Ni loading, agglomeration occurred in the presence and in the absence of Ru which was observed in the Ni crystallite size of the used catalysts, where the value was approximately equal

(~25 nm) for $25NiAl_2O_3$ and $1Ru25NiAl_2O_3$ catalysts. These results proved that the Ni species were responsible for the catalytic activity during the dry reforming of PP. The improvement in the physicochemical properties and catalytic activity of Ni-Ru catalysts compared to Ni-based catalysts can be attributed to the presence of Ru even in small quantities. The Ru promotion improved the metal dispersion of Ni covering the catalyst surface by forming a Ni-Ru cluster, decreased the Ni crystallite size, and increased the reducibility of Ni [7,18]. The CO_2-TPD results in Chapter 2 revealed that in the presence of Ru, more available basic sites were formed which led to better CO_2 adsorption on the surface of the catalysts and consequently better CO_2 conversion. The catalyst's strong adsorption of CO_2 prevented the creation of carbon during the process, which improved catalytic performance [7]. This indicates that the co-impregnation of Ru and Ni on the alumina support increased the syngas production due to the increase in CO_2 conversion.

The carbon deposited on the surface of the catalyst appeared to be filamentous since graphitic carbon was not detected in the XRD analyses for all xNiAl$_2$O$_3$ and 1RuxNiAl$_2$O$_3$ catalysts. At elevated temperatures, the dry reforming reaction is favored rather than the methane decomposition reaction. Therefore, increasing nickel loading led to the promotion of the dry reforming reaction, thus increasing the syngas production, and lowering carbon formation. The increased CO_2 conversion along with lower carbon deposition proved that CO_2 reacted with the carbon deposited on the surface of the catalyst, increased the production of carbon monoxide (reverse-Boudouard reaction), and consequently enhanced the syngas production. Moreover, in the presence of Ru, the carbon deposited on the catalyst surface was oxidized at lower temperatures and decreased in quantity. In fact, the presence of ruthenium can cause the catalyst to become less sensitive and more resistant to coke deposition [19]. Moreover, the considerable dispersion of the active phase in the presence of ruthenium hampers the carbon deposition process due to ruthenium’s ability to provide adsorbed carbon species with a reactional pathway and convert them into gaseous compounds [11,20]. Therefore, in line with the literature [10], the promotion of alumina-supported nickel-based catalysts with ruthenium increased the catalysts’ resistance to carbon deposition.

Tar is a complex mixture of organic compounds (aliphatic, aromatic, and species containing heteroatoms). The formation of tar does not only decrease the quantity of syngas but also condenses on the equipment setup, thus leading to system failure and catalyst deactivation [14]. The GC-MS spectra revealed that the abundance of tar decreased, indicating that heavier tars decomposed into small molecular compounds. This is because, at 800 °C, long-chained tar compounds undergo demethylation, intramolecular bridge bond breaking, and hydrogen bond breakdown, which transforms them into light gaseous hydrocarbons and other small-molecule liquid products [21]. The increasing hydrogen output revealed that macromolecular organic compounds were efficiently transformed into small gaseous molecules. Adsorption of tar is facilitated by the porous structure of the catalyst where more tar molecules can easily access the interior active areas due the catalyst's larger surface area [14]. The Ni loading influenced tar conversion efficiency. The relative abundance of tar was considerably reduced as the Ni loading increased from 5 wt.% to 50 wt.%, demonstrating that aromatic hydrocarbons were efficiently cracked with Al_2O_3-supported Ni catalysts. Moreover, the relative concentrations of benzene and toluene decreased as the Ni loading increased due to the efficient role of highly active Ni in cracking C-C, C-H, and O-H bonds during tar conversion. In the reforming reaction, nickel-based catalysts are known to reduce tar formation and boost hydrogen production [22]. The promotion of the nickel-based catalysts further enhanced the tar conversion, where the promoted catalysts effectively cracked tar compounds and decreased the concentrations of benzene and toluene in tar in comparison to their non-promoted counterparts. Therefore, the improved catalytic characteristics of the catalyst promoted with Ru enhanced carbon gasification and tar cracking, and consequently increased the catalytic activity towards increased syngas production.

2.6. Conclusion

It has been established that the catalytic dry reforming of PP has proven successful in producing synthesis gas. Various nickel percentages impregnated on mesoporous Al_2O_3 support produced substantial quantities of syngas, where the syngas production increased from 76 mmol/g_{PP} to 170 mmol/g_{PP} with the increase of nickel loading from 5 wt.% to 50 wt.%. Moreover, the amount of H_2 produced increased from 0.044 mol to 0.090 mol for these same catalysts. The XRD and H_2-TPR analyses showed that with increasing nickel content, more NiO species having weak interactions with the support are formed on the surface. This improved the reducibility and consequently the catalytic activity. The CO_2-TPD results showed that the basicity of the catalysts increased with Ni loading thus favoring the CO_2 adsorption and consequently its conversion. The results showed that the tar was effectively cracked starting with Ni loading of 25 wt.%. The promotion with a small amount of ruthenium led to an increased surface area due to better metal dispersion on the catalytic surface. This also contributed to enhanced reducibility of the catalytic material and better catalytic performance in the pyrolysis-dry reforming of polypropylene, where 163 $mmol_{syngas}/g_{PP}$ of syngas was produced in the presence of the $1Ru25NiAl_2O_3$ catalyst compared to 155 $mmol_{syngas}/g_{PP}$ for the $25NiAl_2O_3$ catalyst. Moreover, the number of moles of H_2 produced increased from 0.083 moles to 0.087 moles once ruthenium promoted the $25NiAl_2O_3$ catalyst. The ruthenium promoted catalyst was less susceptible to deactivation due to less filamentous carbon deposited on its surface. Therefore, a synergistic effect exists between ruthenium and nickel, leading to a catalytic material that produces considerable amounts of syngas. Therefore, it is concluded that the main effect of Ru in the $Ni\text{-}RuAl_2O_3$ catalyst is to promote the production of small Ni particles on the surface, thus increasing the catalyst's catalytic activity [18].

3. Comparison of $25NiAl_2O_3$ and $1Ru25NiAl_2O_3$ catalysts

According to the catalytic results, $25NiAl_2O_3$, $35NiAl_2O_3$, $50NiAl_2O_3$, and $1Ru25NiAl_2O_3$ catalysts produced roughly comparable quantities of syngas and number of moles of hydrogen. This observation led to the selection of $25NiAl_2O_3$ and $1Ru25NiAl_2O_3$ catalysts for further investigation, as it is preferable to minimize the percentage of active phase to reduce costs. The effect of calcination temperature on these catalysts is studied, and they were subjected to aging test to determine the catalysts' resistance and longevity.

3.1.Effect of calcination temperature

The DSC-TG of the fresh catalyst showed that the catalyst is stabilized around 550 °C. Therefore, a lower calcination temperature of 550 °C was used to study the effect of the calcination temperature on the catalytic activity.

3.1.1. Catalyst Characterization

XRD

Fig. 3.14 shows the XRD patterns of $25NiAl_2O_3$ and $1Ru25NiAl_2O_3$ catalysts calcined at 550 °C and 800 °C.

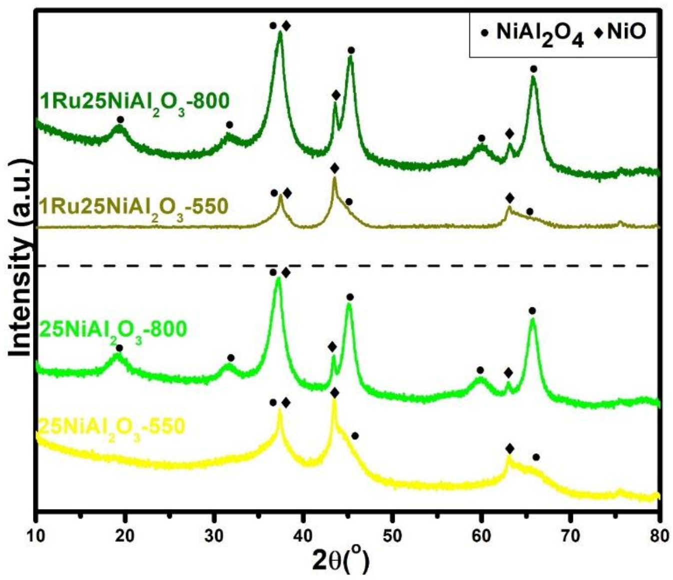

Fig. 3.14 XRD patterns of 25NiAl$_2$O$_3$ and 1Ru25NiAl$_2$O$_3$ catalysts at different calcination temperatures

From the XRD pattern, it is noticed that the intensities of the diffraction peaks of nickel aluminate increased as the calcination temperature increased from 550 °C to 800 °C, indicating that the crystallinities of the $NiAl_2O_4$ phase increase with increasing calcination temperature [23]. In particular, the relative intensity of $NiAl_2O_4$ to NiO increased with calcination temperature, possibly due to stronger NiO–Al_2O_3 interaction at higher temperatures [24]. Moreover, at higher calcination temperature three new peaks at $2\theta = 19°$, 31.7°, and 59.8° emerge, corresponding to the $NiAl_2O_4$ phase.

The Ni species assigned to NiO or $NiAl_2O_4$ in the catalysts calcined at different temperatures cannot be distinguished by XRD data because the diffraction peaks of NiO, Al_2O_3, and $NiAl_2O_4$ overlap. The effect of calcination temperature on the Ni species of NiAl$_2$O$_3$ samples will thus be further investigated using the H_2-TPR technique.

H_2-*TPR*

H_2-TPR was performed to investigate how the reducibility of Ni species was affected by changing the calcination temperature.

Fig. 3.15 (a and b) show the H_2-TPR profiles of 25NiAl$_2$O$_3$ and 1Ru25NiAl$_2$O$_3$ catalysts calcined at 550 °C and 800 °C.

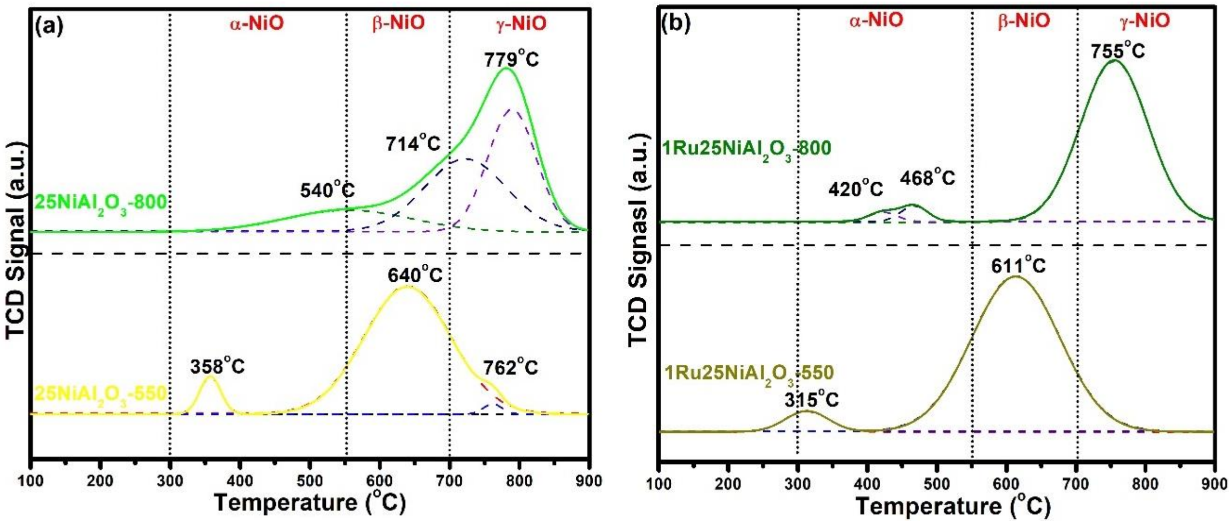

Fig. 3.15 H_2-TPR profiles of (a) 25NiAl$_2$O$_3$ and (b) 1Ru25NiAl$_2$O$_3$ catalysts calcined at 550 °C and 800 °C

The three different forms of reducible NiO species may be distinguished based on the peak position of the H_2-TPR profiles. According to the literature [25,26], the peak in the low temperature region (300 °C-550 °C) is attributed to the α-type NiO species, which interact weakly with the Al_2O_3 support. The peak in the moderate temperature region (550 °C-700 °C) is attributed to the β-type NiO species, which interact strongly with the support. The peak located in the high temperature region (above 700 °C) is ascribed to the γ-type NiO species, which are the stable nickel aluminate spinel phase. The H_2-TPR results show the peaks in the regions attributed to the interaction of NiO species with the support. In the 25NiAl$_2$O$_3$ catalysts (**fig. 3.15** a), it is noticed that the α-type and β-type NiO species shift to high temperatures (α-type: 358 °C to 540 °C; β-type: 640 °C to 779 °C) as the calcination temperature increases from 550 °C to 800 °C. Moreover, the α-type NiO species disappear at high calcination temperatures while the γ-type NiO species attributed to the $NiAl_2O_4$ phase are present. The same trend is observed for the 1Ru25NiAl$_2$O$_3$catalyst (**fig. 3.15** b), where the α-type NiO species reduction shifts from 315 °C to 468 °C and the β-type NiO species reduction shifts from 611 °C to 755 °C as the calcination temperature increases from 550 °C to 800 °C. For this catalyst, the high calcination temperature resulted in the disappearance of α-type NiO species and the emergence of the γ-type NiO species. These results agree with the XRD analyses, where the elevated calcination temperature promotes the interaction of the NiO species with the support and forms the nickel aluminate spinel phase, thus impeding the reduction of the nickel species with hydrogen [25].

The experimental H_2 consumption of both catalysts was determined and is shown in **table 3.3**. The total H_2 consumption of the $25NiAl_2O_3$ catalyst calcined at 550 °C (3351 µH_2/g) is greater than that of the same catalyst calcined at 800 °C (2317 µH_2/g). The same trend is noticed for the promoted catalyst, where the H_2 consumption of $1Ru25NiAl_2O_3$ calcined at 550 °C (4238 µH_2/g) is greater than that of the same catalyst calcined at 800 °C (3624 µH_2/g). This shows that the Ru and Ru-Ni-based catalysts calcined at 550 °C hold more available Ni active sites than the catalysts calcined at 800 °C.

Table 3.3 Experimental H_2 consumption of $25NiAl_2O_3$ and $1Ru15NiAl_2O_3$ catalysts at different calcination temperatures

Catalyst	**H_2 Consumption [µH_2/g catalyst]**			
	Experimental Consumption			
	I	**II**	**III**	**Total**
$25NiAl_2O_3$-550	-	219	3132	**3351**
$25NiAl_2O_3$-800	-	85	2232	**2317**
$1Ru25NiAl_2O_3$-550	-	270	3968	**4238**
$1Ru25NiAl_2O_3$-800	-	236	3338	**3624**

N_2 adsorption/desorption

The influence of calcination temperature on the physiochemical properties of the catalysts was examined using nitrogen adsorption/desorption analysis. The isotherms and the pore size distributions of the $25NiAl_2O_3$ and $1Ru25NiAl_2O_3$ catalysts at different calcination temperatures are presented in **Fig. 3.16** (a and b) and **Fig. 3.17** (a and b), respectively. The textural properties associated with each are listed in **table 3.4**.

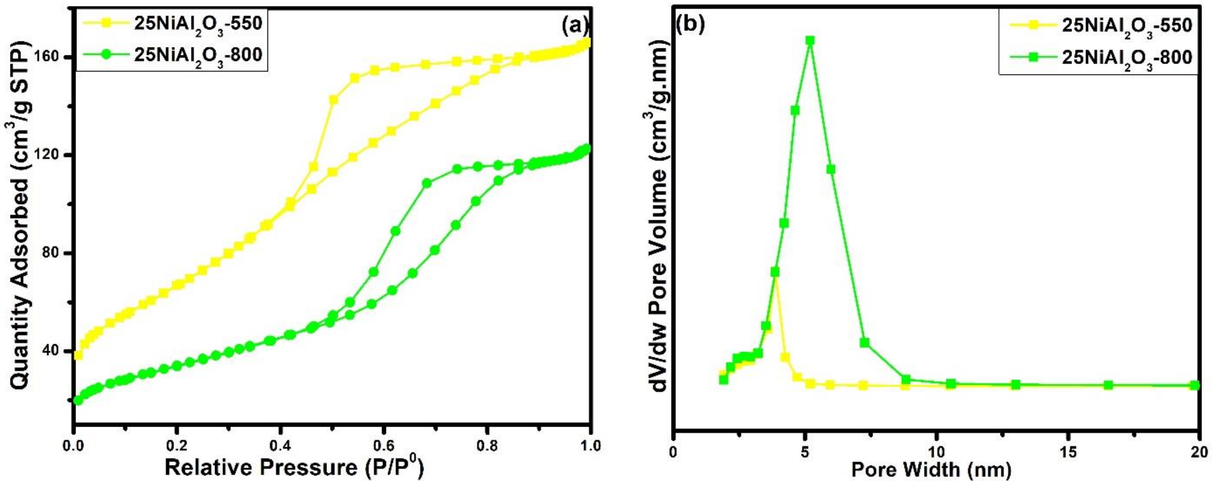

Fig. 3.16 (a) N_2 adsorption/desorption isotherms and (b) pore size distributions of 25NiAl$_2$O$_3$ catalysts calcined at different calcination temperatures

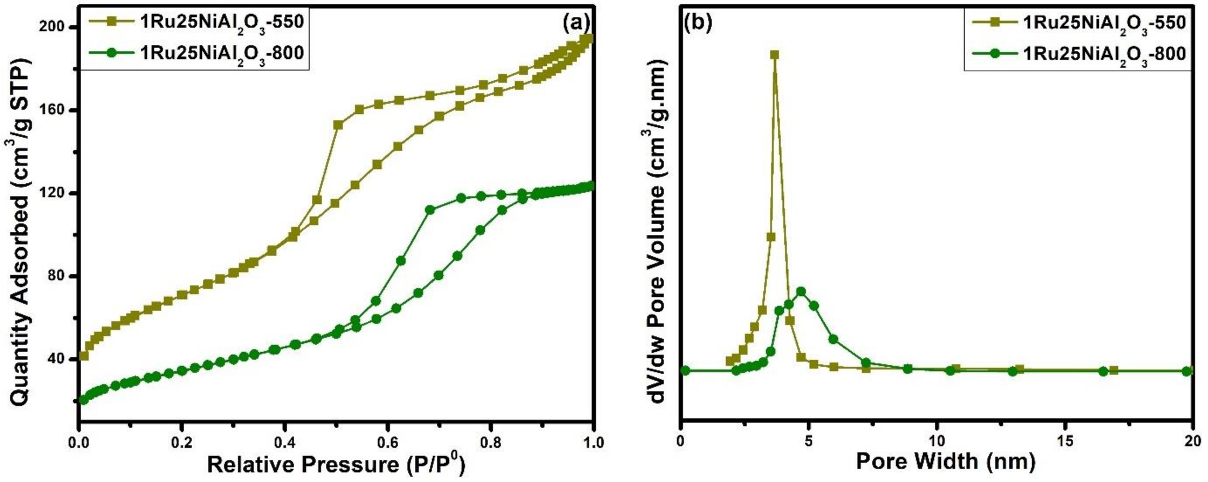

Fig. 3.17 (a) N_2 adsorption/desorption isotherms and (b) pore size distributions of 1Ru25NiAl$_2$O$_3$ catalysts calcined at different calcination temperatures

Table 3.4 Textural properties of 25NiAl$_2$O$_3$ and 1Ru25NiAl$_2$O$_3$ catalysts calcined at 550 °C and 800 °C

Catalyst	S_{BET}^{a} (m^2/g)	Vp^b (cm^3/g)	d$_0$^{c} (nm)	Catalyst	S_{BET}^{a} (m^2/g)	Vp^b (cm^3/g)	d$_0$^{c} (nm)
25NiAl$_2$O$_3$-550	253	0.27	3.582	**25NiAl$_2$O$_3$-800**	124	0.20	5.276
1Ru25NiAl$_2$O$_3$-550	286	0.31	4.105	**1Ru25NiAl$_2$O$_3$-800**	149	0.325	7.293

[a] Specific surface area; [b] Pore volume; [c] Pore diameter

The type IV isotherm indicates that the catalysts calcined at different temperatures exhibit a characteristic mesoporous structure. The amount of N_2 adsorption rose quickly due to capillary condensation when the relative pressure of p/p^o was greater than 0.4-0.45. This led to the appearance of hysteresis loops, showing the presence of mesoporous structures in the catalysts mentioned above [27]. Information about pore volume and pore size was provided by adsorption/desorption isotherm hysteresis curves. As shown in **fig. 3.16** (a) and **fig. 3.17** (a), hysteresis size decreased with an increase in calcination temperature, indicating that the porosity decreased as well. The shift of the hysteresis loop towards higher p/p^o denotes the presence of larger pore diameters [25]. This is consistent with the pore diameter results in **table 3.3** where the pore diameters increased with increasing calcination temperature. It is also noticed that as the calcination temperature increased to 800 °C, the amount of nitrogen adsorbed decreased, which indicated a decrease in surface area available for the adsorption of nitrogen. **Table 3.3** shows that the specific surface area of the $25NiAl_2O_3$ catalyst calcined at 550 °C was 253 m^2/g. The catalyst's surface area lost almost half its value and decreased to 124 m^2/g when calcined at 800 °C. When comparing with the support (Chapter 2), it is noticed that the pore size decreased from 13 nm to 4 nm once impregnated with Ni and calcined at 550 °C. The pore size then increased to 5 nm once calcined at 800°C probably due to the sintering of particles and the strong metal support interaction (SMSI) at high calcination temperature [23]. The same trend is observed for the $1Ru25NiAl_2O_3$ catalyst, where the surface area decreased from 286 m^2/g to 149 m^2/g as the calcination temperature increased from 550 °C to 800 °C. Moreover, at elevated calcination temperature, the position of the hysteresis loop changed from low p/p^o to high p/p^o. Moreover, the pore width increased in both catalysts with the increase in calcination temperature. This indicates that the small mesopores collapsed and sintered, thus forming bigger pores [24].

CO_2-*TPD*

The basic sites crucial for CO_2 adsorption were identified using CO_2-TPD. The CO_2-TPD profiles of $25NiAl_2O_3$ and $1Ru25NiAl_2O_3$ catalysts calcined at two different calcination temperatures are shown **in fig. 3.18** (a and b).

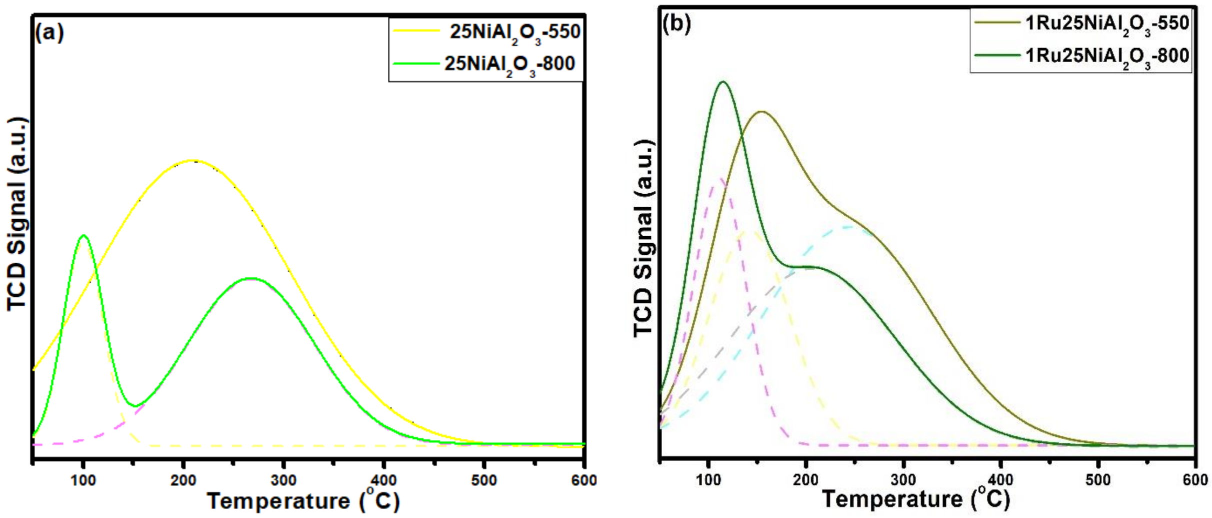

Fig. 3.18 CO_2-TPD profiles of (a) 25NiAl$_2$O$_3$ and (b) 1Ru25NiAl$_2$O$_3$ catalysts calcined at 550 °C and 800 °C

In **fig. 3.18** (a), the 25NiAl$_2$O$_3$ catalyst calcined at 550 °C showed one broad CO_2 desorption peak around 200 °C corresponding to medium basic site. On the other hand, the same catalyst calcined at 800 °C showed a low-temperature CO_2 desorption peak around 100 °C ascribed to weak basic sites on the surface and another peak between 200 °C and 400 °C attributed to medium basic sites. The intensity of the second peak in the catalyst calcined at 550 °C was higher than that calcined at 800 °C indicating that at lower calcination temperature more medium basic sites are available. In **fig 3.18** (b), 1Ru25NiAl$_2$O$_3$ catalyst calcined at 550 °C and 800 °C showed a low temperature desorption peak attributed to weak basic sites and one broad CO_2 desorption peak between 200 °C and 400 °C attributed to medium basic sites. Each CO_2 desorption peak in the 1Ru25NiAl$_2$O$_3$ catalysts calcined at 550 °C was shifted to a higher temperature, compared with the catalysts calcined at 800 °C. Moreover, the intensity of the desorption peak increased at lower calcination temperature. These results show increased basicity in catalysts calcined at lower temperature.

3.1.2. Catalytic activity

Fig. 3.19 shows the effect of calcination temperature on the gas composition (moles) and syngas production after the pyrolysis-dry reforming of polypropylene.

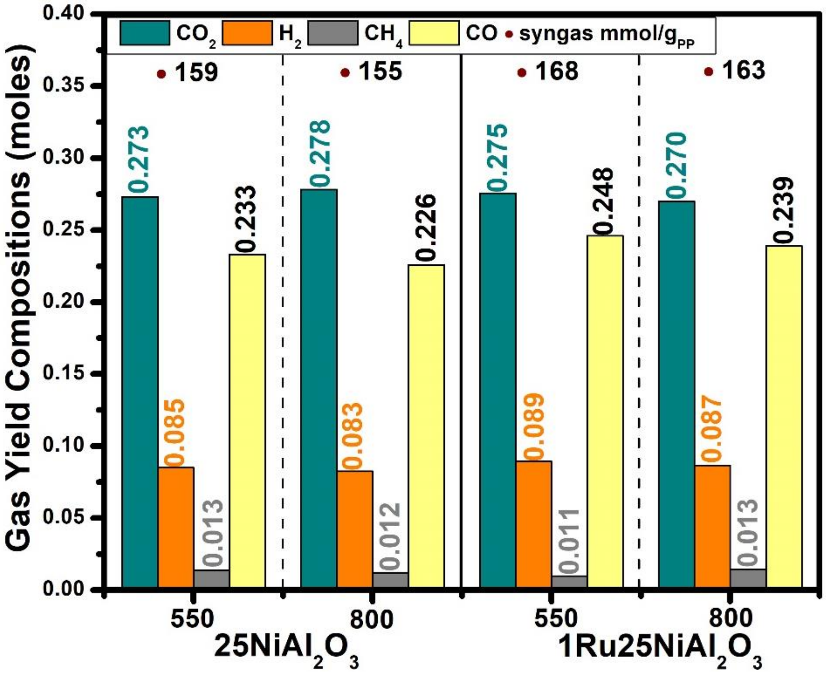

Fig. 3.19 Product gas composition of the pyrolysis-dry reforming of polypropylene over 25NiAl$_2$O$_3$ and 1Ru25NiAl$_2$O$_3$ catalysts at different calcination temperatures

As shown in **fig. 3.19**, the 25NiAl$_2$O$_3$ catalyst calcined at 550 °C produced 0.085 mol of H$_2$ and 159 mmol$_{syngas}$/g$_{PP}$ of syngas, which was slightly higher compared to the same catalyst calcined at 800 °C, which produced 0.083 mol of H$_2$ and 154 mmol$_{syngas}$/g$_{PP}$ of syngas. The same trend was also observed for the 1Ru25NiAl$_2$O$_3$ catalyst, where the one calcined at 550 °C produced slightly more H$_2$ and syngas (0.089 mol; 168 mmol$_{syngas}$/g$_{PP}$) compared to the same catalyst calcined at 800 °C (0.087 mol H$_2$; 163 mmol$_{syngas}$/g$_{PP}$). Since the catalysts were reduced before test, NiO species more readily transform into well dispersed active Ni than NiAl$_2$O$_4$ species thus affecting the catalytic activity.

3.1.3. Discussion

The activity and stability of the catalysts in the dry reforming of plastics relate to their characterization results after being calcined at two different temperatures (550 °C and 800 °C). From the XRD spectra, catalysts calcined at 800 °C showed increased crystallinity compared to those calcined at 550 °C. Furthermore, it is noticed that the NiO phase is the main component in the catalysts calcined at 550 °C, while the NiAl$_2$O$_4$ is the main component in the catalysts calcined at 800 °C. NiO species are more readily reduced into Ni compared to NiAl$_2$O$_4$ species. Therefore, the amount of Ni active sites decreases with increasing calcination temperature because the metal support interaction between Ni and alumina is stronger at higher calcination temperature and thus the Ni species are more difficult to obtain [25].

N_2 adsorption/desorption analyses showed a decrease in surface area and an increase in pore size at higher calcination temperatures. Lower surface area is typically associated with higher catalyst crystallinity [24]. The improved catalytic performance in catalysts calcined at lower temperature could be attributed to the higher surface area and smaller pore size.

From the H_2-TPR profiles, the catalysts showed better reducibility at lower calcination temperatures. These findings show that at lower calcination temperature, the interaction between Ni and the support is weaker [28]. The presence of NiO with weak interactions with the support could explain the improved catalytic performance of the catalysts calcined at 550 °C. On the other hand, the generation of the inactive $NiAl_2O_4$ spinel in the catalysts calcined at 800 °C may be responsible for their poor performance [26]. The experimental H_2 consumption of both catalysts at different calcination temperatures demonstrates that the catalysts calcined at 550 °C have a greater availability of active sites than those calcined at 800 °C, leading to higher catalytic activity. The Ni phase formed from the reduction of NiO showed better catalytic activity compared to that formed from the reduction of $NiAl_2O_4$. Therefore, researchers have focused on synthesizing catalysts with high NiO content to increase the active nickel phase while minimizing the less active nickel aluminate phase [24].

From the CO_2-TPD results, the $25NiAl_2O_3$ catalyst calcined at 550 °C showed a broader peak ascribing to medium basic sites. This indicates that at a calcination temperature of 550 °C, this catalyst had more medium basic sites than when calcined at 800 °C. For the $1Ru25NiAl_2O_3$ catalyst, a lower calcination temperature shifted the CO_2 desorption peaks to higher temperatures. This indicates that the catalyst calcined at 550 °C possessed stronger basic sites than the catalyst calcined at 800 °C. Moreover, as the calcination temperature decreased, the intensity of the desorption peak increased, indicating that more basic sites were present in the samples calcined at 550 °C. Therefore, catalysts calcined at lower temperatures had stronger basic sites, which was consistent with the observed catalytic activity trend. Consequently, it is likely that the enhanced activity of catalysts calcined at lower temperatures was influenced by their basicity [29].

The dispersion of active Ni particles, the degree of reduction, and the interaction between metal and support were all significantly influenced by the calcination temperature, which in turn affects the activity and stability of catalysts [25]. Therefore, in the dry reforming of plastics, the calcination temperature is crucial for determining the activity and stability of the Ni-based catalysts.

3.1.4. Conclusion

It can be concluded that a high catalyst calcination temperature promotes greater interaction between the active phase and the support and leads to the development of inactive species like the $NiAl_2O_4$ spinel. Thus, the catalysts calcined at 550 °C showed better catalytic performance compared to those calcined at 800 °C. Therefore, this temperature will be used for the remaining part of this study since it requires less energy and therefore lower costs while resulting in increased catalytic activity.

3.2. Aging of $25NiAl_2O_3$ and $1Ru25NiAl_2O_3$ catalysts

The $25NiAl_2O_3$ and $1Ru25NiAl_2O_3$ catalysts were aged using a nine-run protocol, which involved reforming 2 g of polypropylene plastic nine successive times. **Fig. 3.20** (a) displays the results of the aging experiments. The number of moles of H_2 generated in the presence of the $25NiAl_2O_3$ catalyst dropped from 0.085 mol during the 1st run to 0.078 mol during the 9th run. However, during the nine successive runs, the amount of hydrogen generated with the $1Ru25NiAl_2O_3$ catalyst remained consistent (at about 0.09 mol). This might be caused by the kind of carbon that has been formed on the catalytic surface. **Fig. 3.20** (b) represents the DSC curves of the spent $25NiAl_2O_3$ and $1Ru25NiAl_2O_3$ catalysts after nine runs. Both catalysts exhibited two oxidation peaks. The peak between 300 °C and 450 °C is attributed to the oxidation of nickel. The second intense exothermic peak was observed in both curves at higher temperatures, attributed to the oxidation of filamentous carbon. However, this peak is more intense for the $25NiAl_2O_3$ catalyst, indicating more carbon was deposited in the absence of ruthenium. The weight loss clearly shows that after the nine runs, more carbon was formed in the $25NiAl_2O_3$ catalyst (20%) compared to the promoted $1Ru25NiAl_2O_3$ catalyst (6%). Since deposited carbons deactivate catalysts, promoting the $NiAl_2O_3$ catalysts with Ru prevented their deposition, delaying the catalytic deactivation [8].

To check if the deactivation rate increases, three additional runs were performed over the $25NiAl_2O_3$ catalyst. The number of moles of H_2 and syngas produced decreased to 0.072 mol and 138 $mmol_{syngas}/g_{PP}$, respectively, showing 12% deactivation.

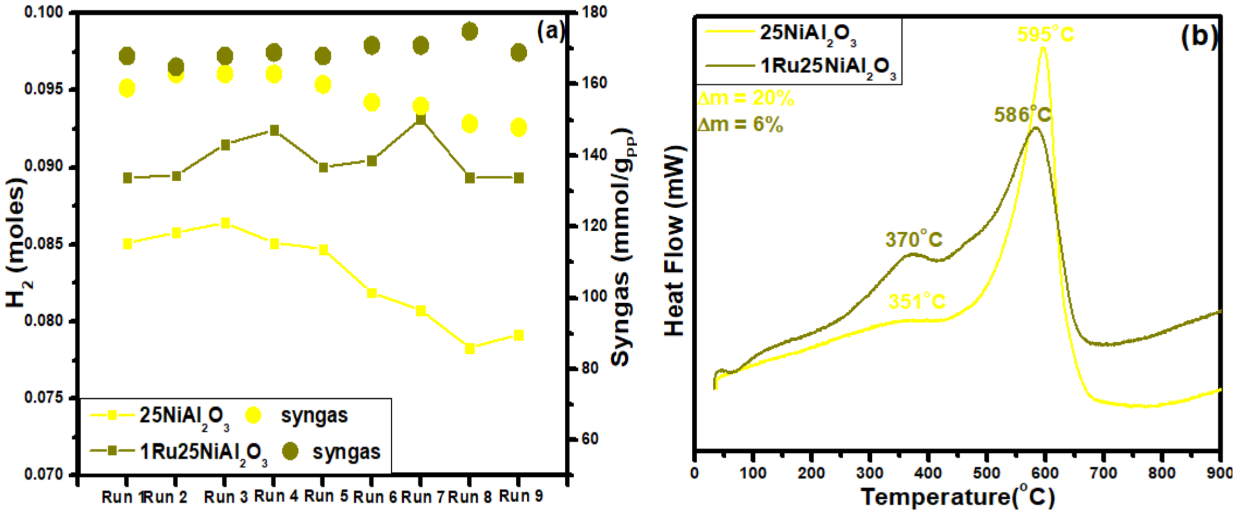

Fig. 3.20 (a) Number of moles of H_2 and syngas produced during the nine consecutive runs over the $25NiAl_2O_3$ and $1Ru25NiAl_2O_3$ catalysts and (b) the DSC curves of the spent catalysts

From an industrial perspective, nickel is more desirable due to its availability and low cost, so high loadings are plausible to attain high catalytic performance. Nevertheless, Ni-based catalysts get easily deactivated by sintering, coke deposition, and nickel oxidation. Therefore, the promotion of the catalyst with a noble metal improves the catalyst's resistance to coke deposition and enhances the catalytic activity [17].

3.3.Conclusion

Since both catalysts were synthesized using the same wet-impregnation technique and same nickel loading, this clearly shows that the co-impregnation with ruthenium can significantly enhance the stability of the nickel-based catalysts at elevated temperatures and lengthen the catalyst lifespan during the dry reforming of polypropylene. No significant deactivation of the $1Ru25NiAl_2O_3$ catalyst was observed after the successive runs. This could be because the quantity of carbon deposited did not reach the level to cause the catalyst deactivation in the present cases. Further runs should be performed to be able to determine the lifetime of the catalyst.

In the next section, the $1Ru25NiAl_2O_3$ catalyst calcined at 550 °C will be used as it showed the best compromise between cost, activity in converting the plastic into syngas, and stability during several reaction runs.

4. Influence of promoting the support with Ce

This section studies the influence of ceria addition on alumina on the activity of the 1Ru25NiAl_2O_3 catalyst.

CeO_2 is employed as a promoter for Al_2O_3-supported catalysts. This enables the combination of CeO_2's ability to store and release oxygen with the large surface area of such mesoporous supports. Additionally, one widely used method of stabilizing alumina involves doping or combining it with various metal oxides [30]. Several studies investigated ceria as an alumina stabilizing agent, and it was found to be a very promising combination for the dry reforming of methane [31]. According to the literature [32], ceria plays a crucial role in transporting active oxygen species that oxidize coke on catalyst surfaces. Therefore, the aim is to study the CeO_2 effect on coke formation over Ce-modified 1Ru25NiAl_2O_3 catalyst in the dry reforming of polypropylene.

4.1. Catalyst preparation

4.1.1. Synthesis of Al_2O_3 promoted with Ce

Mesoporous Al_2O_3 has been employed as a template to synthesize mesoporous *x*CeAl_2O_3 with various CeO_2 weight percentages (*x* = 15, 30, or 60 wt.%).

The preparation of the support was adapted from the literature [33] using the nano casting technique. Calculated amounts of $Ce(NO_3)_3 6H_2O$ were dissolved in absolute ethanol (80 ml). Alumina support (2 g) was added to the above solution and heated at 60 °C under vigorous stirring. Once the ethanol was evaporated, the remaining powder was dried in an oven at 110 °C overnight and then calcined under air at 550 °C for 4 hours with a rate of 1 °C/min. Appendix B contains the calculations used to determine the required mass of the precursor.

4.1.2. Synthesis of the *x*CeAl_2O_3 supported catalysts

The synthesis of the *x*CeAl_2O_3 supported catalysts was done using the wet impregnation technique previously discussed in Chapter 2. The nickel active phase loading was 25 wt.% and that of ruthenium was 1 wt.%. In this section, the catalysts were referred to as 1Ru25Ni*x*CeAl_2O_3 where *x* = 15, 30, or 60 wt.%.

4.2.Catalyst characterization

4.2.1. XRD

Fig. 3.21 shows the XRD pattern of the calcined 1Ru25Ni*x*CeAl$_2$O$_3$ catalysts. **Table 3.5** lists the obtained crystallite sizes and surface areas of the catalysts.

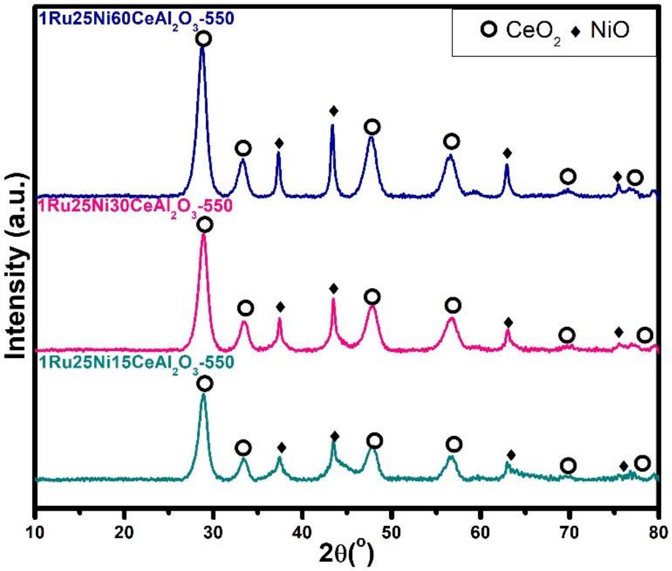

Fig. 3.21 XRD patterns of the1Ru25Ni*x*CeAl$_2$O$_3$ catalysts

All XRD patterns show the ceria crystallized in fluorite phase (JCPDS 34-0394), with the intensity increasing as the Ce percentage increases. NiO peaks are also present in all catalysts. **Table 3.5** shows the crystallite sizes of CeO$_2$ at $2\theta = 28°$ and of NiO at $2\theta = 37°$ determined from Scherrer formula. The crystallite sizes of CeO$_2$ increase with the increase in Ce percentage. Moreover, the NiO crystallite sizes are larger in the Ce-Al$_2$O$_3$ supported catalysts. The table summarizes the NiO crystallite size of the Ce-modified 1Ru25NiAl$_2$O$_3$ catalysts with different Ce content. The 1Ru25NiAl$_2$O$_3$ catalyst without ceria addition shows the smallest NiO size of 10.12 nm. NiO size increases as Ce content increases up to 60 wt.% and reached 21.22 nm. This is most likely caused by Ni particle agglomeration and the production of a solid Ni-CeO$_2$ solution at high Ce loading [32]. The table also shows the surface area of the nonpromoted and promoted 1Ru25NiAl$_2$O$_3$ catalysts. The surface area decreases from 286 m^2/g in the absence of Ce to 118 m^2/g after promotion with 60 wt.% Ce. The decrease in surface area is probably due to the presence of large amount of ceria in the catalyst, which possesses a low surface area of 70 m^2/g.

Table 3.5 Crystallite size and surface area of the1Ru25Ni*x*CeAl$_2$O$_3$ catalysts

Catalyst	Crystallite Size		S_{BET}^{a} (m^2/g)
	CeO_2	NiO	
1Ru25NiAl$_2$O$_3$	-	10.12	286
1Ru25Ni15CeAl$_2$O$_3$	6.3	11.80	201
1Ru25Ni30CeAl$_2$O$_3$	7.4	21.18	160
1Ru25Ni60CeAl$_2$O$_3$	8.20	21.22	118

4.2.2. H_2-TPR

Fig. 3.22 shows the H_2-TPR profiles of the1Ru25Ni*x*CeAl$_2$O$_3$ catalysts calcined at 550 °C.

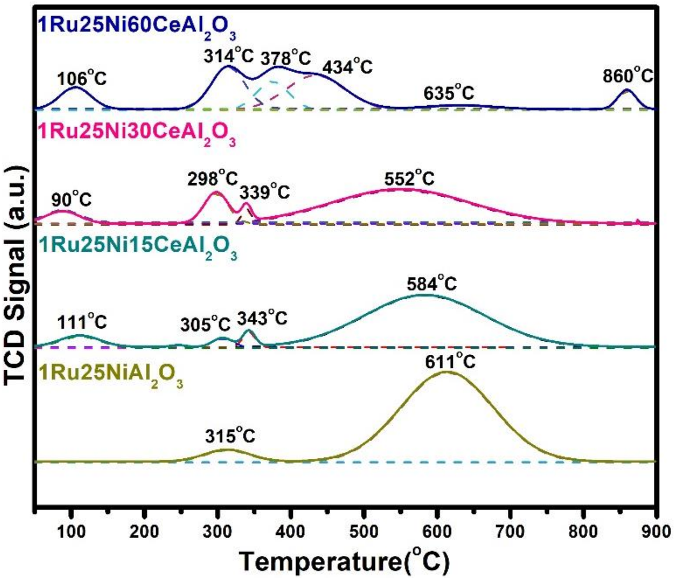

Fig. 3.22 H_2-TPR profiles of the1Ru25Ni*x*CeAl$_2$O$_3$ catalysts

The H_2-TPR peaks attributed to the reduction of RuO_2 were not detected in the 1Ru25NiAl$_2$O$_3$ catalysts. These peaks emerged after promoting the support with Ce. The peaks detected at lower temperatures (below 270 °C) are attributed to the reduction of RuO_2 species [34]. A reduction peak is noticed at low temperature in the Ce-promoted catalysts, and its intensity increases with increasing Ce loading. This reduction peak is due to the oxygen-bridging bonds known as "Ru-Ce-O" formed between ruthenium and surface cerium. At low temperatures, this bridging oxygen is very fragile and is easily reduced [8]. The fragility of Ru-Ce-O bond eases the reducibility of Ru: the ruthenium in RuO_2 is directly reduced to Ru^0 without forming intermediate valence states [34]. Ceria reduction primarily occurs in two temperature ranges: the first between 300 °C and 600 °C and the second between 700 °C and 900 °C. These two ranges are respectively attributed to the reduction of surface and bulk ceria into Ce_2O_3 [34]. Without Ce promotion, $1Ru25NiAl_2O_3$ catalysts exhibit reduction peaks at temperatures around 315 °C and 611 °C. It is well known that the reduction of complex NiOx species, which interact strongly with the support, causes the higher temperature peaks, whereas the reduction of the free NiO species causes the lower temperature peaks [6]. As the Ce content increases, the reduction peak of free NiO species shifts toward a higher temperature (from 315 °C in absence of Ce to 378 °C after promotion with 60 wt.% Ce). This was probably because the NiO is covered by CeO_2 once Ce is added [35]. On the other hand, the higher reduction peak of the promoted catalysts is ascribed to the strong interaction between Ni and CeO_2 in Ni-Ce solid solution [36]. This peak was slightly lower than that of the non-promoted catalyst showing that the interaction between NiO and Al_2O_3 weakened after promoting the support with Ce. Therefore, after the promotion of the catalyst with Ce, its reducibility improved. A weak reduction peak at 860 °C is observed at a high Ce loading of 60 wt.%, which is attributed to the reduction of bulk CeO_2 [32].

4.3. Catalytic activity

Fig. 3.23 shows the effect of promoting the support with Ce on the gas composition and syngas production after the pyrolysis-dry reforming of polypropylene.

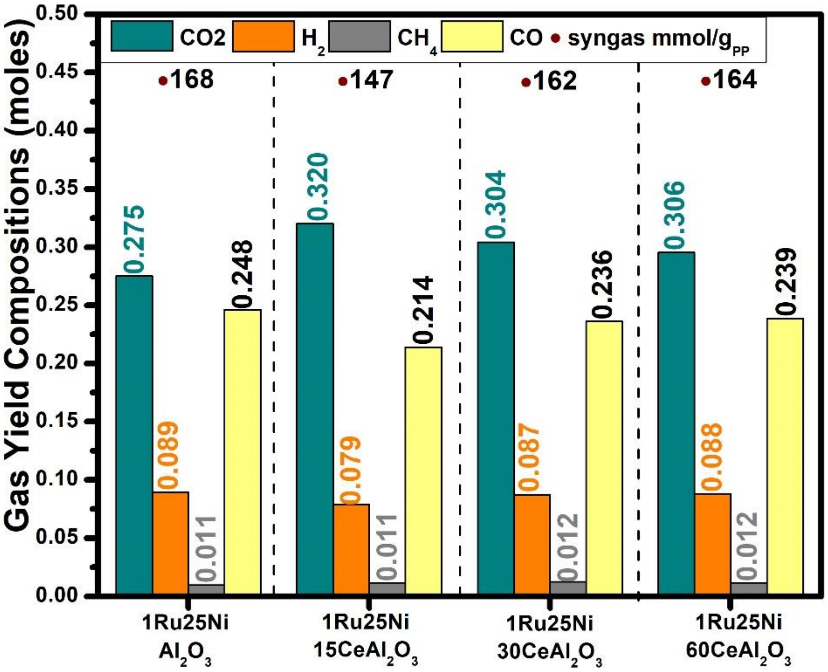

Fig. 3.23 Product gas composition of the pyrolysis-dry reforming of polypropylene over $1Ru25NixCeAl_2O_3$ catalysts

The promotion of the alumina support with 15 wt.% Ce produced fewer number of moles of H_2 and syngas (0.079 mol; 147 $mmol_{syngas}/g_{PP}$) compared to the non-promoted catalyst (0.089 mol; 168 $mmol_{syngas}/g_{PP}$). However, an increase in Ce loading to 30 wt.% and 60 wt.% led to an increase in the production of gaseous products. Both catalysts produced similar amounts of H_2 (0.087 mol and 0.088 mol) and syngas (162 $mmol_{syngas}/g_{PP}$ and 164 $mmol_{syngas}/g_{PP}$). Furthermore, the catalysts promoted with 30 wt.% and 60 wt.% Ce produced almost equivalent quantities of gaseous products as the non-promoted catalyst.

Therefore, the aging of these catalysts was performed over 3 runs to test their stability. The number of moles of H_2 and syngas produced over the three runs are presented in the **fig. 3.24**.

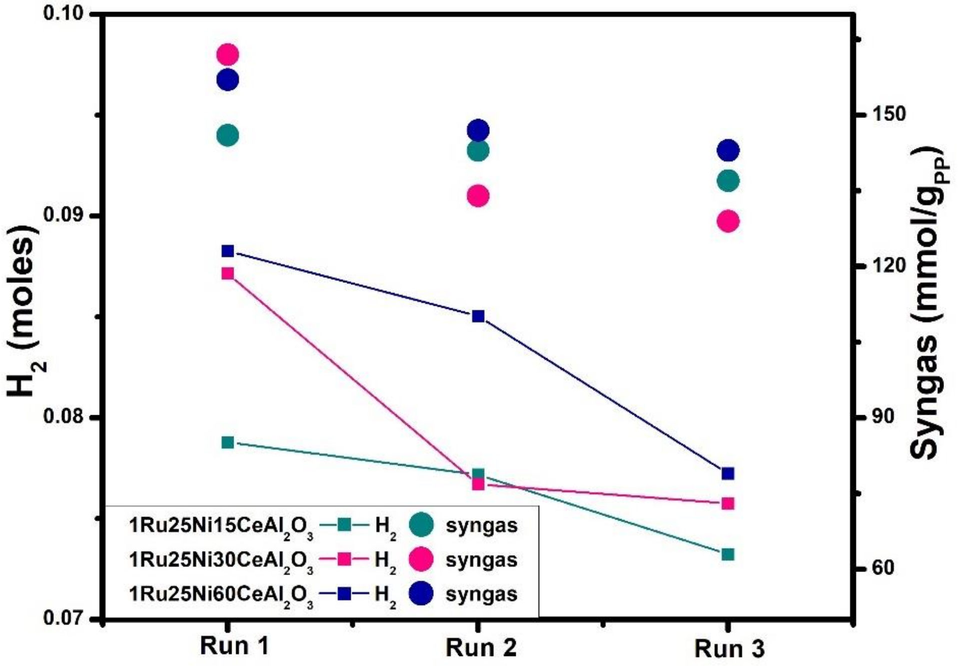

Fig. 3.24 Number of moles of H_2 and syngas produced during the three consecutive runs over 1Ru25Ni*x*CeAl$_2$O$_3$ catalysts

It is evident from the results that the number of moles of H_2 and syngas produced decreased over the consecutive runs. The number of moles of H_2 produced decreased from 0.079 mol to 0.073 mol in the catalyst promoted with 15 wt.% Ce. The syngas produced also decreased from 146 $mmol_{syngas}/g_{PP}$ to 137 $mmol_{syngas}/g_{PP}$ for this same catalyst. The same trend is also observed for the catalysts promoted with 30 wt.% and 60 wt.% of Ce. The number of moles of H_2 decreased from 0.087 mole to 0.075 for the 1Ru25Ni30CeAl$_2$O$_3$ catalyst and from 0.088 mol to 0.077 mol for the 1Ru25Ni60CeAl$_2$O$_3$ catalyst after the three runs. It is worth mentioning that in all three catalysts, an obvious drop in flow was noticed throughout the second and third runs, probably due to the clogging of the reactor. Therefore, the carbon deposited on the catalysts is studied. The DSC curves of the used catalysts are presented in **fig. 3.25**.

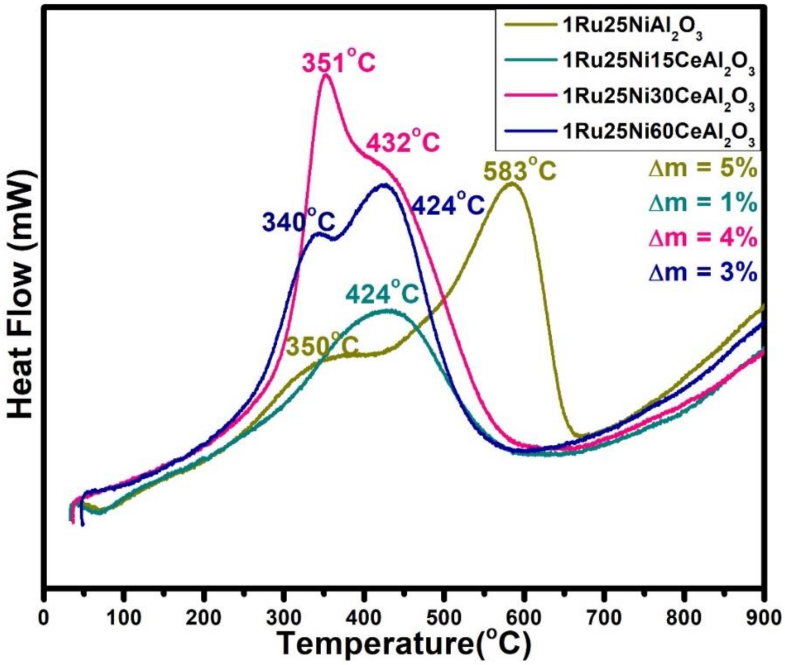

Fig. 3.25 DSC curves of the spent 1Ru25Ni*x*CeAl$_2$O$_3$ catalysts

The DSC profiles showed that the promoted catalysts produced amorphous coke, as indicated by the lower temperature peak (below 500 °C). The intensity of the peaks increased with an increase in Ce loading. On the other hand, the non-promoted catalyst produced filamentous coke (583 °C). Moreover, less carbon was deposited on the surface of the catalyst in the Ce-promoted catalyst. It is to be noted that the low temperature peak (350 °C) in the non-promoted catalyst is accompanied by a weight gain corresponding to the oxidation of nickel. No weight gain peaks were noticed for the Ce-promoted catalysts, indicating that both peaks recorded below 500 °C correspond to the oxidation of amorphous carbon.

4.4.Discussion

Alumina is characterized by its thermal stability and large surface area. Ceria is characterized by its oxygen mobility and physicochemical properties [34]**.** From the textural properties, it is noticed that the surface area decreases with the increase of Ce loading. This is due to the agglomeration of Ni particles and the formation of Ni-CeO$_2$, especially since it is more difficult to reduce the Ni in Ni-CeO$_2$ [32]. This agrees with the NiO crystallite size, where it was greater in the Ce-promoted catalysts compared to the non-promoted 1Ru25NiAl$_2$O$_3$ catalyst. Moreover, the active metal dispersion on a support with a high surface area improves the activity and stability of the catalyst [34]. Therefore, the difference in catalytic performance seems to be related to Ni dispersion and surface area. The catalytic activity decreases when catalysts are promoted with high Ce loadings due to the agglomeration of Ni particles and the segregation of CeO$_2$ [32].

For all the catalysts, TPR analyses revealed that Ce addition increases active phase reduction. The creation of easily reducible, widely diffused ruthenium oxide species is facilitated by the unique interaction established between ruthenium and cerium oxide species. It can be explained that the Ce promotion supplied active oxygen species, thus inhibiting coke formation. According to the literature [32], CeO$_2$ acts as a carrier for active oxygen species that oxidize coke on catalyst surfaces and strengthen metal to support contact. In general, the oxygen vacancies offered by CeO$_2$ during dry reforming reactions inhibit carbon deposition by improving surface oxygen mobility and adsorbing CO$_2$ species on the catalyst surface. This is primarily because systems combining Ru and Ce have good redox characteristics, which enable carbon oxidation processes [37]. The dissociation of carbon dioxide is improved by reduced ceria and absorbed oxygen species react with the surface carbon to produce H$_2$, CO, and CO$_2$. Therefore, less carbon is formed on the surface of the catalysts promoted with Ce. Furthermore, Ce-promoted support revealed the ability to significantly inhibit filamentous carbon growth. However, it was unable to stop the development of amorphous carbon. The aging of the Ce-promoted catalysts showed that these catalysts gradually deactivate.

According to the literature [38], the carbon oxidized at high temperature was due to the oxidation of the filamentous whisker carbons developed on the catalyst’s surface, while the carbon oxidized at low temperature could be attributed to the combustion of the encapsulating carbons. The filamentous type carbons have less of a deactivation effect than the encapsulating layered carbons because they grow away from the catalytic surface [39]. Due to the carbon formed on the 1Ru25NiAl$_2$O$_3$ catalyst (not promoted with Ce), Ni particles will be pushed forward by the expanding carbon whisker and lifted over the catalyst. This way, the Ni particles are still available for reactions, and the conversion of the reactions is not impacted. On the contrary, as amorphous carbon builds up on the catalyst surface, the Ni particles will be shielded, and the reaction conversion will drop. Consequently, it may be the cause of the decrease in conversion in the Ce-promoted catalysts throughout the three runs [40].

Therefore, it is suggested that the amorphous carbon formed on the surface of the Ce-promoted catalysts is responsible for the low catalytic activity due to the blockage of the gaseous reactants to the catalyst during the pyrolysis-dry reforming of polypropylene.

4.5. Conclusion

The results clearly show that the promotion of the support did not enhance the catalytic activity in the dry reforming of the polypropylene reaction. On the contrary, the aging of the catalysts demonstrated catalytic deactivation over three runs. The high Ce content might have segregated CeO_2 and thus led to the deactivation of the catalyst. Moreover, the carbon formed on the surface of the catalyst is amorphous. This type of carbon encapsulates the Ni active site, causing the deactivation. Therefore, the aim to decrease carbon deposition by promoting the support with Ce failed due to the type of carbon formed. Thus, in the upcoming sections, the catalyst of choice is $1Ru25NiAl_2O_3$ calcined at 550 °C.

5. Reaction Parameters

The influence of the plastic to catalyst ratio was investigated to determine the optimum process parameters regarding the mass of starting materials. Three masses of PP plastic, 1 g, 2 g, and 3 g were utilized to generate the corresponding plastic: catalyst ratios of 1:1, 2:1, and 3:1 while maintaining a constant amount of the catalyst at 1 g. **Fig. 3.26** shows the hydrogen produced (moles) in the three tests compared to the corresponding maximum theoretical values. Regardless of the initial mass of plastics utilized, it has been shown that the amounts of H_2 generated are around 53% and 63% of the theoretical quantities. Furthermore, the syngas production was 164 $mmol_{syngas}/g_{PP}$, 168 $mmol_{syngas}/g_{PP}$, and 132 $mmol_{syngas}/g_{PP}$ for plastic: catalyst ratios of 1:1, 2:1, and 3:1, respectively. Saad and Williams [41] investigated the impact of the catalyst to plastic ratio on syngas production by using a constant mass of plastic and various masses of catalyst. They established that the ideal catalyst to plastic ratio for the pyrolysis-dry reforming reaction is 0.5. They hypothesized that by using more catalyst, more pyrolysis gases would be reformed, leading to more production of syngas and less deposition of carbon. However, a further increase in catalyst mass reduces the CO formation because of the CO methanation reaction **(3.3)**.

$$CO + 3H_2 \rightarrow CH_4 + H_2O \qquad \textbf{(3.3)}$$

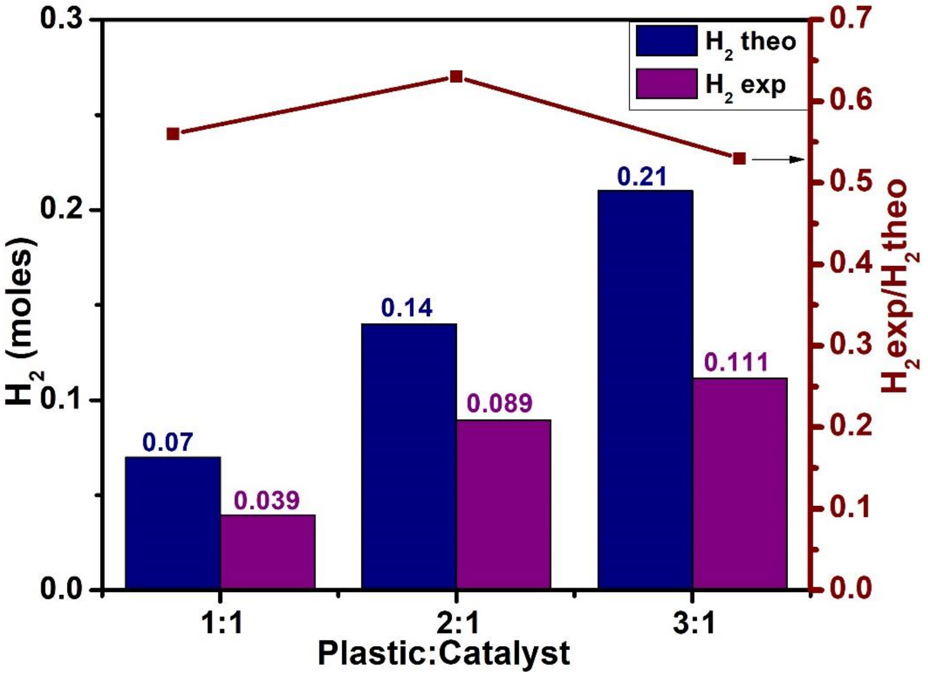

Fig. 3.26 Theoretical and experimental number of moles of H_2 for different plastic:catalyst ratios

The amount of carbon deposited on the catalysts' surface was determined by conducting a thermal study on the used catalysts. Similar weight loss was observed for ratios of 1:1 and 2:1 (4 wt.% and 5 wt.%, respectively). However, for the 3:1 ratio, the weight loss was high (15 wt.%). This could be because pyrolyzing more plastics results in the formation of more methane. As a result, the methane decomposition reaction, favored at 800 °C, resulted in an increase in the carbon deposition on the catalyst's surface [38].

As a result, it is decided that a plastic:catalyst ratio of 2:1 represents the best compromise in this study because it produces a significant amount of syngas while valorizing a larger volume of plastic with a relatively low carbon output.

6. Comparison of $1Ru25NiAl_2O_3$ with a commercial catalyst

The synthesized catalyst in this study was compared with a commercial reforming catalyst purchased from Arcos Organics comprising of 50 wt.% Ni loading on an alumina support, reduced, and stabilized (product code: 326211000). The commercial catalyst is denoted by $50NiAl_2O_3$-comm (the synthesis method and calcination temperature of the commercial catalysts are unknown).

Fig. 3.27 shows the gas composition and syngas production over the two catalysts in the pyrolysis-dry reforming of polypropylene.

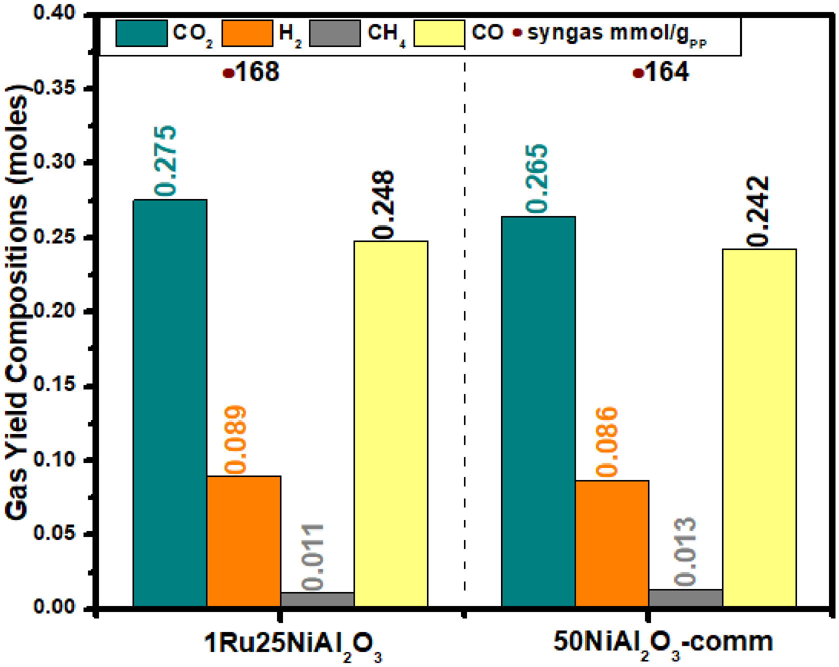

Fig. 3.27 Product gas composition of the pyrolysis-dry reforming of polypropylene over 1Ru25NiAl$_2$O$_3$ and a commercial catalyst

The catalyst synthesized in this study produced a higher number of moles of H_2 and syngas (0.089 mol; 168 $mmol_{syngas}/g_{PP}$) compared to the commercial catalyst (0.086 mol; 164 $mmol_{syngas}/g_{PP}$). Note that the synthesized catalyst required half the Ni loading compared to the commercial catalyst yet showed better catalytic activity. This comparison experiment proved that 1Ru25NiAl$_2$O$_3$ is a promising catalyst for the dry reforming of plastics.

Data from several published studies reporting on the pyrolysis-dry reforming of plastics over different catalysts and under various process parameters is compiled in **Table 3.6**. For comparison, our catalyst is listed in the first row of the table. Compared to the catalysts indicated in the table, the optimum catalyst presented in this study produced more syngas, with a yield of 168 $mmol_{syngas}/g_{PP}$ for the 1Ru25NiAl$_2$O$_3$ catalyst. The amount of syngas produced by the 25NiAl$_2$O$_3$ catalyst synthesized in this study (159 $mmol_{syngas}/g$) was larger than the amounts of syngas produced in prior studies 153.67 $mmol_{syngas}/g$ [42], 138.81 $mmol_{syngas}/g$ [41], under similar process conditions. Ru as a metal promoter produced greater syngas yield (168 $mmol_{syngas}/g$) than Cu (130.56 $mmol_{syngas}/g$) [2], Co (136 $mmol_{syngas}/g$, 149.92 $mmol_{syngas}/g$, 148.6 $mmol_{syngas}/g$, 96

$mmol_{syngas}/g$) [2,41,43,44], and Mg (146.96 $mmol_{syngas}/g$) [2,43]. Furthermore, alumina-supported catalysts produced higher syngas yield than ZSM-5-supported catalysts (112.6 $mmol_{syngas}/g$, 95.2 $mmol_{syngas}/g$) [45,46]. This study is the first to use ruthenium as a promoter transition metal, demonstrating the novelty of the work and the effectiveness of such a catalyst in producing substantial amounts of syngas.

Table 3.6 Syngas yields obtained from the pyrolysis-catalytic dry reforming of plastics reported in the literature under different process parameters

Catalyst	Plastic Used	Operating Conditions	Catalyst: Plastic	Syngas Yield	Reference
$25NiAl_2O_3$	PP	T_{pyr}=500°C	0.5	159 $mmol/g_{PP}$	This Work
$1Ru25NiAl_2O_3$		T_{DR}= 800°C		168 $mmol/g_{PP}$	
$NiAl_2O_3$	MPW	T_{pyr}=500°C T_{DR}= 800°C	0.5	153.67$mmol/g_{MPW}$	[42]
Ni-Al	HDPE	T_{pyr}=500°C	0.5	138.81$mmol/g_{HDPE}$	[2]
Ni-Cu-Al		T_{DR}= 800°C		130.56$mmol/g_{HDPE}$	
Ni-Co-Al				149.92$mmol/g_{HDPE}$	
Ni-Mg-Al				146.96$mmol/g_{HDPE}$	
Ni-Co-Al	LDPE	T_{pyr}=500°C	0.5	154.7$mmol/g_{LDPE}$	[44]
	HDPE	T_{DR}= 800°C		149.4 $mmol/g_{HDPE}$	
	PP			136 $mmol/g_{PP}$	
	PS			126.3 $mmol/g_{PS}$	
	PET			63 $mmol/g_{PET}$	
$Ni-Co/Al_2O_3$	MPW*	T_{pyr}=500°C T_{DR}= 800°C	0.5	148.6$mmol/g_{MPW}$	[41]
$Ni-Co/Al_2O_3$	MPW	T_{pyr}=500°C T_{DR}= 800°C	0.5	96$mmol/g_{MPW}$	[43]
$Ni-Mg/Al_2O_3$	MPW	T_{pyr}=500°C T_{DR}= 800°C	0.5	108$mmol/g_{MPW}$	[43]
$Ni-Mg/Al_2O_3$	HDPE	T_{pyr}=500°C T_{DR}= 800°C	0.5	132$mmol/g_{HDPE}$	[3]
Ni/ZSM-5	MPW	T=850°C	0.5	112.6$mmol/g_{MPW}$	[45]
Ni/ZSM-5	MPW	T=850°C	0.5	95.2$mmol/g_{MPW}$	[46]

***MPW: Municipal Plastic Waste**

7. Pyrolysis-dry reforming of different types of plastics over $1Ru25NiAl_2O_3$ catalyst

The $1Ru25NiAl_2O_3$, was used to investigate the pyrolysis-reforming other types of plastics (PE and PS), as well as a mixture of two plastics (50% PP + 50% PE). The gas yield compositions (moles) and the syngas produced ($mmol_{syngas}/g_{Plastics}$) are depicted in **fig. 3.28** (a). The H_2, CO, and syngas yields (%) with respect to the theoretical calculations are shown in **fig. 3.28** (b).

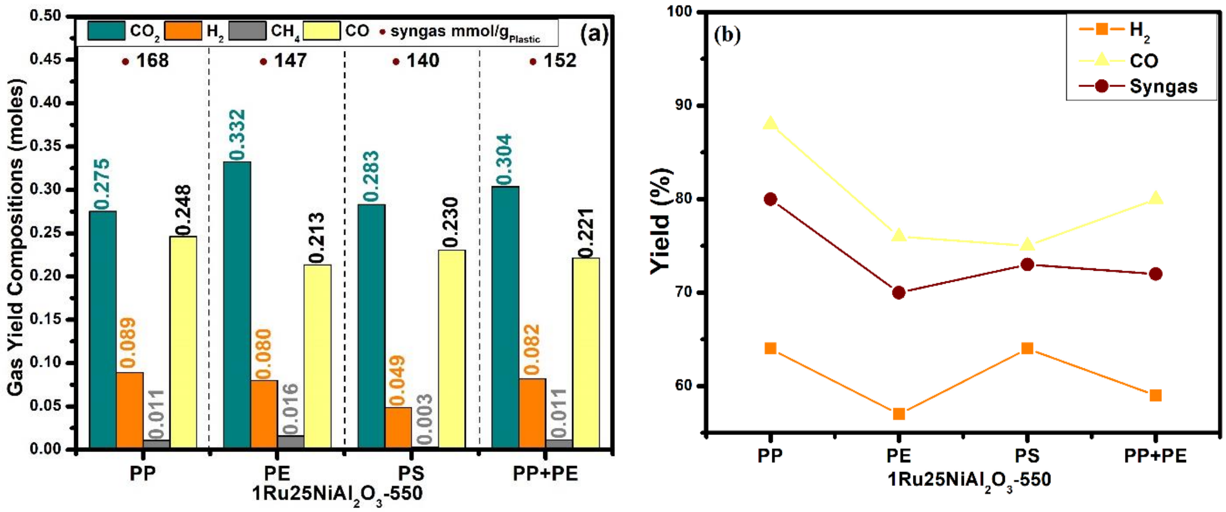

Fig. 3.28 (a) Product gas composition of the pyrolysis-dry reforming of different types of plastics over $1Ru25NiAl_2O_3$ and (b) H_2, CO, and syngas yields

The results show that PP plastic resulted in the highest values of hydrogen (0.089 mol) and syngas (168 $mmol_{syngas}/g_{PP}$) compared to PE (0.08 mol; 147 $mmol_{syngas}/g_{PE}$) and PS (0.049 mol; 140 $mmol_{syngas}/g_{PS}$). According to the theoretical calculations (Appendix B), the dry reforming of PP and PE should produce 0.14 mol of H_2 and 210 $mmol_{syngas}/g_{PP}$ of syngas. PS should theoretically produce 0.077 mol of H_2 and 193 $mmol_{syngas}/g_{PS}$ of syngas. This allowed the computation of the yield of H_2, CO, and syngas produced for each type of plastic over the $1Ru25NiAl_2O_3$ catalyst. The yield of H_2 was 64% for PP, 57% for PE, 64% for PS, and 59% for the mixture of PE and PP. The yield of CO was 88% for PP, 76% for PE, 75% for PS, and 80% for the mixture. The syngas yield was 80% for PP, 70% for PE, 73% for PS, and 72% for the mixture. It is noticed that over $1Ru25NiAl_2O_3$ catalyst, the H_2 yield leveled around 60%, the CO yield leveled around 80%, and that of syngas leveled around 70%.

DSC/TG experiments were carried out for the reacted $1Ru25NiAl_2O_3$ catalysts from the dry reforming of the different types of plastics. The results of the DSC curves are presented in **fig. 3.29**.

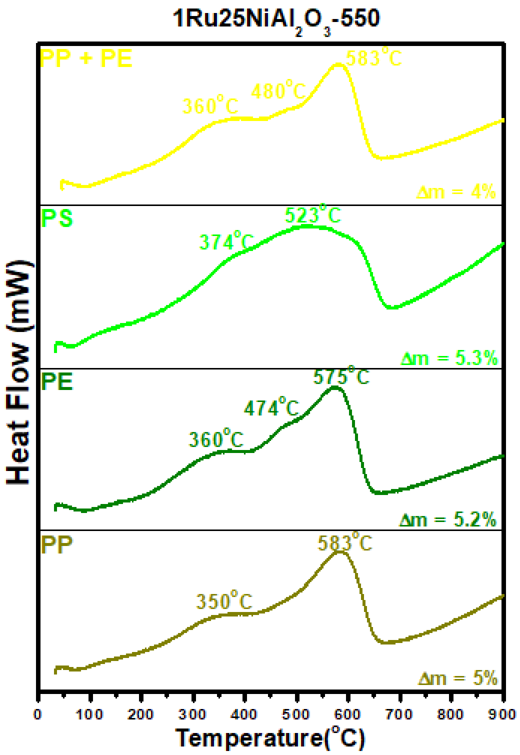

Fig. 3.29 DSC curves of the spent $1Ru25NiAl_2O_3$ catalysts after reforming different types of plastics

Two exothermic peaks are noticed for the spent catalyst after the pyrolysis of different types of plastics. The first peak, accompanied by weight gain (around 360 °C), corresponds to the oxidation of nickel. The second peak, accompanied by weight loss (above 500 °C), corresponds to the oxidation of filamentous carbon formed on the catalyst surface. For PE plastic, a third peak is noticed (at 474 °C for pure PE and 480 °C for the mixture), corresponding to the oxidation of amorphous carbon below 500 °C. Furthermore, the carbon deposited levels around 5%, regardless the type of plastic used.

7.1.Discussion

For the dry reforming of plastics, the insertion of Ru over the $NiAl_2O_3$ catalyst introduced more active sites by improving Ni dispersion and particle size, thus increasing the plastic conversion. However, the behavior of the catalyst toward syngas production may vary based on the type of plastic used. In terms of syngas production from the dry reforming of different types of plastic over 1Ru25NiAl$_2$O$_3$ catalyst, it may be summed up as follows: PP produces a large yield of syngas, followed by PS, a mixture of PP and PE, and then PE. A difference in syngas production is noticed among the different types of plastics. This may be attributed to the carbon formed on the catalyst's surface after reforming. It is therefore concluded that, depending on the waste sample used, the formation of the carbon deposits on the Ni-based catalysts varies [39]. The yield of syngas slightly varied between these plastics, showing that the synthesized catalyst in this study can successfully convert different types of plastics into significant quantities of syngas.

8. Conclusion

Catalytic-dry reforming has a significant impact on the breaking of high molecular weight hydrocarbons into hydrogen and carbon monoxide. The insertion of a catalyst to the dry reforming of plastics increased the production of syngas. The 1Ru25NiAl$_2$O$_3$ catalyst has proven successful in producing significant quantities of syngas after the dry reforming of different types of plastics.

The significant increase in the activity and stability of Ru-Ni bimetallic catalysts was caused by an increase in the metallic dispersion of Ni due to the formation of Ni-Ru clusters with a Ni-covered surface. It is probable that as Ru and Ni are reduced, bimetallic clusters of both metals form.

9. References

[1] PlascticsEurope, Plastics-the Facts 2021 An analysis of European plastics production, demand and waste data, 2021.

[2] J.M. Saad, M.A. Nahil, C. Wu, P.T. Williams, Influence of nickel-based catalysts on syngas production from carbon dioxide reforming of waste high density polyethylene, Fuel Processing Technology. 138 (2015) 156–163. https://doi.org/10.1016/j.fuproc.2015.05.020.

[3] J.M. Saad, M.A. Nahil, P.T. Williams, Influence of process conditions on syngas production from the thermal processing of waste high density polyethylene, J Anal Appl Pyrolysis. 113 (2015) 35–40. https://doi.org/10.1016/J.JAAP.2014.09.027.

[4] J. Abou Rached, M.R. Cesario, J. Estephane, H.L. Tidahy, C. Gennequin, S. Aouad, A. Aboukaïs, E. Abi-Aad, Effects of cerium and lanthanum on Ni-based catalysts for CO_2 reforming of toluene, J Environ Chem Eng. 6 (2018). https://doi.org/10.1016/j.jece.2018.06.054.

[5] L. Guczi, G. Stefler, O. Geszti, I. Sajó, Z. Pászti, A. Tompos, Z. Schay, Methane dry reforming with CO_2: A study on surface carbon species, Appl Catal A Gen. 375 (2010) 236–246. https://doi.org/10.1016/J.APCATA.2009.12.040.

[6] S. Andraos, R. Abbas-Ghaleb, D. Chlala, A. Vita, C. Italiano, M. Laganà, L. Pino, M. Nakhl, S. Specchia, Production of hydrogen by methane dry reforming over ruthenium-nickel based catalysts deposited on Al_2O_3, $MgAl_2O_4$, and YSZ, Int J Hydrogen Energy. 44 (2019) 25706–25716. https://doi.org/10.1016/j.ijhydene.2019.08.081.

[7] N.A. Roslan, S. Zainal Abidin, O.U. Osazuwa, S.Y. Chin, Y.H. Taufiq-Yap, Enhanced syngas production from glycerol dry reforming over Ru promoted -Ni catalyst supported on extracted Al2O3, Fuel. 314 (2022). https://doi.org/10.1016/J.FUEL.2021.123050.

[8] N. Elia, J. Estephane, C. Poupin, B. el Khoury, L. Pirault-Roy, S. Aouad, E.A. Aad, A Highly Selective and Stable Ruthenium-Nickel Supported on Ceria Catalyst for Carbon Dioxide Methanation, ChemCatChem. 13 (2021) 1559–1567. https://doi.org/10.1002/cctc.202001687.

[9] W.A.W. Abu Bakar, R. Ali, S. Toemen, Catalytic methanation reaction over supported nickel-ruthenium oxide base for purification of simulated natural gas, Scientia Iranica. 19 (2012) 525–534. https://doi.org/10.1016/j.scient.2012.02.004.

[10] I. Luisetto, C. Sarno, D. de Felicis, F. Basoli, C. Battocchio, S. Tuti, S. Licoccia, E. di Bartolomeo, Ni supported on γ-Al_2O_3 promoted by Ru for the dry reforming of methane in packed and monolithic reactors, Fuel Processing Technology. 158 (2017) 130–140. https://doi.org/10.1016/J.FUPROC.2016.12.015.

[11] J. Estephane, S. Aouad, S. Hany, B. el Khoury, C. Gennequin, H. el Zakhem, J. el Nakat, A. Aboukaïs, E. Abi Aad, CO_2 reforming of methane over Ni-Co/ZSM5 catalysts. Aging and carbon deposition study, Int J Hydrogen Energy. 40 (2015) 9201–9208. https://doi.org/10.1016/j.ijhydene.2015.05.147.

[12] M.D. Argyle, C.H. Bartholomew, Heterogeneous catalyst deactivation and regeneration: A review, Catalysts. 5 (2015) 145–269. https://doi.org/10.3390/catal5010145.

[13] T. Miyazawa, T. Kimura, J. Nishikawa, S. Kado, K. Kunimori, K. Tomishige, Catalytic performance of supported Ni catalysts in partial oxidation and steam reforming of tar derived from the pyrolysis

of wood biomass, Catal Today. 115 (2006) 254–262. https://doi.org/10.1016/J.CATTOD.2006.02.055.

[14] D. Xu, Y. Xiong, S. Zhang, Y. Su, The influence of preparation method of char supported metallic Ni catalysts on the catalytic performance for reforming of biomass tar, Int J Energy Res. 43 (2019) 6922–6933. https://doi.org/10.1002/ER.4709.

[15] C. Jiménez-González, Z. Boukha, B. de Rivas, J.J. Delgado, M.Á. Cauqui, J.R. González-Velasco, J.I. Gutiérrez-Ortiz, R. López-Fonseca, Structural characterisation of Ni/alumina reforming catalysts activated at high temperatures, Appl Catal A Gen. 466 (2013) 9–20. https://doi.org/10.1016/j.apcata.2013.06.017.

[16] N. Sahli, C. Petit, A.C. Roger, A. Kiennemann, S. Libs, M.M. Bettahar, Ni catalysts from NiAl2O4 spinel for CO_2 reforming of methane, Catal Today. 113 (2006) 187–193. https://doi.org/10.1016/j.cattod.2005.11.065.

[17] M. A. Álvarez, L.F. Bobadilla, V. Garcilaso, M.A. Centeno, J.A. Odriozola, CO_2 reforming of methane over Ni-Ru supported catalysts: On the nature of active sites by operando DRIFTS study, Journal of CO_2 Utilization. 24 (2018) 509–515. https://doi.org/10.1016/j.jcou.2018.01.027.

[18] A. Ishihara, E.W. Qian, I.N. Finahari, I.P. Sutrisna, T. Kabe, Addition effect of ruthenium on nickel steam reforming catalysts, Fuel. 84 (2005) 1462–1468. https://doi.org/10.1016/J.FUEL.2005.03.006.

[19] S. Aouad, E. Saab, E. Abi Aad, A. Aboukaïs, Reactivity of Ru-based catalysts in the oxidation of propene and carbon black, Catal Today. 119 (2007) 273–277. https://doi.org/10.1016/j.cattod.2006.08.030.

[20] C. Gennequin, S. Hany, H.L. Tidahy, S. Aouad, J. Estephane, A. Aboukaïs, E. Abi-Aad, Influence of the presence of ruthenium on the activity and stability of Co–Mg–Al-based catalysts in CO_2 reforming of methane for syngas production, Environmental Science and Pollution Research. 23 (2016) 22744–22760. https://doi.org/10.1007/S11356-016-7453-Z/TABLES/4.

[21] M. Zhai, X. Wang, Y. Zhang, P. Dong, G. Qi, Y. Huang, Characteristics of rice husk tar secondary thermal cracking, Energy. 93 (2015) 1321–1327. https://doi.org/10.1016/J.ENERGY.2015.10.029.

[22] A. Farooq, H. Song, Y.K. Park, G.H. Rhee, Effects of different Al_2O_3 support on HDPE gasification for enhanced hydrogen generation using Ni-based catalysts, Int J Hydrogen Energy. 46 (2021) 18085–18092. https://doi.org/10.1016/J.IJHYDENE.2020.05.199.

[23] Y.S. Seo, Y.S. Jung, W.L. Yoon, I.G. Jang, T.W. Lee, The effect of Ni content on a highly active Ni-Al_2O_3 catalyst prepared by the homogeneous precipitation method, Int J Hydrogen Energy. 36 (2011) 94–102. https://doi.org/10.1016/J.IJHYDENE.2010.09.082.

[24] B.C. Kwon, N.K. Park, M. Kang, D. Kang, M.W. Seo, D. Lee, S.G. Jeon, H.J. Ryu, CO_2 hydrogenation activity of Ni-Mg-Al_2O_3 catalysts: Reaction behavior on NiAl2O4 and MgAl2O4, Korean Journal of Chemical Engineering. 38 (2021) 1188–1196. https://doi.org/10.1007/s11814-021-0778-4.

[25] L. He, Y. Ren, B. Yue, S.C.E. Tsang, H. He, Tuning metal–support interactions on Ni/Al_2O_3 catalysts to improve catalytic activity and stability for dry reforming of methane, Processes. 9 (2021). https://doi.org/10.3390/pr9040706.

[26] M.L. Dieuzeide, V. Iannibelli, M. Jobbagy, N. Amadeo, Steam reforming of glycerol over Ni/Mg/γ-Al_2O_3 catalysts. Effect of calcination temperatures, Int J Hydrogen Energy. 37 (2012) 14926–14930. https://doi.org/10.1016/J.IJHYDENE.2011.12.086.

[27] H. Wu, M. Zou, L. Guo, F. Ma, W. Mo, Y. Yu, I. Mian, J. Liu, S. Yin, N. Tsubaki, Effects of calcination temperatures on the structure–activity relationship of Ni–La/Al_2O_3 catalysts for syngas methanation, RSC Adv. 10 (2020) 4166–4174. https://doi.org/10.1039/C9RA09674D.

[28] J. Gao, C. Jia, J. Li, M. Zhang, F. Gu, G. Xu, Z. Zhong, F. Su, Ni/Al_2O_3 catalysts for CO methanation: Effect of Al_2O_3 supports calcined at different temperatures, Journal of Energy Chemistry. 22 (2013) 919–927. https://doi.org/10.1016/S2095-4956(14)60273-4.

[29] Z. Bian, W. Zhong, Y. Yu, Z. Wang, B. Jiang, S. Kawi, Dry reforming of methane on Ni/mesoporous-Al_2O_3 catalysts: Effect of calcination temperature, Int J Hydrogen Energy. 46 (2021) 31041–31053. https://doi.org/10.1016/J.IJHYDENE.2020.12.064.

[30] K.M.S. Khalil, Synthesis and characterization of mesoporous ceria/alumina nanocomposite materials via mixing of the corresponding ceria and alumina gel precursors, J Colloid Interface Sci. 307 (2007) 172–180. https://doi.org/10.1016/J.JCIS.2006.11.039.

[31] S. Damyanova, B. Pawelec, R. Palcheva, Y. Karakirova, M.C. Capel-Sanchez, G. Tyuliev, E. Gaigneaux, J.L.G. Fierro, Structure and surface properties of ceria-modified Ni-based catalysts for hydrogen production, Appl Catal B. 225 (2018) 340–353. https://doi.org/10.1016/J.APCATB.2017.12.002.

[32] K.Y. Koo, H.S. Roh, U.H. Jung, W.L. Yoon, CeO2 promoted Ni/Al_2O_3 catalyst in combined steam and carbon dioxide reforming of methane for gas to liquid (GTL) process, Catal Letters. 130 (2009) 217–221. https://doi.org/10.1007/S10562-009-9867-4.

[33] M. Piumetti, S. Bensaid, N. Russo, D. Fino, Nanostructured ceria-based catalysts for soot combustion: Investigations on the surface sensitivity, Appl Catal B. 165 (2015) 742–751. https://doi.org/10.1016/J.APCATB.2014.10.062.

[34] M. Safariamin, L.H. Tidahy, E. Abi-Aad, S. Siffert, A. Aboukaïs, Dry reforming of methane in the presence of ruthenium-based catalysts, Comptes Rendus Chimie. 12 (2009) 748–753. https://doi.org/10.1016/j.crci.2008.10.021.

[35] F. Meng, Z. Li, J. Liu, X. Cui, H. Zheng, Effect of promoter Ce on the structure and catalytic performance of Ni/Al_2O_3 catalyst for CO methanation in slurry-bed reactor, J Nat Gas Sci Eng. 23 (2015) 250–258. https://doi.org/10.1016/J.JNGSE.2015.01.041.

[36] K.Y. Koo, H.S. Roh, U.H. Jung, W.L. Yoon, Combined H_2O and CO_2 reforming of CH_4 over Ce-promoted Ni/Al_2O_3 catalyst for gas to liquid (GTL) process: Enhancement of Ni-CeO_2 interaction, Catal Today. 185 (2012) 126–130. https://doi.org/10.1016/J.CATTOD.2011.07.027.

[37] R. Mahfouz, J. Estephane, C. Gennequin, L. Tidahy, S. Aouad, E. Abi-Aad, CO_2 reforming of methane over Ni and/or Ru catalysts supported on mesoporous KIT-6: Effect of promotion with Ce, J Environ Chem Eng. 9 (2021) 104662. https://doi.org/10.1016/J.JECE.2020.104662.

[38] S. Aouad, M. Labaki, S. Ojala, P. Seelam, E. Turpeinen, C. Gennequin, J. Estephane, E.A. Aad, A Review on the Dry Reforming Processes for Hydrogen Production: Catalytic Materials and Technologies, in: 2018: pp. 60–128. https://doi.org/10.2174/9781681087580118020007.

[39] J.M. Saad, P.T. Williams, Catalytic dry reforming of waste plastics from different waste treatment plants for production of synthesis gases, Waste Management. 58 (2016) 214–220. https://doi.org/10.1016/j.wasman.2016.09.011.

[40] W. Chen, G. Zhao, Q. Xue, L. Chen, Y. Lu, High carbon-resistance Ni/CeAl$_2$O$_3$-Al$_{2O3}$ catalyst for CH$_4$/CO$_2$ reforming, Appl Catal B. 136–137 (2013) 260–268. https://doi.org/10.1016/J.APCATB.2013.01.044.

[41] J.M. Saad, P.T. Williams, Pyrolysis-catalytic dry (CO$_2$) reforming of waste plastics for syngas production: Influence of process parameters, Fuel. 193 (2017) 7–14. https://doi.org/10.1016/j.fuel.2016.12.014.

[42] J.M. Saad, P.T. Williams, Catalytic dry reforming of waste plastics from different waste treatment plants for production of synthesis gases, Waste Management. 58 (2016) 214–220. https://doi.org/10.1016/J.WASMAN.2016.09.011.

[43] J.M. Saad, P.T. Williams, Manipulating the H$_2$/CO ratio from dry reforming of simulated mixed waste plastics by the addition of steam, Fuel Processing Technology. 156 (2017) 331–338. https://doi.org/10.1016/j.fuproc.2016.09.016.

[44] J.M. Saad, P.T. Williams, Pyrolysis-Catalytic-Dry Reforming of Waste Plastics and Mixed Waste Plastics for Syngas Production., Energy and Fuels. (2016). https://doi.org/10.1021/acs.energyfuels.5b02508.

[45] S.M. Sajjadi, M. Haghighi, A.A. Eslami, F. Rahmani, Hydrogen production via CO$_2$-reforming of methane over Cu and Co doped Ni/Al$_2$O$_3$ nanocatalyst: impregnation versus sol-gel method and effect of process conditions and promoter, J Solgel Sci Technol. 67 (2013) 601–617. https://doi.org/10.1007/s10971-013-3120-8.

[46] M. Al-asadi, N. Miskolczi, Hydrogen rich products from waste HDPE/LDPE/PP/PET over Me/Ni-ZSM-5 catalysts combined with dolomite, Journal of the Energy Institute. 96 (2021) 251–259. https://doi.org/10.1016/J.JOEI.2021.03.004.

Chapter 4

Simulation of a Process for the Pyrolysis-Dry Reforming of Plastics

Table of Contents

List of Figures

List of Tables

1. Introduction

Plastic waste contains different types of polymers and other materials. Determining the content and yield of the products is rather challenging due to the complexity of plastics structures and their reaction pathway during pyrolysis. Heat carrier temperature, reactor temperature, vapor residence time, and carrier gas flow rate are some of the numerous variables that affect the process [1].

In the industry, engineers frequently use specialized software like ASPEN to tackle complex problems. “ASPEN plus” is a process simulation platform of choice for examining mass and energy balances in addition to phase and chemical equilibria in a chemical engineering process [1]. It is possible then to simulate an actual plant behavior, given accurate thermodynamic data, realistic operating conditions, and reliable equipment models [2]. What-if analysis, sensitivity studies, optimization runs, and running various plant scenarios are additional features of ASPEN plus.

It is important to select the appropriate property method to analyze a process before creating a flowsheet or running a simulation [1]. Equilibrium process models can be created using ASPEN Plus. These models are crucial to predict the thermal efficiency or highest conversion rate a given process can achieve. ASPEN plus includes a large library of models for numerous unit operations (reactions, heat exchange, separation…) Gasification processes have received most of the attention in ASPEN Plus simulation work for the thermochemical conversion of polymers to biofuels. Processes concerning the pyrolysis of biomass or plastic waste, and the co-pyrolysis of these two materials followed by gasification are mainly studied in the literature.

Ismaeli et al., [3] studied the pyrolysis of waste tires using ASPEN plus software. The effect of pyrolysis process temperature was examined using the model, which revealed that higher temperatures caused larger chain fractions to decrease while smaller chains increased. This result is thought to be caused by the extensive cracking of the larger hydrocarbon chains at higher temperatures.

Kannan et al., [4] studied the pyrolysis-gasification of polyethylene plastic. NRTL/REDLICH-KWONG was the property method used in this study. A RYIELD reactor was used as the pyrolysis reactor and RGIBBS was used as the gasification reactor. Equivalence ratio and steam-fuel ratio were the only variables considered in this simulation because they are the two important parameters that affect the reactor temperature and the product distribution.

Zhu et al., [5] simulated the conversion of municipal solid waste (MSW) into syngas using ASPEN Plus. In this simulation, the property method used was PENG–ROBINSON-BOSTON–MATHIAS (PR–BM). RYIELD was the pyrolysis reactor and RGIBBS was the gasifier. They concluded that increase in stream to mass ratio and equivalence ratio decreased methane concentration. Moreover, the team compared different municipal solid waste of different ultimate and proximate analysis; they realized that better volatiles favored the production of light gases, resulting in higher gas yields and conversion efficiencies while also enhancing process efficiency.

Saebea et al., [6] studied the pyrolysis of polypropylene and polyethylene plastic. SOAVE–REDLICH–KWONG property method was used. This study also used RYIELD and RGIBBS blocks as the pyrolysis and gasification pyrolysis respectively. They studied the effects of gasifier temperature and steam to feed (S/F) mass ratio on the syngas flow rate. The results showed that a gasifier temperature of 900 °C and S/F mass ratio of 1.5 provided the maximum syngas flow rate.

Rosha et al., [7] studied the co-gasification of algae and polyethylene for hydrogen production. They used a kinetic free steady state isothermal model and PR–BM was the property method employed. A RYIELD block reactor was used as a decomposition reactor and a RGIBBS block reactor was used as a gasifier. The aim was to maximize the H_2 production by optimizing the parameters. They realized that an increase in gasifier temperature favored the formation of hydrogen and carbon monoxide. In a later study [8], they used a kinetic free steady state isothermal system and PR–BM property method to perform a sensitivity analysis on the pyrolysis of biomass. The sensitivity analysis showed that the pyrolysis temperature is important for product distribution, where an increase in pyrolysis temperature increases the gaseous and char yield while decreasing the oil yield.

Salisu et al., [9] studied the co-gasification of rice husk and sachet water plastic waste with CaO as a catalyst. PR–BM was the employed property method. The pyrolysis of the waste occurred in a RYIELD reactor, and the products were mixed with the catalyst in a mixer before entering the gasifier (RGIBBS). They concluded that a gasification temperature of 800 °C and feed rate of 70 kg/h plastic and 30 kg/h rice husk showed the highest combined heat and power efficiency.

Singh et al., [10] developed a detailed process model with kinetic-based models for the co-gasification of biomass and plastics. The aim was to study the synergistic effect of plastic biomass co-gasification and effect of process parameters on syngas composition. A RYIELD block reactor was used as a pyrolysis reactor; RGIBBS and RPLUG were used as gasifiers. They concluded that increase in plastic content increases hydrogen production at gasification temperature of 750 °C.

Moreover, dry reforming of methane and biogas processes are also simulated in the literature. For instance, Gopaul et al., [2] compared the syngas production from dry reforming of methane. The IDEAL property method was chosen and RGIBBS reactor was employed for the reforming reaction. They also studied the partial oxidation and hydrogen oxidation along the dry reforming reaction in the RGIBSS reactor. They concluded that the dry reforming reaction at 950 °C and 1 atm produced the highest syngas yield.

Phan et al., [11], studied the dry reforming, steam reforming, and tri reforming of biogas in an RGIBBS reactor block and using PENG ROBINSON property method. They realized that it was possible to optimize hydrogen production by changing methane reforming process.

However, to our knowledge, the pyrolysis-catalytic dry reforming of plastic waste is not yet studied. This adds to the novelty of this study as it appears to be the first of its kind to use the ASPEN Plus simulation to carry out a sensitivity analysis of the pyrolysis-catalytic dry reforming of plastic waste process for synthesis gas production. During a sensitivity analysis, Aspen repeats its calculation sequence through a range of values provided for an independent variable, to obtain a specified result for a dependent variable. Some parameters are considered to account for their effect on the integrated system [8].The performance of an integrated system, which consists of a pyrolyzer, a dry reformer, a cleaning separator, and a splitter of recycling stream was assessed. Kinetic-based models are known to be highly accurate for simulation goals and process design objectives; nevertheless, it is computationally intensive and only useful when kinetic data is available [12]. By entering experimental test values, this simulation model may accurately estimate or compute the syngas yield and allows the optimization of the pyrolysis-reforming process operating parameters. In our case, a realistic model would have required the development of a kinetic model for the reforming reaction over the best performing catalyst identified in Chapter 3 ($1Ru25NiAl_2O_3$). Since the kinetic experimental parameters are not available yet, we used the equilibrium condition for the dry reforming reaction which will give us the syngas yield in the best-case scenario in the absence of a catalyst. In most cases, the equilibrium constant or the minimization of Gibbs free energy are used to determine the thermodynamic equilibrium in a certain reactor [11]. In the dry reforming reaction, carbon is usually a by-product, which makes it difficult to use the equilibrium constant method. As a result, this study uses an in-built reactor model known as 'RGIBBS' available in the ASPEN Plus V12.1 software which functions based on Gibbs free energy minimization approach. This enables the calculation of the gas composition at equilibrium under different operating conditions. Additionally, a RYIELD block reactor was used to convert the nonconventional plastic component into conventional hydrocarbons, and Peng-Robinson is the employed property method in this simulation. The aim of this chapter is to develop a preliminary model, validate it, and use it in the future to incorporate kinetic characteristics specific to the synthesized catalyst.

2. Materials and method

2.1. Feedstock

This simulation study established sequential pyrolysis, reforming, and cleaning of plastic for syngas production using the ASPEN Plus simulator. Three different plastic feedstocks were assumed, namely, 100% polypropylene (PP) plastic, 100% polyethylene (PE) plastic, or 100% polystyrene (PS) plastic. The plastic stream labeled as "PLASTIC" was defined as a non-conventional stream and the ultimate and proximate analyses are provided as input to the model based on the type of plastic used. HCOALGEN and DCOALIGT models were used to evaluate the enthalpy and density of the feed. In this process, the HCOALGEN model requires these component attributes for nonconventional components: proximate analysis results (denoted as PROXANAL), ultimate analysis results (denoted as ULTANAL), and sulfur analysis results (denoted as SULFANAL). Proximate analysis gives the moisture, volatile matter, fixed carbon, and ash contents. Ultimate analysis gives the weight content of carbon, hydrogen, oxygen, nitrogen, and sulfur. The sulfur analysis gives the contents of pyritic, sulfate, and organic sulfur. The DCOALIGT model requires only the two component attributes ULTANAL and SULFANAL. **Table 4.1** shows the proximate and ultimate analyses of PP, PE, and PS polymers. Moisture (M), volatile matter (VM), fixed carbon (FC), ash contents, and weight contents of carbon and hydrogen were retrieved from the literature [13]. It was assumed that the raw material before entering the pyrolysis stage is dried and the moisture is reduced to a minimum value. The flow class

"MIXCINC" is chosen, which signifies a mixture (MIXED) of a pure solid (CISOLID) and a nonconventional heterogeneous solid (NC) [14].

Table 4.1 Proximate and ultimate analyses of PP, PE, and PS polymers

Proximate Analysis	*PP*	*PE*	*PS*	Ultimate Analysis	*PP*	*PE*	*PS*
Moisture (wt.%)	0.120	0.110	0.09	***Carbon***	85.714	85.714	92.308
Fixed Carbon (wt.%)	0.042	0.051	0.071	***Hydrogen***	14.286	14.286	7.692
Volatile (wt.%)	99.821	99.816	99.814	***Oxygen***	0.000	0.000	0.000
Ash (wt.%)	0.017	0.023	0.025	***Nitrogen***	0.000	0.000	0.000
				Sulfur	0.000	0.000	0.000

2.2. Model Development

In a pyrolysis process, the long polymer chains in plastic are broken down into much shorter hydrocarbons by rapid heating and in the absence of oxygen. This results in the production of hydrocarbons consisting of char and vapors. The pyrolysis vapors include condensable and non-condensable gases [15]. These hydrocarbons are sent into a reforming reactor, where the dry reforming reaction occurs in the presence of carbon dioxide. The produced gases are then mixed with isopropanol solution, which serves as tar trap. The mixture is then sent into a separator which separates the syngas and discards the isopropanol solution. Some factors can affect this process such as the properties of the polymers used and process parameters. This work employed ASPEN plus simulator to explore the viability of producing syngas using plastic as feedstock.

A kinetic-free steady-state isothermal system was considered when modeling this plastic to syngas conversion system. The non-conventional plastic stream was identified using polypropylene, polyethylene, and polystyrene proximate and ultimate analyses. Although high temperature and low pressure could be used to choose the IDEAL property methods, however this method will require more assumptions. Therefore, the PENG-ROBINSON method has been preferred as an alternative property method since it is based on a cubic equation of state (**4.1**), which can take into consideration potential non-ideal behaviors [12]. Moreover, this method can be applied to processes that operate at high temperatures [11]. It is the latest development among all other cubic equations of state, which gives the more accurate value of state variable calculation (P, V, T) for liquid as well as non-polar gases. Therefore, because the PENG-ROBINSON model is one of the most reliable equations of state for this kind of process, this property method is employed in our model. Additionally, a calculator block based on FORTRAN programming language was employed to optimize the flow rate of carbon dioxide and argon to maximize the recycling of these gases.

$$P = \frac{RT}{V-b} - \frac{a(T)}{V(V+b)+b(V-b)} \tag{4.1}$$

$$a(T) = \alpha a(T_c) \qquad \alpha a(T_c) = 0.45725\frac{\alpha R^2 {T_c}^2}{P_c}$$

$$b = 0.07780\frac{RT_c}{P_c} \qquad \alpha = (1 + k(1-\sqrt{T/T_c})^2 \qquad k = 0.37464 + 1.54226\omega - 0.26992\omega^2$$

Where:

P is the pressure (Pa)

V is the molar volume (m^3mol^{-1})

R is the gas constant (8.314 $Jmol^{-1}K^{-1}$)

T is the absolute temperature (K)

Pc is the critical pressure for the component of interest (Pa)

Tc is the critical temperature for the component of interest (K)

ω is the acentric factor for the component of interest

The ability to determine any reaction system's phase and equilibrium composition under predetermined parametric parameters makes thermodynamic analysis suitable for a wide range of applications [7]. Therefore, using Gibbs' free energy minimization method, a sensitivity analysis of the entire reforming system was performed. According to the literature [7], the reforming reactor typically runs below the temperature at which ash sinters; as a result, the reforming temperature ranges between 500 °C and 1000 °C to prevent the creation of excessive sintered agglomerates.

Based on some literature considering pyrolysis processes [8,16], the parameters in our simulation were chosen based on the following assumptions:

- Plastic feed rate is 1000 kg/h.
- Inlet stream (Plastic and Argon) temperature 30 °C and pressure 1 atm
- The plastic is considered dry and free of moisture before entering the system.

- The reactions take place at equilibrium state and no pressure drop.
- Ash is treated as an inert substance and does not participate in the reaction.
- It is considered that the coke formed consists entirely of carbon and undergoes complete conversion.
- The following products are produced following the pyrolysis of PP, PE, and PS: hydrogen, methane, ethane, ethylene, propylene, propane, n-butane, 1-octane, cyclooctane, 1-octocosene, and carbon.
- The isopropanol solution assumably traps all tar formed from the reaction and is completely discarded after separation.
- Syngas produced consists of hydrogen and carbon monoxide.

Fig. 4.1 depicts a comprehensive process design used in the simulation study, including plastic pyrolysis, hydrocarbon dry reformer, mixer, separator, and splitter.

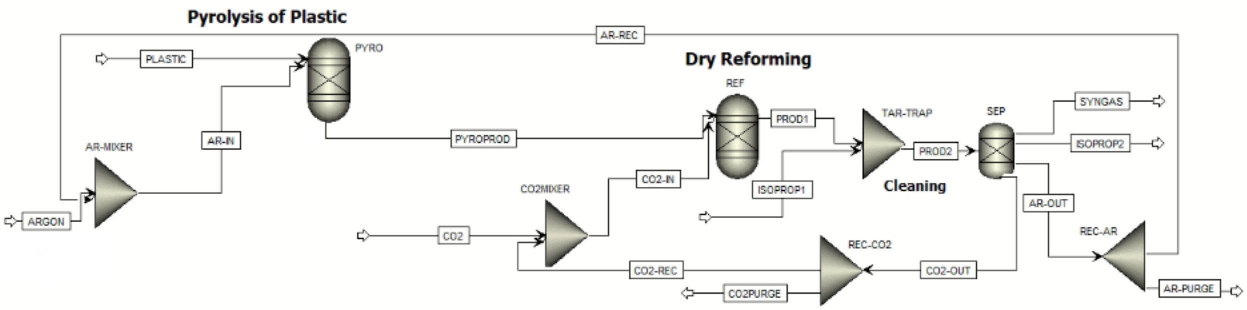

Fig. 4.1 Detailed process scheme of reforming plastic into syngas

The plastic polymer "PLASTIC" enters pyrolyzer "PYRO" modeled as a RYIELD block in Aspen Plus. An operating temperature of 500 °C and a pressure of 1 atm were chosen to set the exiting stream "PYROPROD" to a pre-heated temperature of 500 °C. The RYIELD reactor was chosen to convert the non-conventional feed into conventional products [7]. **Table 4.2** represents the mass fractions of the components around the pyrolysis reactor as retrieved from the literature [16].

Table 4.2 Mass fractions of the produced gases after the pyrolysis of PP, PE, and PS plastics [16]

Component	PP Vap-liq Frac and Char Residue	PE Vap-liq Frac and Char Residue	PS Vap-liq Frac and Char Residue
Hydrogen	0.0849	0.0868	0.0477
Methane	0.0324	0.0434	0.0231
Ethane	0.0152	0.0227	0.0106
Ethylene	0.0099	0.0067	0.0079
Propene	0.0002	0.0001	0.0003
Propane	0.0008	0.0007	0.0008
n-butane	0.0004	0.0004	0.0004
1-octane	0.3214	0.3180	0.3208
Cycloocatane	0.4225	0.4020	0.4764
1-octocosene	0.0868	0.0855	0.0890
Carbon	0.0256	0.0337	0.0233

The hydrocarbons produced are then fed into the reforming reactor “REF” modeled as a RGIBBS block and carbon dioxide is simultaneously fed into the same reactor for the dry reforming reaction to occur. Due to the lack of reaction kinetics, RGIBBS block was chosen to estimate the product distributions from the reforming reactor. The product stream “PROD1” was cleaned with isopropanol solution “ISOPROP1” in “TAR-TRAP” mixer. The resulting stream “PROD2” was sent into a separator “SEP” where the “SYNGAS” is separated, and isopropanol solution “ISOPROP2” is discarded. Carbon dioxide “CO2-OUT” and argon “AR-OUT” streams are also separated in this separator block, and these streams respectively enter splitter “REC-CO2” and “REC-AR” to recycle them. The recycled streams are then sent into mixers where the calculator block was employed to optimize the flow rate of CO_2 and Ar.

Table 4.3 shows the model blocks used in the ASPEN Plus along with their description.

Table 4.3 Model blocks used in Aspen Plus flowsheet and their detailed description.

Unit	Block	ASPEN name	Description
Pyrolysis	PYRO	RYIELD	Conversion of non-conventional components into conventional ones based on a mass basis; pressure 1 atm and temperature 500 °C
Reformer	REF	RGIBBS	Reforming performed with restricted chemical equilibrium reactions, pressure 1 atm and temperature 800 °C
Cleaning	TAR-TRAP	MIXER	Mixing of isopropanol solution with the resulting hydrocarbons
Separator	SEP	SEP.	Separates the syngas, isopropanol solution, carbon dioxide, and argon
Recycling stream	REC-AR	FSPLIT	Divides argon based on splits specified for the recycling stream
Recycling stream	REC-CO2	FSPLIT	Divides carbon dioxide based on splits specified for the recycling stream
Ar Flow mixer	AR-MIX	MIXER	Mixes initial and recycled argon streams
CO_2 Flow mixer	CO2-MIX	MIXER	Mixes initial and recycled carbon dioxide streams

The sensitivity analysis with respect to different parameters including reforming temperature (range from 500 °C to 1000 °C with an increment of 100 °C) and flow of carbon dioxide (ranged from 1000 kg/h to 6000 kg/h with an increment of 1000 kg/h) were studied to evaluate the syngas overall process performance.

3. Results and Discussion

In this section, the pyrolysis-reforming of different types of plastics is investigated. This section also presents the effect of reforming temperature and carbon dioxide mass flow rate on syngas production.

3.1. Effect of plastic type

After inserting the feedstock elemental analyses of each type of plastic separately into the ASPEN plus simulator, various simulation runs were performed at same parametric conditions: 800 °C reforming temperature and 3000 kg/h CO_2 mass flow rate. **Fig. 4.2** shows the flow rate of the gaseous products produced after the pyrolysis-dry reforming of the three types of plastics.

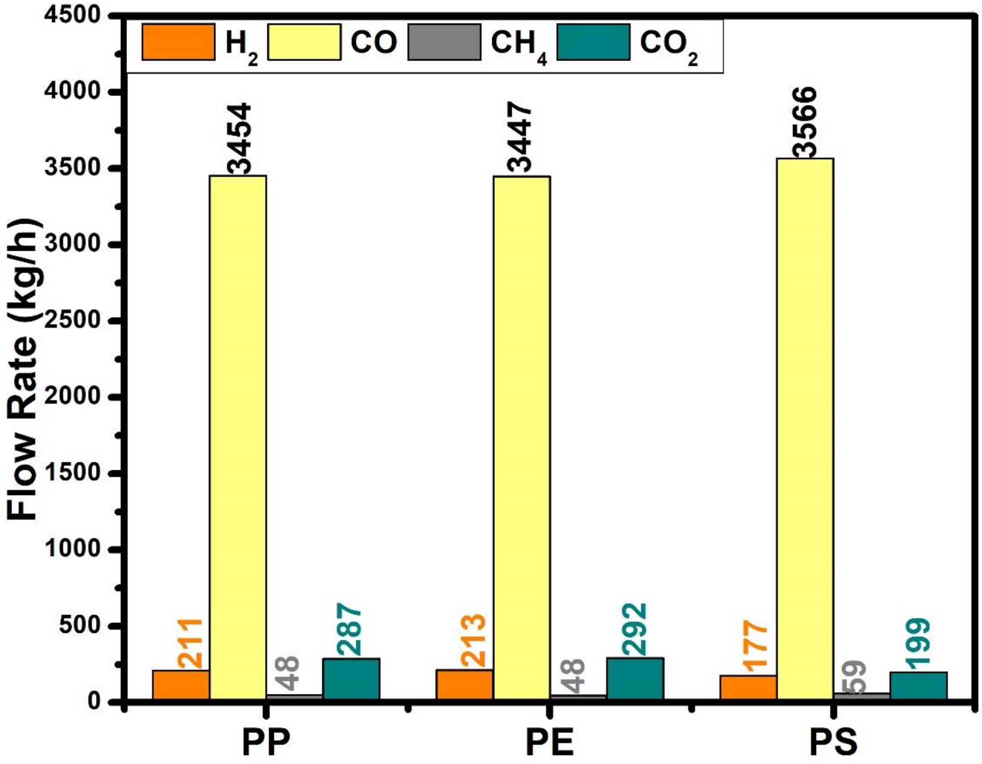

Fig. 4.2 Gas flow rates obtained after the pyrolysis-reforming of PP, PE, and PS

As shown in **fig. 4.2**, PP and PE plastics produced almost equivalent values of gaseous products, where PP produced 211 kg/h H_2 and 3454 kg/h CO, and PE produced 213 kg/h H_2 and 3447 kg/h CO. On the other hand, PS produced slightly lower H_2 values (177 kg/h) and higher CO values (3566 kg/h). This slight difference between the olefins and polystyrene is due to the ultimate analyses' values, where PS had higher carbon content and lower hydrogen content compared to PP and PE, which had similar C and H contents, justifying the lower H_2 and higher CO production from PS reforming. Moreover, the mass fractions of the pyrolysis products produced from each plastic (**table 4.2**) show that PS produced lower vap-liq fractions compared to PP and PE. A study by Zhu et al., [5] investigated the influence of proximate and ultimate analyses of feedstock on the process performance. Their results showed that higher volatiles favored the production of light gases, leading to higher conversion efficiencies and gas yield, thus enhancing the process performance. It is evident from **fig. 4.2** that the produced gases after the pyrolysis-reforming of different types of plastic polymers are approximately similar probably because the plastic polymers studied have approximately equal volatile matter content. These results agree with the ones presented in Chapter 3, where the synthesized catalyst could convert the different types of plastics into almost equivalent values of syngas.

After inserting the feedstock elemental analyses of polypropylene into the Aspen plus simulator, various simulation runs were performed at different parametric conditions. First, the sensitivity analysis involves maximizing the syngas production (H_2 + CO) under different reforming temperatures (500 °C to 1000 °C). Second, different flows of carbon dioxide (1000 kg/h to 6000 kg/h) were inserted in the reforming reactor to see its effect on the reforming reaction and consequently on syngas production.

3.2. Effect of reforming temperature

To study the effect of reforming temperature on syngas production, the CO_2 flow rate was kept constant at 3000 kg/h. **Fig. 4.3** was obtained by varying reaction temperature in the simulation and monitoring the syngas production from the reactor block. **Fig. 4.3** shows the H_2, CO, CH_4, and CO_2 mass flow rates at various temperatures (500 °C to 1000 °C) for the dry reforming of PP Results show that the H_2 content increased with increasing temperature and became constant at reforming temperature of 800 °C and higher. The CO mass flow rate also increased with temperature, and its value exceeded that of H_2. On the other hand, the CH_4 and CO_2 flow rates followed an opposite trend. The CH_4 mass flow decreased with increasing temperature and became almost negligible at temperature of 800 °C, suggesting almost complete conversion of methane at this temperature. The CO_2 mass flow rate also decreased with increasing temperature and reached 158 kg/h at 1000 °C.

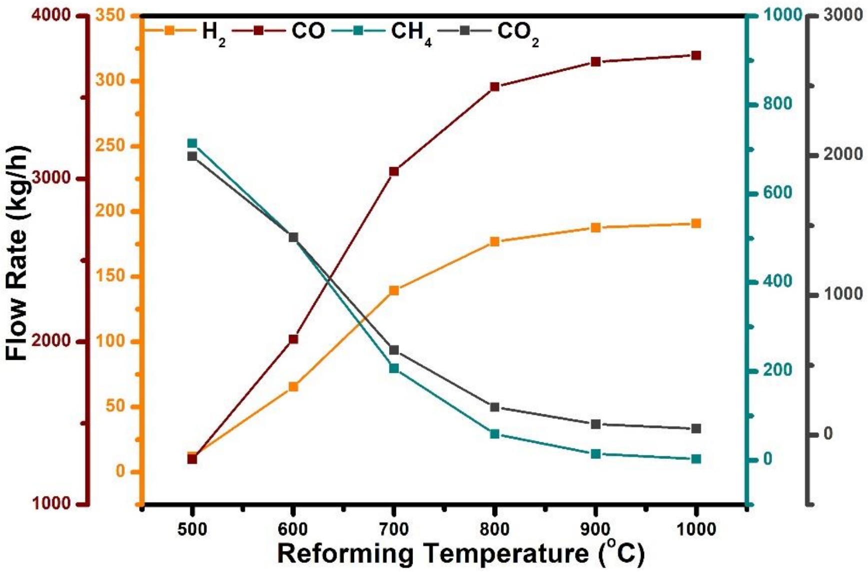

Fig. 4.3 Effect of reforming temperature on mass flow rate of gas products obtained from the dry reforming of PP

Fig. 4.4 illustrates the effect of reforming temperature on methane and carbon dioxide conversion. Syngas mass flow rates increased with increasing temperature as reactant conversion increased. The methane conversion increased from 20 % at 500 °C to 99.9% at 1000 °C. It is noticed that near-total methane conversion was observed at high temperature ranges (more than 95% of methane converted at temperature above 800 °C) which is in line with the literature [2]. A 3000 kg/h CO_2 flow rate was sent into the reforming reactor. At 500 °C, 22% of CO_2 was converted in the dry reforming reaction. The conversion increased to 90% at 800 °C reforming temperature and reached 95% conversion at 1000 °C.

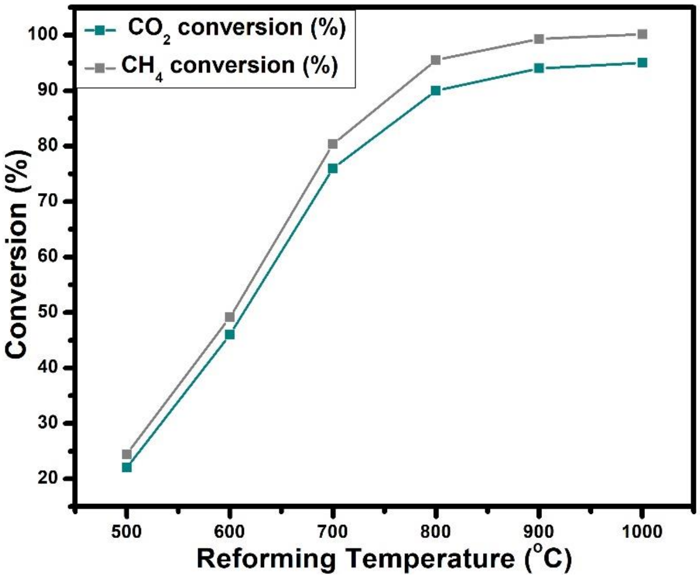

Fig. 4.4 Effect of reforming temperature on CH_4 and CO_2 conversion during the dry reforming of PP

According to the thermodynamic study of the dry reforming reaction presented in Chapter 1, the dry reforming reaction is favored at temperatures exceeding 700 °C. Due to energy deficiency, endothermic reactions are less prevalent at low temperatures (500 °C to 600 °C), therefore the pyrolysis is dominant at this temperature range. The endothermicity of dry reforming reaction may be responsible for the syngas stream's increased H_2 and CO contents [7]. Therefore, increasing the reforming temperature favored the dry reforming reaction resulting with an increase in H_2 and CO production. Moreover, the enhanced CO formation could be a result of the reverse-Boudouard reaction favored at elevated temperatures. Some previous research [2,7–9] also showed a similar trend on the effect of temperature on syngas composition

It can be summarized that the conversion is maximized at temperatures exceeding 800 °C. Results showed that the CH_4 and CO_2 conversion and H_2 and CO production increased with increasing temperature from 500 °C to 1000 °C. At 800 °C, almost maximum CH_4 (95%) and CO_2 (90%) conversion and H_2 (211 kg/h) and CO (3454 kg/h) production was achieved; then, it starts to follow constant trends when increasing temperature (>800 °C). From an economic and environmental standpoint, the ideal reforming reaction temperature for the pyrolysis of waste polypropylene is 800 °C.

3.3. Effect of CO_2 flow rate

Fig. 4.5 was obtained by varying CO_2 flow rate in the simulation and monitoring the H_2 and CO production from the reactor block. **Fig. 4.5** shows the H_2 (a) and CO (b) mass flow rates at various CO_2 flow rates (1000 kg/h to 6000 kg/h) during the dry reforming of PP at different reforming temperatures (500 °C to 1000 °C).

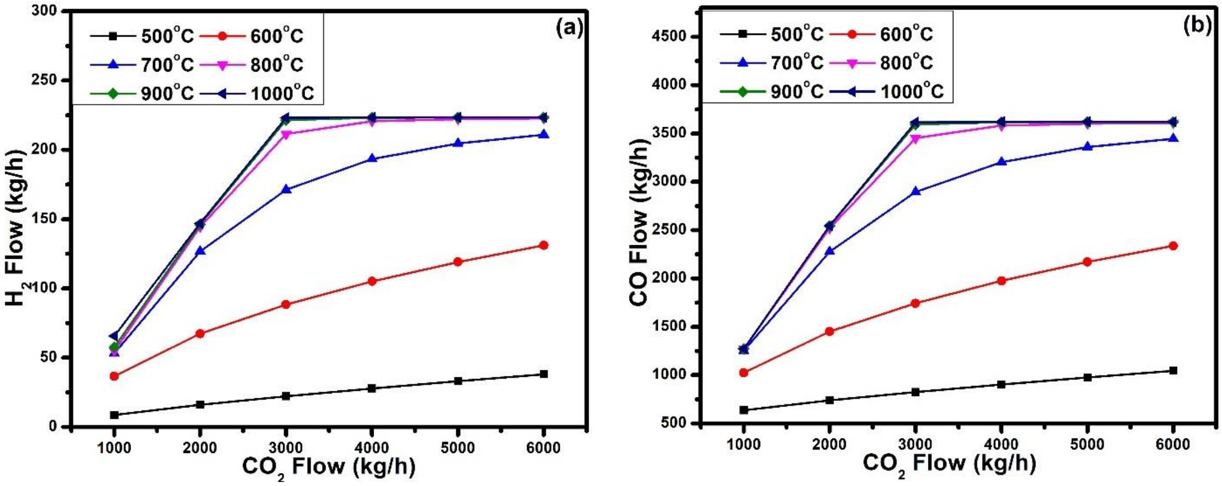

Fig. 4.5 Effect of CO_2 flow rate on H_2 (a) and CO (b) production at different reforming temperatures

The CO_2 flow rate influenced the syngas production. It is noticed that the H_2 and CO production increased with increasing CO_2 flow rate regardless of the reforming temperature. However, as already mentioned in the previous section, the mass flow rates of H_2 and CO increased with increasing reforming temperature and stabilized around 800 °C. At 3000 kg/h CO_2 flow rate, the H_2 flow rate was 211 kg/h at 800 °C. It increased to 223 kg/h at 1000 °C. At 6000 kg/h CO_2 flow rate, the H_2 flow rate was 223 kg/h at 800 °C and stabilized at this value at 1000 °C. It is also noticed at elevated reforming temperatures (800 °C, 900 °C, and 1000 °C) the H_2 and CO production maximized at 3000 kg/h and remained almost constant when the CO_2 flow increased to 6000 kg/h. Therefore, it can be summarized that a CO_2 flow rate of 3000 kg/h is sufficient for the dry reforming reaction at a reforming temperature of 800 °C.

4. Conclusion

A simulation model on ASPEN Plus platform was developed to evaluate the influence of plastic type, reforming temperature, and carbon dioxide flow rate on the syngas composition in the product stream. Since the different plastics used (PP, PE, and PS) possessed similar values from proximate and ultimate analyses, almost equivalent composition of gaseous products resulted after the pyrolysis-dry reforming of these plastics. Moreover, the simulation results indicated that the increase in reforming temperature favored the H_2 and CO production while both CH_4 and CO_2 production decreased. This implies that as the temperature increases, the dry reforming reaction predominates and consumes both CH_4 and CO_2. Therefore, from the sensitivity analysis it was possible to determine the optimal process conditions for high H_2 and CO yields: 800 °C reforming temperature and 3000 kg/h CO_2 flow rate.

Based on the findings, consistency in the simulation results was observed compared with the experimental results in Chapter 3. In the dry reforming of PP, 2 g of plastic needed 6.2 g of CO_2. Therefore, for 1000 kg/h of PP, 3100 kg/h CO_2 is needed. Since the results clearly showed a flow of 3000 kg/h is sufficient for the dry reforming reaction at 800 °C, it is concluded that the process parameters applied in Chapter 3 are nearly optimized for the dry reforming reaction.

However, the current simulation results are based on the equilibrium condition of the dry-reforming reactor and therefore, the H_2 and CO yields observed in the product flow stream should be considered as the ‘best case scenario’. To develop a more realistic model, it is important to determine the kinetics of the reactions involved. Therefore, as a future perspective, the pyrolysis-dry reforming reaction can be carried out at different operating temperatures and gas hourly space velocities. The experimental results thus obtained can be used to determine the different kinetic parameters through model regression and incorporate in the in-built reactor models like RPLUG (based on plug-flow reactor model) for validation of the simulation model.

5. References

[1] E. Ansah, Experimental Investigation and Aspen Plus Simulation of the MSW Pyrolysis Process, 2013.

[2] S.G. Gopaul, A. Dutta, Dry reforming of multiple biogas types for syngas production simulated using Aspen Plus: The use of partial oxidation and hydrogen combustion to achieve thermo-neutrality, Int J Hydrogen Energy. 40 (2015) 6307–6318. https://doi.org/10.1016/J.IJHYDENE.2015.03.079.

[3] H.Y. Ismail, A. Abbas, F. Azizi, J. Zeaiter, Pyrolysis of waste tires: A modeling and parameter estimation study using Aspen Plus®, Waste Management. 60 (2017) 482–493. https://doi.org/10.1016/J.WASMAN.2016.10.024.

[4] P. Kannan, A. al Shoaibi, C. Srinivasakannan, Optimization of Waste Plastics Gasification Process Using Aspen-Plus, Gasification for Practical Applications. (2012). https://doi.org/10.5772/48754.

[5] L. Zhu, L. Zhang, J. Fan, P. Jiang, L. Li, MSW to synthetic natural gas: System modeling and thermodynamics assessment, Waste Management. 48 (2016) 257–264. https://doi.org/10.1016/J.WASMAN.2015.10.024.

[6] D. Saebea, P. Ruengrit, A. Arpornwichanop, Y. Patcharavorachot, Gasification of plastic waste for synthesis gas production, Energy Reports. 6 (2020) 202–207. https://doi.org/10.1016/J.EGYR.2019.08.043.

[7] P. Rosha, S. Kumar, S. Vikram, H. Ibrahim, A.H. Al-Muhtaseb, H2-enriched gaseous fuel production via co-gasification of an algae-plastic waste mixture using Aspen PLUS, Int J Hydrogen Energy. (2021). https://doi.org/10.1016/J.IJHYDENE.2021.11.092.

[8] P. Rosha, S. Kumar, H. Ibrahim, Sensitivity analysis of biomass pyrolysis for renewable fuel production using Aspen Plus, Energy. 247 (2022). https://doi.org/10.1016/J.ENERGY.2022.123545.

[9] J. Salisu, N. Gao, C. Quan, Techno-economic Assessment of Co-gasification of Rice Husk and Plastic Waste as an Off-grid Power Source for Small Scale Rice Milling - an Aspen Plus Model, J Anal Appl Pyrolysis. 158 (2021). https://doi.org/10.1016/J.JAAP.2021.105157.

[10] M. Singh, S.A. Salaudeen, B.H. Gilroyed, A. Dutta, Simulation of biomass-plastic co-gasification in a fluidized bed reactor using Aspen plus, Fuel. 319 (2022). https://doi.org/10.1016/J.FUEL.2022.123708.

[11] T.S. Phan, D. Pham Minh, F. Espitalier, A. Nzihou, D. Grouset, Hydrogen production from biogas: Process optimization using ASPEN Plus®, Int J Hydrogen Energy. (2022). https://doi.org/10.1016/J.IJHYDENE.2022.01.100.

[12] A. Visconti, M. Miccio, D. Juchelkova, An Aspen Plus® tool for simulation of lignocellulosic biomass pyrolysis via equilibrium and ranking of the main process variables, INTERNATIONAL JOURNAL OF MATHEMATICAL MODELS AND METHODS IN APPLIED SCIENCES. 9 (2015).

[13] I. Janajreh, I. Adeyemi, S. Elagroudy, Gasification feasibility of polyethylene, polypropylene, polystyrene waste and their mixture: Experimental studies and modeling, Sustainable Energy Technologies and Assessments. 39 (2020). https://doi.org/10.1016/J.SETA.2020.100684.

[14] W.T. Ouazzani, L. el Farissi, E. Monteiro, A. Rouboa, Automotive plastic waste and olive pomace valorization using the pyrolysis process, Energy Reports. 8 (2022) 628–637. https://doi.org/10.1016/J.EGYR.2022.08.067.

[15] A. Fivga, I. Dimitriou, Pyrolysis of plastic waste for production of heavy fuel substitute: A techno-economic assessment, Energy. 149 (2018) 865–874. https://doi.org/10.1016/J.ENERGY.2018.02.094.

[16] B. Rama, J. Mishra, K.B.V.S.R. Subrahmanyam, R. Deshmukh, L. Cardoso, S. Nandhini, S. Bhrathi, D.D. Goud, K.P. Krishna, D.B. Priya, A. Sumathi, J.R. Murugadoss, R.P. Vaijayanthi, N. Lokhande, E.P. Akhator, D.I. Igbinomwanhia, A.I. Obanor, N. Kohli, S. Sivarajan, V.I. Loganina, M.A. Sadovnikova, Yu.P. Skachkov, T. Selvaganapathy, R. Muthuvelayudham, M.J. Kumar, S. Malik, P. Sharma, M. Sharanya, B. Banakara, M. Sasikala, M. Duraisamy, W.J. Singh, E.T. el Shenawy, A. Hegazy, A. Garcia, J. Trujillo, J.F. Jurado, Emerging Trends in Engineering Research and Technology Vol. 2, Book Publisher International (a part of SCIENCEDOMAIN International), 2020. https://doi.org/10.9734/bpi/etert/v2.

Conclusion and Perspectives

This work aims to find a solution to the plastic waste issue while valorizing the greenhouse gas carbon dioxide. Different catalytic materials are synthesized to catalyze the dry reforming reaction of plastics pyrolysates. The study describes the synthesis and characterization of Ni and Ru-Ni-based catalysts supported on mesoporous alumina and investigates the impact of incorporating ceria to the alumina support. Some process parameters are investigated to determine the best conditions for the dry reforming reaction.

Prior to catalytic testing, the support and catalysts were exhaustively studied for their porosity, crystal structures, reducibility, and basicity. All calcined catalysts showed a type IV isotherm, accounting for their mesoporous structures. Following the active phase impregnation, the mesoporous structure of the support was partially destructed, as seen by the change in shape of the isotherms and the decrease in surface areas and pore volumes. Once the nickel-based catalysts were promoted with Ru, the metal active phase dispersion, the NiO reducibility at lower temperatures, and the surface areas were improved.

In this study, the hydrocarbon-cracking efficiency was significantly increased when using a catalyst, resulting in higher hydrogen production and lower concentrations of methane and other hydrocarbons. In the dry reforming of polypropylene plastics, the nickel loading impregnated on the mesoporous alumina support affected the syngas production. As the nickel loading increased, the catalytic activity improved, and more syngas was produced. The findings of this study demonstrated that Ru reduces carbon production while simultaneously enhancing the activity of the monometallic catalyst in the pyrolysis-dry reforming of plastics. The presence of ruthenium close to active nickel sites stabilizes a reduced surface and facilitates carbon gasification by preventing the buildup of carbon inside the nickel particle. Because of its well-dispersed small Ni particles, high reduction degree, and high basic site concentration, the ruthenium promoted nickel-based catalysts supported on alumina and calcined at 550 °C showed the best catalytic performance in the investigated reaction. Ru-Ni catalysts outperform Ni-catalysts in the dry reforming reaction of plastics, where the $1Ru25NiAl_2O_3$ catalyst remained active after several runs, while the $25NiAl_2O_3$ catalyst deactivated. This indicates that the stability and catalytic activity of Ni-catalysts were greatly enhanced following the incorporation of ruthenium in the catalytic matrix. It was discovered that the support also plays a crucial role in preventing the development of coke, which enhances the stability of the catalyst. The lower carbon deposition in the pyrolysis-dry reforming of PP was probably due to the reaction between filamentous carbon and carbon dioxide, which in turn increased the production of carbon monoxide. The syngas production after dry reforming over the best catalysts was 8.4 times higher than the non-catalytic reforming of PP. Furthermore, CO_2 conversion increased from 10% for the non-catalytic dry reforming of PP to around 40% after reforming over Ni-based catalysts. The promotion of the support with certain percentages of Ce did not significantly affect the syngas production and led to the deactivation of the catalyst after consecutive runs. This is because of the amorphous carbon formed after test which covered the active sites and hampered the catalytic performance. The best results for the pyrolysis-catalytic dry reforming of polypropylene were achieved over a catalyst calcined at 550 °C and a plastic: catalyst ratio of 2:1. The $1Ru25NiAl_2O_3$ catalyst synthesized via wet impregnation and calcined at 550 °C is proven successful in reforming different types of plastics and producing significant quantities of syngas.

A simulation model using ASPEN Plus software was developed to assess the influence of plastic-type, reforming temperature, and carbon dioxide flow rate on the syngas composition in the product stream. The pyrolysis-dry reforming of different types of plastic resulted in similar gaseous product composition. Moreover, 800 °C reforming temperature and 3000 kg/h CO_2 flow rate were the optimal process conditions for high H_2 and CO yields. These parameters were determined using a sensitivity analysis study.

Additional research must be conducted to build on this work and assist in scaling the processes up to pilot plant scale. To begin with, additional characterization techniques must be performed on the catalysts, including SEM and EDX mapping (for active phase dispersion), microscopy techniques (for morphologies of formed carbon), XPS (for determining surface oxygen capacity), and ICP (for verification of active phase loading, especially in bimetallic catalysts). Furthermore, mechanistic studies could be applied where reactive intermediates are identified to comprehend the function of each catalytic component in the reaction. It will be intriguing to study the effect of the synthesis method on catalytic performance and further optimize the reaction's parameters to increase syngas production. Also, additional runs should be performed on the catalyst to study its degree of deactivation. Lower Ce loadings should be used to comprehensively study the effect of Ce on catalytic performance. Moreover, using biochar as support could be a novel green approach to implement for this reaction. It should be emphasized that steam might be used to advance the process by causing the product's carbon monoxide to undergo a water gas shift reaction, resulting in the production of hydrogen. This would increase the H_2:CO ratio and make it closer to 1. A complete analysis of the plastics and its pyrolysis products would add to the value of the work. Furthermore, clean, pure plastics were used in this study. However, to scale up the process it will be interesting to perform the dry reforming of mixed impure plastics to study the effect of impurities on the catalytic performance. Also, in this study, a batch reactor was used. Therefore, a continuous feed of plastic waste will be more appealing for potential industrial use.

To develop a more realistic model using the ASPEN Plus software, the kinetics of the reactions involved in the dry reforming process should be determined. Therefore, as a future perspective, the pyrolysis-dry reforming reaction can be carried out at different operating temperatures and gas hourly space velocities. The experimental results thus obtained can be used to determine the different kinetic parameters through model regression and incorporate in the in-built reactor models like RPLUG (based on the plug-flow reactor model) for validation of the simulation model.

Appendix A

All the experimental information pertaining to the pyrolysis catalytic dry reforming of plastics is contained in this appendix. This includes the characterization of plastics, characterization of catalysts, and characterization of produced gases and trapped tar.

All types of plastics used were studied using Simultaneous Differential Scanning Calorimetry and Thermogravimetry (DSC/TG) and Pyrolysis coupled to Gas Chromatography-Mass Spectrometry (Pyro-GC-MS).

All synthesized calcined catalysts were characterized using the following techniques: X-Ray Diffraction (XRD), Nitrogen adsorption/desorption, Hydrogen-Temperature Programmed Reduction (H_2-TPR), and Carbon Dioxide-Temperature Programmed Desorption (CO_2-TPD).

The gases produced from the dry reforming reaction and collected in a Tedlar^{TM} gas sample bag were identified using offline gas chromatography (micro-GC). The spent catalysts were characterized using Simultaneous Differential Scanning Calorimetry and Thermogravimetry (DSC/TG) and X-Ray Diffraction (XRD). The tar trapped in isopropanol solutions were studied using Gas Chromatography/Mass Spectrometry (GC/MS).

A two-stage setup was utilized for the catalytic dry reforming of plastic wastes. The XRD, N_2 adsorption/desorption, Pyro-GCMS and GC/MS were performed in UCEIV (Unité de Chimie Environnementale et Interactions sur le Vivant) laboratories at the Université du Littoral Côte d’Opale (ULCO) in Dunkerque, France. The H_2-TPR, CO_2-TPD, DSC/TG, and the pyrolysis-catalytic dry reforming experiments were carried out in the Chemistry Lab at the University of Balamand (UOB), Lebanon. The calcination of the synthesized catalysts was performed in the Chemical Engineering Laboratory at the University of Balamand (UOB).

1. Characterization of Plastics

1.1. Differential Scanning Calorimetry/ Thermogravimetry Analysis (DSC/TGA)

Prior to the pyrolysis experiments, the thermal degradation behavior of plastics was studied under an inert atmosphere using a thermogravimetric analyzer. Simultaneous DSC/TG combines two thermal analysis techniques: Differential scanning calorimetry (DSC) is a technique for identifying a solid's endothermic and exothermic transitions versus temperature. Thermogravimetric analysis (TGA) is a technique for identifying the temperature difference between a sample and a reference sample. These techniques were performed concurrently using a Setaram Labsys EVO apparatus (**fig. A.1**). On a support inside a furnace, two alumina crucibles are positioned. The first is an empty reference crucible. Around 20 mg of plastics are added to the second crucible, which is then heated at a rate of 10 °C/min with a 30 ml/min argon flow from ambient temperature to 900 °C. The basic idea is to compare the heat flux of a plastic sample in an aluminum crucible to an empty reference crucible. The temperature of the sample is controlled and measured via a thermocouple device. Gravimetric (mass loss or gain) and thermal differential (temperature difference) analyses are both possible with the difference measured between the reference and the sample.

Fig. A.1 Setaram Labsys EVO apparatus for DSC-TG analysis

1.2. Pyrolysis-Gas Chromatography/Mass Spectrometry (Py-GC/MS)

Analytical pyrolysis technique (Py) linked to gas chromatography/mass spectrometry (GC/MS) is used for the characterization of plastic polymers. Products from the initial polymer sample are generated under regulated conditions: at 550 °C and in the presence of helium as an inert gas. A silica capillary column is then used to chromatographically separate the pyrolysis products, and a mass spectrometer is used to identify them by the interpretation of the mass spectra and with the aid of the mass spectral libraries (NIST). This pyrolysis method enables us to directly perform the analysis on the solid sample polymer without any need for pretreatment. The pyrolysis system used was the flash pyrolyzer, where the pyrolyzer reaches the desired temperature almost instantly (in about 30 seconds). The pyrolyzer is attached to the injector port of the gas chromatograph using a heated transfer line. Helium serves as the carrier gas for volatile fragments as they are transported into the gas chromatograph and separated into their component parts, then detected using mass spectrometry.

A very small amount of the plastic being analyzed is cut off with a scalpel and placed on a quartz wool bed in a small quartz tube without any additional preparation. The tube is then placed in a probe consisting of a platinum wire, which is instantly heated to the desired pyrolysis temperature. Based on the DSC-TG results of the studied plastics, a fixed temperature of 550 °C was implemented to operate the pyrolyzer. Py-GC/MS measurements were done using two apparatuses: the CDS pyro probe 5000 series pyrolyzer **(fig. A.2)** was connected to a Perkin Elmer Clarus 680 gas chromatograph with a Perkin Elmer Clarus 600S mass spectrometer **(fig. A.3)**. After flash pyrolysis, the formed gases are injected into the GC using a heated transfer line at 300 °C into Perkin Elmer Elite 5MS, 30 m x 0.25 mm x 0.25 µm, with a split of 50, followed by MS in scan mode between 35 and 600 µma. Helium, grade 6.0, was used as a carrier gas. The following were the GC conditions: the capillary column's temperature was programmed to rise from 40 °C (hold for 2 min) to 300 °C (hold for 10 min) at a heating rate of 10 °C/min and a constant helium flow of 1 ml/min throughout the entire analysis.

Fig. A.2: Plastic pyrolyzer CDS pyroprobe 5000 series linked to the injection port of the gas chromatograph

Fig. A.3 Perkin Elmer Clarus 680 Gas Chromatograph/ Perkin Elmer Clarus Mass Spectrometry for pyrolysis-gas chromatography/mass spectrometry (Py-GC/MS)

2. Characterization of Catalysts

2.1. X-ray diffraction

X-ray diffraction (XRD) is a non-destructive method used to analyze the catalysts' crystalline structure. The method comprises of the transmission of X-rays, of wavelength λ, onto a powdered sample positioned on a sample holder. These beams are emitted by a source, and once they reach the sample, they are diffracted by an angle θ and captured by a detector. The relationship between the incident X-ray wavelength, the incident angle, and the spacing between the atoms' crystal lattice planes is known as Bragg's Law, and is conveyed as follow:

$$n\lambda = 2dsin\theta$$

Where:

n: diffraction order (an integer)

λ: incident X-rays' wavelength

d: crystal's interplanar spacing

θ: incident angle

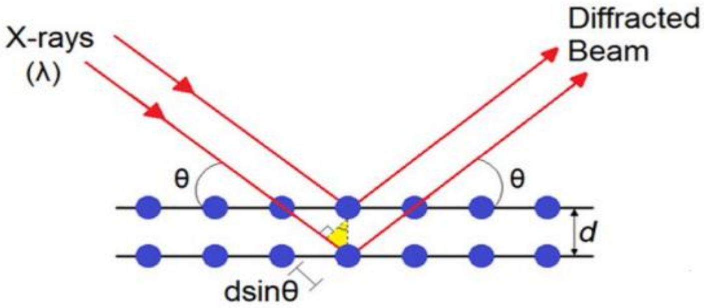

The Bragg equation can be used to determine the 3D structure of a molecule by utilizing the position and intensity of the measured diffraction spots. Once the travel path difference *d* is equal to integer *n* of wavelength, a constructive interference occurs. This will cause the diffracted X-ray beam to leave the crystal at the same angle θ as the incident X-ray beam.

Therefore, a constructive interference will be detected when X-rays collide with a crystal structure formed by a well-organized arrangement of atoms. This interference is converted by the detector into an electronic signal, which appears as a peak at a specific angle on a diffractogram. The position of the peaks can be correlated with the position of certain species likely to be present on the surface of the analyzed sample via pre-established database. Since constructive interference occurs according to structure, this technique can thus determine the composition of crystalline elements on the surface and the structure of compounds with the same formula.

The XRD analysis was performed on a Brucker D8 advance diffractometer. The X-ray beam is produced by a tungsten filament fitted with a copper anode at wavelength λ = 1.5406 Å. The X-ray detector used is a Lynxeye. The angular range 10° < 2θ < 80° was used for calcined, reduced, and spent samples with a step size of 2θ = 0.02° and an integration time of 2 s. Prior to the analysis, the sample was ground to a powder consistency and a smooth layer was applied on the sample holder. The crystalline phases were identified through the comparison of the attained diffraction patterns with reference patterns obtained from the Joint Committee on Powder Diffraction Standards (JCPDS) database maintained by the International Center for Diffraction Data (ICDD) using EVA software. This method allowed the computation of the crystallite size using the Debye-Scherrer equation as follow:

$$D = \frac{K\lambda}{\beta cos\theta}$$

D: crystallite size (nm)

λ: X-ray wavelength (1.5406 Å)

β: line broadening full width at half maximum FWHM (radians)

θ: Bragg’s angle (°)

K: dimensionless shape factor, typical value of 0.9

2.2. N_2 adsorption-desorption analysis

The existence of pores on the catalyst's surface enhances the surface contact and the likelihood of a gaseous mixture adsorption on the catalyst. N_2 adsorption-desorption analysis was performed to study catalysts' textural properties, surface area, and porous properties. The experiments were recorded on a 3-flex micromeritics apparatus (**fig. A.4**). The physical adsorption of nitrogen gas at liquid nitrogen temperature (-196 °C) is used in N_2 adsorption-desorption. The resulting adsorption isotherm was determined by measuring the amounts of nitrogen gas adsorbed as a function of relative pressure. The isotherm's form reveals both the catalyst surface and the pores' type. The multipoint Brunauer–Emmet–Teller (BET) method was utilized to determine the surface area. The amount of nitrogen desorbed at a relative pressure of $p/p^o = 0.99$ was useful in calculating the pore volumes. The Barrett–Joyner–Halenda (BJH) method was employed to evaluate the pore size distributions. The degasification of the adsorbents was conducted, preceding the analysis, at 90 ºC for 1 hour, then at 350 ºC for 4 hours, to eliminate atmospheric contaminants and water molecules.

Fig. A.4 3-flex micromeritics apparatus for N_2 adsorption/desorption analysis

$$\frac{\frac{P}{P^0}}{V(1-\frac{P}{P^0})} = \frac{1}{V_m C} + \frac{(C-1)P}{V_m C P^0}$$

P: partial pressure

P^0: saturation pressure at the experimental temperature

V: volume of N_2 adsorbed (cm^3/g)

V_m: volume of N_2 adsorbed at monolayer coverage (cm^3/g)

C: constant

The surface area is then calculated based on the following formula:

$$S(m^2/g) = \frac{\alpha V_m N_A}{V}$$

N_A= 6.023*10^{23} mol^{-1}

V_m= 22400 cm^3/mol

α = 16.2*10^{-20}

2.3. H_2- Temperature Programmed Reduction (H_2-TPR)

TPR is a method that measures a catalyst's degree of reduction and calculates its reversible redox capacity. It is employed for metal oxides characterization which constitute the catalysts' active phase to ascertain the most effective reduction conditions needed for the investigated reaction. H_2-TPR experiments were conducted in a Micromeritics Autochem II chemisorption analyzer (**fig. A.5**) to identify reducible species and their corresponding reduction temperatures. Inside a U-shaped quartz tube, 50 mg of the calcined catalyst are uniformly dispersed on the surface of a quartz cotton. The tube is then placed in an oven, where the catalyst's temperature is measured via a thermocouple. A reducing gas mixture is then fed over the catalyst as it is subjected to a programmed increase in temperature. The catalyst is purged under 30 ml/min Ar flow (at 150 °C for 1 hour) to discard any physiosorbed water. The sample is then heated from ambient temperature to 900 °C under a 50 ml/min 5 vol% H_2 in Ar at a heating rate of 5 °C/min. Water was contained in a salted ice recipient during the analysis. A thermal conductivity detector (TCD) is used to record the variation of the amount of hydrogen consumed as a function of temperature.

Fig. A.5 Micromeritics Autochem II chemisorption analyzer for H_2-TPR and CO_2-TPD analyses

The experimentally determined hydrogen consumptions were compared with those calculated theoretically using the following formula.

$$M_xO_y + yH_2 \rightarrow xM + yH_2O$$

(**M_xO_y**: metal oxide; **M**: reduced metal)

x mol of MO → y mol of H_2

$n_{MO} = \frac{m_{MO}}{MM_{MO}} \rightarrow x$ mol of H_2 (in µmol H_2/g)

The reduction reactions were the following:

$Ni^{2+} + H_2 \rightarrow Ni^0 + 2H^+$

$Ru^{4+} + 2H_2 \rightarrow Ru^0 + 4H^+$

2.4. CO_2- Temperature Programmed Desorption

TPD is used to measure the desorbed species from a catalyst at a specific heating rate. After the catalyst contacts the adsorbate for a predetermined amount of time, the temperature is raised at a specific rate. The adsorbate and adsorbent's chemical bond will eventually be broken as the temperature rises, resulting in the desorption of the adsorbate. The variations in the desorbed gas concentration are tracked using a TCD detector. In this study, CO_2-TPD tests were conducted to examine the basicity of each catalyst. Carbon dioxide is used as an adsorbate since it is sufficiently acidic to assess all basic sites. The amount of desorbed carbon dioxide helps determine the total basicity of the catalyst, while the desorption temperature helps determine the strength of the basic sites. The same Micromeritics Autochem II chemisorption analyzer that was utilized for the H_2-TPR tests was used to measure the basicity of the supports and catalysts. 50 mg of the sample were positioned in U-tube quartz reactor and preheated under 30 ml/min He flow (500 °C for 1 hour). The catalysts were cooled and subjected to a 30 ml/min 10% CO_2 in He flow (50 °C for 1 hour). The samples were then purged for 30 min with 30 ml/min He flow and then heated to 600 °C (10 °C/min) to desorb the carbon dioxide. The TCD monitors the variations in the desorbed gas concentration.

3. Characterization of produced gases

The gases stored in the sample bag were analyzed by an Agilent 3000A micro-gas chromatography (**fig. A.6**) equipped with two parallel columns: a Plot U column that separates carbon dioxide using helium carrier gas and a molecular sieve column that separates methane, hydrogen, and carbon monoxide using argon carrier gas. These products were detected using a Thermal Conductivity Detector (TCD).

Fig. A.6 Agilent 3000A micro-gas chromatography for GC analysis

4. Characterization of Trapped Tar

After reforming 2g of polypropylene using 1g of reduced Ni or Ru-Ni catalysts impregnated on alumina support, the tar formed was trapped in gas bubblers containing isopropanol solution and placed in ice recipients. The tar components were ascertained by a Varian CP-3800 gas chromatography connected with a series 1200 quadrupole mass spectrometer operated in electron impact ionization (EI) mode (**fig. A.7)** using helium as a carrier gas. Using a capillary column (VF-5MS, 30 m x 0.25 mm x 0.25 µm) with a split of 5, the organic phases were separated. Injector and interface temperatures were maintained at 295 °C and 310 °C respectively.

The capillary column's temperature was programmed to increase from 40 °C (hold for 5 min) to 310 °C (hold for 60 min) at a 5 °C/min heating rate and 1 ml/min helium flow during the entire analysis.

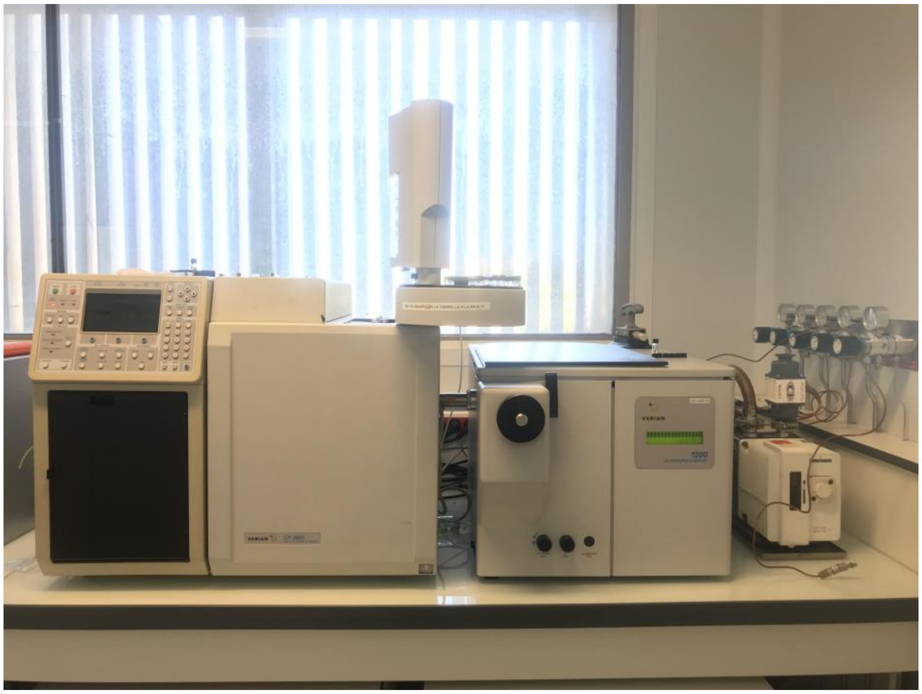

Fig. A.7 Varian CP-3800 gas chromatograph/ Varian 1200 quadrupole Mass Spectrometer Gas chromatography/mass spectrometry (GC/MS) analysis

5. Characterization of spent catalysts:

All used catalysts were characterized using previously mentioned DSC-TG (under flow of air) and XRD techniques.

Appendix B

1. Active phase calculations

Wet impregnation technique was employed to synthesize all catalysts. The following formula is used to calculate the quantity of precursor needed to obtain an active phase of 5-50 % Ni (from $Ni(NO_3)_26H_2O$) and 1 % Ru (from $Ru(NO)(NO_3)_3$).

$$x = \frac{m_{a.p}}{m_{support} + m_{a.p}} \times 100$$

Where x is the percentage of active phase, $m_{a.p}$ is the mass of active phase, and $m_{support}$ is the mass of the support used.

2. Test conditions

After extensive literature review and several preliminary tests, we were able to determine the most suitable experimental conditions. Below are the CO_2 calculations and the H_2, CO, and syngas theoretical calculations for each type of plastic used.

From the DSC-TG curve, we were able to determine the beginning and end of the pyrolysis reaction thus permitting us to calculate the quantity of carbon dioxide needed for the reforming reaction. The carbon dioxide was sent to the system right before the plastic transforms to gas. This is also when the Tedlar bag is opened. the pyrolysis temperature of polypropylene was set at 500 °C, that of polyethylene was set at 550 °C, and that of polystyrene was set at 475 °C

Polypropylene and Polyethylene plastic:

According to the DSC-TG analysis of PP plastic, the pyrolysis starts at 330 °C and ends at 490 °C. During these 32 min, 6.25 g of CO_2 must be sent into the system to perform the dry reforming reaction of polypropylene. This permitted the calculation of the flow of CO_2 needed for the reforming reaction to be 105 ml/min.

According to the DSC-TG analysis of PE plastic, the pyrolysis starts at 410 °C and ends at 530 °C. During these 24 min, 6.25 g of CO_2 must be sent into the system to perform the dry reforming reaction of polyethylene. This permitted the calculation of the flow of CO_2 needed for the reforming reaction to be 143 ml/min.

According to theoretical calculations based on reaction (**A.1**), 2 g of polypropylene/polyethylene plastic should produce 0.14 mol of H_2, 0.28 mol of CO, and 210 $mmol/g_{plastic}$ of syngas.

$$-(CH_2)- + CO_2 \rightarrow H_2 + 2CO \qquad \textbf{(A.1)}$$

Polystyrene plastic:

According to the DSC-TG analysis of PS plastic, the pyrolysis starts at 330 °C and ends at 460 °C. During these 26 min, 6.77 g of CO_2 must be sent into the system to perform the dry reforming reaction of polystyrene. This permitted the calculation of the flow of CO_2 needed for the reforming reaction to be 116 ml/min.

According to theoretical calculations based on reaction (**A.2**), 2 g of polystyrene plastic should produce 0.077 mol of H_2, 0.308 mol of CO, and 193 mmol/g_{PS} of syngas.

$$-(CH)- + CO_2 \rightarrow \frac{1}{2} H_2 + 2CO \qquad \textbf{(A.2)}$$

Since the Tedlar bag can only hold 25 L, and after determining the time needed for the experiment to finish, we used an Argon flow of 50 ml/min, which was sufficient to carry the gases towards the Tedlar bag.

3. Carbon balance

For the carbon balance, the loop is closed during all the performed tests. Below is an example of a carbon balance during the dry reforming test over the $15NiAl_2O_3$ catalyst. The balance is correct with an error less than 2.5%. This the case for all other catalysts.

Catalyst	**$15NiAl_2O_3$**		
$m_{catalyst}$ (g)	1.0742	**m_{PP} (g)**	2.0171
Carbon Input			
Mass PP (g)	2.0171	**Mass of C (g)**	1.7289
Volume of CO_2 (L)	10.5		
Number of moles of CO_2 (mol)	0.4294		
Mass of CO_2 (g)	18.8927	**Mass of C (g)**	5.1526
		Total C Input (g)	6.8815
Carbon Output			
Liquid Analysis			

Compound	**mass (g)**	**mass of C (g)**
Benzene	1.0805	0.9975
Toluene	0.0505	0.0461
Ethyl benzene	0.0004	0.0004
o-xylene	0.0082	0.0075

m-xylene	0.0023		0.0021
	Total C Liquid (g)		1.0536 g
	Gas Analysis		
Volume in Tedlar (L)	20.65		
	CO_2	**CH_4**	**CO**
Mole%/volume%	33.3779	1.4014	19.2729
Volume (L)	6.8926	0.2894	3.9799
Number of moles (mol)	0.3079	0.0129	0.1778
Mass of C (g)	3.6948	0.1551	2.1334
	Total C Gas (g)		5.9833
	Total C Output (g)		7.0369

4. Carbon deposition

The carbon deposition of each catalyst was determined based on the weight loss detected from the thermal gravimetric analysis of the catalyst sample. Since at high Ni loadings two exothermic peaks are noticed, the first accompanied with weight gain (oxidation of nickel) and the second accompanied with weight loss (carbon oxidation), the DSC-TG of 50 wt.% Ni loading catalyst after reduction and after the reforming reaction were compared to determine the mass of carbon deposited on the sample. **Fig. B.1** (a and b) shows the DSC-TG profiles of the reduced and used $50NiAl_2O_3$ catalysts, respectively.

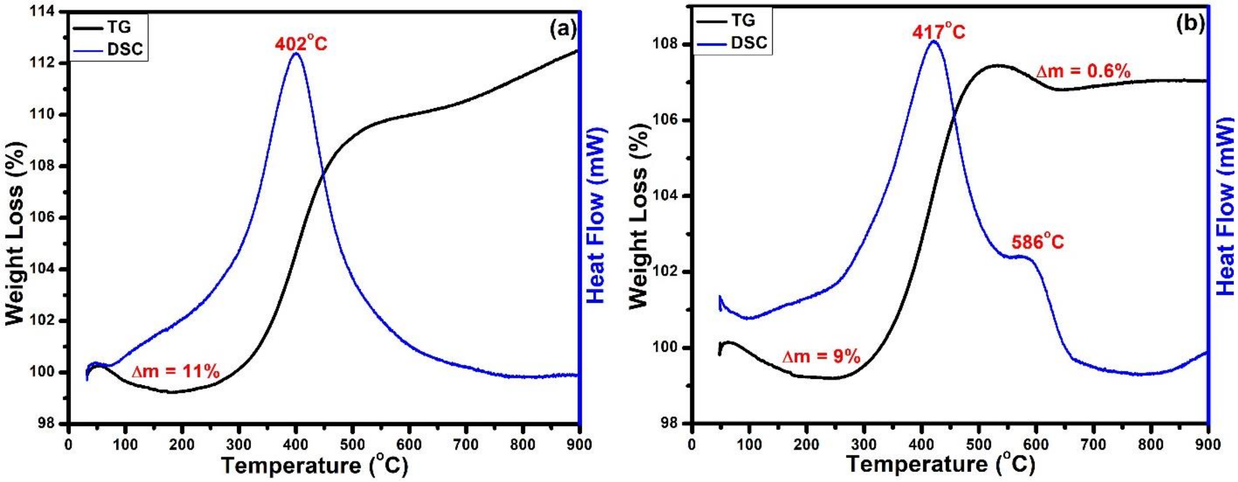

Fig. B.1 DSC-TG profiles of (a) reduced and (b) used $50NiAl_2O_3$ catalysts

It is noticed that the weight gain peaks in both samples are approximately equal, therefore the weight loss resulting from the second exothermic peak is considered the percentage of carbon deposited on the catalyst. This trend is applied for all catalysts with high nickel loadings (25 wt.% and above).

5. Tar yield

The tar yield (mg/g) was calculated according to this formula

$$Tar\ yield = \frac{m_{tar}}{m_{plastic}}$$

Where m_{tar} is the mass of tar in mg and $m_{plastic}$ is the mass of plastic feedstock in g.

6. Tar conversion efficiency

The tar conversion efficiency was calculated according to this formula

$$Tar\ conversion\ efficiency = \frac{w_{pyr} - w_{cat}}{w_{pyr}} \times 100$$

Where w_{pyr} is the tar yield (mg/g) in the absence of catalyst and w_{cat} is the tar yield (mg/g) in the presence of Ni and Ru-Ni supported catalysts.

7. Ce percentages calculations

The following formula is used to calculate the quantity of $Ce(NO_3)_36H_2O$ precursor needed to obtain $x$$CeAl_2O_3$.

$$x = \frac{m_{Ce}}{m_{CeO_2 + m_{support}}} \times 100$$

$$m_{Ce} = n_{Ce} \times MM_{Ce}$$

$$m_{CeO_2} = n_{Ce} \times MM_{Ce} + n_{Ce} \times MM_{O_2}$$

For example, the calculation of the precursor needed to get $15CeAl_2O_3$ was as follow:

$$0.15 = \frac{140.116 \times n_{Ce}}{(140.116 \times n_{Ce} + 32 \times n_{Ce}) + 2}$$

$$n_{Ce} = 2.62 \times 10^{-3}\ mol$$

$$1\ mol\ Ce \rightarrow 1\ mol\ precursor$$

$$m_{precursor} = n_{precursor} \times MM_{precursor}$$

$$m_{precursor} = 2.62 \times 10^{-3} \times 434.22$$